

# ELECTRO-OPTICAL SYSTEMS, INC.

A Subsidiary of Xerox Corporation



Study and Development Report  
on  
HIGH-PERFORMANCE THERMIONIC CONVERTERS

A. E. Campbell

2 September 1966

FACILITY FORM 602

N 67 11843	
(ACCESSION NUMBER)	(THRU)
181	1
(PAGES)	(CODE)
CR 74388	03
(NASA CR OR TMX OR AD NUMBER)	(CATEGORY)

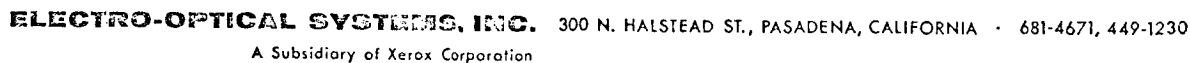
GPO PRICE \$ \_\_\_\_\_  
CFSTI PRICE(S) \$ \_\_\_\_\_

Hard copy (HC) 5.00

Microfiche (MF) 1.00

ff 653 July 65

Prepared for  
Jet Propulsion Laboratory  
California Institute of Technology  
4800 Oak Grove Drive  
Pasadena, California



Date 27 September 1966

TO: California Institute of Technology  
Jet Propulsion Laboratory  
4800 Oak Grove Drive  
Pasadena, California

Attn: John Heie

Reference (Contract No.) 951225

Report No. and Type	6952-Final	Date of Issue	2 September 1966
Short Title	Thermionic Converter	Covers Period	19 May 1965 - 19 July 1966
Classification	U - <del>C</del> - <del>S</del>	EOS Classified	Doc. No.

Transmitted herewith are the required copies of the report described above. Fund and labor reports, if required, are included and distributed as tabulated below. Should additional information be desired, please direct your inquiries to the undersigned.

Very truly yours,

ELECTRO-OPTICAL SYSTEMS, INC.

*Richard N. Strong*  
Richard N. Strong, Manager  
Contract Administration

EOS Form No. 7503 (7/64)

Final Report

HIGH-PERFORMANCE THERMIONIC CONVERTERS

Prepared for

Jet Propulsion Laboratory

California Institute of Technology

4800 Oak Grove Drive

Pasadena, California

Attention: Mr. John Heie, Contract Negotiator

Contract 951225


EOS Report 6952-Final

2 September 1966

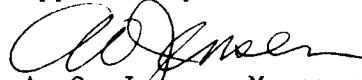
Prepared by

  
A. E. Campbell

Approved by

  
D. G. Worden, Manager  
Electron Device Research Section

Approved by

  
A. O. Jensen, Manager  
Electro-Optical Technology Laboratory

ELECTRO-OPTICAL SYSTEMS, INC.-- PASADENA, CALIFORNIA  
A Subsidiary of Xerox Corporation

## CONTENTS

1.	INTRODUCTION	1
2.	ELECTRODE MATERIALS INVESTIGATION	5
2.1	Emitter Processing and Stabilizing Schedule	5
2.1.1	Tantalum Emitter Schedule	6
2.1.2	Rhenium Emitter Schedule	13
2.2	Variable Parameter Test Vehicle	14
2.2.1	Variable Parameter Test Vehicle Design	17
2.2.2	Variable Parameter Test Vehicle Fabrication and Assembly Procedure	32
2.2.3	Variable Parameter Test Vehicle Drive Mechanism	37
2.2.4	Variable Parameter Test Vehicle Mounting Fixture	41
2.2.5	Rhenium-Rhenium Electrode Measurements and Interpretation	44
2.2.6	VPTV Investigation of the Rhenium Emitter/Molybdenum Collector System	86
3.	SECONDARY EXPERIMENTS SUPPORTING CONVERTER TECHNOLOGY	93
3.1	Heat Transfer/Heat Rejection Investigation	93
3.1.1	Rokide "C" Emittance Investigation	93
3.1.2	Nonintegral Collector-Radiator Investigation	101
3.1.3	L/A Design Curves for Collector " $\Delta T$ "	104
3.2	Feasibility Experiments Related to Converter Fabrication	106
3.2.1	Converter Seal-Off	106
3.2.2	Ceramic-Metal Seal	111
3.2.3	Electron Beam Welding	112
3.2.4	Interelectrode Spacing Experiments	118
4.	HIGH PERFORMANCE THERMIONIC CONVERTER DESIGN	129
4.1	Converter Efficiency	130



## CONTENTS (contd)

4.2	Definition of Emitter Area	133
4.3	Collector-Radiator Structure	136
4.3.1	Collector Heat Load	137
4.3.2	Radiator Heat Rejection	138
4.4	Assembly Procedure	139
5.	THERMIONIC CONVERTER PERFORMANCE	143
5.1	Methods of Measurement	143
5.1.1	Current-Voltage Data	143
5.1.2	Temperature Measurement	147
5.2	Converter SN-101 (rhenium-rhenium)	147
5.2.1	SN-101 Electrode Processing	149
5.2.2	SN-101 Interelectrode Spacing	150
5.2.3	SN-101 Optimized dc Performance	150
5.2.4	SN-101 Miscellaneous Data	152
5.3	Converter SN-102 (rhenium-rhenium)	154
5.3.1	Electrode Processing	154
5.3.2	SN-102 Interelectrode Spacing	154
5.3.3	Converter SN-102 Performance	156
5.4	Converter SN-103 (rhenium-molybdenum)	158
5.4.1	Electrode Processing	158
5.4.2	SN-103 Interelectrode Spacing	158
5.4.3	Converter SN-103 Steady-State, Optimized Performance	158
5.5	Converter SN-104 (rhenium-molybdenum)	160
5.5.1	Electrode Processing	160
5.5.2	SN-104 Interelectrode Spacing	163
5.5.3	Converter SN-104 Performance	163
6.	CONTRIBUTOR LIST	165
	REFERENCES	167
	APPENDIX A - PROCEDURE FOR CHEMICAL CLEANING OF TANTALUM	169
	APPENDIX B - DERIVATION OF COLLECTOR HEATING POWER	173

## ILLUSTRATIONS

2-1a	Tantalum Emitter Vacuum-Fired at 2100°C for 2 Hours in a Vac-Ion Pumped Atmosphere of $1 \times 10^{-7}$ Torr	10
2-1b	Same Emitter after Operation at 1735°C for 100 Hours in a Vac-Ion Pumped Environment of $5 \times 10^{-8}$ Torr	10
2-2a	Tantalum Emitter Vacuum-Fired at 2250°C for 2 Hours in a Vac-Ion Environment of $4 \times 10^{-7}$ Torr	11
2-2b	Same Emitter after Operation at 1735°C for 100 Hours in a Vac-Ion Pumped Environment of $5 \times 10^{-8}$ Torr	11
2-3a	Tantalum Emitter Vacuum-Fired at 2450°C for 2 Hours in a Vac-Ion Pumped Environment of $6 \times 10^{-7}$ Torr	12
2-3b	Same Emitter after Operation at 1735°C for 100 Hours in a Vac-Ion Pumped Environment of $5 \times 10^{-8}$ Torr	12
2-4a	Rhenium Process Sample Vacuum-Fired at 2450°C for 24 Hours in a Vac-Ion Pumped Atmosphere of $3 \times 10^{-7}$ Torr	15
2-4b	Same Sample after 100-Hour Operation at 1735°C in a Vac-Ion Pumped Atmosphere of $4 \times 10^{-8}$ Torr	15
2-5a	Rhenium Process Sample Vacuum-Fired at 2450°C for 10 Hours in a Vac-Ion Pumped Atmosphere of $3 \times 10^{-7}$ Torr	16
2-5b	Same Sample after 100-Hour Operation at 1735°C in a Vac-Ion Pumped Atmosphere of $4 \times 10^{-8}$ Torr	16
2-6	Variable Parameter Test Vehicle	19
2-7	Setup for Collector Heat Transfer Experiment	23
2-8	Idealized Collector-Radiator System	25
2-9	Collector Surface Temperature as a Function of Collector Current Density (calculated)	27
2-10	Interelectrode Potential Distributions	30
2-11	VPTV Components and Subassemblies Prior to Final Joining	33
2-12	Test Vehicle Layout	36
2-13	Variable Parameter Test Vehicle Drive Mechanism	39
2-14	Variable Parameter Test Vehicle Mounting Fixture	42

# ILLUSTRATIONS (contd)

2-15	Reservoir Temperature versus Current with 0.002, 0.003, and 0.004 Inch Spacing, $T_{\text{Collector Root}} = 570^{\circ}\text{C}$	47
2-16	Reservoir Temperature versus Current with 0.003, 0.004, and 0.005 Inch Spacing, $T_{\text{Collector Root}} = 596^{\circ}\text{C}$	48
2-17	Reservoir Temperature versus Current with 0.002, 0.003, 0.004, and 0.005 Inch Spacing, $T_{\text{Collector Root}} = 610^{\circ}\text{C}$	49
2-18	Reservoir Temperature versus Current with 0.002, 0.003, 0.004, and 0.005 Inch Spacing, $T_{\text{Collector Root}} = 660^{\circ}\text{C}$	50
2-19	Converter Optimization Data for 0.7 Volt Output. $T_{\text{Collector Root}} = 575^{\circ}\text{C}$	51
2-20	Converter Optimization Data for 0.7 Volt Output. $T_{\text{Collector Root}} = 610^{\circ}\text{C}$	52
2-21	Converter Optimization Data for 0.7 Volt Output. $T_{\text{Collector Root}} = 656^{\circ}\text{C}$	53
2-22	Converter Optimization Data for 0.6 Volt Output. $T_{\text{Collector Root}} = 650^{\circ}\text{C}$	54
2-23	Converter Optimization for 0.6 Volt Output. $T_{\text{Collector Root}} = 685^{\circ}\text{C}$	55
2-24	Interelectrode Spacing versus Current at 0.8 Volt Output. Collector, Emitter, and Cesium Reservoir Constant Temperatures	56
2-25	Interelectrode Spacing versus Voltage. Emitter, Collector, and Cesium Reservoir Temperatures Constant	58
2-26	Voltage-Spacing Relationship for Constant Emitter, Collector, and Cesium Reservoir Temperatures	59
2-27a	Interelectrode Spacing versus Voltage Output at a Constant Current of 60 Amperes	61
2-27	I-V Characteristics for the Operating Regions of Space-Charge Limited, Incipient Breakdown, and Fully Developed Plasma	64
2-28	Potential Distribution Diagram for Space-Charge, Incipient Breakdown, and Fully Developed Plasma at the dc Points "A", "B", and "C"	65
2-29	First Derivative of Voltage-Spacing Curve	67
2-30	I-V Characteristics Showing that Saturated Electron Emission is Independent of Spacing	70

# ILLUSTRATIONS (contd)

2-31	Thermocouple Calibration Data	72
2-32	Saturated Electron Emission from Polycrystalline Rhenium	73
2-33	Saturated Emission Measured from Collector (Rhenium Surface)	76
2-34	Circuit for Bare-Work Function Measurements	78
2-35	I-V Curves for Bare-Work Measurements	79
2-36	Cesium Conduction Measurements Compared with Semi-Empirical Theory	83
2-37	Comparison of Voltage Output versus Interelectrode Spacing for Rhenium-Rhenium and Rhenium-Rhenium/Molybdenum Electrode System	88
2-38	Voltage Output versus Interelectrode Spacing for Rhenium-Rhenium/Molybdenum Electrode System	89
2-39	Composite Plot of Optimum Converter Performance for Rhenium-Rhenium/Molybdenum Electrode System	92
3-1	Thermocouple Locations and Sample Dimensions of Molybdenum-Rokide "C" Experiment	94
3-2	Rokide "C"-Coated Molybdenum Sample After 500 Hours of Operation	96
3-3	Cooldown Curves of Rokide "C"-Coated Molybdenum Sample	98
3-4	Cooldown Curves of Rokide-Coated Copper Sample	100
3-5	Nonintegral Collector-Radiator Assembly	103
3-6	Thermal Design Curves for Molybdenum Collector	107
3-7	Annealed OFHC Copper Tubing 1/4" O.D., 0.030" Wall. Kane Hand Pinch-Off Tool	109
3-8	Annealed OFHC Copper Tubing 1/4" O.D., 0.030" Wall. Varian Hand Pinch-Off Tool	109
3-9	Annealed OFHC Copper Tubing 1/4" O.D., 0.030" Wall. Kane Hydraulic Pinch-Off Tool with 1/4"-Radius Roller	110
3-10	Annealed OFHC Copper Tubing 1/4" O.D., 0.030" Wall. Kane Hydraulic Pinch-Off Tool with 1/8"-Radius Roller	110
3-11	Electron-Beam Weld of 0.020-Inch Thick Niobium Ring to 0.060-Inch Thick Niobium Ring.	114

## ILLUSTRATIONS (contd)

3-12	Rhenium Sheet to Rhenium Sheet Electron-Beam Weld. Beam Voltage of 150 kV x Current of 3.4 mA. Part Speed of 100 in/min	116
3-13	Rhenium Sheet to Rhenium Sheet Electron-Beam Weld. Beam Voltage of 150 kV x Current of 3.4 mA. Part Speed of 90 in/min	116
3-14	Rhenium Sheet to Rhenium Sheet Electron-Beam Weld. Beam Voltage of 150 kV x Current of 4.7 mA. Part Speed of 80 in/min	117
3-15	Rhenium Sheet to Rhenium Sheet Electron-Beam Weld. Beam Voltage of 150 kV x Current of 6 mA. Part Speed of 80 in/min	117
3-16	Thermal Mock-Up for Interelectrode Spacing Measurements	119
3-17	Emitter Heat Choke Temperature (true) Distribution	120
3-18	Spacing Experiment Setup	123
3-19	Photograph of Interelectrode Spacing at an Emitter Temperature of 1735°C	125
3-20	Change in Interelectrode Spacing as a Function of Emitter Temperature	126
4-1	Thermionic Converter Design with Envelope Sidewall Contributing to Performance Output	134
4-2	Thermionic Converter Design with Envelope Sidewall Unable to Provide Performance Output	135
4-3	Layout of Principal Subassemblies of EOS High-Performance Thermionic Converters	140
4-4	Completed Diode Assembly	142
5-1	Electrical Circuit for dc Performance Testing of Thermionic Converters	144
5-2	Electrical Circuit for ac Performance Testing of Thermionic Converters	145
5-3	Calibration Record of Micro-Optical Pyrometer Used for Converter Testing	148
5-4	Converter SN-101 Performance Plot	151
5-5	Converter SN-101 Performance Plot Comparing Electrode Potential to Terminal Output Voltage	153

## ILLUSTRATIONS (contd)

5-6a	SN-102 Characteristic at 1735°C Emitter Temperature, 349°C Cesium Reservoir Temperature, and Collector Root Temperature at 592°C	155
5-6b	Rhenium-Rhenium Variable Parameter Test Vehicle Characteristic at 1735°C Emitter Temperature, 348°C Cesium Reservoir Temperature, and Collector Root Temperature at 600°C	155
5-7	Converter SN-102 Performance Plot	157
5-8	Converter SN-103 Initial Performance Plot	159
5-9	Converter SN-103 Performance Plot after 60 Hours	161
5-10	Converter SN-103 after Evaporation of Rhenium onto the Collector	162
5-11	Converter SN-104 Performance Plot	164

## 1. INTRODUCTION

This is the final report of the research and development program on high-performance cesium-vapor thermionic converters conducted by Electro-Optical Systems, Inc., for the Jet Propulsion Laboratory under Contract JPL 951225. The program period extended from 19 May 1965 to 19 July 1966.

The major objectives of the program were: (1) to provide a thorough, definitive experimental and analytical research background on the converter performance capabilities of selected electrode materials and converter engineering design parameters and, (2) to demonstrate the actual performance of practical operating converters designed on the basis of the results of this study. To achieve this objective, the program was organized in two major tasks, the first of which was concerned primarily with the properties of the electrode materials selected and experimental parametric investigations, and the second, with converter design and subsidiary studies of converter fabrication techniques.

Task I included the design and construction of precision variable parameter test vehicles with which complete parametric investigations of plane-parallel cesium-vapor converter performance characteristics could be conducted over a wide range of converter parameters applicable to practical converter design. These vehicles were capable of operation with emitter temperatures from  $1300^{\circ}\text{K}$  to  $2100^{\circ}\text{K}$ , collector temperatures from  $700^{\circ}\text{K}$  to  $1300^{\circ}\text{K}$ , and cesium reservoir temperatures from  $400^{\circ}\text{K}$  to  $750^{\circ}\text{K}$ . The interelectrode spacings could be varied from less than 0.0002 inch to over 0.015 inch and were accurately reproducible. During this program, two such vehicles were fabricated and parametric studies were made with two sets of electrode materials, namely rhenium emitter/rhenium collector, and rhenium emitter/molybdenum collector.

Prior to the use of these materials in the variable parameter test vehicles, samples were subjected to processing experiments and were characterized chemically and physically in both the as-received and processed conditions.

Task II included the design, fabrication and test of high-performance plane parallel converters as well as a number of experiments on fabrication technology. The aspects of converter design that were related to operational parameters (emitter temperature, inter-electrode spacing, etc.) were based directly on the data acquired in the Task I investigations. This provided the means for immediate and unambiguous correlations between hardware performance and research results. The experiments in fabrication technology included the formulation of reliable electron-beam welding schedules, thermal cycling of active-alloy brazed metal-to-ceramic seals, heat transfer experiments and thermal emittance measurements for radiator design, and experiments with a thermal mock-up of a thermionic converter to ascertain the influence of thermal loads on interelectrode spacing.

#### Outline of Program Accomplishments

Task I was highlighted by the outstanding results obtained on two variable parameter test vehicles which operated for a combined period of 1500 hours without failure. The test vehicles exceeded their design goals in scope, precision and reliability. The prolonged period of operation permitted extensive parametric testing which completely covered the plasma modes of the converter and defined the potentialities of cesium-vapor converters with the electrode materials utilized in these tests. Precise measurements were made of output characteristics for interelectrode spacings in the range from 0.0002 to over 0.010 inch for several settings of emitter, collector, and reservoir temperatures and under optimized power output conditions as well as off-optimum conditions. The interelectrode spacings were reproducible to within 0.0001 inch, and the output performance was reproducible within 1 to 2 percent during the entire period of testing. The details of these experiments are discussed in Section 2 of this report.



Four high-performance prototype converters were fabricated during Task II and the performance goal of 20 watts/cm<sup>2</sup> power output at 0.8 volts for an emitter temperature of 1735°C (true) was achieved. The interelectrode spacings of these converters were selected for specific output characteristics from the data acquired from the parametric test vehicles of Task I. A significant achievement of the program was the exact correlation between the performances of the prototype converters and the parametric vehicles. The prototype converters of Task II were fabricated using a new fabrication method developed during the program, wherein prefabricated subassemblies, including metal-ceramic seals, were electron beam welded together to form the final converter assembly. This modular approach is inherently highly reliable since the final step in the converter assembly is a metal-to-metal joint rather than a seal braze. The converters and their fabrication are discussed in Section 4.

The Task II investigations in fabrication technology are discussed in detail in Section 3. Briefly, the results were:

1. An electron beam welding schedule was developed which permitted a reliable weld between a solid rhenium emitter and rhenium envelope. Two test vehicles and four thermionic converters utilized this weld schedule without failure or reweld.
2. A seal testing program demonstrated that active brazed, metal-to-ceramic seals can withstand hundreds of thermal cycles at a cycle rate of 100°C/min. Moreover, it was established that those seals could be prefabricated and then electron beam welded to the converter structures.
3. Heat transfer and heat rejection investigations were completed which established that the emittance value of Rokide "C" coatings at 0.78 demonstrated a reliable molybdenum-copper radiator heat rejection system, and permitted a collector design of minimum thermal design for calculated thermal heat loads.

4. A thermal mockup of thermionic converter together with a high-resolution optical system permitted direct measurements of interelectrode spacings. The mockup was operated at converter operating conditions. The spacing measurements agreed within 0.0002 inch with the design calculations.

## 2. ELECTRODE MATERIALS INVESTIGATION

### 2.1 Emitter Processing and Stabilizing Schedule

The objective of this study was the generation of a processing schedule for the materials selected as electrodes in the variable parameter vehicle or high performance converters. The process schedule includes a detailed chemical cleaning treatment and vacuum outgassing procedure for achieving uncontaminated, stable electrode surfaces.

The emitting electrode in a high-performance thermionic converter operates at a temperature of  $2000^{\circ}\text{K}$  which will result in excessive grain growth and unstable emission if the emitter surface has not been previously heat-treated sufficiently to establish a stable grain structure. The core of the problem, therefore, is to determine a surface finishing and vacuum outgassing schedule that will not only remove gaseous and high vapor pressure elements but will also set the grain structure of the emitter such that subsequent operation for an extended length of time (i.e., much greater than 100 hours) at a temperature of  $2000^{\circ}\text{K}$  will not effect changes in the emitter surface structure.

The materials selected for this process study were Rembar high-purity, plate-stock rhenium and NRC high-purity, rod-stock tantalum. The following paragraphs discuss the analyses of the stock in the "as received" condition, the sample preparation, vacuum outgassing schedules, and results of the surface stability.

As a starting point for the processing study, a detailed mill history for each material was requested from the supplier. Upon receipt of each material, a spectrographic analysis was performed by the Materials Testing Laboratory (MTL), a division of the Magnaflux

Corporation, to provide a comparison with the supplier's certification of purity (Tables 2-IA and 2-IIA). Tables 2-IB and 2-IIB present the data obtained from the MTL tests.

The analyses differ significantly on the type and amount of impurities present in each sample. The differences are due to the conditions of testing, such as electrode selection and chamber cleanliness, as well as the interpretation of the spectra; the latter may account for impurity values that were optimistically reported in the range from 1 to 10 ppm.

#### 2.1.1 Tantalum Emitter Schedule

##### 2.1.1.1 Surface Finish and Chemical Cleaning

Three bar-stock tantalum disks of 0.800-inch diameter and 0.200-inch thickness were machined to achieve a tolerance of 0.0001-inch flatness and 0.0001-inch perpendicularity without the use of oil lubricants. Such tolerances are required in the variable parameter vehicle study for accurate measurements of thermionic power output at 0.0005-inch interelectrode spacings. The actual machined tolerances were: flatness to within 30 millionths of an inch and perpendicularity or "squareness" to within 19 millionths of an inch, both as measured by the EOS Quality Assurance Laboratory with a Pratt & Whitney electronic micrometer capable of determining accuracy to 10 millionths of an inch. A profilometer reading indicated that the surface smoothness on the sample surfaces ranged from 20 to less than 16 microinches.

The samples were chemically cleaned in accordance with the procedure described in Appendix A and were stored in evacuated containers until required for vacuum outgassing.

##### 2.1.1.2 Vacuum Outgassing Schedule for Tantalum

The tantalum emitters which were machined and chemically cleaned as described in the previous paragraphs were mounted in refractory metal firing stands for electron bombardment

TABLE 2-IA

## NRC REPORT ON ANALYSIS OF HIGH-PURITY TANTALUM BAR STOCK

Tantalum	Remainder (99.87 percent)
Chromium	0.0001 percent*
Copper	0.0001 percent*
Iron	0.0005 percent
Molybdenum	0.0048 percent
Tungsten	0.01 percent
Aluminum	0.0001 percent
Columbium	0.0095 percent
Total other elements	0.106 percent*

\* Less than

TABLE 2-IB

MATERIALS TESTING LABORATORY REPORT  
ON SPECTROGRAPHIC ANALYSIS (SEMIQUANTITATIVE)  
OF HIGH-PURITY TANTALUM BAR STOCK

Tantalum	Remainder (99.62 percent)
Chromium	0.003 percent
Copper	0.001 percent
Iron	0.01 percent
Molybdenum	0.01 percent
Tungsten	0.10 percent*
Aluminum	0.0001 percent
Calcium	0.001 percent
Columbium	0.10 percent*
Total other elements	0.15 percent

\* Less than

TABLE 2-IIA

## REMBAR REPORT ON ANALYSIS OF HIGH-PURITY RHENIUM PLATE STOCK

Rhenium	Remainder (99.99 percent)
Aluminum	0.0001 percent
Nickel	0.0005 percent
Copper	0.0001 percent
Gold	0.0042 percent
Manganese	0.0001 percent
Silicon	0.0001 percent
Total other elements	Not detected

TABLE 2-IIB

MATERIALS TESTING LABORATORY REPORT  
ON SPECTROGRAPHIC ANALYSIS (SEMIQUANTITATIVE)  
OF HIGH-PURITY RHENIUM PLATE STOCK

Rhenium	Remainder (99.96 percent)
Aluminum	0.002 percent
Calcium	0.005 percent
Titanium	0.002 percent
Molybdenum	0.01 percent
Magnesium	0.003 percent
Chromium	0.01 percent
Silicon	0.007 percent
Others	Not detected

heating in a vac-ion pumped vacuum environment. The tantalum firing stands were fitted with high-purity, vacuum-fired tantalum tubes that supported the samples. Tantalum was purposely selected as the support material to prevent the formation of eutectics or the diffusion of a dissimilar metal support into the tantalum sample during the high-temperature firing operation.

As a starting point for this investigation, an outgassing schedule of  $2100^{\circ}\text{C}$  for 2 hours was selected for the first emitter sample. A second sample was outgassed at  $2250^{\circ}\text{C}$  for 2 hours and a third sample, at  $2450^{\circ}\text{C}$  for 2 hours. All temperature measurements were made by viewing a 10:1 hohlraum with a calibrated micro-optical pyrometer. The sample surfaces were subsequently examined on a Zeiss metallograph. Selected grains were marked by a microhardness tester and photographed without metallographic preparation such as etching or polishing. The samples were returned for 100-hour operation at  $1735^{\circ}\text{C}$ , the specified emitter temperature for the program performance goals.

#### 2.1.1.3 Surface Stability Examination of Vacuum Outgassed Tantalum

Figures 2-1a and 2-2a are photographs of samples outgassed at  $2100^{\circ}\text{C}$  and  $2250^{\circ}\text{C}$ , respectively, and then operated at  $1735^{\circ}\text{C}$  for 100 hours (Figs. 2-1b and 2-2b). The grooves that appear in the photographs of the sample surface are machining marks. The samples were not lapped or polished since tantalum becomes contaminated with embedded particles from lapping and polishing operations. On both sets of photographs, there is ample evidence of grain boundary movement, which indicates that the processing schedule was not sufficient to produce a stable electrode surface. However, the third emitter sample which was outgassed at  $2450^{\circ}\text{C}$  for 2 hours and then operated at  $1735^{\circ}\text{C}$  for 100 hours displayed little or no grain boundary movement, as shown in Figs. 2-3a and 2-3b. Therefore, the recommended minimum outgassing schedule for tantalum emitters operating near  $2000^{\circ}\text{K}$  is  $2450^{\circ}\text{C}$  for 2 hours.

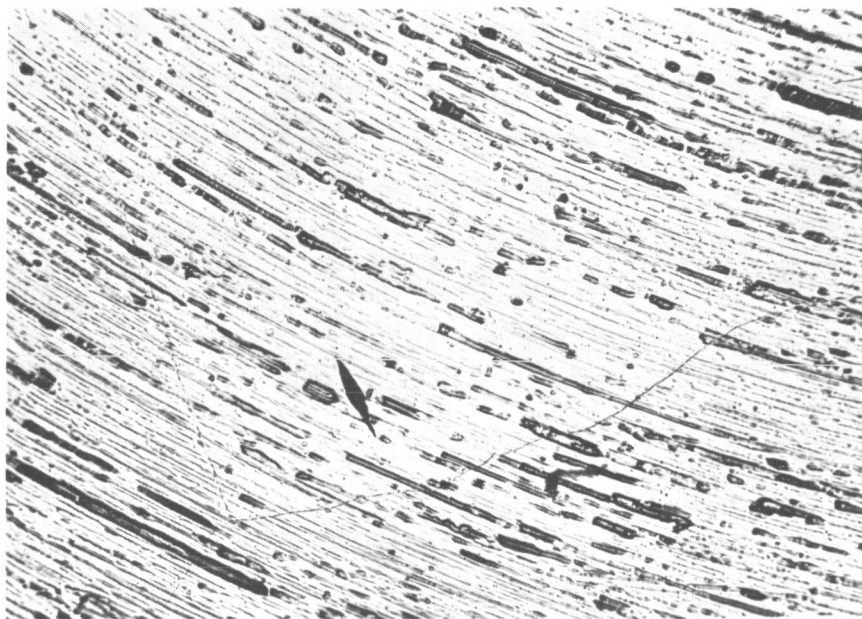


FIG. 2-1a TANTALUM EMITTER VACUUM-FIRED AT 2100°C  
FOR 2 HOURS IN A VAC-ION PUMPED ATMOS-  
PHERE OF  $1 \times 10^{-7}$  TORR (X100)

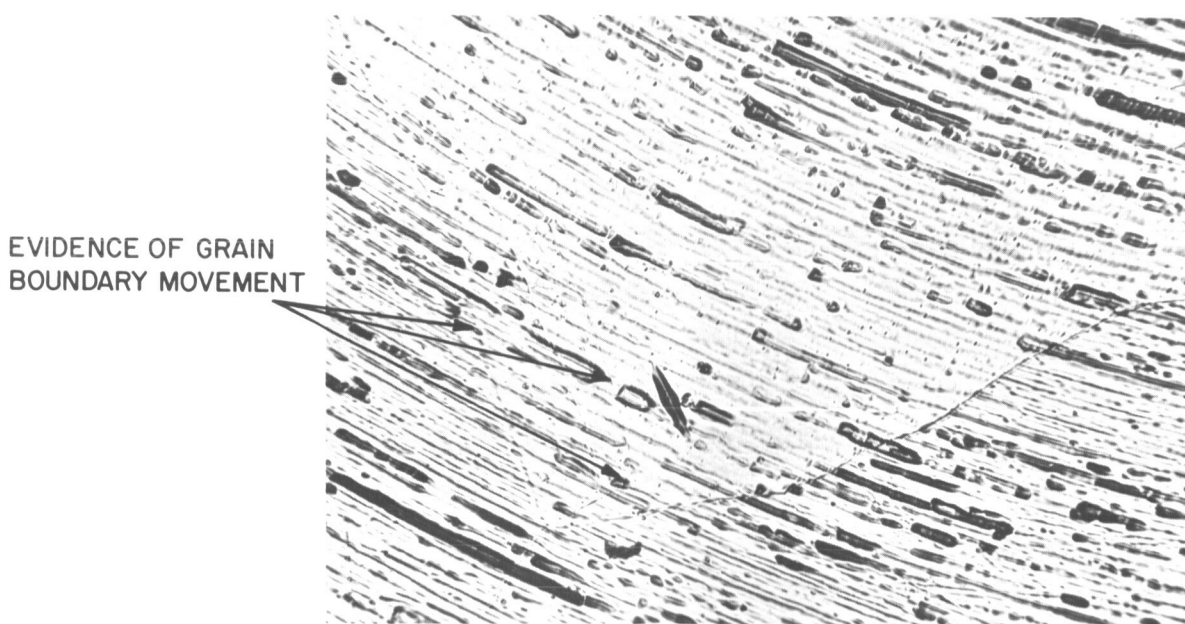


FIG. 2-1b SAME EMITTER AFTER OPERATION AT 1735°C  
FOR 100 HOURS IN A VAC-ION PUMPED EN-  
VIRONMENT OF  $5 \times 10^{-8}$  TORR (X50)



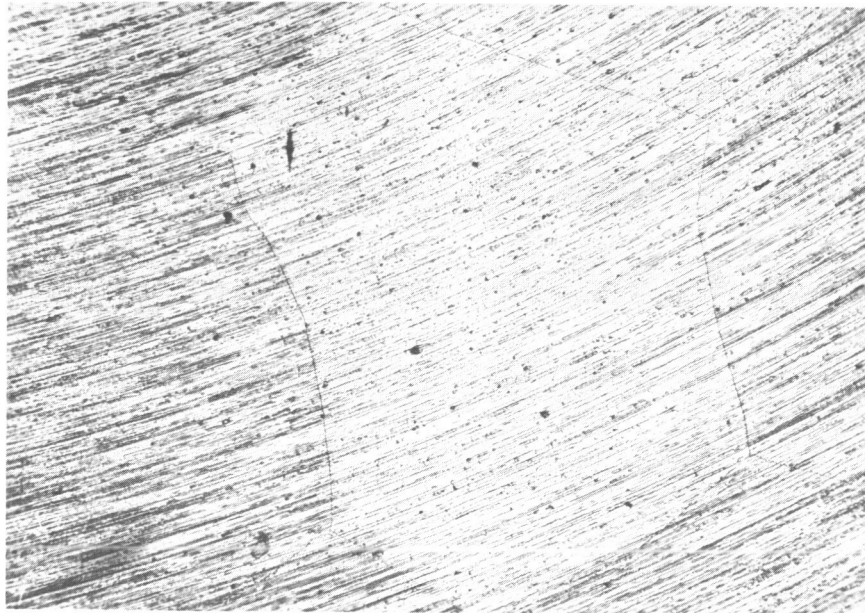


FIG. 2-2a TANTALUM EMITTER VACUUM-FIRED AT 2250°C  
FOR 2 HOURS IN A VAC-ION PUMPED EN-  
VIRONMENT OF  $4 \times 10^{-7}$  TORR (X50)

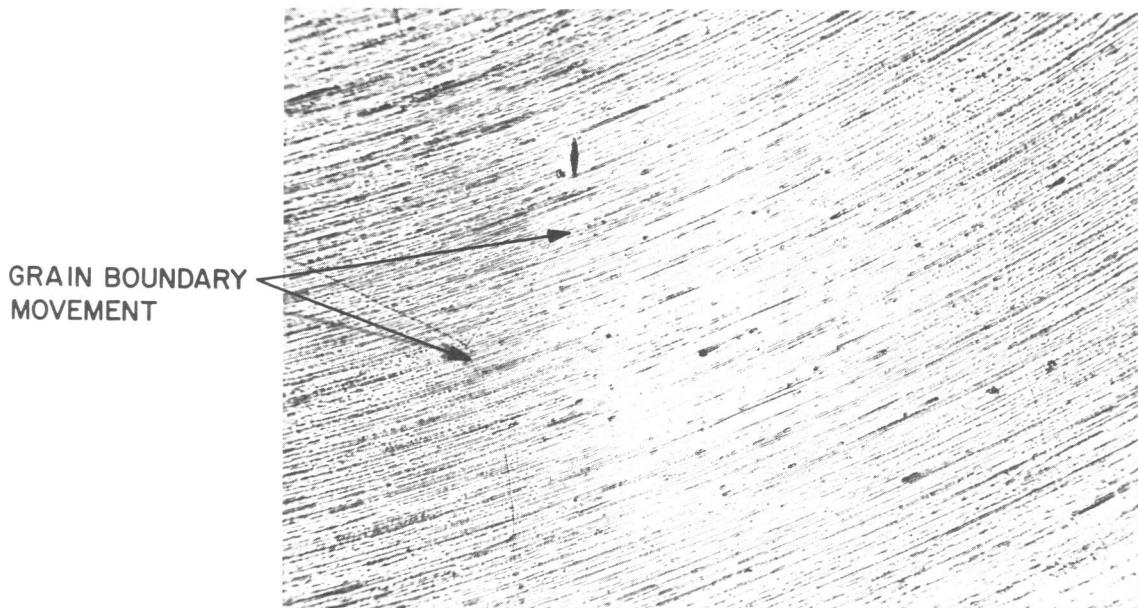


FIG. 2-2b SAME EMITTER AFTER OPERATION AT 1735°C  
FOR 100 HOURS IN A VAC-ION PUMPED EN-  
VIRONMENT OF  $5 \times 10^{-8}$  TORR (X50)

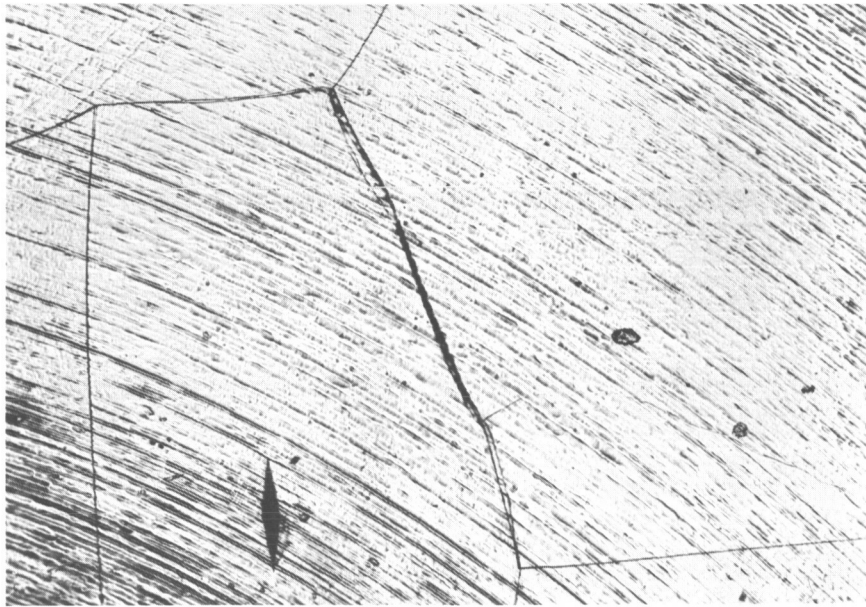


FIG. 2-3a TANTALUM EMITTER VACUUM-FIRED AT  $2450^{\circ}\text{C}$   
FOR 2 HOURS IN A VAC-ION PUMPED ENVIRON-  
MENT OF  $6 \times 10^{-7}$  TORR (X50)

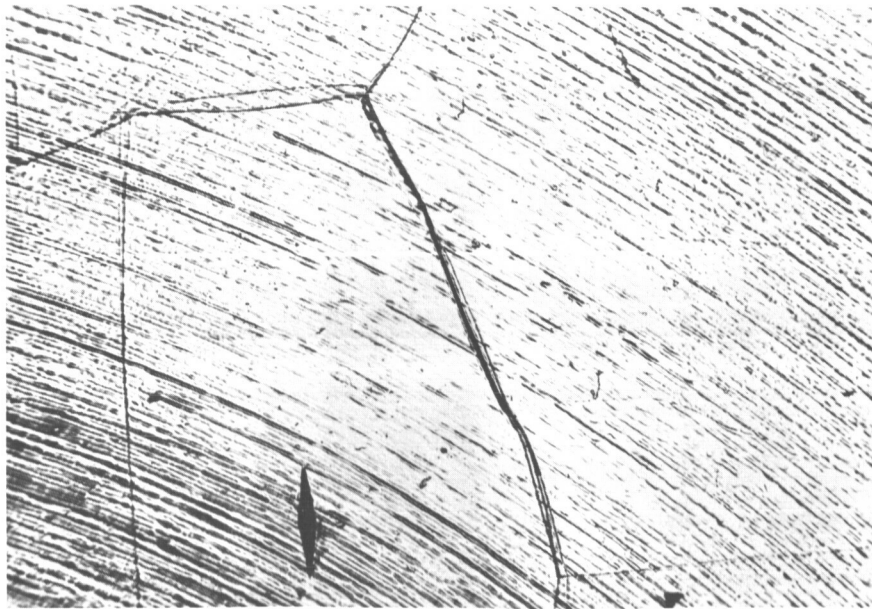


FIG. 2-3b SAME EMITTER AFTER OPERATION AT  $1735^{\circ}\text{C}$   
FOR 100 HOURS IN A VAC-ION PUMPED EN-  
VIRONMENT OF  $5 \times 10^{-8}$  TORR (X50)

## 2.1.2 Rhenium Emitter Schedule

### 2.1.2.1 Surface Finish and Chemical Cleaning

Three plate-stock rhenium disks of 0.800-inch diameter and 0.200-inch thickness were ground to achieve flatness and perpendicularity to 0.0001-inch tolerances. Measured tolerances on an electronic micrometer were less than 10 millionths of an inch, the limit of the measuring instrument. The grinding operation, performed with fine-grit diamond wheels, was followed by diamond-dust lapping and polishing to achieve final surface smoothness. Profilometer readings indicated a surface smoothness of less than 10 microinches.

Grinding and polishing are acceptable techniques for working rhenium, since the material is not amenable to standard machining practices of facing and turning. Rhenium work-hardens so easily that neither fully treated tool steel nor cemented tungsten carbide is capable of taking accurate cuts of the material. In addition, rhenium does not pick up polishing or lapping compounds as does tantalum; hence, it remains free of imbedded contaminants. Pyrometer sight holes having 10:1 depth-to-diameter ratios were electric-discharge machined in ethyl alcohol.

The samples were chemically cleaned in accordance with the procedure for cleaning tantalum as described in Appendix A with the exception that the hot chromic acid dip was limited to 4 seconds duration.

### 2.1.2.2 Vacuum Outgassing Schedule for Rhenium

The rhenium emitter samples, which were prepared as described in the previous paragraphs, were mounted in refractory metal firing stands for electron bombardment heating in a vacuum pumped environment. The firing stands are fitted with high-purity, vacuum-fired rhenium legs which support the samples.

An outgassing schedule of 2450°C for 24 hours was selected for the first sample. The second sample was outgassed at

2450°C for 10 hours and the third sample, at 2450°C for 3 hours. All temperature measurements were made by viewing the 10:1 hohlraum with a calibrated micro-optical pyrometer. The sample surfaces were subsequently examined on a Zeiss metallograph. Selected grains were marked by a microhardness tester and photographed without metallographic preparation, as in the case of tantalum. The samples were returned for 100-hour operation at 1735°C and reexamined on the metallograph.

#### 2.1.2.3 Surface Stability Examination of Rhenium

The reexamined surfaces, shown in Figs. 2-4b and 2-5b, indicate no surface structure changes with the possible exception of some thermal etching at grain boundaries. There appears to be no significant movement of grain boundaries as a result of the 100-hour operation. The fiducial marks which stressed the surface in the immediate neighborhood of the marks show expected signs of stress relief. Note their different appearance in the "before" and "after" photographs. The last rhenium sample, fired at 2450°C for 3 hours, also displayed no grain boundary movement after the 100-hour operation at 1735°C and consequently is recommended as the rhenium emitter outgassing schedule.

#### 2.2 Variable Parameter Test Vehicle

A variable parameter test vehicle was designed for the wide range of operation necessary to characterize electrode material performance for application to thermionic energy conversion. Specifically, the test vehicle was designed to meet the following work statement design criteria:

1. Interelectrode spacing to vary from 0.0005 to 0.010 inch separation.
2. Emitter to operate over the temperature range from 1300°K to 2100°K; collector to operate from 700°K to 1300°K; cesium reservoir to operate from 400°K to 750°K.

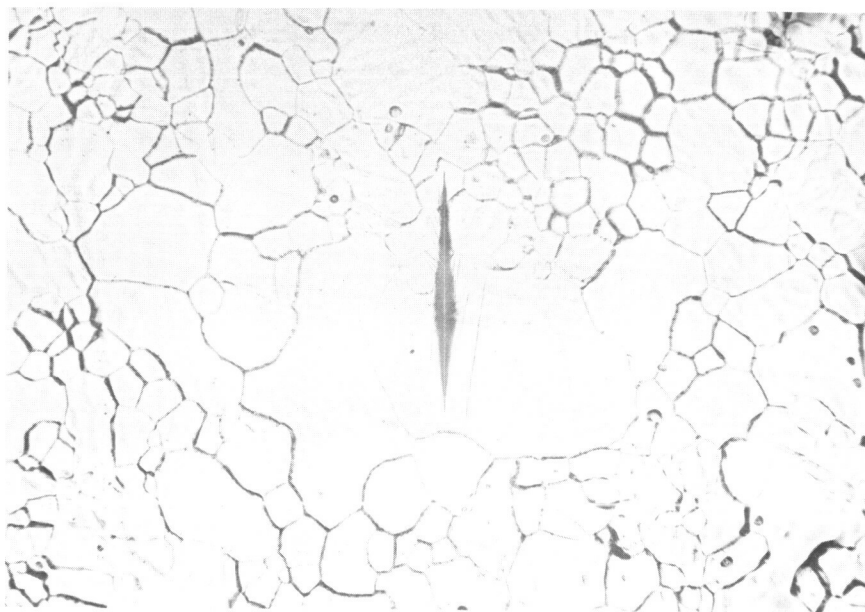


FIG. 2-4a RHENIUM PROCESS SAMPLE VACUUM-FIRED AT  
2450°C FOR 24 HOURS IN A VAC-ION PUMPED  
ATMOSPHERE OF  $3 \times 10^{-7}$  TORR (X200)

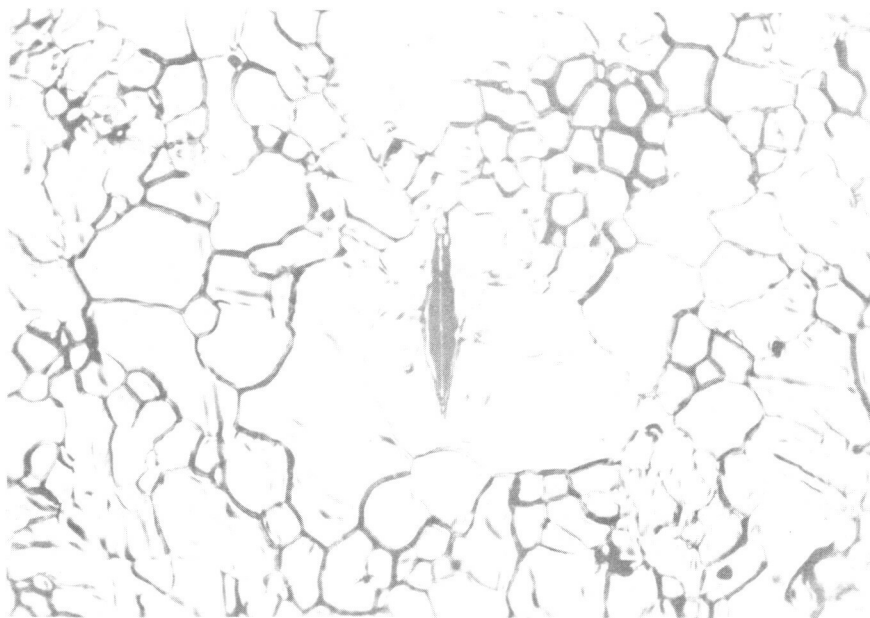


FIG. 2-4b SAME SAMPLE AFTER 100-HOUR OPERATION AT  
1735°C IN A VAC-ION PUMPED ATMOSPHERE OF  
 $4 \times 10^{-8}$  TORR (X200)

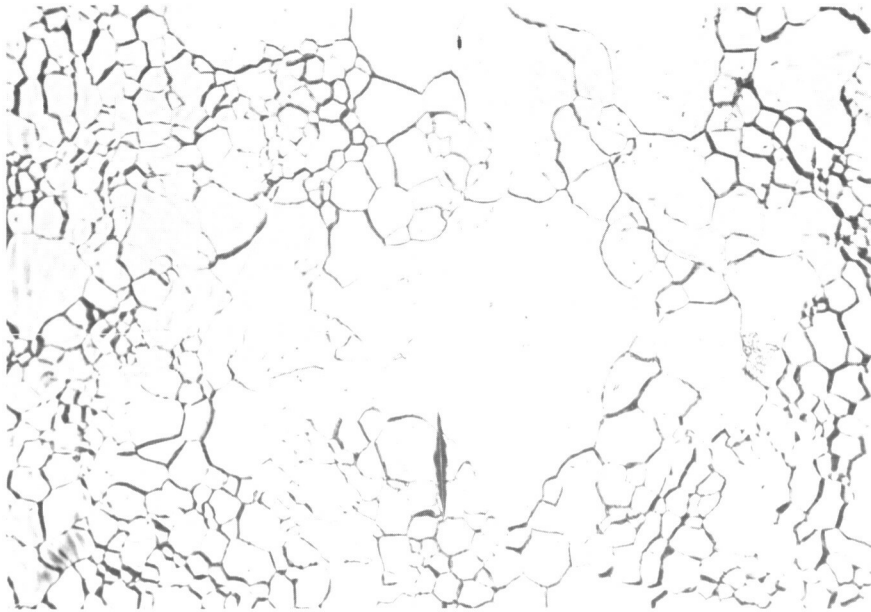


FIG. 2-5a RHENIUM PROCESS SAMPLE VACUUM-FIRED AT  
2450°C FOR 10 HOURS IN A VAC-ION PUMPED  
ATMOSPHERE OF  $3 \times 10^{-7}$  TORR (X200)

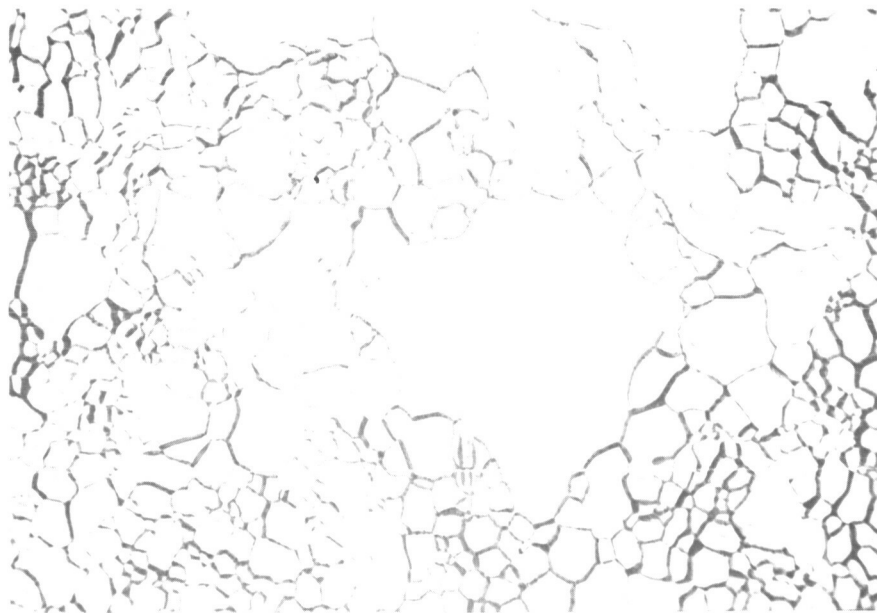


FIG. 2-5b SAME SAMPLE AFTER 100-HOUR OPERATION AT  
1735°C IN A VAC-ION PUMPED ATMOSPHERE OF  
 $4 \times 10^{-8}$  TORR (X200)

3. A guard ring assembly which follows the potential and temperature profile of the collector.
4. Steady-state operation with output current densities of 200 amperes/cm<sup>2</sup>.

The test vehicle was also designed to be capable of obtaining both cesiated and vacuum electron emission measurements from the emitter and cesiated electron emission from the collector for minimum work function determination. In addition, the design permitted power output measurements, as a function of interelectrode spacing and element temperatures which could be compared directly to converter results.

In retrospect, the variable parameter test vehicle exceeded all its design objectives and demonstrated that: (1) it is a superb research instrument capable of sufficient precision and control for fundamental thermionic measurements; and (2) it is a hardware-type device with a projected lifetime of 10,000 hours of reproducible performance obtained by direct measurement of power output and emitter temperature.

#### 2.2.1 Variable Parameter Test Vehicle Design

Before a detailed design and thermal analysis of a variable parameter test vehicle could begin, a basic decision concerning temperature measurement was required. A design which allowed the accurate determination of emitter (cathode) temperatures had to be selected. Due to the high-temperature instability of thermocouple measurements during long term operation (a result of material diffusion at the bimetal junction), a pyrometer method of measurement, utilizing a 10:1 blackbody hole was chosen. Since the largest contribution to measurement inaccuracy in this method is extraneous radiation, a device geometry was selected which allowed an unobstructed view of the blackbody hole by a micro-optical pyrometer. This geometry is identical to the plane-parallel converter wherein the blackbody hole is located in the circumference of the emitter and at right angles to the bombardment heater.

Based on these considerations, the design geometry utilizes a concentric guard ring and a collector barrel with exposed emitter. Figure 2-6 shows the geometry of the vehicle. An added benefit of this design is the elimination of a "parasitic" cesium reservoir which occurs when a location within the device approaches the reservoir temperature. By keeping the vehicle compact, with the bellows, seals, and guard ring concentric to the collector barrel, the device proper will operate at least  $150^{\circ}\text{C}$  higher than the reservoir.

The length of the collector barrel is determined by both heat transfer considerations and, mechanically, the fact that it must be coaxial with a guard ring of a particular length. The length of the guard ring is mainly set by the mechanical limitations which are introduced by the requirement that the guard ring-collector must move with respect to the emitter and emitter envelope.

#### 2.2.1.1 Variable Parameter Test Vehicle Thermal Analysis

A primary consideration in the thermal design of the emission vehicle was to provide equal temperature distributions (zero contact potential) along the guard ring and collector barrel and, at the same time, minimize the collector barrel length to reduce  $\Delta T$  in the collector barrel at high heat fluxes.

To determine whether the guard ring and collector have equal or nearly equal thermal gradients and hence zero contact potential difference since they are fabricated of the same material, consider the following derivation. The heat conducted down the collector barrel is

$$Q_{\text{coll}} = k_{\text{coll}} A_{\text{coll}} \left. \frac{dT}{dx} \right|_{\text{coll}} \quad (2-1)$$

where  $Q_{\text{coll}}$  is the heat flux conducted down the collector,  $k_{\text{coll}}$  is the thermal conductivity of the collector material,  $A_{\text{coll}}$  is the cross-sectional area of the conducting path, and  $\left. \frac{dT}{dx} \right|_{\text{coll}}$  is the thermal



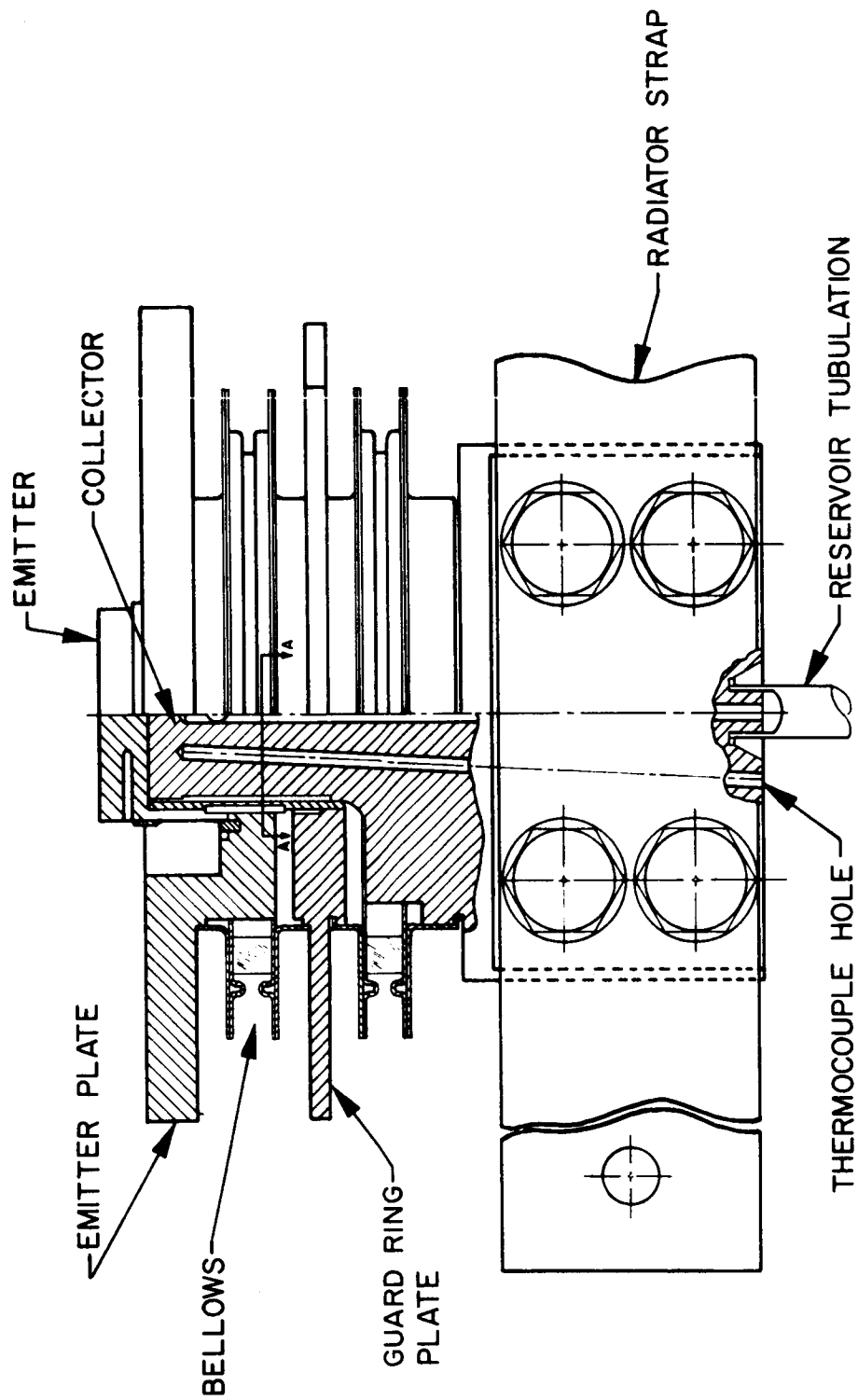


FIG. 2-6 VARIABLE PARAMETER TEST VEHICLE

gradient down its length. The heat conducted down the guard ring is given by

$$Q_{g.r.} = k_{g.r.} A_{g.r.} \left. \frac{dT}{dx} \right|_{g.r.} \quad (2-2)$$

where the quantities in Eq. 2-2 are the same as in Eq. 2-1 except that they apply to the guard ring structure. Now, the heat flux input to the collector barrel is

$$Q_{coll} = J \phi_{coll} A_{coll} \quad (2-3)$$

and the heat flux input to the guard ring is

$$Q_{g.r.} = J \phi_{g.r.} A_{g.r.} \quad (2-4)$$

where  $J$  is the electron current density emitted by the emitter (cathode),  $\phi_{coll}$  and  $\phi_{g.r.}$  are the effective thermal work functions of the collector and guard ring, and  $A_{coll}$  and  $A_{g.r.}$  are the collector areas for the collector and guard ring, respectively. The effective thermal work function for heat transfer purposes is dependent upon the apparent surface work function  $\phi_c$  (as determined from emission data), the plasma electron energy ( $E_{plasma} = 4kT_{plasma}/\pi e$ ), and the energy gained (or lost) at the accelerating (or retarding) sheath at the collector or guard ring surface. In the condition where the collector is matched to the plasma, there is no sheath at the anode surface and, for heat transfer purposes,

$$\phi_{eff_{th}} = \phi_c + \frac{\epsilon kT_p}{e} \pm V_s \quad 0$$

where  $1.3 \leq \epsilon \leq 1.5$  depending on the plasma electron energy distribution. Appendix B contains a detailed discussion of the origin and nature of the plasma potential term.

It is apparent from the foregoing discussion that a heat transfer analysis cannot be valid without consideration of plasma conditions within the interelectrode space. The effect of these plasma conditions on the thermal power input can be demonstrated by considering the case of a matched plasma at the collector (anode) (i.e., no collector sheath), a plasma electron temperature of  $6000^{\circ}\text{K}$  (a probable maximum condition), and an apparent minimum work function for cesiated molybdenum of 1.55 eV (Reference 1). In this case,  $V_p = 4kT_{\text{plasma}}/e = 0.66 \text{ eV}$ . This results in  $\phi_{\text{effth}} = 2.21 \text{ eV}$  (for heat transfer purposes), which is a correction of 40 percent to the thermal power input to the collector or guard ring over apparent work function considerations.

Returning to the derivation, since the guard ring and collector are of the same material, the conductivities and work functions are identical, if equal temperatures are assumed. In addition, due to the noncontoured geometry, the collecting area is the same as the cross-sectional area of the conducting path. Therefore, substitution of Eqs. 2-3 and 2-4 into Eqs. 2-1 and 2-2 yields

$$J \phi_{\text{coll}} = k_{\text{coll}} \left. \frac{dT}{dx} \right|_{\text{coll}} ; J \phi_{\text{g.r.}} = k_{\text{g.r.}} \left. \frac{dT}{dx} \right|_{\text{g.r.}} \quad (2-5)$$

and, since the collector and guard ring are identical,

$$k_{\text{coll}} \left. \frac{dT}{dx} \right|_{\text{coll}} = k_{\text{g.r.}} \left. \frac{dT}{dx} \right|_{\text{g.r.}} \quad (2-6)$$

$$\left. \frac{dT}{dx} \right|_{\text{coll}} = \left. \frac{dT}{dx} \right|_{\text{g.r.}}$$

Thus, the temperature gradients are identical down the guard ring and collector, resulting in equivalent temperature distribution. This produces equal cesiated work functions and thus a zero contact potential difference.

The method chosen for heat rejection from the collector is the mechanical attachment of a copper, water- or air-cooled heat sink. The heat sink consists of 1-inch copper straps, 1/8-inch thick, which are connected to copper bus bars by flexible copper straps. The bus bars have been fitted with copper tubing which can be used for air or water cooling to accomplish a variable thermal conduction. An experiment was conducted to determine the heat transfer characteristics of such a mechanically clamped collector-radiator combination. Figure 2-7 shows the experimental arrangement and the position of thermocouples. Table 2-III summarizes the results of a heat transfer experiment on this combination.

TABLE 2-III

BOLTED COLLECTOR RADIATOR HEAT TRANSFER EXPERIMENT  
FOR VARIABLE PARAMETER EMISSION TEST VEHICLE

Constant Electrical Power Input to Gun: approx. 350 watts  
Collector Surface Temperature: approx. 900°C

Collector Base Temperature (°C)	Power Conducted Out Lead Strap (watts)	Type of Auxiliary Cooling
617	158.3	Flexible leads
608	239.2	Flexible leads with air cooling, 20 psi air pressure
603	245.6	Flexible leads with H <sub>2</sub> O cooling, flow rate of 1 liter/min
593	265.3	Flexible leads with H <sub>2</sub> O cooling, flow rate of 2 liters/min

The difference between power conducted out lead straps and electrical power input to gun is the power radiated by the gun and the collector. As can be seen from Table 2-III, over 100 watts of additional power can be conducted out the collector radiator

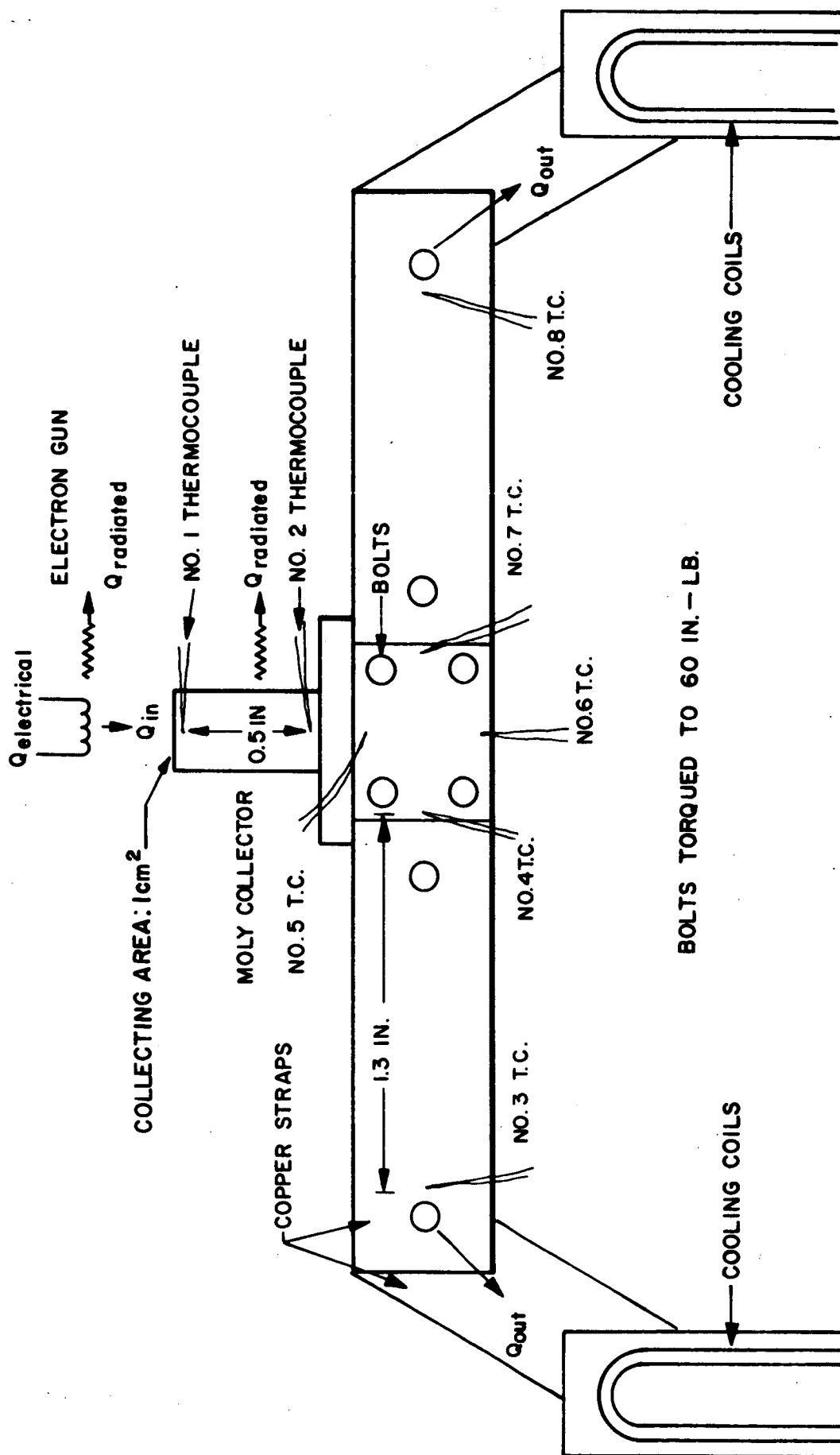


FIG. 2-7 SETUP FOR COLLECTOR HEAT TRANSFER EXPERIMENT

straps by varying the means of cooling. This results in a 25°C variation of the collector root temperature, which is the more significant result. In addition to controlling the collector root temperature by cooling, heaters have been added to the radiator straps for maintaining the collector temperature at desirable levels at low currents. To determine the collector root temperature as a function of heater power, consider the idealized system shown in Fig. 2-8. In the illustration,  $Q$  is the thermal power into the collector,  $(1/2)Q$  is the thermal power out each radiator strap assuming no radiation losses,  $q$  is the heater power into each radiator strap,  $T_T$  is the collector top temperature,  $T_r$  is the collector root temperature, and  $T_s$  is the collector radiator strap temperature. Now,

$$Q = \frac{k_1 A_1 (T_T - T_r)}{L} \quad (2-7)$$

and

$$(1/2)Q - q = \frac{k_2 A_2 (T_r - T_s)}{l}, \quad (2-8)$$

where  $k_1$ ,  $k_2$ ,  $A_1$ , and  $A_2$  are the conductivities and cross-sectional areas of the collector and radiator strap, respectively. Combining Eqs. 2-7 and 2-8 and solving the  $T_r$  yields:

$$T_r = \frac{\left(\frac{k_1 A_1}{L}\right) T_T + \left(\frac{2k_2 A_2}{l}\right) T_s - 2q}{\frac{k_1 A_1}{L} + \frac{2k_2 A_2}{l}} \quad (2-9)$$

Equation 2-9 is used to determine the heater power necessary to control the collector temperatures. If a collector surface temperature of 700°C is desired, the required heater power can be calculated. In addition to  $T_T = 700^\circ\text{C}$ , it will be assumed that  $T_r = 500^\circ\text{C}$  and  $T_s = 450^\circ\text{C}$ . Thus, Eq. 2-9 yields  $q = 70$  watts for the geometry of the designed collector radiator.

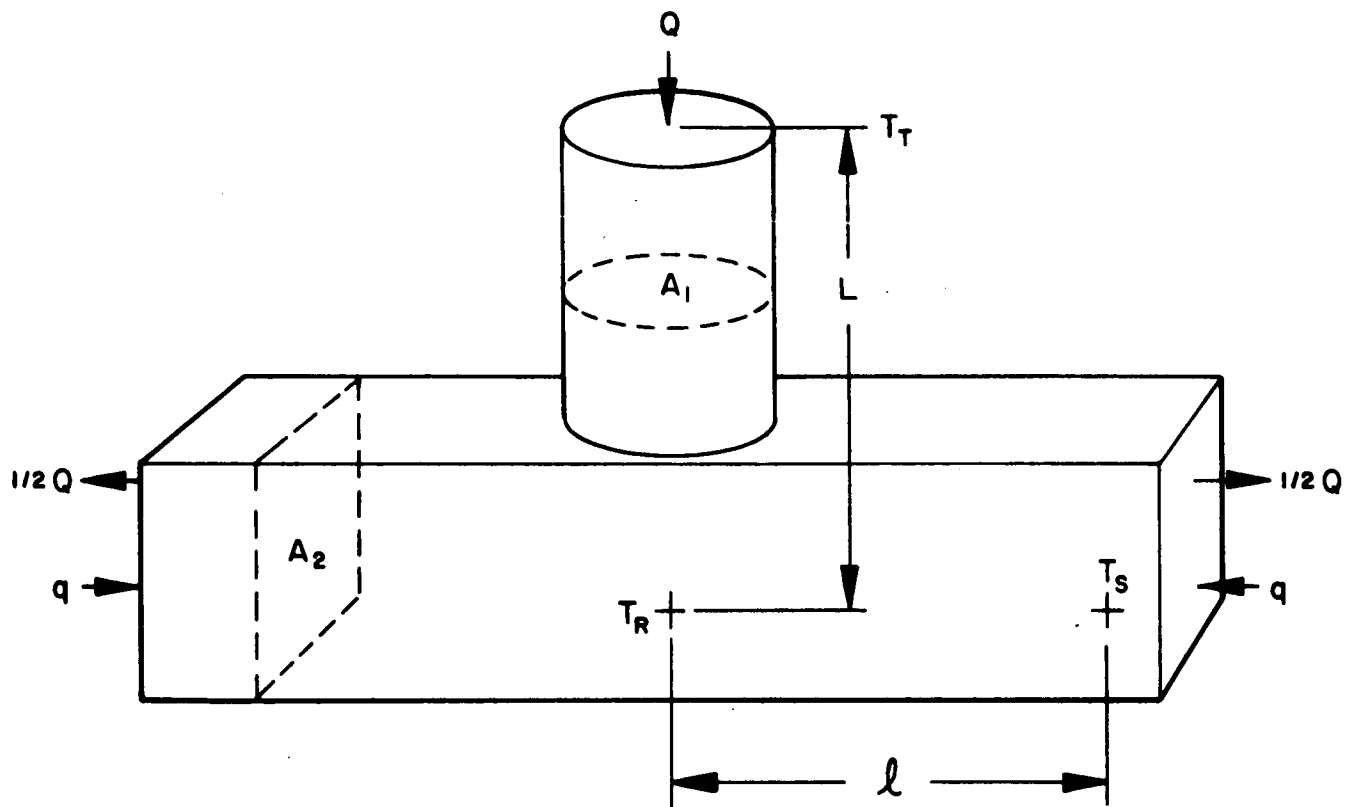


FIG. 2-8 IDEALIZED COLLECTOR-RADIATOR SYSTEM

Figure 2-9 shows the variation of collector surface temperature with collector current density. The curve was calculated assuming a constant collector root temperature of 450°C. The significance of Fig. 2-9 lies in the result that steady-state optimized power measurements will be limited to currents less than 125 amperes/cm<sup>2</sup>. This is due to EOS' experience that minimum collector work functions cannot be achieved for collector temperatures in excess of 900°C. This result does not place a limitation on emission measurements at much higher current densities than 125 amperes/cm<sup>2</sup>. When optimized power output is of no interest, the allowable collector surface temperature is limited only by structural considerations; therefore, currents of 200 amperes/cm<sup>2</sup> can be easily measured.

The last item to receive thermal design analysis was the emitter support structure which is normally referred to as an envelope. This envelope is coaxial with the guard ring and collector and provides the electrical connection between the emitter and emitter lead straps. The envelope is a critical member of the vehicle and accomplishes three important tasks: (1) It must act as an effective heat choke, thermally isolating an emitter which may operate at temperatures in excess of 1800°C from structural members of the device, such as seals, which should not exceed temperatures of 800°C to 900°C; (2) it must carry currents in excess of 400 amperes without a large voltage drop over the length of the envelope; and (3) it must maintain ultra-high vacuum and mechanical integrity.

The "optimum" heat choke design requires balancing of the electrical losses with the thermal losses. From the following equation, a practical L/A ratio must be obtained that minimizes  $\alpha$ , the ratio of electrical loss to thermal loss.

$$\alpha = \frac{I^2 \rho \frac{L}{A}}{K \Delta T \left( \frac{A}{L} \right) - \frac{1}{2} I^2 \rho \left( \frac{L}{A} \right)}, \quad (2-10)$$



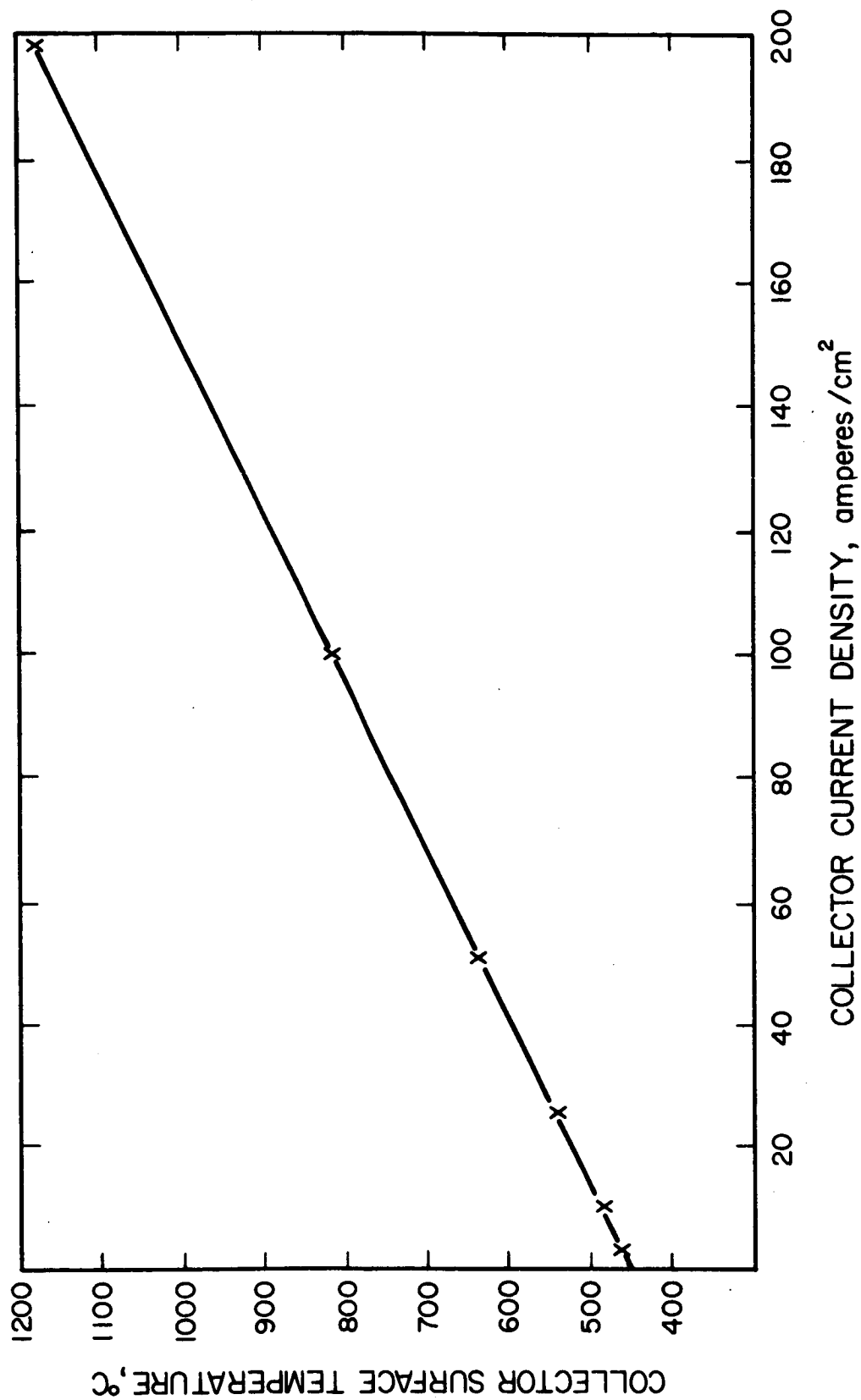


FIG. 2-9 COLLECTOR SURFACE TEMPERATURE AS A FUNCTION OF COLLECTOR CURRENT DENSITY (CALCULATED)

where  $I$  is the total current (in amperes) passing through the heat choke,  $\rho$  is the resistivity of the material,  $L$  is the length of the heat choke,  $A$  is the cross-sectional area of the heat choke wall,  $K$  is the thermal conductivity of the material, and  $\Delta T$  is the temperature drop across the heat choke. The terms in the denominator of Eq. 2-10 are the thermal losses in the envelope. This consists of heat conduction (the first term) and half the joule heating (the second term) due to the possibility of joule losses flowing out either end of the envelope.

Heat choke envelopes of two different materials were designed: one of rhenium for rhenium emitters, and one of tantalum for tantalum emitters. The reason for selecting identical envelope and emitter materials is discussed in Section 4. The design procedure is to determine practical values of  $L$  and  $A$  and evaluate  $\Delta T$  from Eq. 2-10 as a function of the parameter  $\alpha$ . Table 2-IV summarizes the results based on this approach. Heat conduction,  $K$ , is evaluated for an average temperature of  $1000^{\circ}\text{C}$ .

TABLE 2-IV  
HEAT CHOKE ENVELOPE DESIGN PARAMETERS

	Rhenium	Tantalum
$L$	0.200 inch	0.150 inch
$t$	0.005 inch (wall)	0.003 inch (wall)
$I$	250 amperes	250 amperes
$\rho$	$80 \times 10^{-6} \Omega\text{-cm}$	$60 \times 10^{-6} \Omega\text{-cm}$
$K$	$0.48 \text{ watt/cm-}^{\circ}\text{C}$	$0.67 \text{ watt/cm-}^{\circ}\text{C}$
$\Delta T$	$1165^{\circ}\text{C}$	$1005^{\circ}\text{C}$
$\alpha$	0.48	0.48

From the values shown in the table, the thermal power conducted down the rhenium heat choke is 86 watts, the joule heating power generated in the heat choke is 33 watts, and the power radiated by the envelope is 9 watts. Therefore, the total power lost by the emitter down the rhenium envelope is 62 watts for an emitter temperature of  $1700^{\circ}\text{C}$  and an emitter current of 250 amperes. For tantalum, the thermal power conducted down the heat choke is 80 watts, the joule heating power generated in the envelope is 31 watts, and the radiated power is 11 watts. Then the total power drained from the emitter by a tantalum heat choke envelope is 60 watts for an emitter temperature of  $1700^{\circ}\text{C}$  and an emitter current of 250 amperes.

#### 2.2.1.2 Interelectrode Potential Distribution and Analysis

Utilizing a teledeltos analog field plotter, the interelectrode electrostatic potential distribution was obtained for an equivalent interelectrode spacing of 5 mils for three cases: (1) the guard ring at the same potential as the collector; (2) the guard ring at a potential intermediate between those of the collector and emitter; and (3) the collector at a potential between those of the guard ring and emitter. For the first case, the penetration potential in the collector-guard ring gap is reduced to 1 percent of the collector-emitter potential in one gap width. This situation is shown in Fig. 2-10. In addition, the shifts in the potential distribution as the guard ring potential varies are evident.

There are two major conclusions to be drawn from these distributions: (1) the potential distribution in the interelectrode area between emitter and collector is insensitive to guard ring potential; and (2) the maximum error in the emission area determination is less than 2 percent. These conclusions result from observing that with deviations of the guard ring potential as large as  $\pm 10$  percent, the potential distribution perturbations within the interelectrode space due to guard ring potential variations are completely

# EMITTER STRUCTURE

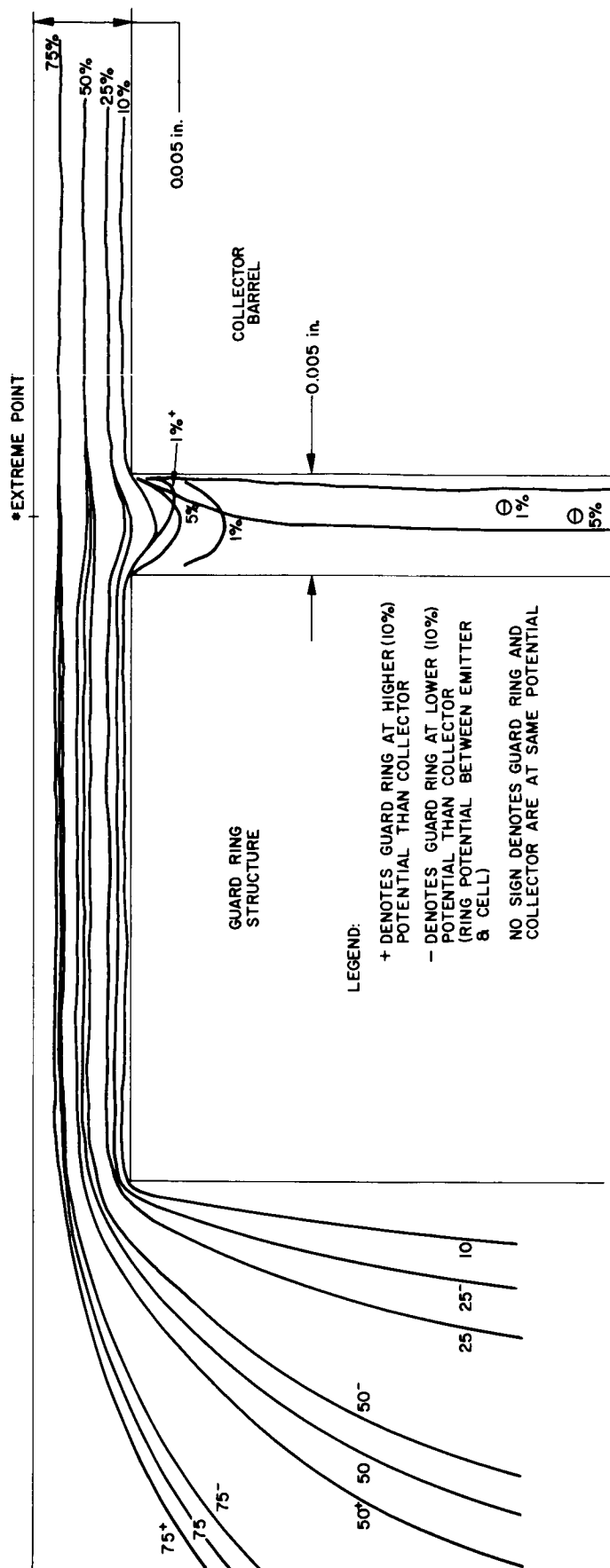


FIG. 2-10 INTERELECTRODE POTENTIAL DISTRIBUTIONS

suppressed in a distance only 0.002 inch from the edge of the collector surface. The estimate of emission area error is based on the symmetry of the potential lines. The line of electrostatic potential symmetry bisects the guard ring-collector gap. The drift electrons in the interelectrode spacing have thermal energies of only approximately 0.5 volts. If the energies of the drift electrons are comparable to or less than the potential drop of the spacing, the electron trajectories are essentially perpendicular to the potential lines. If the electron energies are much greater than the total potential drop in the gap, they are free to travel at large angles to the potential lines. In the case of a thermionic converter, approximately the total potential drop is across the sheath at the cathode, since the interelectrode spacing is predominantly a very weak field region. In this case, though, the drift electrons enter the emitter sheath from the emitter (cathode) with energies of only  $2kT$  and, with the very steep potential gradient in the sheath, they are easily forced into a trajectory of normal incidence. Therefore, it seems apparent that the farthest point from the collector (anode) from which electrons can originate and be collected by the collector is the point on the emitter opposite the midpoint of the collector-guard ring spacing. This point has been marked in Fig. 2-10. Using this point for measuring the emitting area results in a maximum effective emitter area of  $2.04 \text{ cm}^2$ , an error of 2 percent in the desired emitter area of  $2.00 \text{ cm}^2$ .

These potential plots were made for the vacuum case. In a plasma-filled environment with a cathode sheath, the sheath acts as a virtual cathode and the potential distribution in the plasma column is still represented by the indicated teledeltos plots.

A final comment concerning the potential distribution in the interelectrode spacing is that the lines of electric field between the emitter and collector/guard ring will be normal

to these surfaces if their current densities or lines of flux per square centimeter are equal. A dc driving source is normally applied to the guard ring to maintain an equal current density with the collector for varying load conditions, and therefore the E-field is normal to all the electrode surfaces.

#### 2.2.2 Variable Parameter Test Vehicle Fabrication and Assembly Procedure

The variable parameter vehicle utilizes a prefabricated approach wherein as many subassemblies as possible are preassembled before being joined into the test vehicle final configuration. Figure 2-11 is a layout of the components and subassemblies of the test vehicle. The key to the fabrication of the test vehicle was the development of a single-convolution, refractory-metal bellows formed by the welding of niobium flanges to prefabricated niobium-alumina seal subassemblies. The advantage of this method is the use of a high-purity, high-temperature bellows assembly which does not compromise the design objectives with ferrous alloys exposed to a device interior of high pressure cesium vapor. A bellows subassembly was fabricated and measured to have an excursion greater than 0.040 inch without failure, more than sufficient to satisfy the work statement design goals. The same assembly was then cycled 3500 times at a 0.025 inch displacement, leak-checked, found leak-tight, and cycled to destruction, which occurred at 8000 cycles. Since this testing was performed at room temperature, the bellows assembly did not receive the benefit of stress-relief which it would when operating in the vehicle at temperatures near 600°C. Equally important to the bellows development was the EOS high-temperature, high-strength, ceramic-metal seal which was prefabricated from high-purity niobium (99.9%) and unmetallized high-purity ceramics (AL 995 WESGO) per the EOS active sealing process discussed in Section 3. The critical juncture in the test vehicle fabrication is the heli-arc welding of these seal subassemblies to mating parts of the emitter and collector subassemblies.

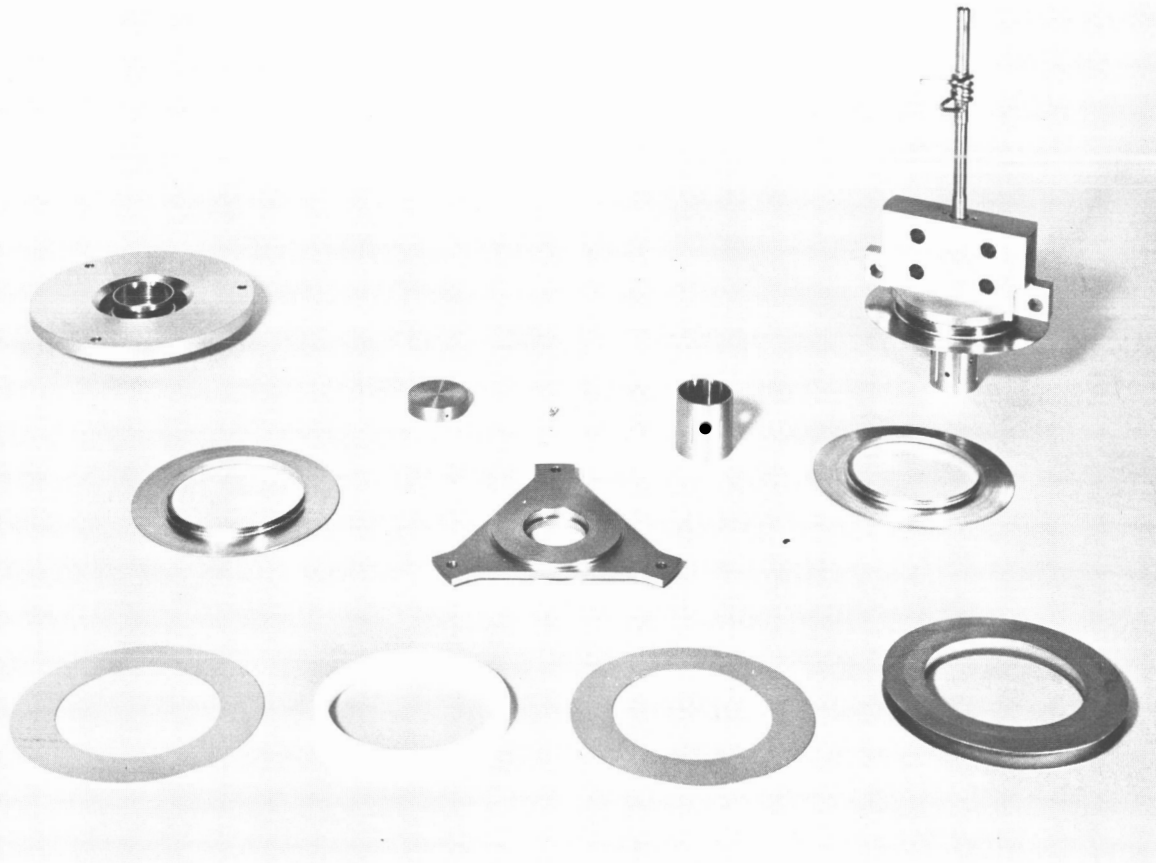


FIG. 2-11 VPTV COMPONENTS AND SUBASSEMBLIES PRIOR TO FINAL JOINING

However, heli-arc welded joints are inherently more reliable to make on one-of-a-kind devices, than seal brazing a three-electrode system, particularly if sealing is the final assembly step.

A rhenium emitter/rhenium collector electrode system was selected as the first set of materials for investigation in the test vehicle. The choice of a rhenium emitter automatically selected rhenium as the envelope material. This point is discussed in more detail in Section 3, but briefly the argument for a rhenium emitter/rhenium envelope is as follows: First, since the envelope and emitter are pierce-welded on an electron beam welder, both parts are brought to the melting point in a localized area. Rhenium forms brittle inter-metallic compounds and alloys with almost every common high-temperature material candidate, especially at the melting point. The easiest solution is to also make the envelope out of rhenium. Second, even if the material or materials were found to circumvent this problem, the high temperature ( $2000^{\circ}\text{K}$ ) and long-time requirements for reliable operation most surely lead to diffusion of such dissimilar materials. For example, it has been EOS's experience that the tantalum-rhenium system leads to surface contamination and work function changes within 200 hours at temperatures near  $2000^{\circ}\text{K}$ .

The test vehicle is comprised of four major subassemblies: the emitter plate subassembly, the guard ring subassembly, the collector subassembly, and the ceramic-metal seal subassemblies.

The emitter plate subassembly, which consists of the molybdenum emitter plate and rhenium envelope, was titanium brazed at  $1700^{\circ}\text{C}$ , although backup assemblies were brazed with vanadium at  $1900^{\circ}\text{C}$ . Both brazes were structurally sound and leak-tight; however, the vanadium braze is probably more reliable since there are no phase transitions to contend with as there are in titanium.

The guard ring subassembly fabrication procedure consisted of brazing the molybdenum guard ring barrel to the molybdenum guard ring support plate and joining two niobium bellows flanges



to the top and bottom of the plate. All of these joints were brazed simultaneously using a titanium braze.

The collector subassembly is comprised of a 0.040-inch rhenium shim brazed to the surface of the molybdenum collector, a niobium collector flange, and the cesium reservoir tubulation made from tantalum. The rhenium shim was vanadium-brazed to the molybdenum collector. After the braze, the collector and shim were machined to the finish dimensions. The niobium flange and tantalum reservoir were then titanium-brazed to the collector. After the titanium braze, the rhenium collector surface was surface-ground to remove any condensed brazing material. Finally, sheathed thermocouples were inserted into the collector barrel with thin (0.001 inch) copper foil wrapped around the end of the thermocouple. The collector was raised to a temperature of 1100°C to effect a copper braze. The collector surface was lapped, cleaned, and vacuum-fired at 800°C for 20 hours to remove any trace impurities.

Upon completion of these subassemblies and the seals, the final assembly proceeded wherein all items are re-leak-checked on a  $5 \times 10^{-10}$  cc-atm/sec sensitive mass spectrometer leak detector and stacked for final joining at the periphery of the flanges and seals. During stacking, three specially machined screws are used primarily to position the guard ring with respect to the collector, hence insuring a concentrically preset spacing of 0.005 inch. The location of the screws is shown in Section A-A of Fig. 2-12. The secondary purpose of the screws is to mechanically fasten the guard ring and collector at a common reference plane so that thermal expansion of both members will be identical during operation of the vehicle. Electrical isolation is provided by ceramic sleeve inserts. During operation it was observed that external holding fixtures served equally well to contain the guard ring plate and hence, the guard ring itself. The second variable parameter test vehicle, discussed in succeeding paragraphs, employed internal tie-down by way of screw attachment in a different location,

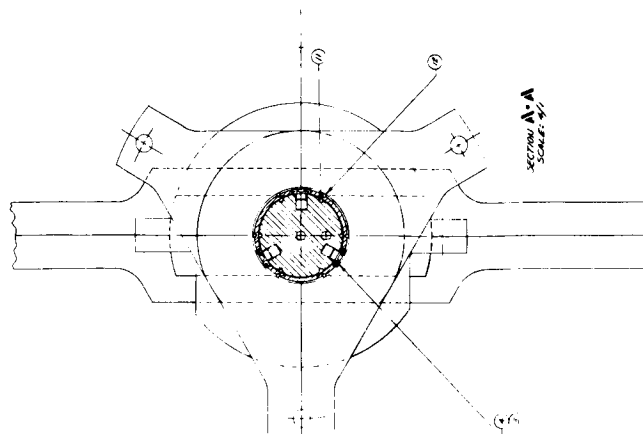
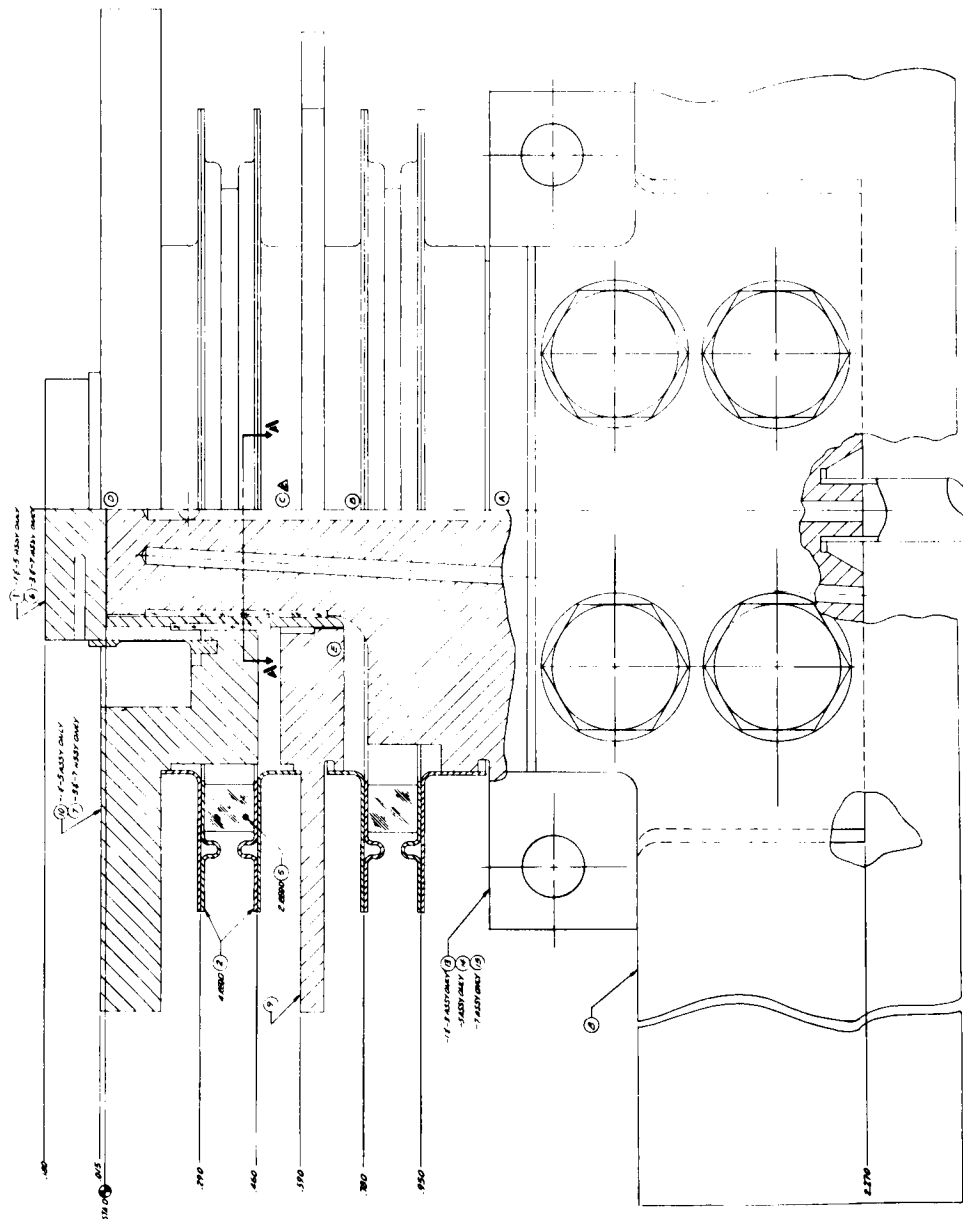


FIG. 2-12 TEST VEHICLE LAYOUT

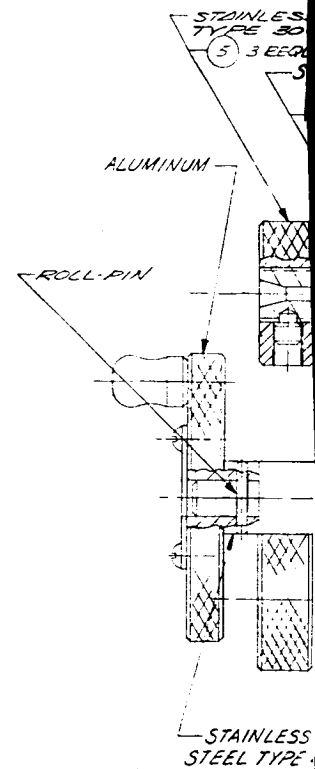
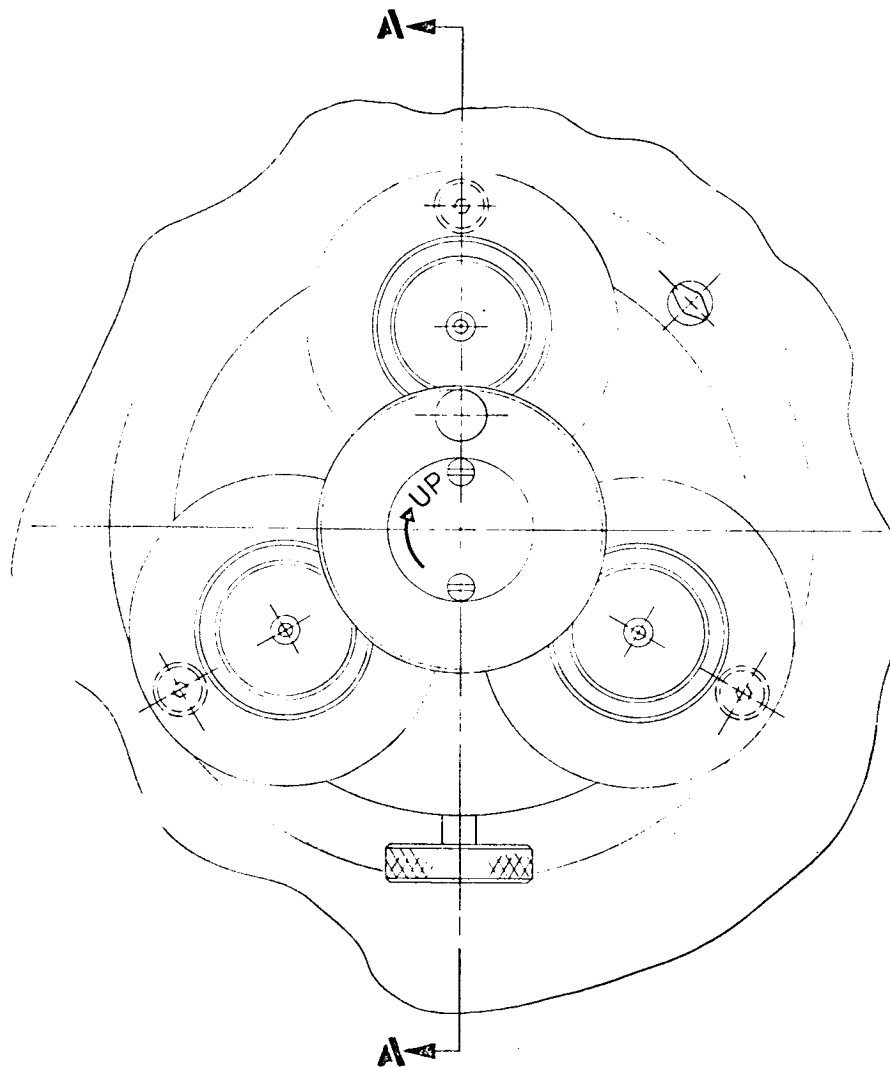
namely, the guard ring plate to the collector root which would be at right angles to section A-A. At any rate, throughout the operation of both test vehicles, the collector surface remained at least 0.0003 inch above the guard ring surface, a condition preset during final assembly to allow the interelectrode spacing to be measured only between emitter and collector.

After the bellow seals were welded, the structure was mounted in a jig which expands the bellows by 0.005 to 0.008 inch, and the rhenium emitter, which was preprocessed in accordance with the schedule developed in Subsection 2.1, is inserted into the rhenium envelope and electron beam welded into place. The weld is a pierce-type joint requiring no burn-off lips or other projections for effecting the weldment. The emitter is purposely allowed to be in contact with the collector surface (with bellows expanded) to achieve a controlled shorting at the emitter-collector operating temperatures. If the bellows were not preexpanded, it would be necessary to effect the bellows action in the ceramic-metal seal alone to achieve the condition of a controlled short, since there is always an inherent thermal expansion in the envelope of 0.003 to 0.005 inch.

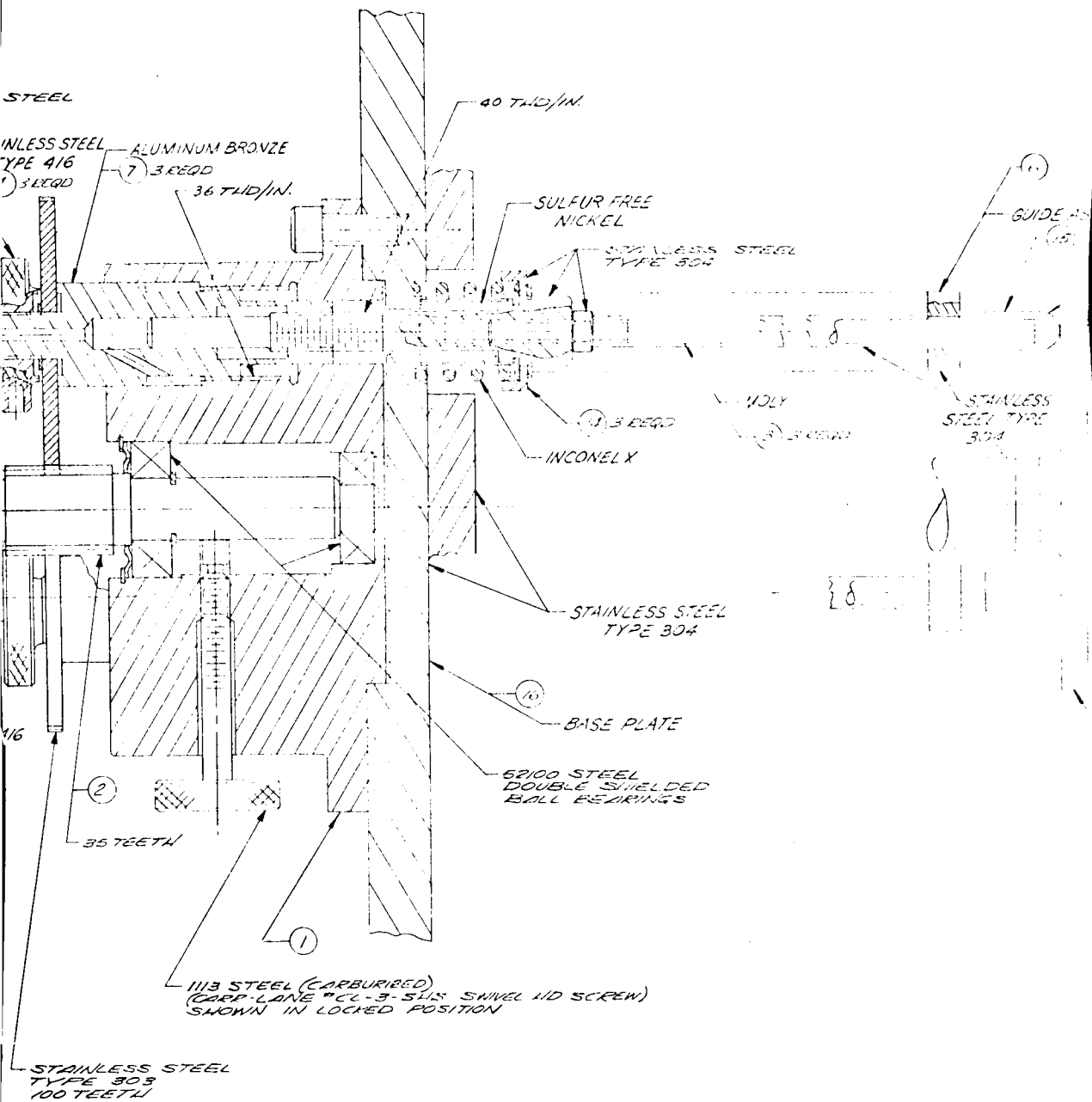
The final process procedure for the test vehicle is terminal exhaust on a vac-ion pump accompanied by a 12 to 14 hour bake-out at 600°C seal temperature, 900°C collector temperature, and 1700°C-1800°C emitter temperature. The vehicle is then pinched off and loaded with cesium. Over 20 sets of thermocouples are attached to the vehicle for precision temperature measurement, and the vehicle is then mounted for test.

#### 2.2.3 Variable Parameter Test Vehicle Drive Mechanism

The interelectrode spacing of the variable parameter test vehicle is varied by applying force to three spring-loaded rods which are inserted from the bell jar top plate. These rods apply pressure to the emitter plate seen in Fig. 2-13. The individual rods are controlled by a differential thread drive to allow independent movement of each rod. One complete rotation of the control nut on the



38-1



SECTION A-A

FIG. 2-13 VARIABLE PARAMETER TEST VEHICLE



### DRIVE MECHANISM:

individual rods results in a vertical displacement of 0.002 inch. The three rods can be ganged for uniform motion controlled by a single drive. One complete rotation of the main control knob results in a uniform displacement of 0.0008 inch by the ganged rods. The return movement is obtained by spring-loaded ceramic rods mounted beneath the emitter plate. These rods maintain a continuous upward force on the bellows section of the vehicle. The spacing measurement device is also mounted beneath the emitter plate. The measuring device is supported from a second ceramic rod while measuring the movement of the ceramic return rod. This temperature compensating method allows the measuring device to indicate only true mechanical movement of the emitter with respect to the collector, and not the thermal expansion in the support and return rods. The measuring device is a 0.0001-inch dial-gage depth indicator which may be read to within 0.00005 inch.

In practice, the 0.0001-inch indicators must be replaced after 400 to 600 hours of operation, since their internal moving parts will not permit smooth tracking for longer periods. It should be pointed out that the gages will still register accurate displacements, but the needle movement of the individual indicators track discontinuously, creating more nuisance than error.

Inconel X was selected for the spring material used throughout the drive mechanism, and has performed satisfactorily at nominal temperatures of 150 to 200°C for over 1100 hours of continuous loading. The other structural materials of the drive mechanism are Type 304 stainless steel and sulfur-free nickel. The alumina rods were selected to provide electrical isolation between the drive mechanism and test vehicle; in addition, they conducted only minimal heat away from the emitter plate.

#### 2.2.4 Variable Parameter Test Vehicle Mounting Fixture

Figure 2-14 illustrates the support or mounting fixture used to secure the test vehicle for operation. The basic structure consists of three parallel stainless steel rings separated by

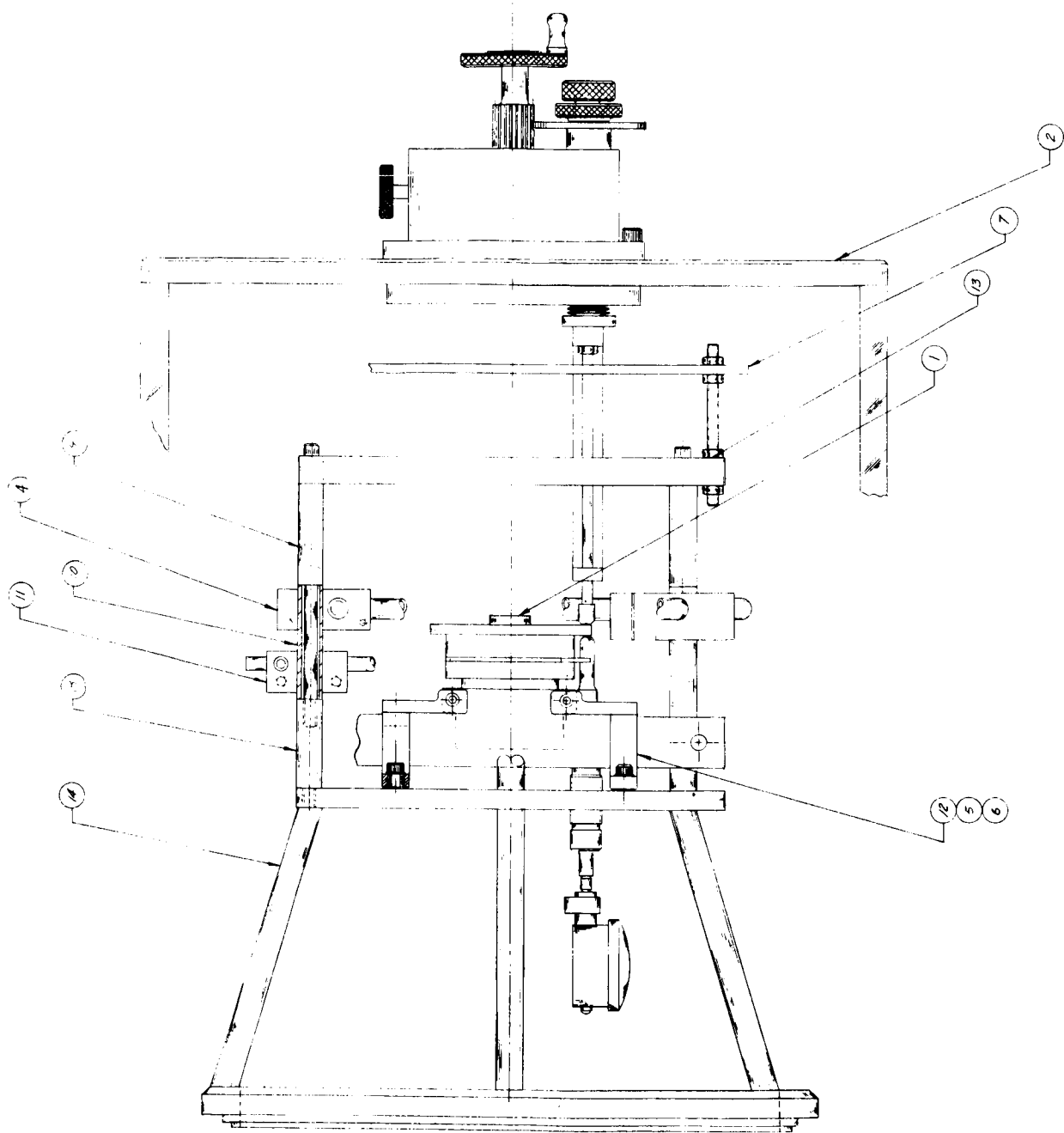


FIG. 2-14 VARIABLE PARAMETER TEST VEHICLE MOUNTING FIXTURE



stainless steel rods. The bottom ring mates with the inside edge of the vacuum test station base plate. The middle ring, actually a disk, supports the return drive mechanism and the test vehicle support fixture. This disk is covered by 10 sheets of 0.002-inch-thick dimpled molybdenum heat shields to limit the temperature of the dial indicators as well as the disk itself, since the disk serves to support the test vehicle. Two molybdenum brackets are bolted to the collector root and terminate on insulated base straps, as shown in the figure. The bolts are made of Inconel-X and contain hand-polished shanks which mate to the insides of collector mounting holes. The bolts are torqued in place at a value of 95 ft-lb to insure even and firm attachment of the test vehicle.

The electron bombardment gun is composed of a well-shielded, counter-wound, pancake tungsten filament to provide uniform heating of the test vehicle emitter. As the interelectrode spacing is varied, the gun remains stationary; however, the variation amounted to 0.015 inch, at most, and the emitter temperature variation caused by this corresponding gun-to-emitter spacing change is controlled with a fine-adjust potentiometer on the bombardment voltage.

The electrical connections were made in the following manner: The collector-radiator straps are connected by flexible leads to copper bus bars equipped with cooling coils on either side of the device. The guard ring and emitter connections are made with closed copper tubes which serve both as water-cooling coils and current conductors. Since the emitter carries a much higher current load than the guard ring, the cross section of the emitter tubing wall is greater than that of the guard ring conductor in order to permit current densities of  $200 \text{ amperes/cm}^2$  without large IR losses. As indicated in Fig. 2-14, the two copper cooling rings are supported at the stainless steel supports and insulated by ceramic sleeving. Flexible copper straps provide electrical connection between the emitter and guard ring and their respective cooling rings at three symmetric positions.

It was observed during the course of secondary experimentation supporting the test vehicle design that symmetric attachment of current leads and cooling coils with torque wrench settings was essential to reliable heat transfer as well as mechanical support. For example, during the operation of the variable parameter test vehicle, an identical "zero" reference for the interelectrode spacing was maintained through hundreds of hours of operation; that is, for the same element temperatures, current load, etc., the individual dial indicators would register the same absolute position of emitter and collector at the condition of electrical short within less than 0.0001 inch.

#### 2.2.5 Rhenium-Rhenium Electrode Measurements and Interpretation

Over 1100 hours of reproducible electrical output was obtained from the rhenium-rhenium variable parameter test vehicle, a testament to the design philosophy and fabrication technology discussed in the preceding paragraphs. The reproducibility was within millivolts of dc voltage output and milliamperes of dc current as measured with 0.1% accurate meters and shunts.

The ranges of parametric operations covered during this period were:

$T_{\text{emitter}}$	973°K-2400°K
$T_{\text{cs reservoir}}$	400°K-700°K
$T_{\text{collector}}$	450°K-1300°K
Interelectrode spacing	0.0001-0.015 inch
$J_{\text{sat}}$	180 amperes/cm <sup>2</sup>

These values either approximated or exceeded the design objectives listed in Subsection 2.2.

The data offered in the following paragraphs is considered to be experimentally absolute wherein no attention to detail has been spared. For instance, all pyrometers were calibrated against

an NBS certified standard lamp before, during, and immediately after the test vehicle operation. The pyrometers were of the micro-optical type with bulb filaments approximately one-sixth the diameter of the blackbody holes sighted upon. The thermocouples consisted of continuous wire from the surface being measured through the vacuum station port and ending in a 0°C ice bath. Potential leads were attached at the device terminals with wire of the same material as the terminal to insure that no thermal emf was generated.

The principal purpose of the variable parameter test vehicle was to obtain thermionic converter optimization data, particularly as a function of spacing between the electrodes. In addition, and perhaps of equal importance, the test vehicle offers a measurement of basic plasma parameters such as the pressure-distance product. The paragraphs that follow contain the results of over 450 I-V characteristics and 1100 dc, steady-state data points yielding the most definitive characterization of thermionic performance known to date.

#### 2.2.5.1 Converter Optimization Data for the Rhenium-Rhenium Electrode System

The converter optimization consisted of optimizing the dc current output of the vehicle as a function of spacing, cesium temperature, and collector temperature, at a true emitter temperature of 1735°C at three voltage outputs of 0.8 volt, 0.7 volt, and 0.6 volt as measured at the test vehicle terminals. The experimental procedure consisted of employing an electronic load to maintain a constant voltage output and setting a fixed collector temperature, fixed spacing, and varying the reservoir temperature until an absolute maximum in output current had been obtained. The cesium reservoir temperature was varied between 310°C and 350°C. At each fixed collector temperature, the spacing was varied between 0.002 and 0.005 inch. This procedure was repeated for collector root temperatures of 570°C, 596°C, 610°C, and 660°C. Collector root temperatures are quoted since the upper collector surface immersion thermocouple opened during the

first few hours of vacuum outgassing. The precise matching collector surface temperature could be determined when the device is disassembled.

While exceptional performance is noted at very close spacings of less than 0.0003 inch, the following data are intended for practical, reproducible converters operating in the arc-mode. The optimum parameters for maximum power output (15.44 watts/cm<sup>2</sup>) at 0.8 volt are: collector root temperature 610°C, cesium reservoir temperature 331°C, and interelectrode spacing between 0.0032 and 0.0038 inch - nominally 0.0035. The 0.80-volt data are shown in Figs. 2-15 through 2-18. The optimum parameters for maximum power output (21.0 watts/cm<sup>2</sup>) at 0.70 volt are: collector root temperature 622°C, cesium reservoir temperature 342°C, and an interelectrode spacing of 0.0026 ± 0.0002 inch. The 0.70-volt data are shown in Figs. 2-19, 2-20, and 2-21. At this point, it should be noted that the collector surface temperature is expected to be different for 0.8 volt than for 0.70 volt even though the root temperature is the same. Subsequent measurements in operating converters and other test vehicles have substantiated this. Figures 2-22 and 2-23 show optimization data for 0.6-volt operation.

The 0.8-volt output was re-examined in more detail since the contract work statement identified converter performance level. Since only 15.4 watts/cm<sup>2</sup> at 0.8 volt are available at practical converter spacings, it was of interest to investigate the spacing where more output was available but with the spacing very close.

The power output variation at 0.8 volt as a function of spacing was measured with the collector root and reservoir temperature set at their optimum values of 610°C and 331°C, respectively. Keeping the voltage output constant at 0.8 volt and only varying spacing, the current output variation was determined. This is shown in Fig. 2-24. Of particular interest is the minimum power point observed at a spacing of 0.001 inch. As the spacing decreases further,

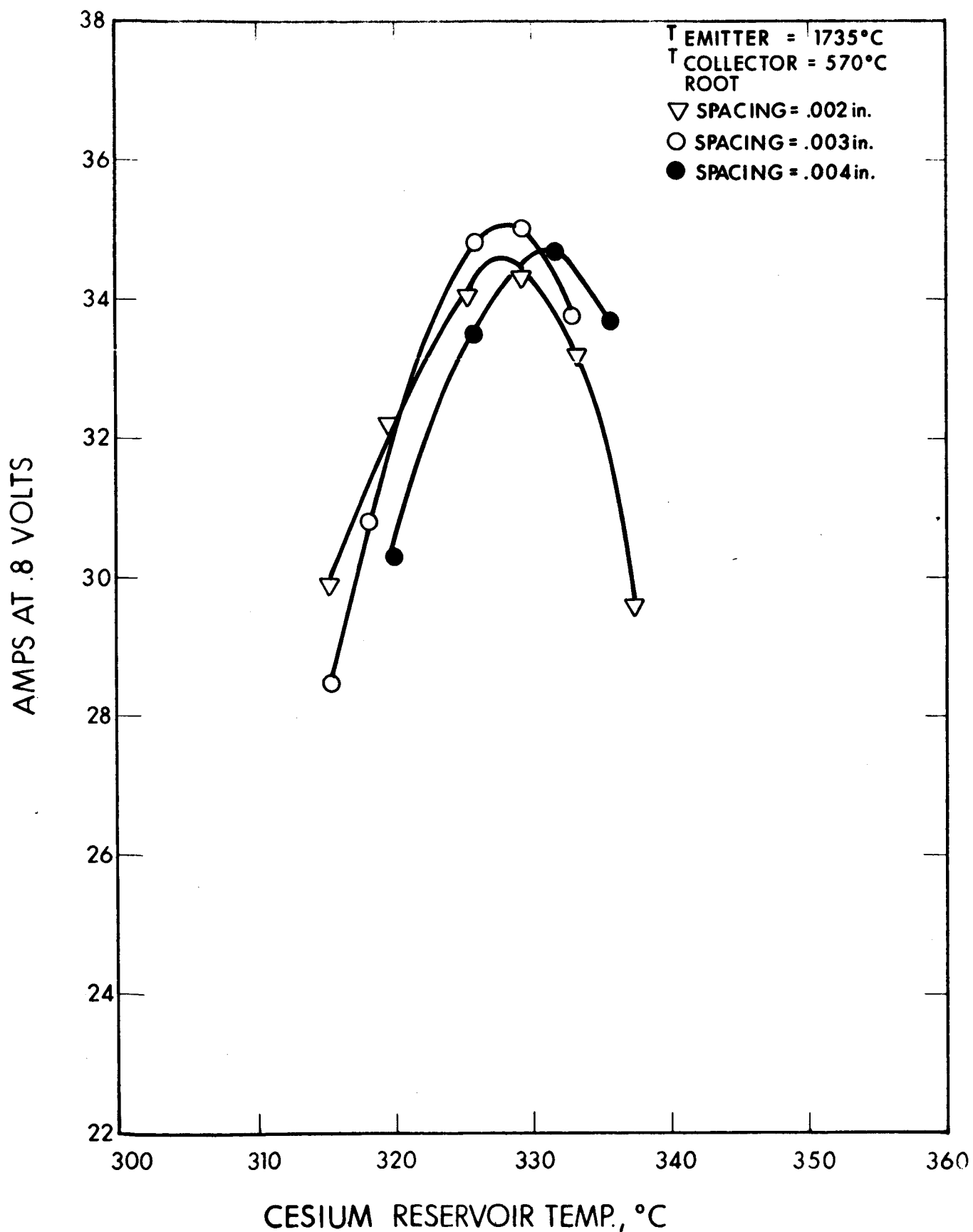


FIG. 2-15 RESERVOIR TEMPERATURE VERSUS CURRENT WITH 0.002, 0.003, AND 0.004 INCH SPACING,  $T_{\text{COLLECTOR}} = 570^{\circ}\text{C}$  (all dc data points)  
 ROOT

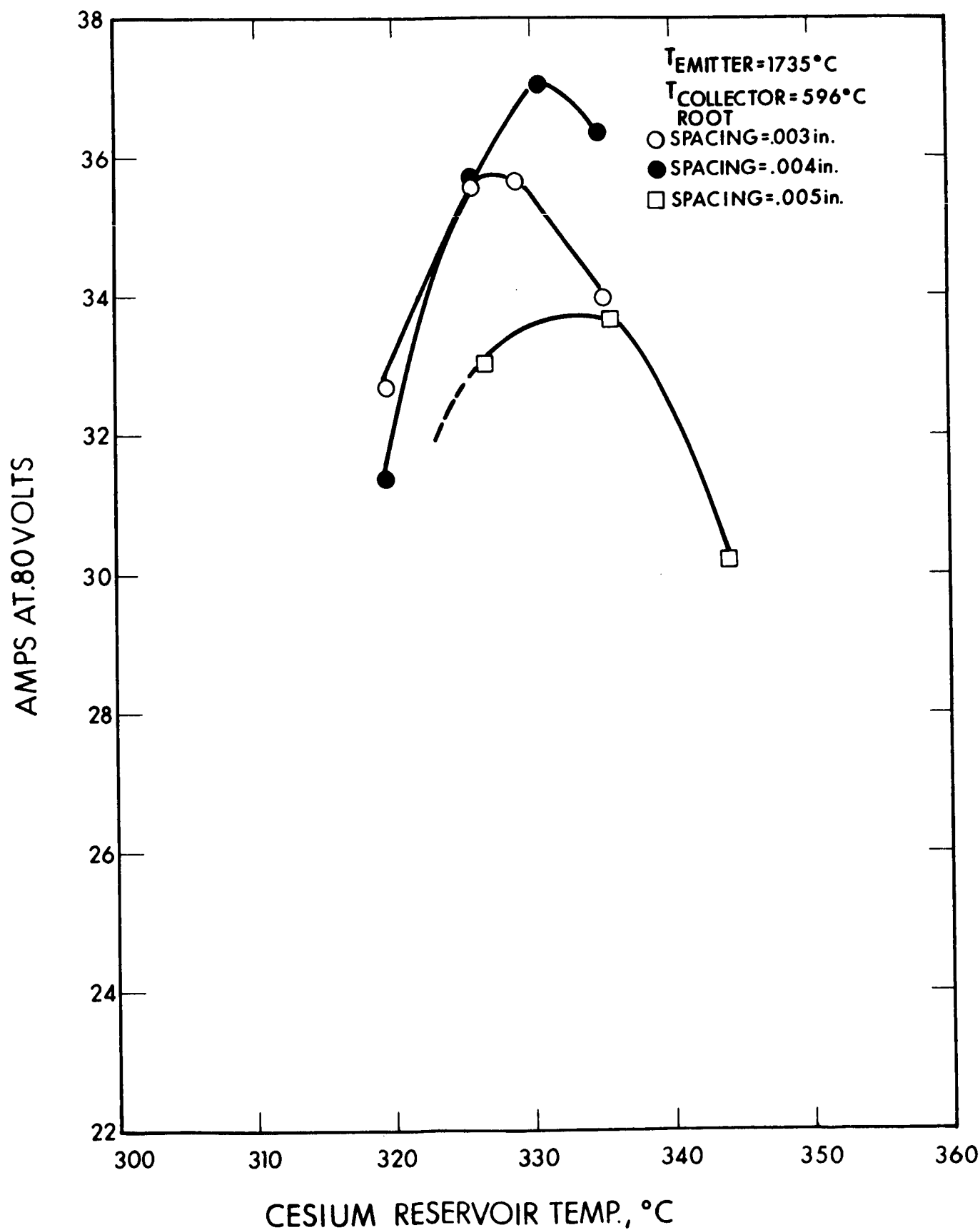


FIG. 2-16 RESERVOIR TEMPERATURE VERSUS CURRENT WITH 0.003, 0.004, AND 0.005 INCH SPACING  $T_{\text{COLLECTOR}} = 596^{\circ}\text{C}$  (all dc data points)

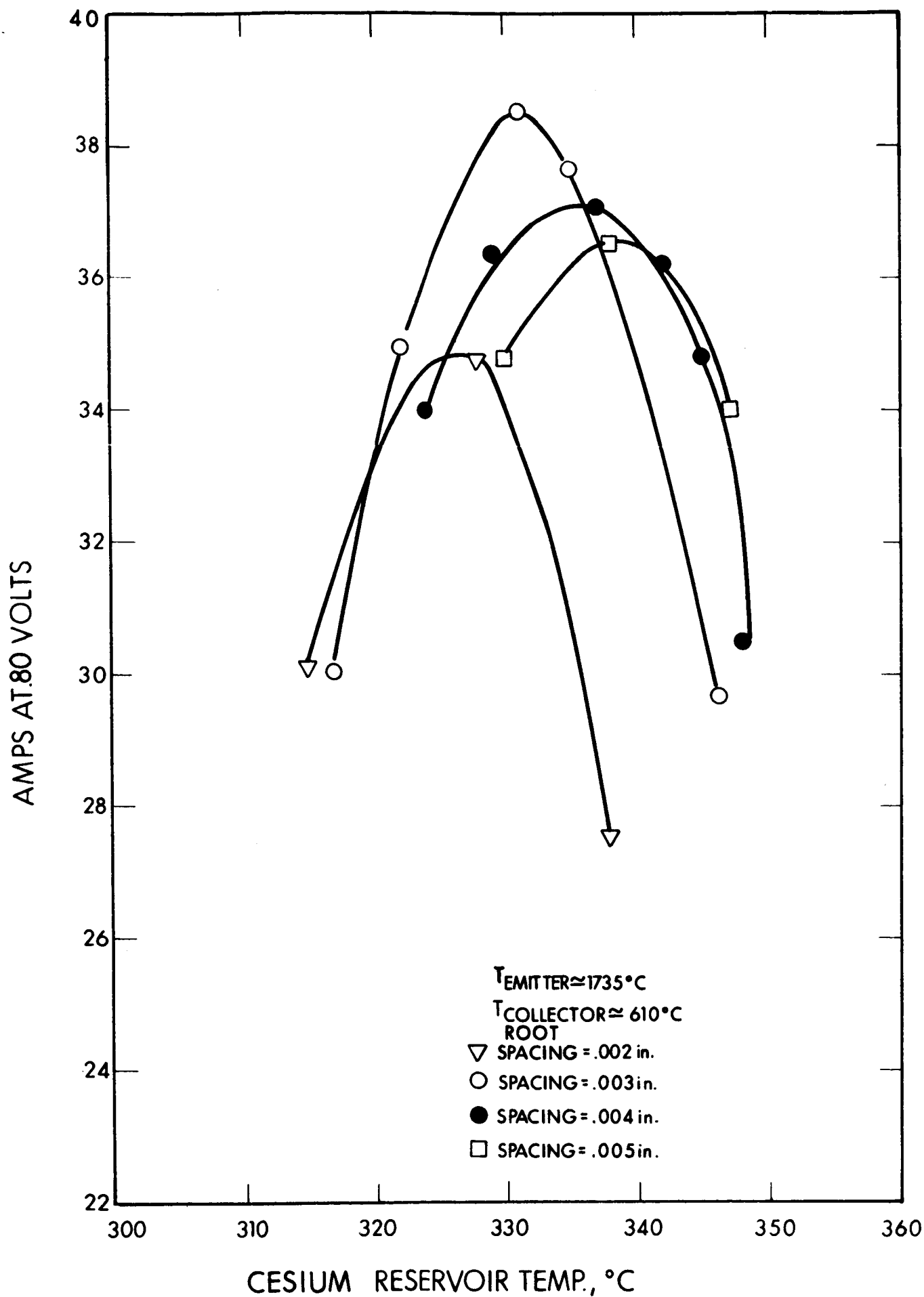


FIG. 2-17 RESERVOIR TEMPERATURE VERSUS CURRENT WITH 0.002, 0.003, 0.004, AND 0.005 INCH SPACING,  $T_{\text{COLLECTOR}} = 610^{\circ}\text{C}$  (all dc data points)

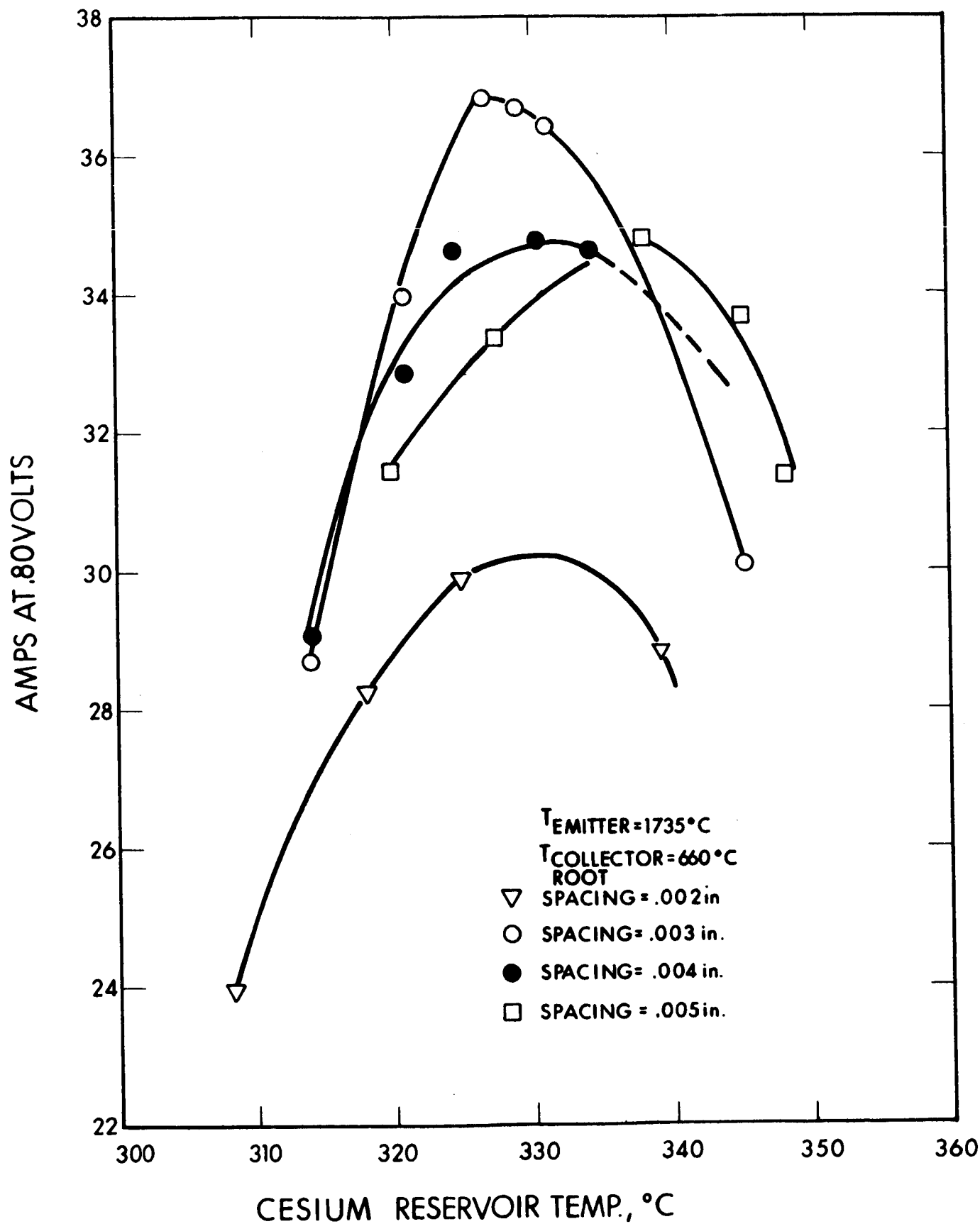


FIG. 2-18 RESERVOIR TEMPERATURE VERSUS CURRENT WITH 0.002, 0.003, 0.004, AND 0.005 INCH SPACING,  $T_{\text{COLLECTOR}} = 660^{\circ}\text{C}$  (all dc data points)  
ROOT



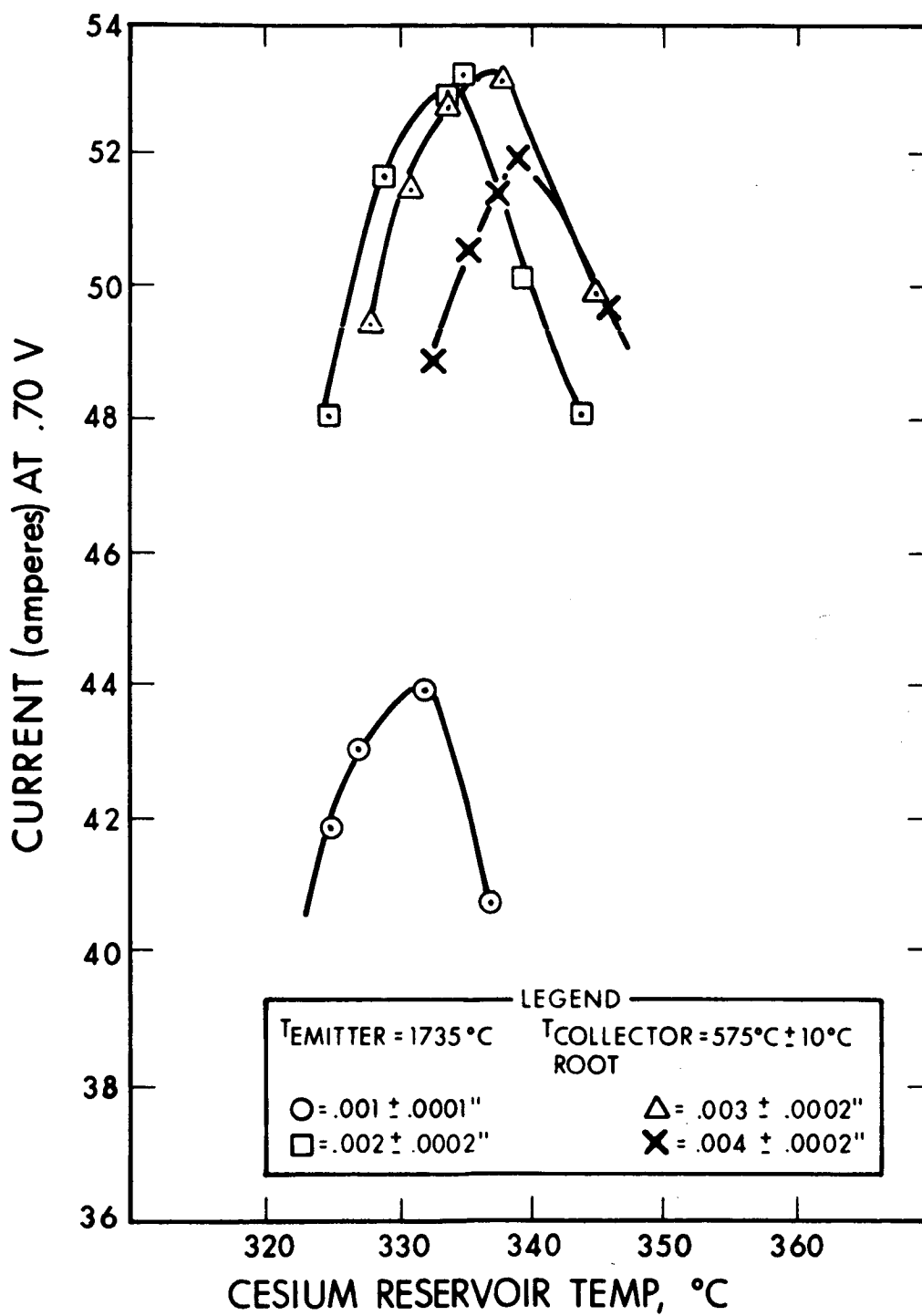


FIG. 2-19 CONVERTER OPTIMIZATION DATA FOR 0.7 VOLT OUTPUT.  
 $T_{\text{COLLECTOR}} = 575^{\circ}\text{C}$  (all dc data points)  
 ROOT

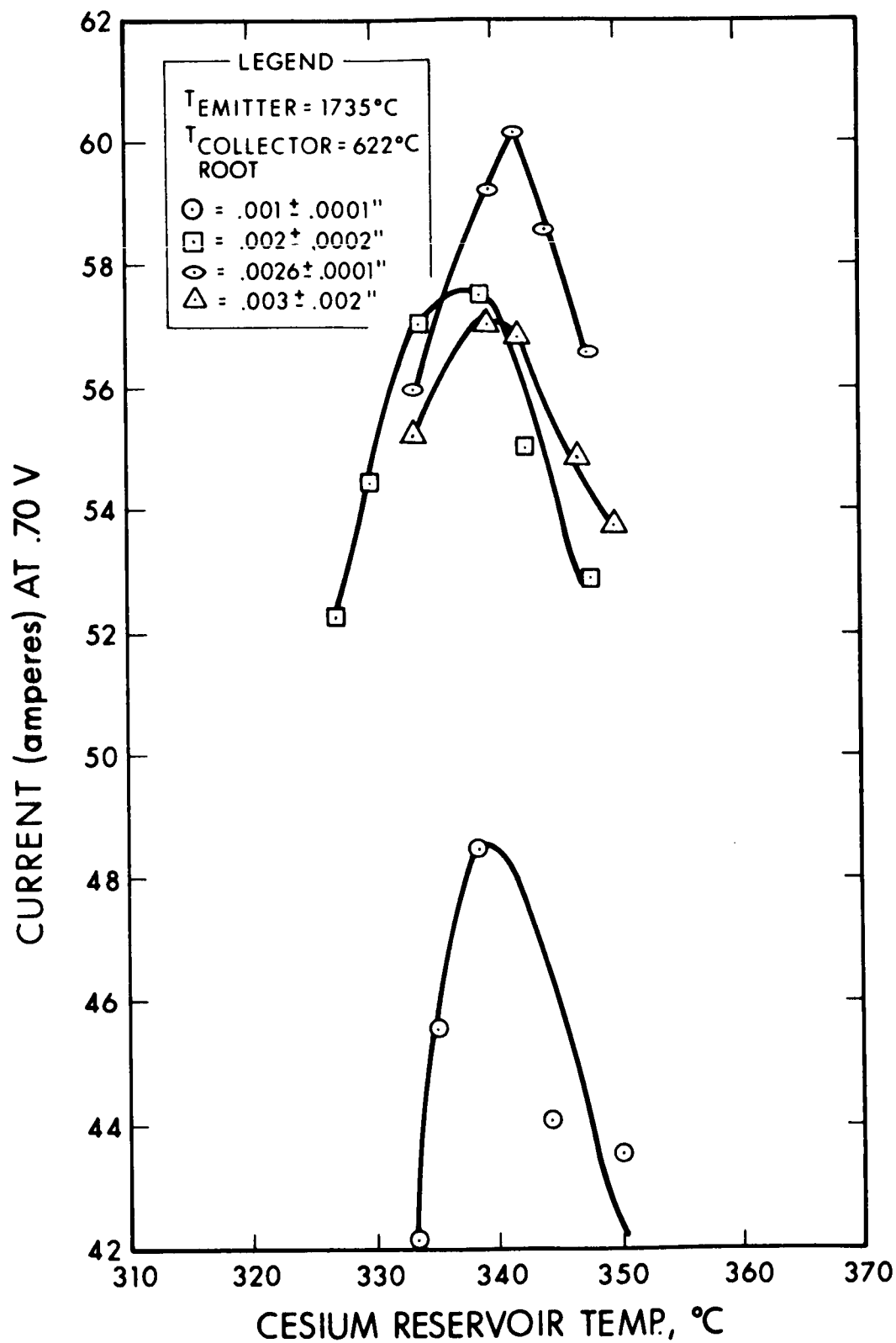


FIG. 2-20 CONVERTER OPTIMIZATION DATA FOR 0.7 VOLT OUTPUT.

$T_{\text{COLLECTOR}} = 610^{\circ}\text{C}$  (all dc data points)  
 ROOT

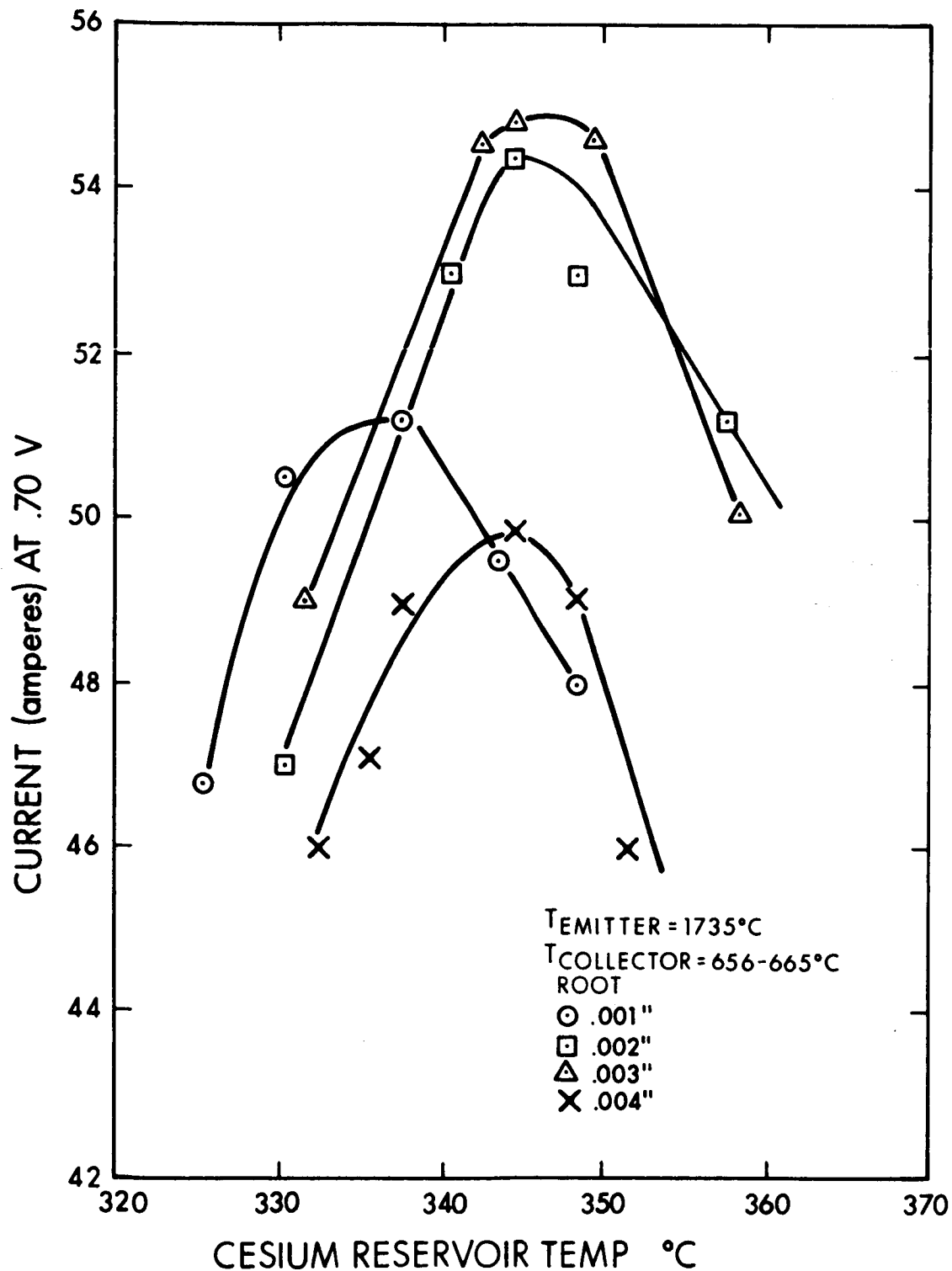


FIG. 2-21 CONVERTER OPTIMIZATION DATA FOR 0.7 VOLT OUTPUT.  
 $T_{\text{COLLECTOR}} = 656^{\circ}\text{C}$  (all dc data points)  
 ROOT

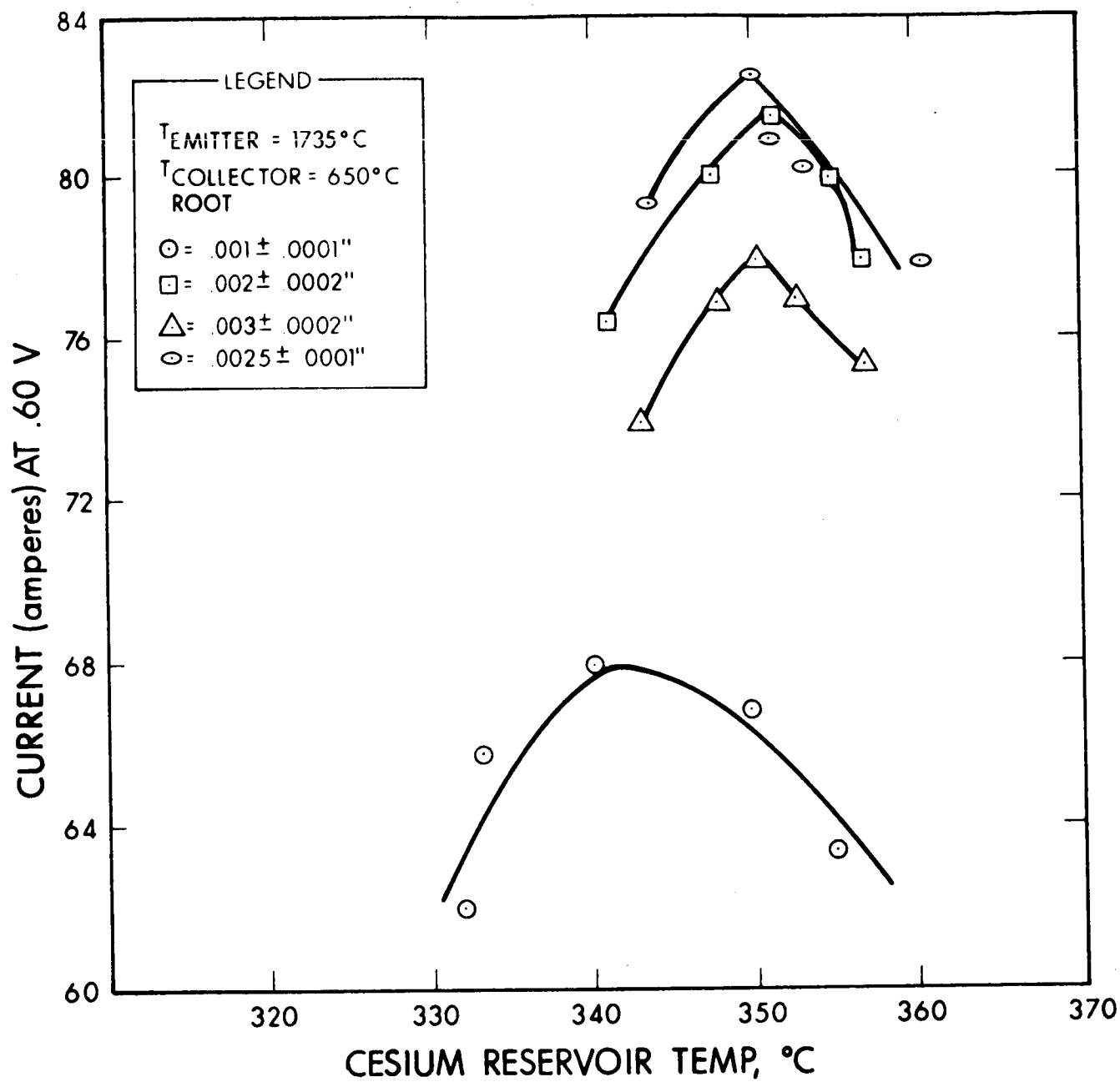


FIG. 2-22 CONVERTER OPTIMIZATION DATA FOR 0.6 VOLT OUTPUT.  
 $T_{\text{COLLECTOR}} = 650^{\circ}\text{C}$  (all dc data points)  
 ROOT

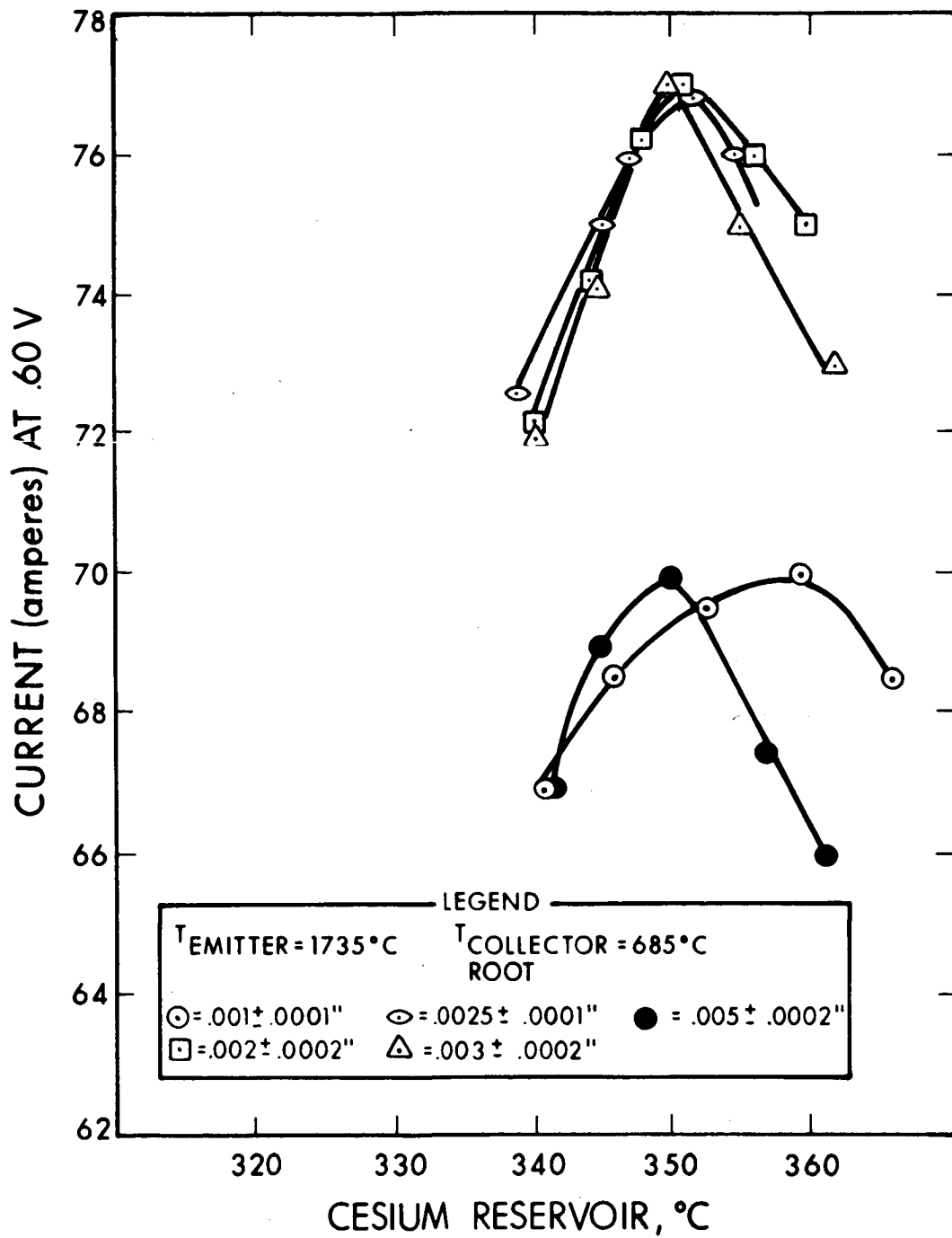


FIG. 2-23 CONVERTER OPTIMIZATION FOR 0.6 VOLT OUTPUT.  
 $T_{\text{COLLECTOR}} = 685^{\circ}\text{C}$  (all dc data points)  
 ROOT

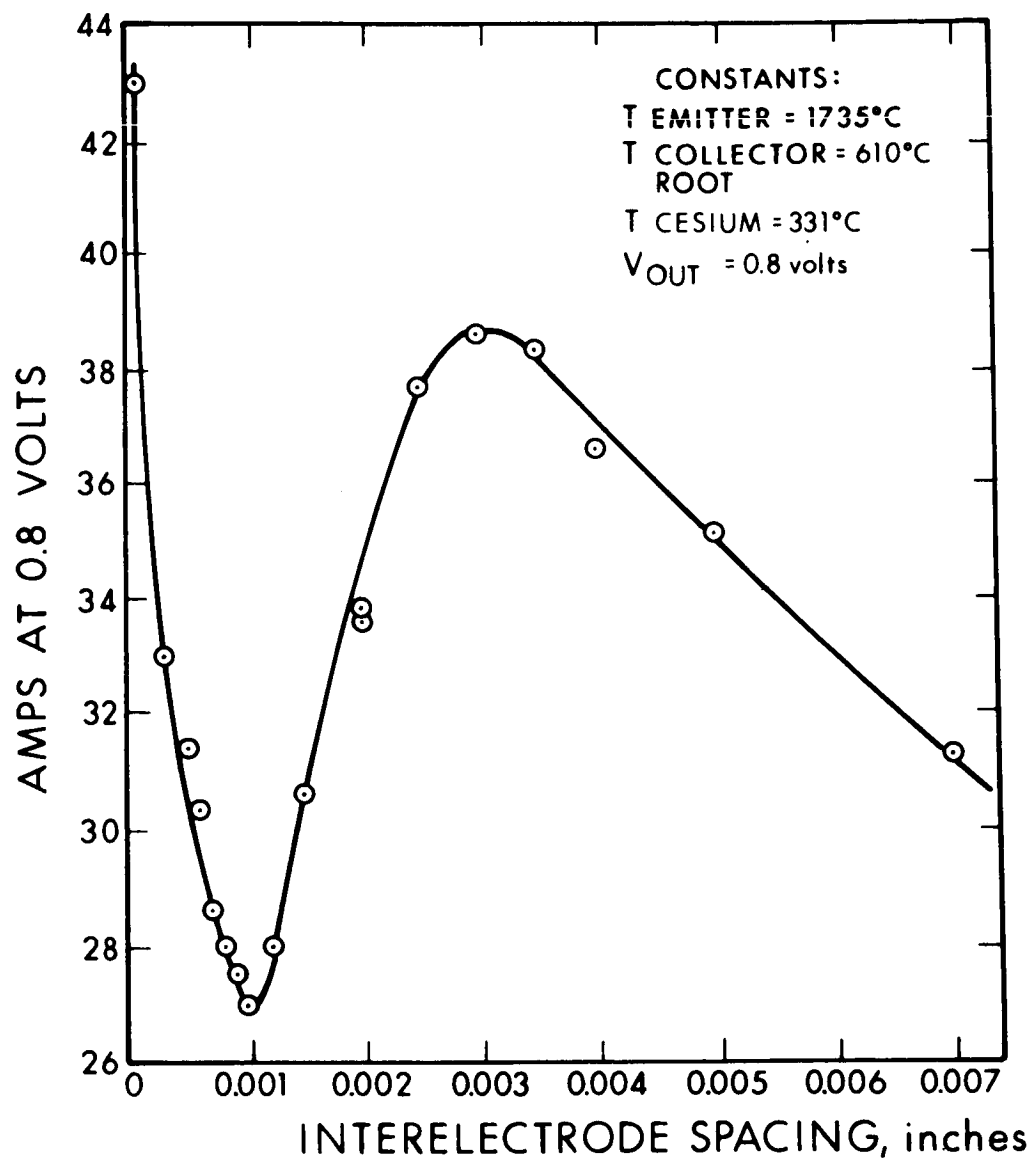


FIG. 2-24 INTERELECTRODE SPACING VERSUS CURRENT AT 0.8 VOLT OUTPUT. COLLECTOR, EMITTER, AND CESIUM RESERVOIR CONSTANT TEMPERATURES (all dc data points)

the current (power) output increases again. This was the first time behavior of this type had been obtained in the emitter temperature region above  $1300^{\circ}\text{C}$  (Ref. 2). The data show that only at spacings of less than 0.0003 inch will the power output exceed that available at a spacing of approximately 0.003 inch. An inherent difficulty was encountered in taking these data: The collector temperature is extremely difficult to maintain at a constant value since the current load continually varies; moreover, at the closer spacings (less than 0.0005 inch) small collector temperature changes produce erroneous spacing measurements.

#### 2.2.5.2 Voltage-Spacing Relationships for the Rhenium-Rhenium Electrode System

After establishing the variation of power output (at 0.8 volt) with spacing, shown in Fig. 2-24, it was desirable to relate the variation to the cesium plasma parameters. To achieve this, the power output was measured as a function of spacing at a constant dc current. The measured quantity is the voltage output variation with spacing. This variation of voltage with spacing at constant current is shown in Fig. 2-25. The advantage of this method over the previous method is that all spacing problems due to differential expansion are eliminated due to the steady-state vehicle temperature distribution.

Figure 2-25 is the voltage variation at a constant 38 amperes at the vehicle parameters for maximum power output of 0.8 volt, i.e., collector root temperature of  $610^{\circ}\text{C}$  and cesium reservoir temperature of  $331^{\circ}\text{C}$ . Figure 2-26 is a similar plot at a higher cesium pressure,  $T_{\text{cesium}} = 350^{\circ}\text{C}$ . The dc current is the same in Figs. 2-25 and 2-26, but the power output is lower for the higher reservoir temperatures. This is as expected, since the optimum power was determined to occur at  $T_{\text{cesium}} = 331^{\circ}\text{C}$ .

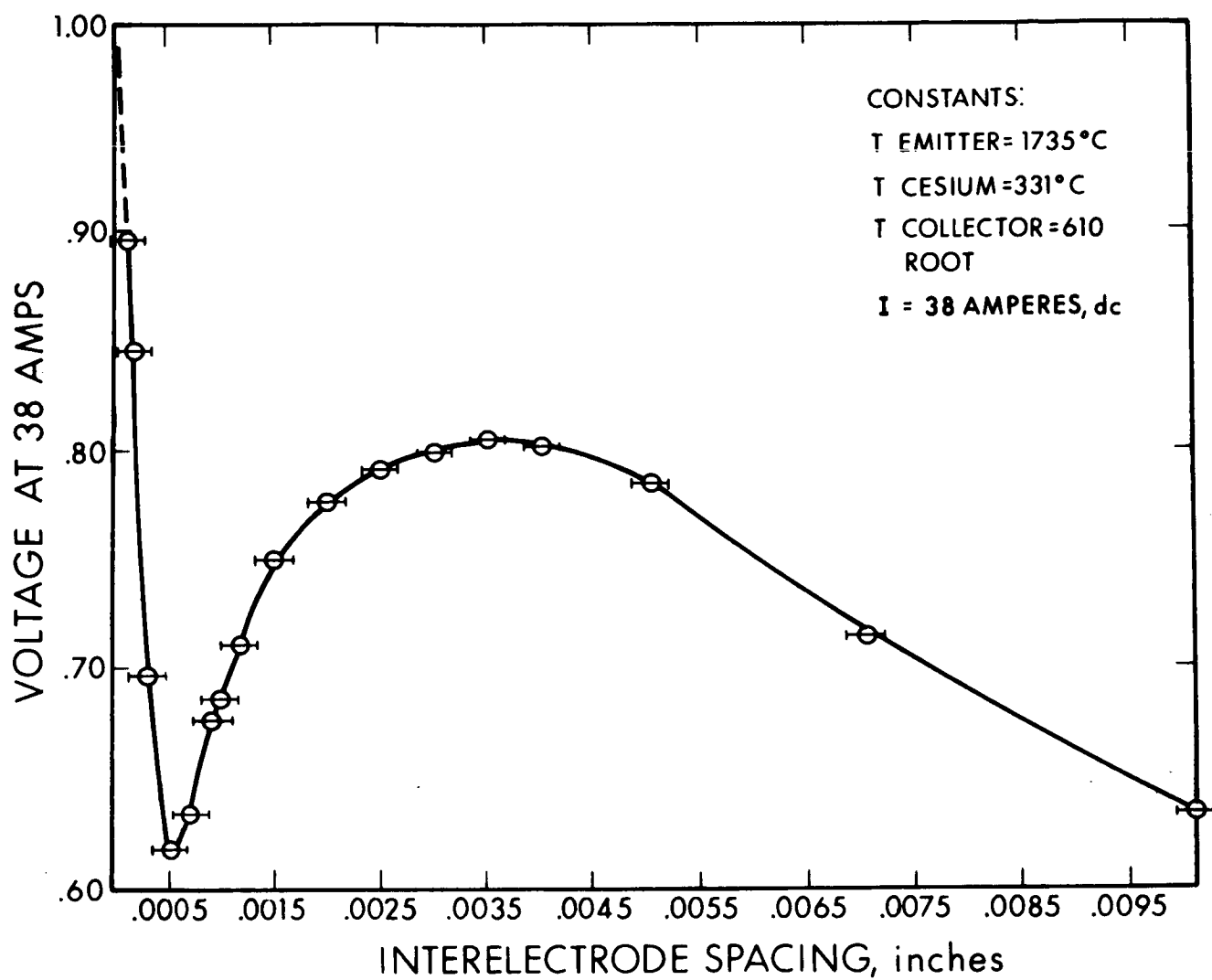


FIG. 2-25 INTERELECTRODE SPACING VERSUS VOLTAGE. EMITTER, COLLECTOR, AND CESIUM RESERVOIR TEMPERATURES CONSTANT (all dc data points)



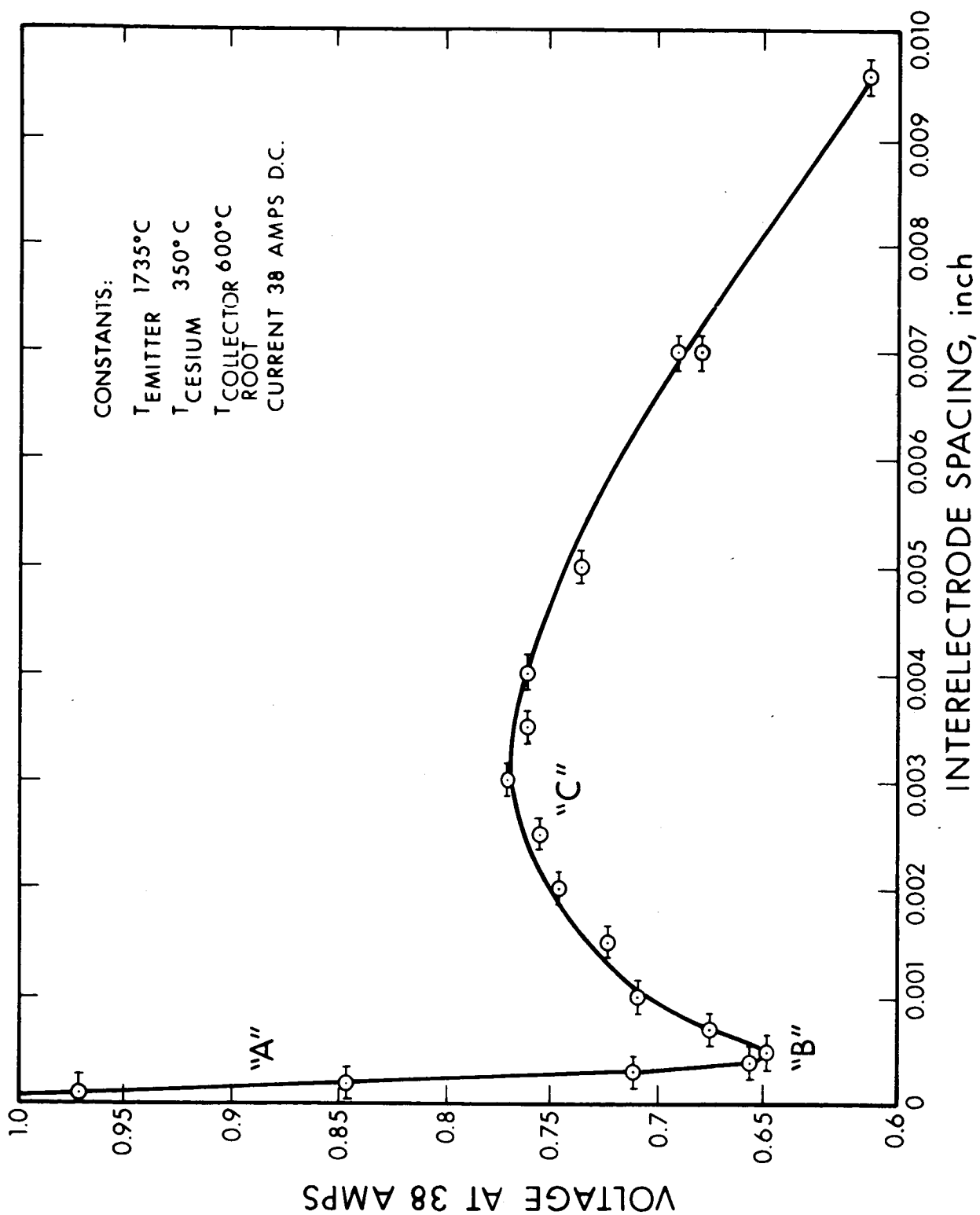


FIG. 2-26 VOLTAGE-SPACING RELATIONSHIP (all dc data points) FOR CONSTANT EMITTER, COLLECTOR, AND CESIUM RESERVOIR TEMPERATURES

Figure 2-27a is the voltage output-spacing relationship at a constant current of 60 amperes at the vehicle parameters for maximum power output of 0.7 volt, i.e., collector root temperature of 622°C and cesium reservoir temperature of 344°C. The voltage output minimum of 0.37V in Fig. 2-27a is much less than the minimum corresponding voltage output of 0.62V in Fig. 2-25. This is consistent with gas discharge phenomena since the extraction voltage or cathode sheath voltage required for drawing 60 amperes is greater than that for 38 amperes and appears as less voltage output from the test vehicle.

Several interesting observations were made during accumulation of the experimental data: (1) at all spacings less than the minimum at 0.0005 inch, the test vehicle was operating in the space charge mode; (2) the minimum power point was a very unstable operating point due to the fact that at this spacing (0.0005 inch), the ignition point coincides with the dc operating point and slight variations in reservoir temperature cause ignitions and extinctions of the arc; and (3) the data were obtained by taking dc data points and then sweeping the vehicle with 60 cycles ac to take an oscilloscope I-V characteristic. Due to the increased collector heating and emitter cooling resulting from operation at the high current portion of the sweep, spacings of less than 0.0002 inch cannot be maintained if the sweep is applied for more than approximately 30 seconds; that is, high current sweep operation causes shorting of the vehicle at close spacings due to thermal expansion of the collector.

Utilizing Langmuir's equation to determine the cesium vapor pressure associated with a particular reservoir temperature:

$$\log_{10} P_{\text{mm}} = 11.0531 - 1.35 \log_{10} T_{\text{OK}} - \frac{4041}{T_{\text{OK}}} \quad (2-11)$$

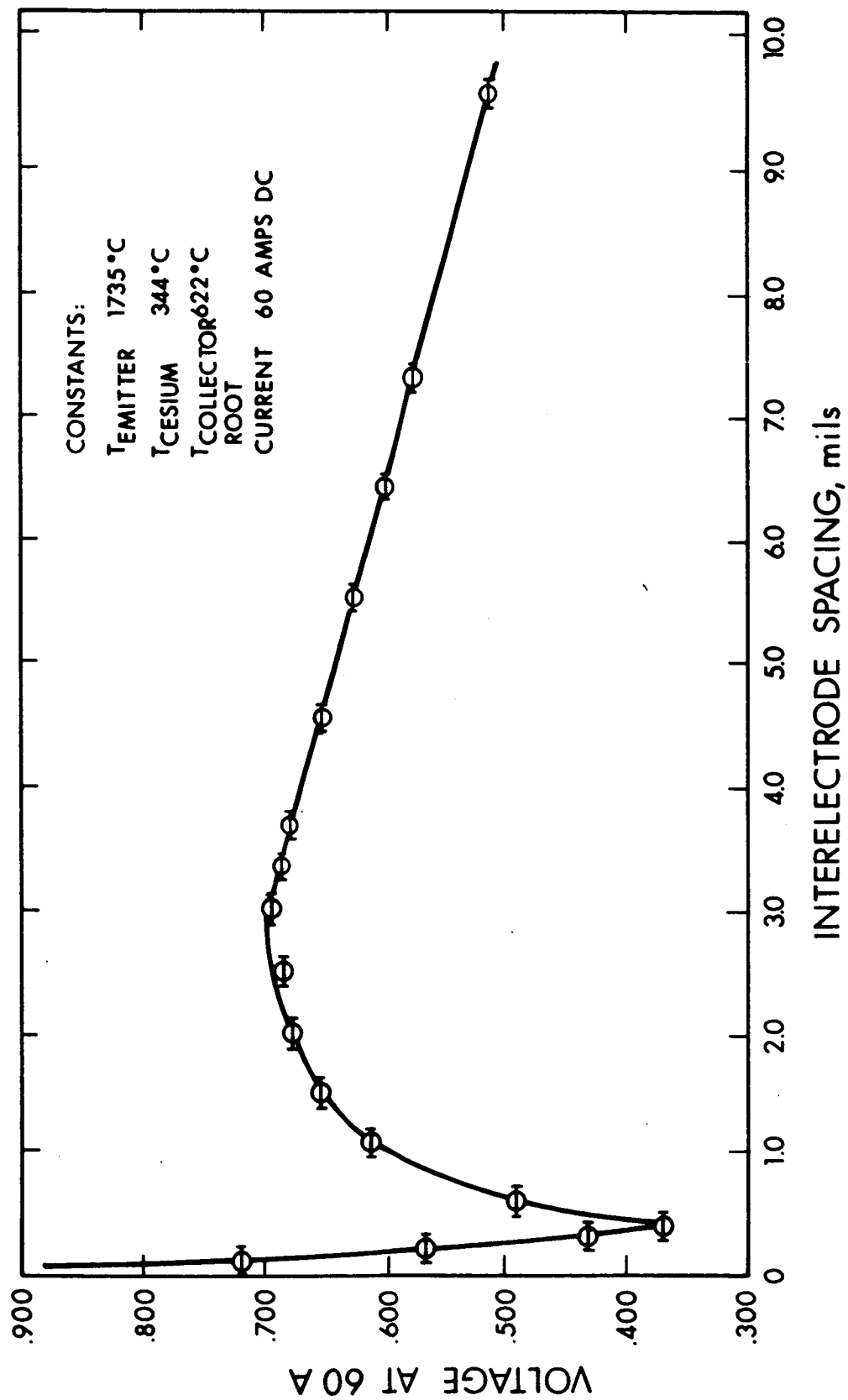


FIG. 2-27a INTERELECTRODE SPACING VERSUS VOLTAGE OUTPUT AT A CONSTANT CURRENT OF 60 AMPERES  
 (all data points are dc data)

The pressure-spacing products (pd) in mil-torr for the relative maximums in Figs. 2-25, 2-26, and 2-27a were determined. The results are shown in Table 2-V. The fundamental feature of the pd product results from the similarity relationships; that is, certain characteristics of a sustained discharge obey a similarity law relating dimensions and basic parameters. Therefore, for a discharge in identical gases and identical electrode materials, the vapor pressure, field intensities, and space potentials are directly related to the ratio of the spacings. Thus, as expected, the maximum power points of Figs. 2-25, 2-26, and 27a occur at the same pressure-spacing product.

TABLE 2-V

<u>T<sub>cesium</sub></u> °C	<u>P<sub>mm</sub></u>	<u>d (mil)</u>	<u>pd (mil-torr)</u>
331	4.1 ±0.2	3.9	16.0 ±0.8
344	5.3 ±0.2	3.0	15.9 ±0.8
350	6.22 ±0.3	2.7	16.8 ±0.8

In all of these voltage-spacing measurements, the constant cesium reservoir temperature, collector root temperature, and emitter temperature along with constant current density results in a constant sheath thickness at the cathode and anode, constant plasma density, and constant plasma electron temperature. Therefore, the voltage output variation with spacing may be related to a voltage profile of the vehicle interelectrode space. This is not to say that the voltage output can be interpreted as a direct measurement of the discharge potential. In fact, the voltage output of the test vehicle is related to the internal voltages by the following equation:

$$V_{\text{out}} = V_{\text{cpd}} + V_m - V_{\text{cathode sheath}} - V_{\text{plasma}} \pm V_{\text{anode sheath}} \quad (2-12)$$

where

$V_{cpd}$  = contact potential difference between the cathode and anode

$V_m$  = space charge minimum voltage; i.e., if a double sheath exists at the cathode,  $V_m$  = voltage barrier necessary for an electron to overcome as it proceeds from the cathode surface to the accelerating portion of the sheath

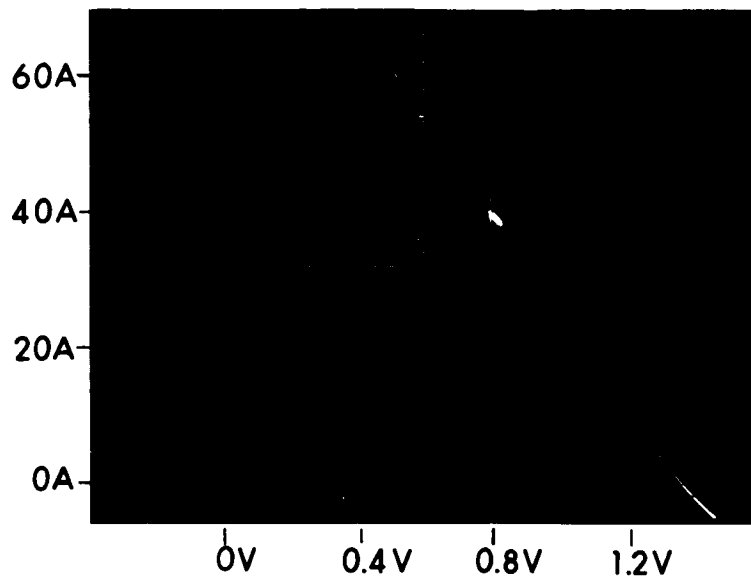
$V_{cathode\ sheath}$  = potential drop from the voltage minimum to the plasma

$V_{plasma}$  = potential drop in the plasma

$V_{anode\ sheath}$  = value of the accelerating or retarding voltage at the collector

$V_{anode\ sheath}$  may be zero under certain conditions of electrode geometry, anode temperature, and spacing. Thus, the variation of output voltage with spacing is a summation of all the spacing dependent terms of Eq. 2-12.

Three areas of interest have been designated on the curve in Fig. 2-26 for the voltage variation with spacing at a cesium temperature of 350°C. I-V characteristics for each of the points of interest are shown in Fig. 2-27. Point A shows the characteristic at an interelectrode spacing of 0.0002 inch; the dc point of 38 amps current is plainly visible on the characteristic. The ignition point can be observed at the top of the photograph occurring at approximately 60 amps and 0.5 volt. It is apparent from this characteristic that the vehicle, for a spacing of 0.0002 inch and at the dc point, is operating in the space charge limited mode. Figure 2-28 shows the potential distribution in the interelectrode space at the specific points on the voltage spacing curve. Again, point A indicates the classical double-diode space charge distribution. Point B is at the minimum of the voltage-spacing curve. Figures 2-27 and 2-28 show the I-V characteristic and potential distribution at this point of operation. As can



Pt. "A"

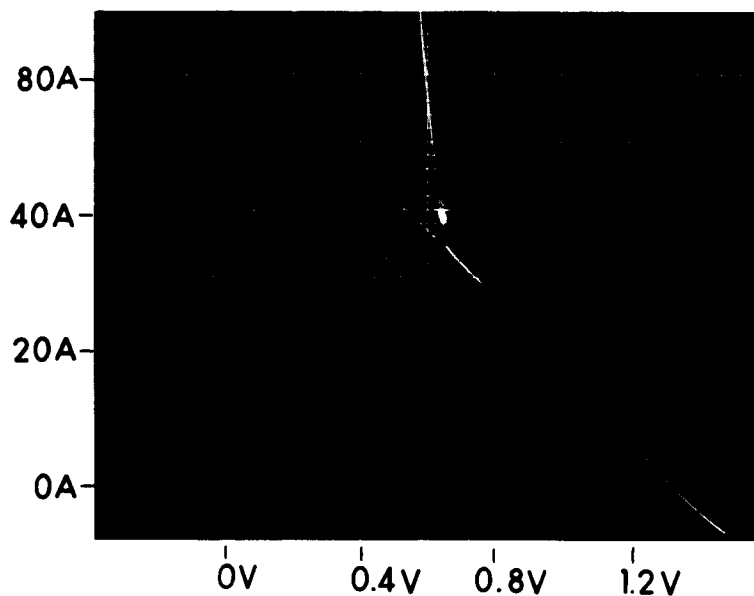
$T_e = 1735^\circ\text{C}$

$T_{Cs} = 348^\circ\text{C}$

Spacing = 0.2 mil

$I_{dc} = 38$  amps

$T_{coll \text{ root}} = 600^\circ\text{C}$



Pt. "B"

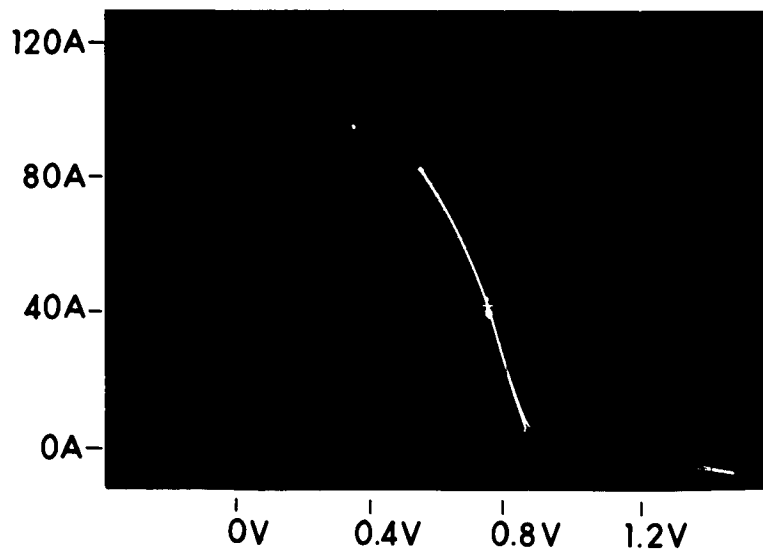
$T_e = 1735^\circ\text{C}$

$T_{Cs} = 350^\circ\text{C}$

Spacing = 0.5 mil

$I_{dc} = 38$  amps

$T_{coll \text{ root}} = 600^\circ\text{C}$



Pt. "C"

$T_e = 1735^\circ\text{C}$

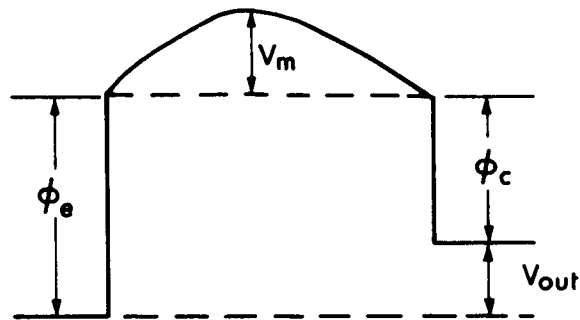
$T_{Cs} = 348^\circ\text{C}$

Spacing = 3.5 mils

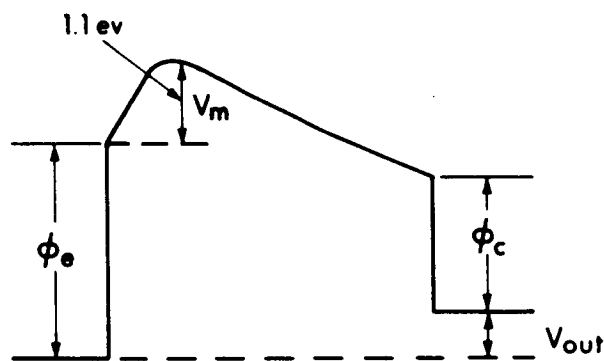
$I_{dc} = 38$  amps

$T_{coll \text{ root}} = 600^\circ\text{C}$

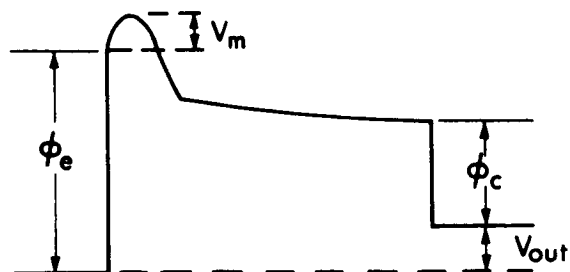
FIG. 2-27 I-V CHARACTERISTICS FOR THE OPERATING REGIONS OF SPACE-CHARGE LIMITED, INCIPIENT BREAKDOWN, AND FULLY DEVELOPED PLASMA (Ref. Fig. 2-26)



POINT "A"



POINT "B"



POINT "C"

FIG. 2-28 POTENTIAL DISTRIBUTION DIAGRAM FOR SPACE-CHARGE, INCIPIENT BREAKDOWN, AND FULLY DEVELOPED PLASMA AT THE dc POINTS A, B, AND C (Ref. Fig. 2-27)

be seen in Fig. 2-28, the dc operating point for point B occurs directly at ignition. This operating point is very unstable since the constant current point can occur at two different voltages. Compared to point A, the voltage output has decreased to allow for the accelerating potential distribution for electrons into the anode. A plasma has not developed yet, but as this potential approaches the first excitation potential for cesium, the ionization mechanisms can be optimized. This process continues until point C is reached. At this point, a fully developed plasma exists, as typified by the potential diagram of point C in Fig. 2-28. In all of the potential diagrams of Fig. 2-28, the plasma potential is assumed to be matched to the anode for the sake of simplicity.

Returning to the data at close spacing, a preliminary analysis was performed on the space charge region of the voltage-spacing curve of Fig. 2-29. Using both the Childs-Langmuir space charge equation and the collision dominated space charge equation,  $dV/dx$  was calculated:

$$J = \frac{1}{9\pi} \sqrt{\frac{2e}{m}} \frac{V^{3/2}}{d^2} \quad \text{Childs-Langmuir} \quad (2-13)$$

$$J = \frac{9}{8} \epsilon_0 \frac{\Lambda^2 \nu}{T_{\text{electron}} x^3} \frac{V^2}{3} \quad \text{Collision dominated} \quad (2-14)$$

where  $\Lambda$  = electron-atom mean free path

$\nu$  = electron-atom collision frequency

$T_{\text{electron}}$  = electron temperature

The transition from the classical space charge limited mode and the plasma dominated region results from the increase in the space charge current (86 percent) produced by ion neutralization and the increased contribution of the collision dominated space charge current given by Eq. 2-14.  $dV/dx$  was evaluated at point A where  $X = 0.0002$  inch and  $J$  is a constant  $19 \text{ amperes/cm}^2$ . The results are shown in Table 2-VI.



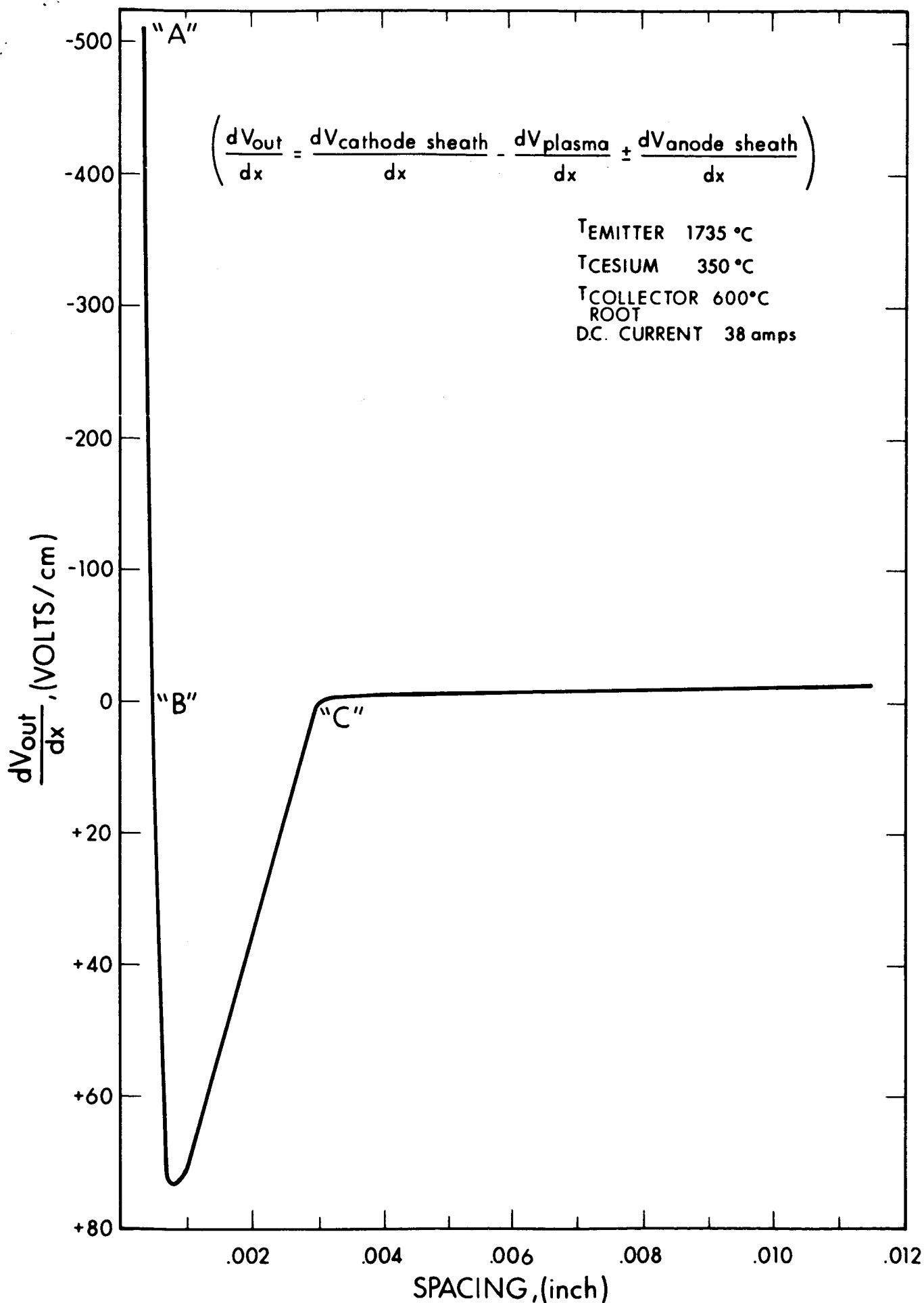


FIG. 2-29 FIRST DERIVATIVE OF VOLTAGE-SPACING CURVE  
6952-Final

TABLE 2-VI

	<u>dV/dX at 0.0002 inch</u>	
Eq. 2-13	Eq. 2-14	Experimental
431 volts/cm	22.6 volts/cm	512 volts/cm

Table 2-VI indicates that within the accuracy of experimental determination, the Childs-Langmuir law applies to region A of Fig. 2-26 and for these short spacings the vehicle is definitely operating in the classical space charge limited mode.

A point-by-point differentiation of the curve in Fig. 2-26 is shown in Fig. 2-29. This is not a plot of the internal field intensity since the plot is of  $dV_{out}/dx$ . Differentiating Eq. 2-12 results in:

$$\frac{dV_{out}}{dx} = \frac{dV_{cathode\ sheath}}{dx} - \frac{dV_{plasma}}{dx} \pm \frac{dV_{anode\ sheath}}{dx} \quad (2-15)$$

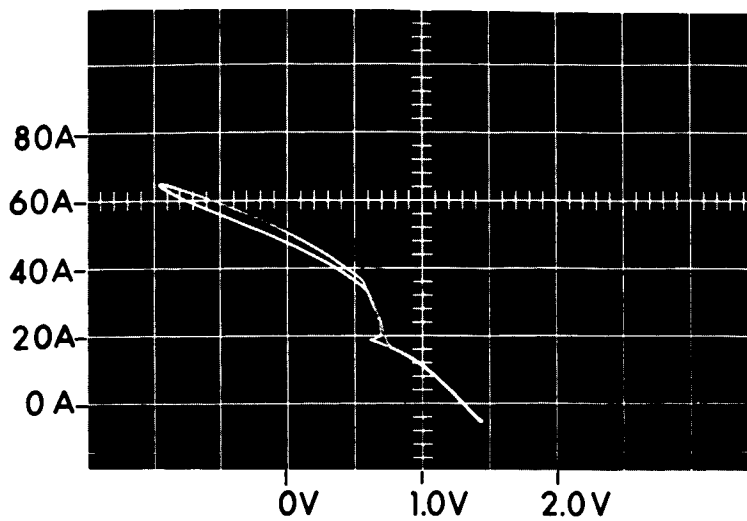
Therefore, Fig. 2-29 represents the contributions of several spacing dependent terms in the voltage output equation. The shape of the curve is similar to the field intensity distribution of a gas discharge, but additional analysis is required to completely pinpoint the regions of influence of each of the voltage output equation terms. One observation can be made at the present time. The constant  $dV_{out}/dx$  beyond point "C" seems indicative of the formation of a positive column in the plasma of a thermionic converter for interelectrode spacings greater than 0.0035 inch and at the test conditions stated.

#### 2.2.5.3 Cesiated Work Function Measurements from Polycrystalline Rhenium

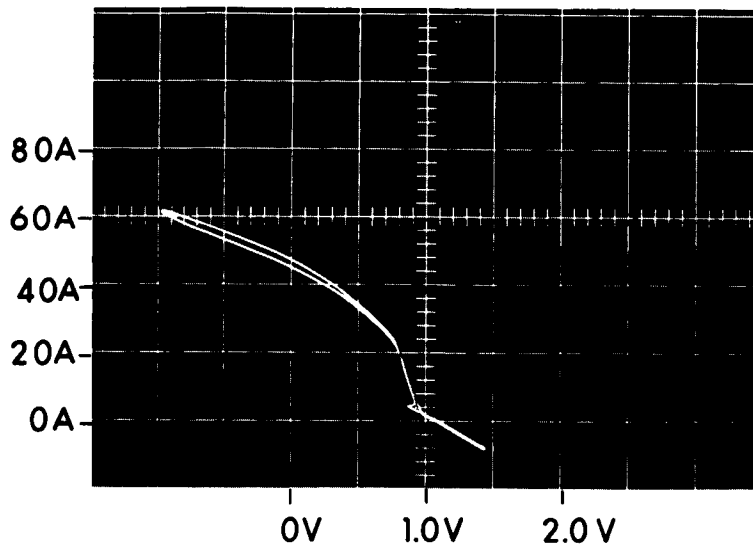
In all of the cesiated work function measurements, the volt-ampere characteristics were obtained by the combined

dc and ac method. This method is utilized since it traces an instantaneous characteristic at fixed parameter temperatures. The dc operating point is usually set by an electronic load. The sweep transformer then sweeps out a portion of the I-V characteristic around this dc point after it is ascertained that the element temperature, particularly the emitter, maintains the same value. Collected current is determined by measuring the voltage drop across a calibrated, 0.1-percent-accurate shunt and displayed on the y-axis of an x-y scope. Applied voltage or generated voltage is measured directly across the test vehicle terminals and displayed on the x-axis of the oscilloscope. To accurately determine saturated emission, it is sometimes necessary to sweep the arc voltage as much as 2 volts into the applied voltage quadrant. Since the zener diodes in the electronic load cannot hold off more than 0.5 volts in the forward direction, the electronic load was replaced by a resistive load across the test vehicle and a low inductance, low impedance, secondary stepdown transformer employed as a sweep source. The saturated emission is defined as the intersection of the extrapolated Schottky slope and the slope of the plasma region. Figure 2-30 consists of three I-V characteristics with an applied voltage of between 1.5 and 2.0 volts. To insure that the saturated electron emission is independent of interelectrode spacing, three spacings were selected for emission measurement: 0.001, 0.003, and 0.006 inch. The characteristics show that the measured saturated emission was constant within  $\pm 5$  percent for the same conditions of emitter and reservoir temperature while the spacing varied by a factor of six.

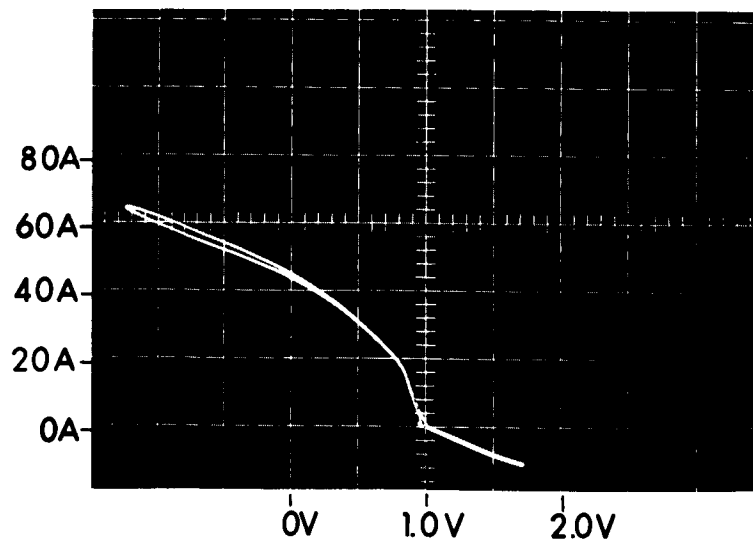
Exact determination of temperature is a very important part of accurate electron emission measurements. For all temperature determinations, other than the emitter and collector, calibrated Chromel-Alumel thermocouples traceable to the National Bureau of Standards were used. The emission measurements were conducted over the emitter temperature range between  $1000^{\circ}\text{K}$  and  $2000^{\circ}\text{K}$ .



$T_e = 1700^\circ\text{C}$   
 $T_{Cs} = 316^\circ\text{C}$   
 Spacing = 1 mil  
 Saturated emission = 42 amps



$T_e = 1700^\circ\text{C}$   
 $T_{Cs} = 316^\circ\text{C}$   
 Spacing = 3 mils  
 Saturated emission = 39 amps



$T_e = 1700^\circ\text{C}$   
 $T_{Cs} = 315^\circ\text{C}$   
 Spacing = 6 mils  
 Saturated emission = 39.5 amps

FIG. 2-30 I-V CHARACTERISTICS SHOWING THAT SATURATED ELECTRON EMISSION IS INDEPENDENT OF SPACING

The temperature for the higher portion of the emitter range (above  $1200^{\circ}\text{C}$ ) can be determined very accurately by comparing the color of a 10-to-1 blackbody hole in the emitter with a micro-optical pyrometer. Below  $1200^{\circ}\text{C}$ , optical temperature measuring methods require large corrections due to radiation reflections and emissivity changes. Therefore, thermocouples are required to measure the temperature ranges below  $1200^{\circ}\text{C}$ . Tungsten-rhenium thermocouples (W-5Re/W-26Re) were attached to the emitter by tantalum pads. These thermocouples were calibrated by platinum-rhodium couples in the lower range and blackbody holes in the higher range to give the saturated emission data continuity over the complete temperature range. Figure 2-31 shows the thermocouple calibration with a considerable range of cross-correlation.

Figure 2-32 is a plot of the saturated electron emission from polycrystalline rhenium for three different cesium reservoir temperatures. There are two significant results to be obtained from this figure: the electron current density and the minimum work function. The electron density measured from the polycrystalline rhenium emitter is a factor of two higher than {110} single crystal tungsten emission (Ref. 3) measured for approximately the same cesium reservoir temperatures (arrival rate), and a factor of ten higher than the cesiated electron emission measured from polycrystalline molybdenum. The minimum work function for the polycrystalline rhenium converges to a value of approximately 1.45 volts. This work function is approximately 0.1 volt less than the minimum work function reported for polycrystalline tantalum and polycrystalline molybdenum.

The importance and value of these data is that they were obtained in a system and manner directly related to operational thermionic energy converters.

To determine collector surface work functions, the saturated emission from the collector must be measured. This is

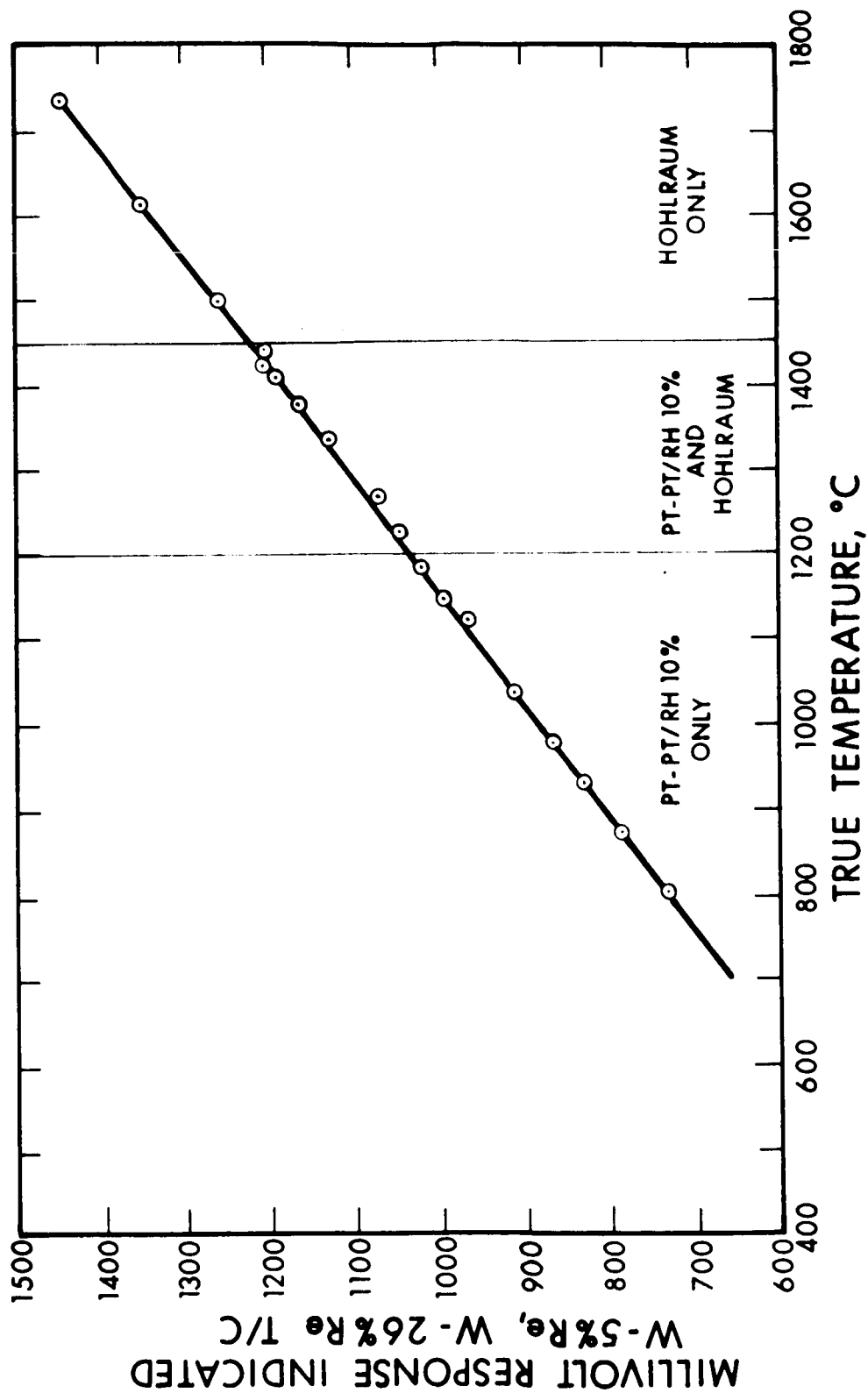
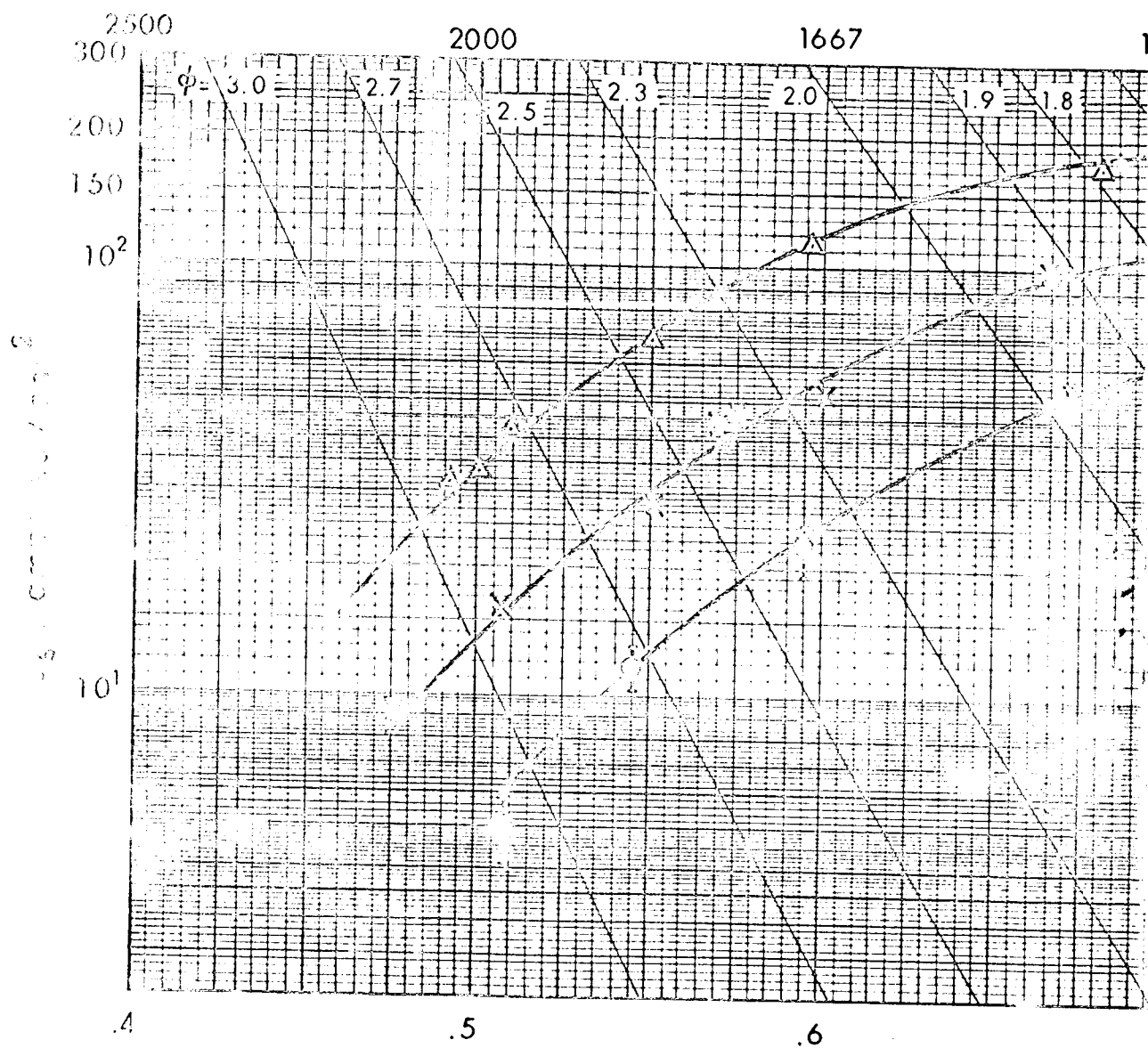


FIG. 2-31 THERMOCOUPLE CALIBRATION DATA



1000 / T

6952-1 [na]

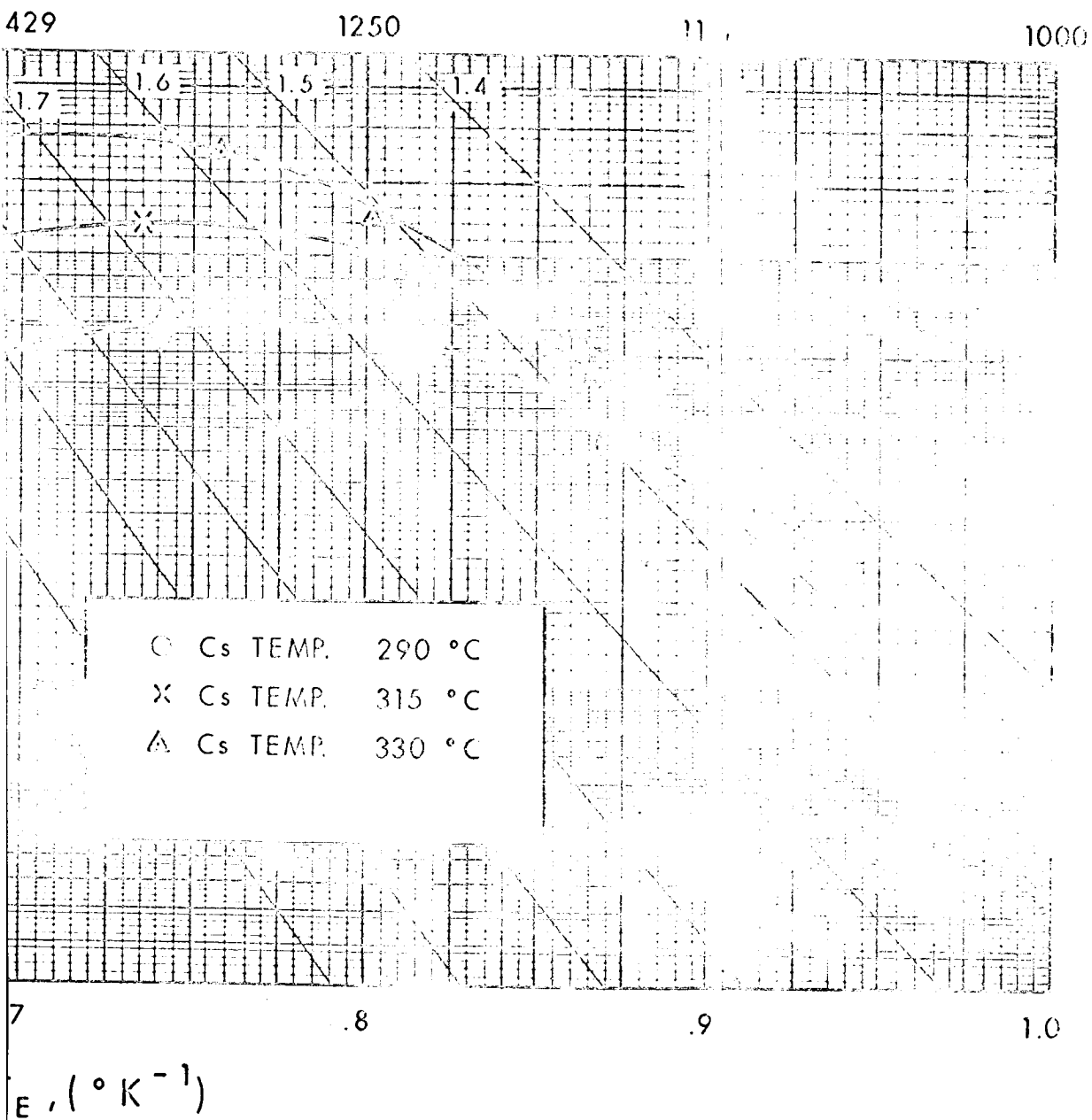


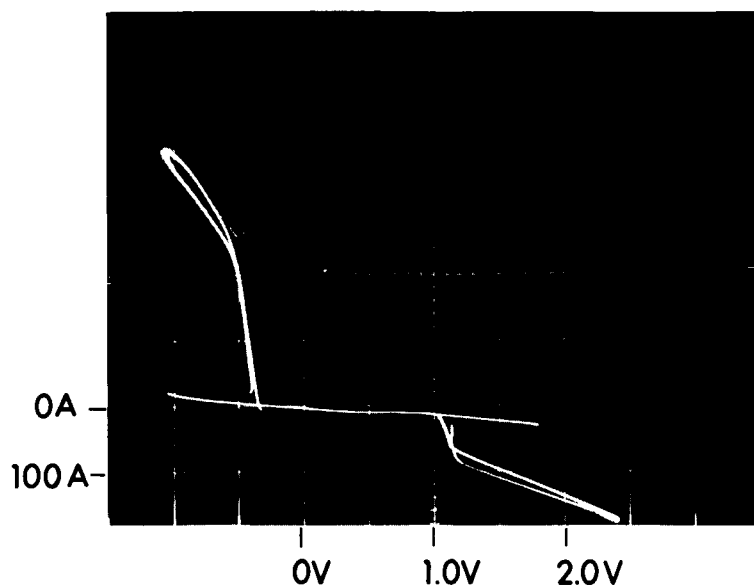
FIG. 2-32 SATURATED ELECTRON EMISSION FROM POLYCRYSTALLINE RHENIUM



obtained by examining the I-V characteristic beyond open circuit voltage. This is, in effect, reversing the potential distribution within the interelectrode space, allowing the collector to act as an emitter. Figure 2-33 shows I-V traces for two sets of parameters. In these photographs, the forward saturated emission is obtained in the positive applied voltage quadrant, and the reverse saturated emission (from the collector) is obtained in the negative applied voltage quadrant. Knowing the collector surface temperature, the saturated emission can be plotted versus temperature in the same manner as the emitter data were presented. Since the collector surface thermocouple was inoperative, no accurate determination of collector work function could be made during these tests. An approximate collector work function can be determined by estimating the collector surface temperature as follows: The temperature drop down the collector barrel as measured during the test vehicle design should be no greater than  $100^{\circ}\text{C}$  for a thermal input of  $265 \text{ watts/cm}^2$  and no less than  $40^{\circ}\text{C}$  for a thermal input to the collector surface of  $150 \text{ watts/cm}^2$ . Therefore, for a collector root temperature of  $727^{\circ}\text{C}$  and a collector saturated emission of  $42.5 \text{ A/cm}^2$  as shown in Fig. 2-33a, a collector work function between 1.42 and 1.34 volts is obtained. For the second case, in Fig. 2-33b, the work function would lie between 1.45 and 1.36 volts. This correlates well with the work function determination of the emitter.

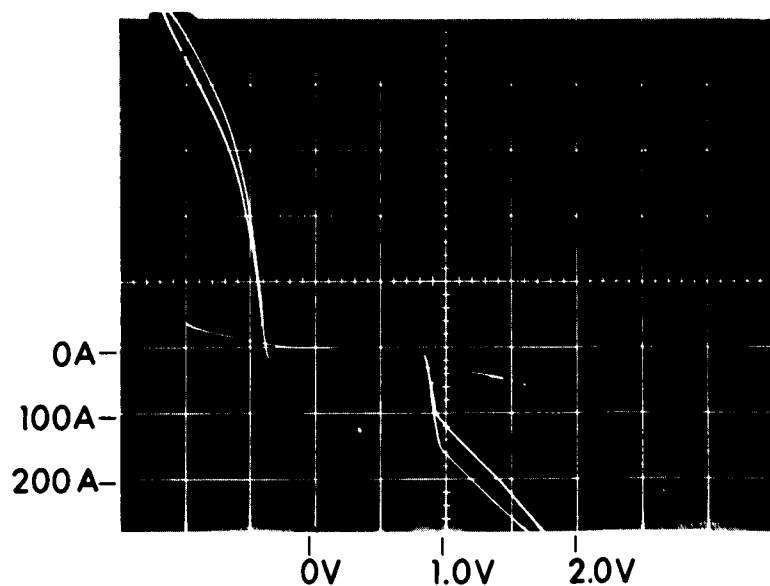
#### 2.2.5.4 Miscellaneous Measurements from the Rhenium-Rhenium Electrode System

Bare work function, or more properly, low cesium coverage (i.e.,  $\theta \leq 0.01$ ), measurements were taken from the polycrystalline rhenium emitter. The saturated electron emission was measured over the emitter temperature range from  $1973^{\circ}\text{K}$  to  $2133^{\circ}\text{K}$  at a reservoir temperature of  $122^{\circ}\text{C}$  which was the minimum achievable. The work function was computed by way of the Richardson-Dushman equation assuming a pre-exponential A value of  $120 \text{ amps/cm}^2 - ^{\circ}\text{K}^2$ . The work function values are indicative of the upper portion, or high-temperature



$T_{\text{coll root}} = 727^{\circ}\text{C}$   
 $T_{\text{cesium}} = 315^{\circ}\text{C}$   
 Collector  
 saturated  
 emission = 85 amps

FIG. 2-33 a



$T_{\text{coll root}} = 783^{\circ}\text{C}$   
 $T_{\text{cesium}} = 330^{\circ}\text{C}$   
 Collector  
 saturated  
 emission = 155 amps

FIG. 2-33 b

FIG. 2-33 SATURATED EMISSION MEASURED FROM COLLECTOR (Rhenium) SURFACE

end, of the Langmuir S curve, ranging in value from 4.45 volts to 4.75 volts; the latter value represents the closest condition of no cesium coverage on the emitter surface.

There are two problem areas in obtaining electron emission measurements where current densities are low and emitter temperatures high. Low current density measurements are difficult to make since leakage paths are available across cesium-coated ceramics. To eliminate this leakage source, a dc null circuit was employed which voided current leakage over the collector and guard ring insulators. The schematic for this null circuit is shown in Fig. 2-34. All instruments used in the circuit were Sensitive Research meters certified at 0.1 percent accuracy. A point-by-point dc measurement of the test vehicle I-V output was plotted utilizing the null circuit. Figure 2-35 shows three such curves where each point on the curves is a dc, steady-state value read from high accuracy meters.

The second problem in obtaining emission data is accurate temperature measurement of the emitting surface. Identical to all emitter temperature measurements in excess of 1100°C reported from the test vehicle, the temperature was determined by directly viewing a 10:1 depth-to-diameter hohlraum with a micro-optical pyrometer which is periodically calibrated against a NBS standard lamp. For the high emitter temperatures (i.e., 2000°K), the normal transmission loss through the bell jar increases. It was therefore necessary to correct the observed temperature by an additional 8°C to 13°C depending on the temperature.

Table 2-VII summarizes the measurements taken from the emitter at the conditions described. The bottom of the "S" curve is evident from the work function change of only 0.02 volt over a 100°C increase in emitter temperature. Emitter temperatures higher than 2133°C are desirable to complete the picture of a non-cesium-covered value of 4.75 volts; however, higher emitter temperatures may alter the surface structure of the emitter and render the previous pd data and cesiated emission measurements nonreproducible.

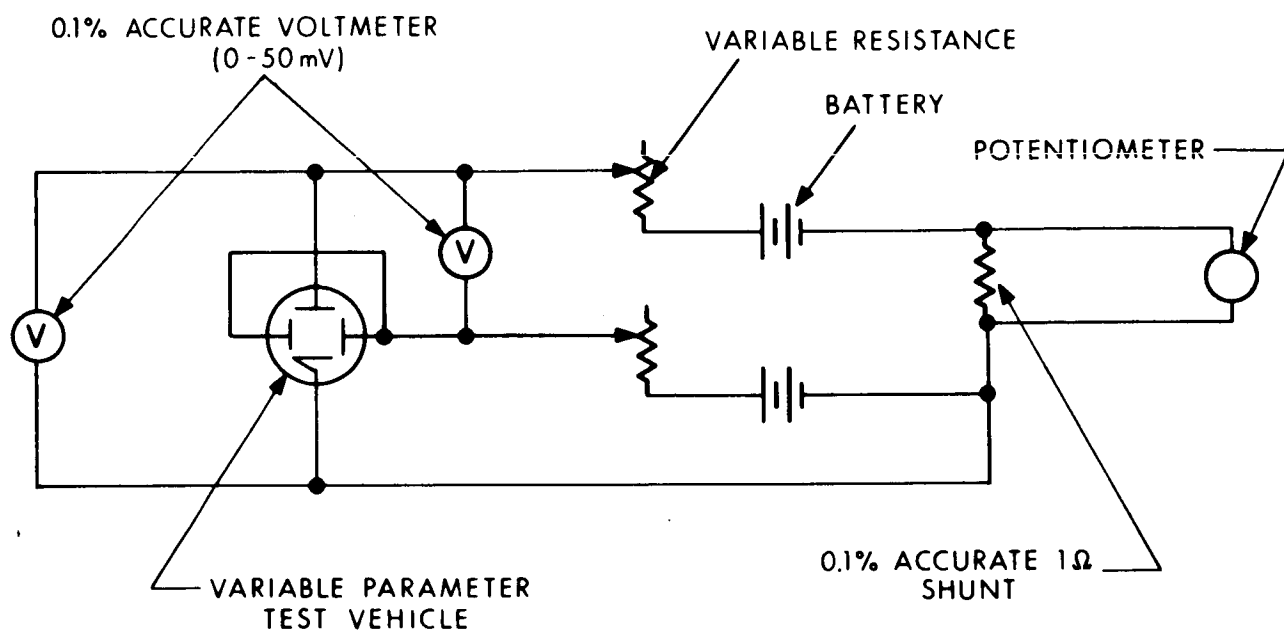


FIG. 2-34 CIRCUIT FOR BARE-WORK FUNCTION MEASUREMENTS

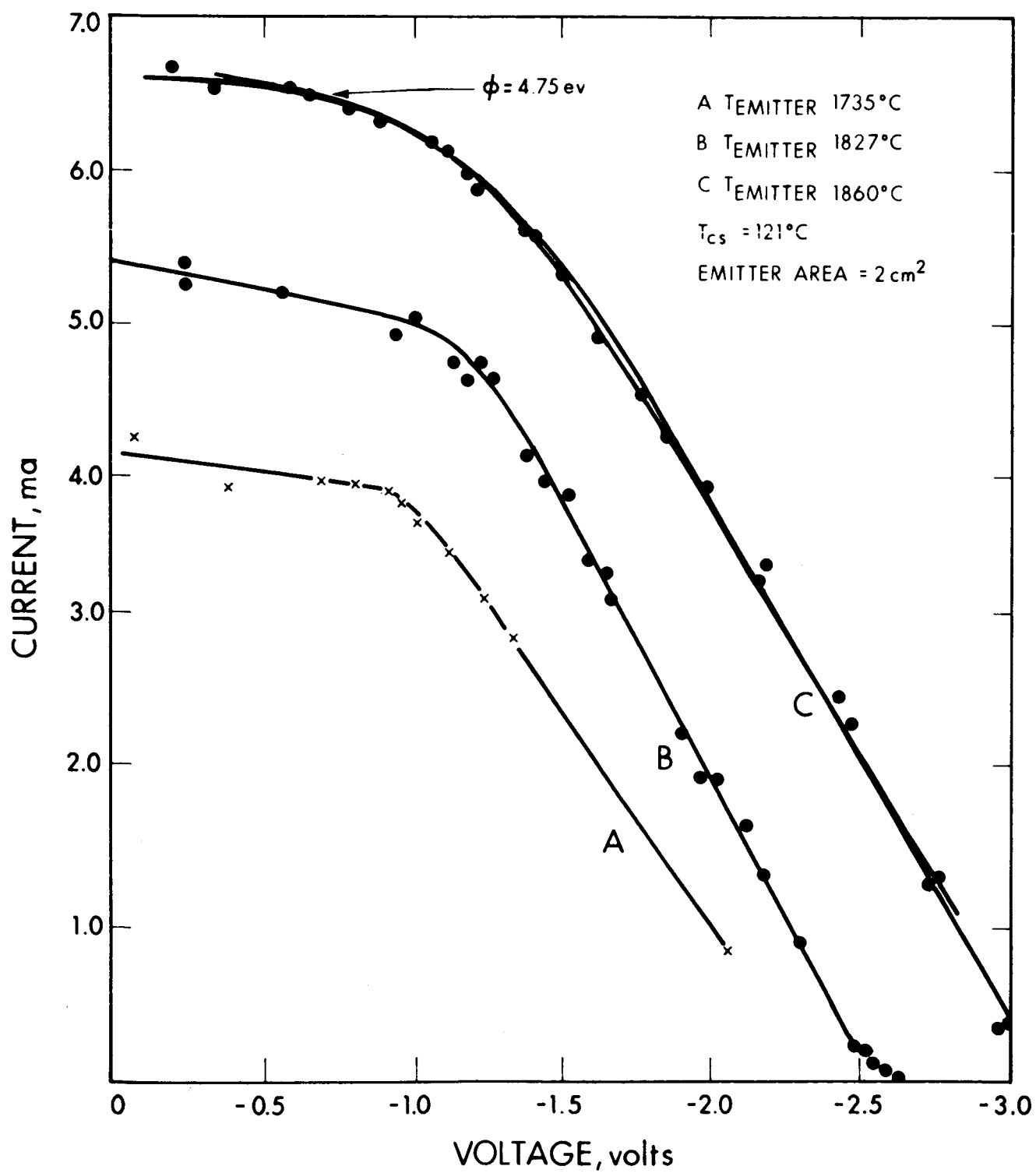


FIG. 2-35 I-V CURVES FOR BARE-WORK MEASUREMENTS (all dc data points)

TABLE 2-VII  
SUMMARY OF BARE WORK FUNCTION MEASUREMENTS

$J_S$ (amp/cm <sup>2</sup> x 10 <sup>-3</sup> )	T(°K)	$\phi$ (volts) A = 120 amps/cm <sup>2</sup> - °K <sup>2</sup>
1.8	1973	4.45
1.85	2008	4.53
2.42	2100	4.55
3.25	2133	4.75

(NOTE: Data taken at a constant cesium reservoir temperature of 122°C.)

Curve B from Fig. 2-35 was plotted on semilog paper to analyze the Boltzmann slope of the I-V curve. Except at the bottommost portion of the curve, where some exponential behavior is apparent, there does not appear to be a true retarding field portion of the curve. This lack of linearity is probably caused by the presence of cesium atoms in the interelectrode spacing which gives rise to collisions. As noted previously, it was not possible to lower the reservoir temperature below 122°C without major structural changes.

The last miscellaneous measurements to be taken from the rhenium-rhenium test vehicle were cesium conduction measurements.

To measure the heat transfer from a thermionic emitter due to cesium vapor conduction requires the detection of small changes in heat input to the emitter. Therefore, it is desirable to reduce or completely omit electron emission from the emitter during the course of these measurements since the heat transfer associated with electron evaporation from an emitting surface may be 10 times that of cesium conduction. The measurements of cesium conduction heat transfer were always taken at a condition of no current flow in the test vehicle.

The procedure for taking cesium conduction measurements is as follows:

1. The emitter temperature is set at  $1735^{\circ}\text{C}$  true; the collector root temperature is set at  $465^{\circ}\text{C}$ ; and an initial interelectrode spacing of some arbitrary value (e.g., 1 mil) is set.
2. The cesium reservoir temperature is set at some initial low value such as  $300^{\circ}\text{C}$ , and the electron bombardment voltage-current is measured for the preset conditions of  $T_E = 1735^{\circ}\text{C}$  (true),  $T_{\text{coll. root}} = 465^{\circ}\text{C}$ , and spacing of 1 mil.
3. Progressively increasing cesium reservoir temperatures are established and the increase in bombardment power to maintain the preset emitter temperature is recorded. The collector root temperature is fixed by a temperature controller which regulates the heater input power to the collector to account for the additional heat input via cesium conduction. Measurements were also taken by decreasing the cesium vapor pressure to reproduce the data.

The sources of possible error in these measurements are: reading accuracy of the meters which is about 0.5 percent, the spacing gages which are accurate to within  $\pm 0.0001$  inch, and thermocouple readings of the reservoir which is a  $\pm 1$  percent Chromel-Alumel thermocouple.

Measurements were made according to the procedure outlined above for interelectrode spacings of 0.2, 0.5, 1, 2, and 3 mils and cesium reservoir temperatures ranging from  $573^{\circ}\text{K}$  to  $700^{\circ}\text{K}$ . In all cases, the collector root temperature was preset and controlled at a constant  $738^{\circ}\text{K}$  while the emitter bombardment power was adjusted to maintain an emitter temperature of  $2008^{\circ}\text{K}$ .

The results of the measurements at the two closest spacings are shown in Table 2-VIII. The cesium reservoir temperatures are shown in the first column and the corresponding cesium vapor pressures in the second column. The vapor pressures were calculated from the equation:

$$\log P_{\text{cs}} (\text{torr}) = 6.91 - (3.80 \times 10^3)/T_{\text{cs}}$$

or

$$\log_{10} P_{\text{mm}} = 11.0531 - 1.35 \log_{10} T(^{\circ}\text{K}) - \frac{4041}{T(^{\circ}\text{K})}$$

TABLE 2-VIII  
BOMBARDMENT POWER REQUIRED FOR  $T_e = 1735^\circ\text{C}$   
AS A FUNCTION OF  $T_{cs}$  FOR INTERELECTRODE SPACINGS  
OF 0.2 AND 0.5 MIL

$T_{cs}$ (°K)	$P_{cs}$ (torr)	$W = 0.2 \text{ mil}$		$W = 0.5 \text{ mil}$	
		$H$ (W)	$\Delta H$ (W)	$H$ (W)	$\Delta H$ (W)
573	1.9	261.9	15.5	257.4	17.5
603	4.1	271.6		271.9	
617	5.5	277.4	10.9	274.9	10.0
741	9.3	282.5		281.9	

The third and fifth columns show the total bombardment power delivered to the emitter to maintain the emitter at  $1735^\circ\text{C}$  at the indicated cesium reservoir temperatures for the spacings of 0.2 and 0.5 mil, respectively. Note that these values represent several power losses in addition to cesium vapor conduction losses and, therefore, their magnitudes are less important than their differences. The power differences between the first and third reservoir temperatures and the second and fourth reservoir temperatures are shown in the fourth and sixth columns. Since each power measurement is made by measuring bombardment current and bombardment voltage with a meter reading accuracy of 0.5 percent, the reading error is about 1 percent in the absolute magnitudes. This results in an error in the differences in power that can be as high as 2.5 watts.

The results of the measurements at the larger spacings are shown graphically in Fig. 2-36. The plotted points are power differences calculated from the measured power levels. Each curve is identified by the interelectrode spacing in mils. The errors in these data points are comparable to those of the close-spacing data of Table 2-VIII, although the relative error is less. The solid lines are calculated from the semiempirical equation determined by Kitrilakis and Meeker (Ref. 4), with the constants shown in the figure.



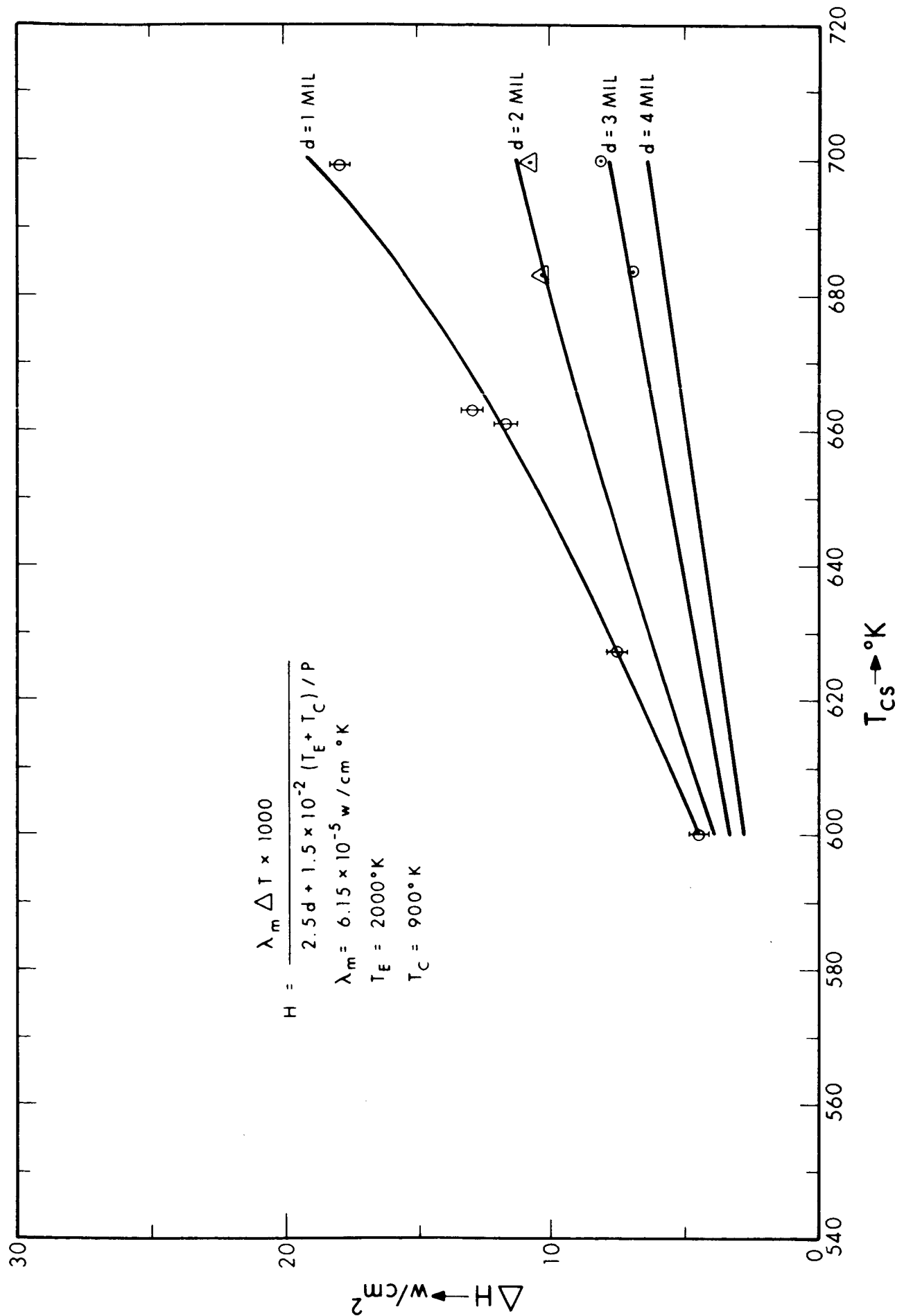


FIG. 2-36 CESIUM CONDUCTION MEASUREMENTS (DATA POINTS) COMPARED WITH SEMI-EMPIRICAL THEORY (SOLID LINES)

Although all the cesium conduction measurements were made at relatively high cesium pressures from about 1 torr to 30 torr, there are two transport regimes represented by the data of Table 2-VIII and Fig. 2-30. The data from the measurements at 0.2 and 0.5 mil spacings indicate a free-molecular transport while those made at the larger spacings indicate transport is occurring in the transition region between free-molecular and mass or viscous flow.

Free molecular heat transport will occur when the cesium mean free path is approximately equal to, or greater than, the interelectrode spacing and is characterized by its independence of spacing. This characteristic is shown by the power differences of Table 2-VIII for the two close spacings. Within experimental error, these differences are identical although the spacings differ by a factor of 2.5. Estimates of the cesium mean free path based on hard-sphere interactions are consistent also with this interpretation. Assuming a cesium diameter of 4 to 7 Å and cesium atom number densities ranging from  $3.2 \cdot 10^{16} \text{ cm}^{-3}$  at the lowest reservoir temperature to  $1.4 \cdot 10^{17} \text{ cm}^{-3}$  at the highest temperature, the mean free path ranges from a maximum of 1.7 mils for the low pressure and smaller diameter to 0.1 mil at the higher pressure and larger diameter. The equation used for these estimates is

$$L (\text{cm}) = (\sqrt{2} \pi \sigma^2 n)^{-1}$$

where

$\sigma$  = hard-sphere diameter

$n$  = number density

For free-molecular transport, the heat flow between parallel plates for monatomic cesium is given by:

$$H = 2 \alpha_e \mu k S (T_e - T_c)$$

where

- $\alpha_e$  = effective accommodation coefficient for heat transfer
- $\mu$  = cesium arrival rate
- $k$  = Boltzmann's constant
- $S$  = area of the plates
- $T_e, T_c$  = emitter and collector temperatures

The arrival rate is calculated by

$$\mu = P_{cs} / (2\pi mkT)^{1/2}$$

where

- $m$  = mass of the cesium atom
- $P_{cs}$  = vapor pressure of cesium in the reservoir

The appropriate temperature in this equation is the temperature at the point where the cesium enters the interelectrode region from the channel connecting this region and the reservoir. For the test vehicle, this temperature is the collector temperature. Using  $T_e - T_c = 1.24 \cdot 10^3$  °K and  $T_c = 760$  °K,

$$H \text{ (watts)} = 3.8 \alpha_e S P_{cs}$$

for  $P_{cs}$  in torr and  $S$  in  $\text{cm}^2$ . The difference,  $\Delta H$ , between the heat conducted at two cesium pressures is

$$\Delta H = 3.8 \alpha_e S \Delta P_{cs}$$

assuming constant  $\alpha_e$  and  $S$ . Using the data of Table 2-IV for the four power differences shown,  $\alpha_e S$  varies from  $0.5 \text{ cm}^2$  to  $1.3 \text{ cm}^2$  with an average of  $0.9 \text{ cm}^2$ . For an area of  $2.4 \text{ cm}^2$ , this indicates the effective accommodation coefficient is 0.4. This result, although based on data with considerable relative error, is consistent with the results of others (Ref. 5) for heat transport in the molecular flow

regime. Since the accommodation coefficient at the low cesium coverages on the emitter at these temperatures and pressures is undoubtedly very close to unity, it is reasonable to conclude that the value 0.4 is characteristic of the collector surface covered by at least one monolayer of cesium.

The data for spacings of 1 mil and larger were not examined completely; within experimental error, it follows the predictions of the semiempirical formulation.

#### 2.2.6 VPTV Investigation of the Rhenium Emitter/Molybdenum Collector System

A second variable parameter test vehicle, similar to the first, was assembled to investigate the thermionic performance of a rhenium emitter/molybdenum collector system. A second vehicle was constructed rather than cutting apart the rhenium-rhenium device, since it is estimated that at least 1000 to 2000 hours more of test time are available in the first vehicle for characterizing the low-temperature behavior of the rhenium-rhenium system.

The rhenium-molybdenum test vehicle contained only one major structural change: The guard-ring was secured by vertically positioned screws to the collector root rather than horizontally into the collector barrel. The same techniques of fabrication and processing were applied to both vehicles.

It was predicted that the same shape of voltage-spacing curves would be observed and that the  $pd$  product for maximum power output would be identical within experimental determination. The major expected difference between the two systems of electrodes was the voltage output for equivalent conditions of temperature and current load. The cesium-on-molybdenum system yields a minimum work function of 1.55 eV as compared to the cesium-on-rhenium system which yields 1.47 eV. Therefore, the voltage versus spacing curves for rhenium-molybdenum would be similar but displaced by approximately 0.080 volt. Likewise,

the converter optimization data for the rhenium-molybdenum system would indicate less performance output by 0.080 volt for current densities on the order of 30 amperes/cm<sup>2</sup>.

The paragraphs that follow reveal the interesting nature of a nonidentical electrode system wherein work function changes on the collector surface were observed and measured. Spacing versus voltage output data was taken for the rhenium-molybdenum system and a hybrid system of rhenium-rhenium/molybdenum deliberately created by vacuum evaporation of rhenium from the emitter onto the collector. Converter optimization data was obtained at 0.8V, 0.7V, and 0.6V.

#### 2.2.6.1 Voltage-Spacing Relationships for the Rhenium-Molybdenum System

The first data obtained from the rhenium-molybdenum test vehicle is shown in Fig. 2-37, where the rhenium-rhenium data for identical test conditions is shown as the dotted curve. That the performance was near-identical suggested that a small amount of rhenium might have been evaporated onto the collector surface during terminal exhaust processing prior to cesium loading. Referring to the process data sheets, it was ascertained that the emitter had operated at 1800°C for 12 hours. An elementary calculation based on vacuum evaporation weight losses indicated that three angstrom layers were evaporated from the emitter and, assuming an accommodation coefficient of unity on the collector surface, condensed on the collector.

The lifetime of this performance was limited and within 7 hours of operation the voltage output was reduced by 10 to 15 millivolts. This reduction continued during further operation until after 33 hours, the voltage output versus spacing curve appeared as shown in Fig. 2-38. The collector surface thermocouple being operable in this vehicle afforded an accurate measure of the collector work function, which was determined to be 1.51 to 1.53 eV. It was reasoned that the initially evaporated rhenium had diffused into the molybdenum (bulk diffusion) or around the molybdenum (surface diffusion).

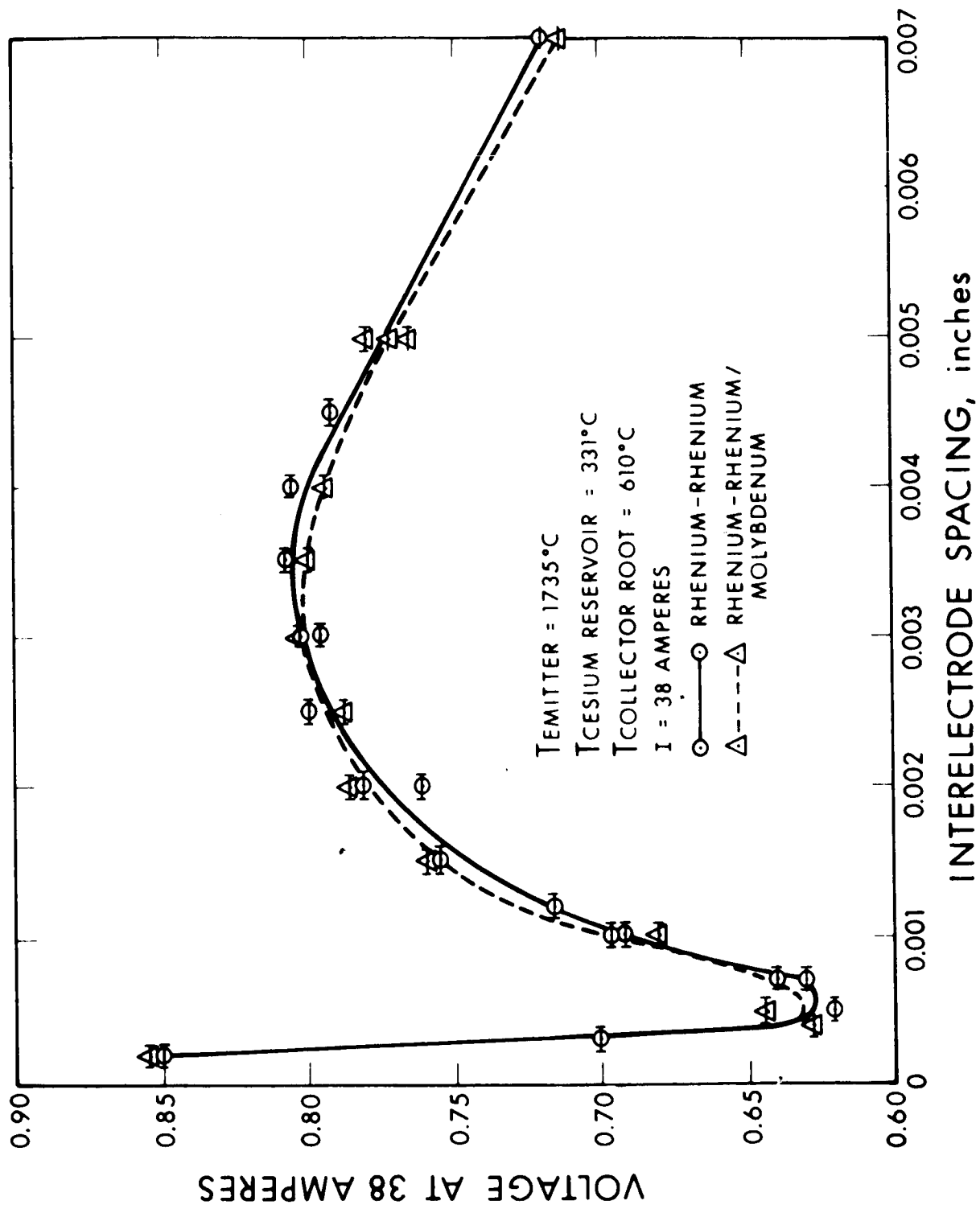


FIG. 2-37 COMPARISON OF VOLTAGE OUTPUT VERSUS INTERELECTRODE SPACING FOR RHENIUM - RHENIUM AND RHENIUM-RHENIUM/MOLYBDENUM ELECTRODE SYSTEM

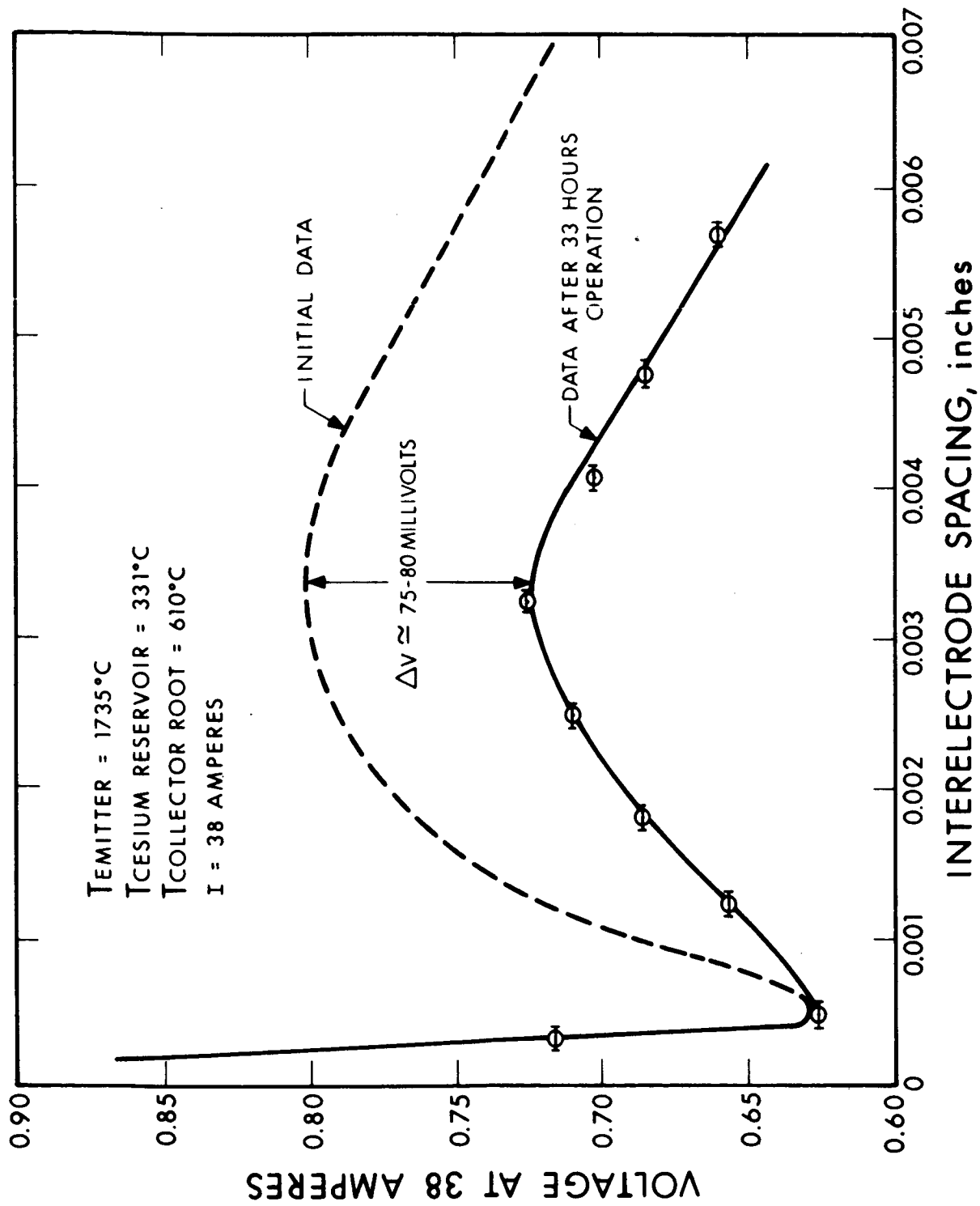


FIG. 2-38 VOLTAGE OUTPUT VERSUS INTERELECTRODE SPACING FOR RHENIUM - RHENIUM/MOLYBDENUM ELECTRODE SYSTEM

In either case, the rate of diffusion is highly dependent upon the collector surface temperature. The length of time required to deplete the surface would depend upon the initial amount present on the surface, the rate of diffusion, and the rate of replacement from the emitter. Since there is almost an absolute lack of diffusion data for these systems, and particularly for thin coatings, it was felt that the balance of data taking should be conducted on stable surfaces to eliminate possible concern that the test vehicle itself was failing or that the drive mechanism had become faulty. The collector surface was therefore replenished with evaporated rhenium from the emitter operating at  $2100^{\circ}\text{C}$  with the cesium reservoir heaters secured. The collector work function, after this processing, was determined to be 1.45 to 1.43 eV which agrees quite well with the work function determinations from the rhenium-rhenium test vehicle. The average difference of 0.080 volt from these successive measurements also corresponds to the voltage output lost in the spacing-voltage curves. This same phenomenon was later observed in a rhenium-molybdenum thermionic converter wherein the converter optimization data for both the rhenium-molybdenum and rhenium-rhenium/molybdenum systems was carefully documented and once again, a difference of 0.080 volt in performance output was noted (see Section 5).

Before proceeding to the converter optimization data, a voltage output versus spacing curve was obtained for 38 amperes fixed current level and the initial data of the test vehicle was reproduced within 3 to 4 millivolts throughout the entire range of spacing. In addition, a voltage-spacing curve at 60 amperes was obtained which reproduced Fig. 2-27 within 5 millivolts over the entire spacing range from 0.0002 inch to 0.009 inch. These data further substantiated the rhenium nature of the collector surface after the evaporation process.



#### 2.2.6.2 Converter Optimization Data for the Rhenium-Rhenium/Molybdenum System

As the title of this section implies, the system of electrodes contained a molybdenum collector which had received an evaporated coating of rhenium from the emitter. Moreover, this was done to stabilize the process of data taking as just discussed. Figure 2-39 is a composite plot of the 0.8V, 0.7V, and 0.6V optimum performance from the rhenium-rhenium/molybdenum system for an emitter temperature of 1735°C (true hohlraum). The optimum data from the rhenium-rhenium system is plotted for comparison. The only discernible difference between the two systems is the location of the optimum reservoir, which for all other conditions of operation equivalent, is shifted 3°C to 4°C higher. While there may be some physical significance to this shift, a value of 3°C to 4°C is certainly within  $\pm 0.5\%$  error of the total reading — an acceptable limit for thermocouple response. Moreover, the location of the reservoir thermocouple junctions on the two test vehicles could vary a sixteenth inch and account for small differences in temperature readings.

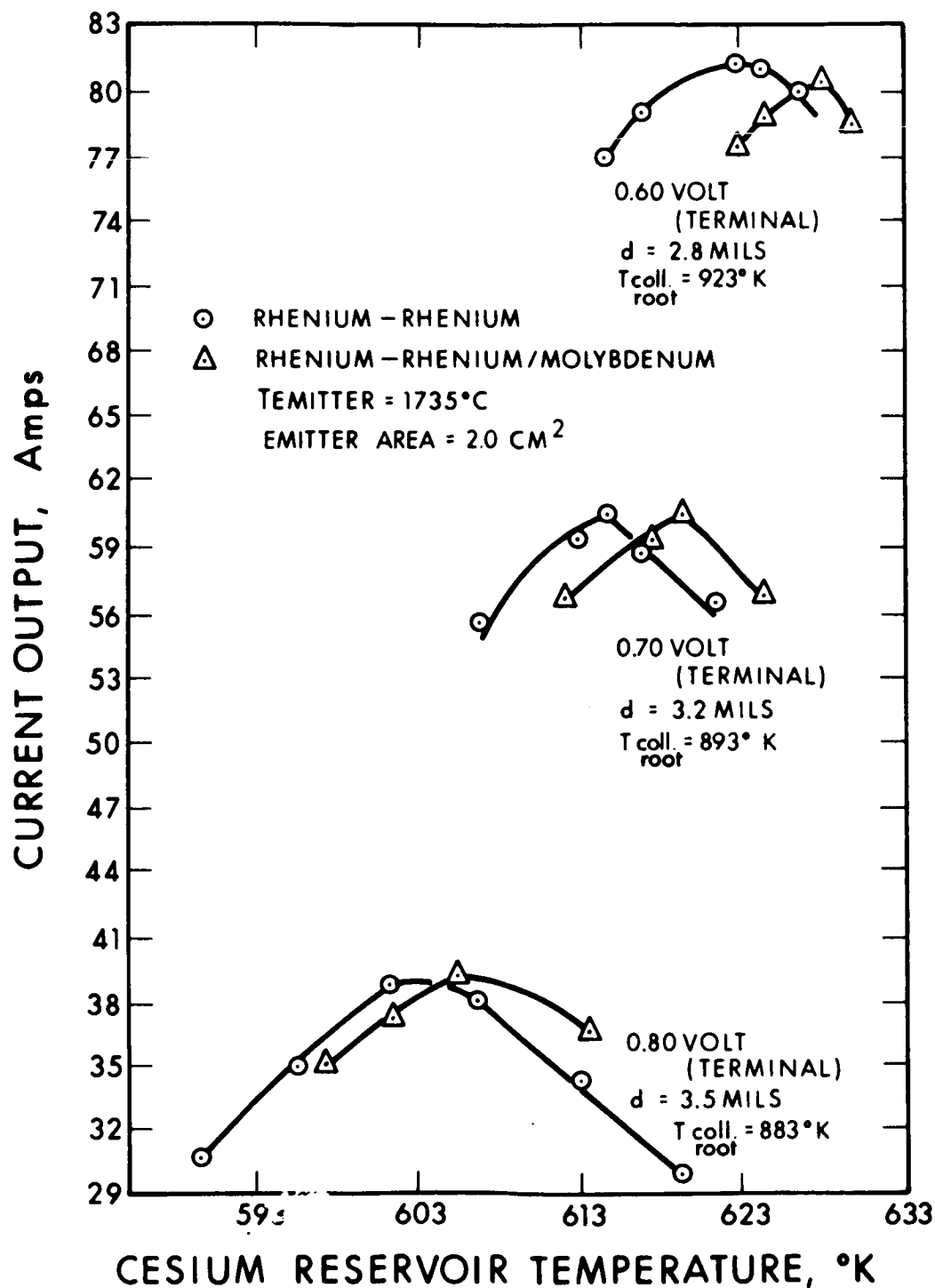


FIG. 2-39 COMPOSITE PLOT OF OPTIMUM CONVERTER PERFORMANCE  
 FOR RHENIUM-RHENIUM/MOLYBDENUM ELECTRODE SYSTEM  
 (rhenium-rhenium plotted for reference)

### 3. SECONDARY EXPERIMENTS SUPPORTING CONVERTER TECHNOLOGY

#### 3.1 Heat Transfer/Heat Rejection Investigation

##### 3.1.1 Rokide "C" Emittance Investigation

The coating material most frequently applied to converter radiators for efficient heat rejection has been Rokide "C", a chromium oxide composite that has been reported (Ref. 6) to have a total emittance as high as 0.9. In addition to their high emittance, Rokide "C" coatings have been reported to be structurally stable at temperatures as high as 1200°C (Ref. 7). However, converter users have observed the deterioration of Rokide "C" on several converter radiator extended life tests of 8,000 hours and longer. There is also a wide spread in reported data concerning the emittance of Rokide "C" which has led to an uncertainty in converter design. An investigation was therefore undertaken to study the structural stability of Rokide "C" on copper and molybdenum substrates and to measure the total emittance of Rokide "C" as a function of operating time, coating thickness, and substrate material.

##### 3.1.1.1 Stability of Rokide "C" Coated Molybdenum

A molybdenum rod was coated with Rokide "C", instrumented with Chromel-Alumel thermocouples for temperature measurement, and mounted on a refractory fixture for extended operation at temperatures of 600°C. Figure 3-1 is a sketch of a coating specimen showing the coated and uncoated portions and the thermocouple locations. Measurements of the rod diameter were taken before plasma spraying and were compared with the measurements of the rod diameter after plasma spraying to determine the Rokide thickness. The thickness of Rokide was determined to be  $0.0025 \pm 0.005$  inch. To provide a reproducible coating schedule, close documentation of the plasma spraying procedure was maintained.

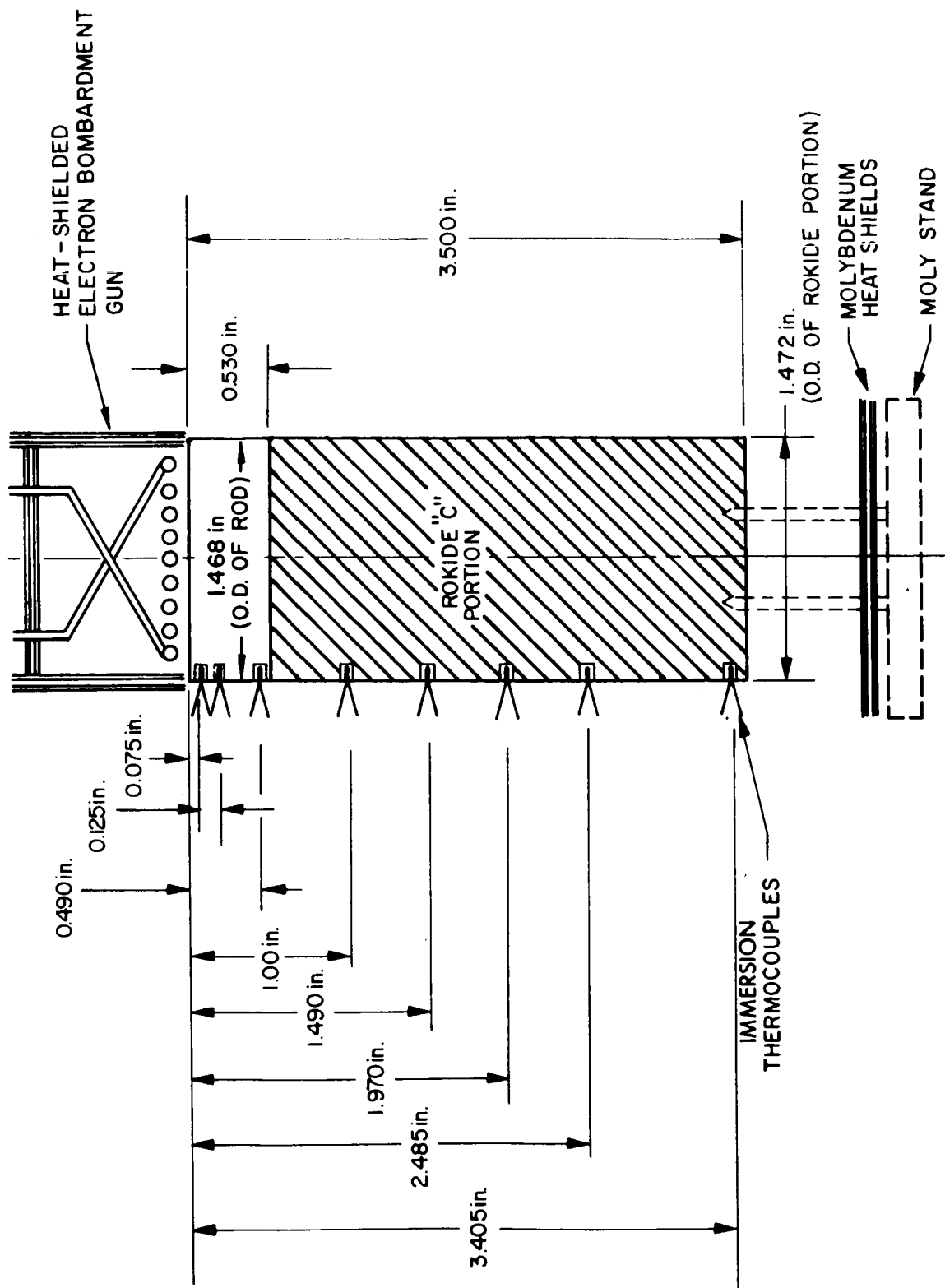


FIG. 3-1 THERMOCOUPLE LOCATIONS AND SAMPLE DIMENSIONS OF MOLYBDENUM-ROKIDE "C" EXPERIMENT

The sample was heated to 600°C by electron bombardment in a vac-ion pumped environment of less than  $5 \times 10^{-8}$  torr for 500 hours. The physical appearance of the coating did not change during this period of time. There was no peeling, blistering, or cracking of the Rokide even though a number of rapid thermal cycles (greater than 30) occurred during test. Figure 3-2 is a photograph of the sample after test. Ceramic-sheathed couples facing the Rokide showed no evidence of discoloration which would be indicative of coating deterioration. The electron bombardment input power remained constant (as did the sample temperature distribution) during the 500 hours of operation.

The bell jar used for this test was calibrated against a standard tungsten ribbon filament lamp before any testing of the sample. It was again calibrated at 210 hours and at 492 hours. This was done to determine what increase in light transmission losses could be expected due to prolonged periods of testing. After 500 hours of operation, there was only a slightly noticeable coating on the test bell jar. Table 3-I shows the increase in transmission losses at three different times during the test run. There is no evidence that the slight jar discoloration was due to heating of the Rokide sample, but it appeared to have been caused by the evolution of material from some of the stainless steel fittings inside the bell jar which normally operate at 200-300°C during test.

TABLE 3-I  
BELL-JAR TRANSMISSION LOSS AS A FUNCTION OF TEST TIME  
DURING ROKIDE "C" STABILITY EXPERIMENT\*

Increase in Transmission Loss (Bell-Jar Surrounding Std. Lamp)			Test Time (Hours)
<u>1000°C</u>	<u>1600°C</u>	<u>1700°C</u>	
0°C	0°C	0°C	0 hours
3°C	10°C	10°C	210 hours
4°C	15°C	19°C	492 (final)

\*Most likely caused from steel fittings in vacuum station operating at 200-300°C

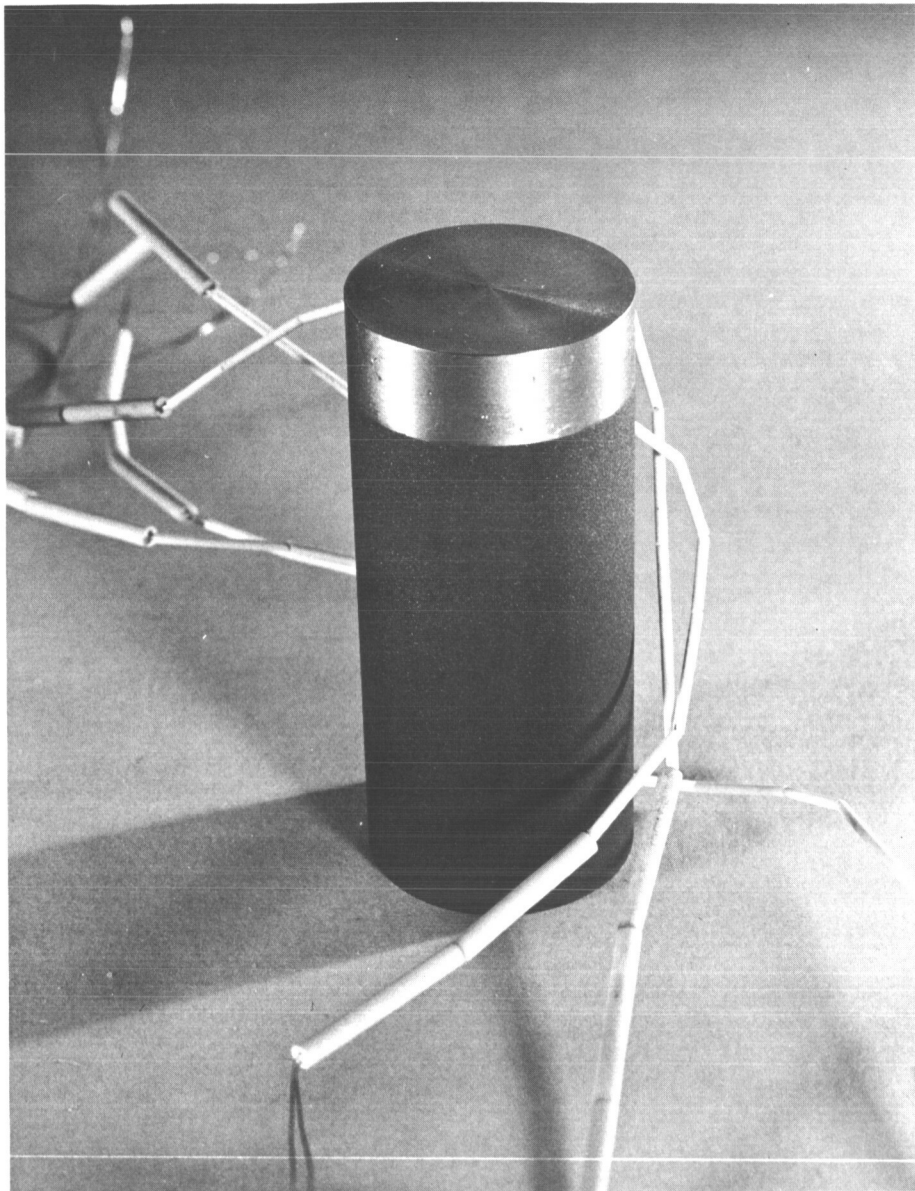


FIG. 3-2 ROKIDE "C"-COATED MOLYBDENUM SAMPLE AFTER 500 HOURS OF OPERATION (Note: the alumina tubes facing the Rokide coating are not discolored)

### 3.1.1.2 Rokide "C" Emittance Measurements

On several occasions during the 500-hour test of the Rokide "C" coatings, the power to the sample was interrupted and the sample was permitted to cool to room temperature. Since the sample mounting arrangement prevented significant heat losses by heat conduction, the major heat rejection during cooling was by radiation. The rate of temperature decrease was dependent, therefore, upon the radiative properties of the sample surface. A comparison of temperature-time cooling curves taken at various stages of the 500-hour test indicated that the radiative properties of the sample surface, i.e., the emittance of the surface, did not alter during the test period. The cooling curves taken at the beginning of the test and after approximately 500 hours, shown in Fig. 3-3, are identical within experimental error. This confirms the visual evidence discussed in the preceding section for the stability of the Rokide "C" coating at temperature.

Each time the power to the sample was turned off to observe the cooling curves, the temperatures indicated by all thermocouples attached to both the uncoated and coated surfaces became identical within about 8 seconds. This time interval is small compared to the total cooling period. The small differences in initial temperatures caused by the asymmetric sample heating arrangement essentially were eliminated during the cooling period, and it is possible to describe the cooling curve by

$$mC_p (dT/dt) = - [\epsilon_R A_R \sigma T^4 + \epsilon_M A_M \sigma T^4] \quad (3-1)$$

where

m = mass of the sample

C<sub>p</sub> = specific heat at constant pressure

T = sample temperature

t = time

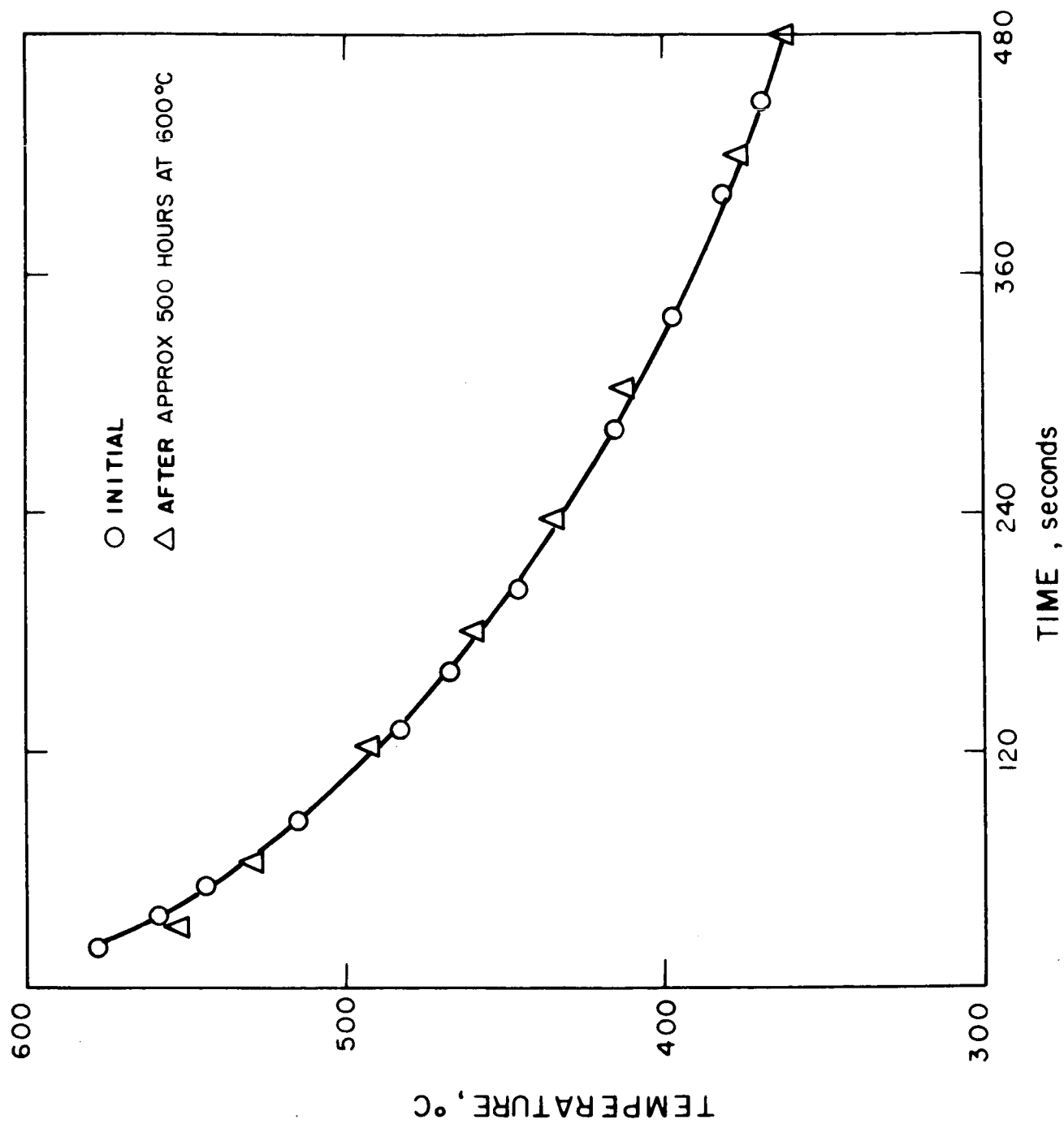


FIG. 3-3 COOLDOWN CURVES OF ROXIDE "C"-COATED MOLYBDENUM SAMPLE



$\epsilon_R$  = Rokide "C" emittance  
 $A_R$  = area of the Rokide "C" coating  
 $\epsilon_M$  = molybdenum emittance  
 $A_M$  = area of the bare molybdenum  
 $\sigma$  = Stefan-Boltzmann constant

Over the small temperature range covered by the cooling curves of Fig. 3-3, it is reasonable to assume (Ref. 8) that  $C_p$ ,  $\epsilon_R$ , and  $\epsilon_M$  are independent of temperature. With this assumption, Equation 3-1 can be integrated and solved for the emittance of the Rokide "C" coating,  $\epsilon_R$ :

$$\epsilon_R = \frac{mC_p}{3\sigma A_R (t_f - t_i)} \left[ \frac{1}{T_f^3} - \frac{1}{T_i^3} \right] - \epsilon_M \frac{A_M}{A_R} \quad (3-2)$$

where the subscripts i and f refer to the initial and final values, respectively. From Fig. 3-3, for  $t_i = 60$  sec and  $t_f = 480$  sec,  $T_i = 803^\circ\text{K}$  and  $T_f = 633^\circ\text{K}$ . Using  $\epsilon_M = 0.2$  (Ref. 7)  $\epsilon_R = 0.79$ . This value of the emittance of Rokide "C" is about 10 percent lower than values generally quoted. This indicates that, in practice, an increase in radiator area of approximately 13 percent is required to give the same heat rejection as that computed using the cited data for Rokide "C" emittance. In the design of the converters of this program, this difference was considered and is discussed in the section on converter design.

#### 3.1.1.3 Rokide "C" Coated Molybdenum versus Rokide "C" Coated Copper

A copper rod, with dimensions similar to those of the molybdenum rod just described, was coated with Rokide "C", using the same process schedule and achieving the same coating thickness. The sample was instrumented with thermocouples, placed in a vac-ion pumped test chamber, and heated by electron bombardment to determine the Rokide coating emittance and stability for 500 hours of operation. Initial and final cooldown curves, shown in Fig. 3-4, were

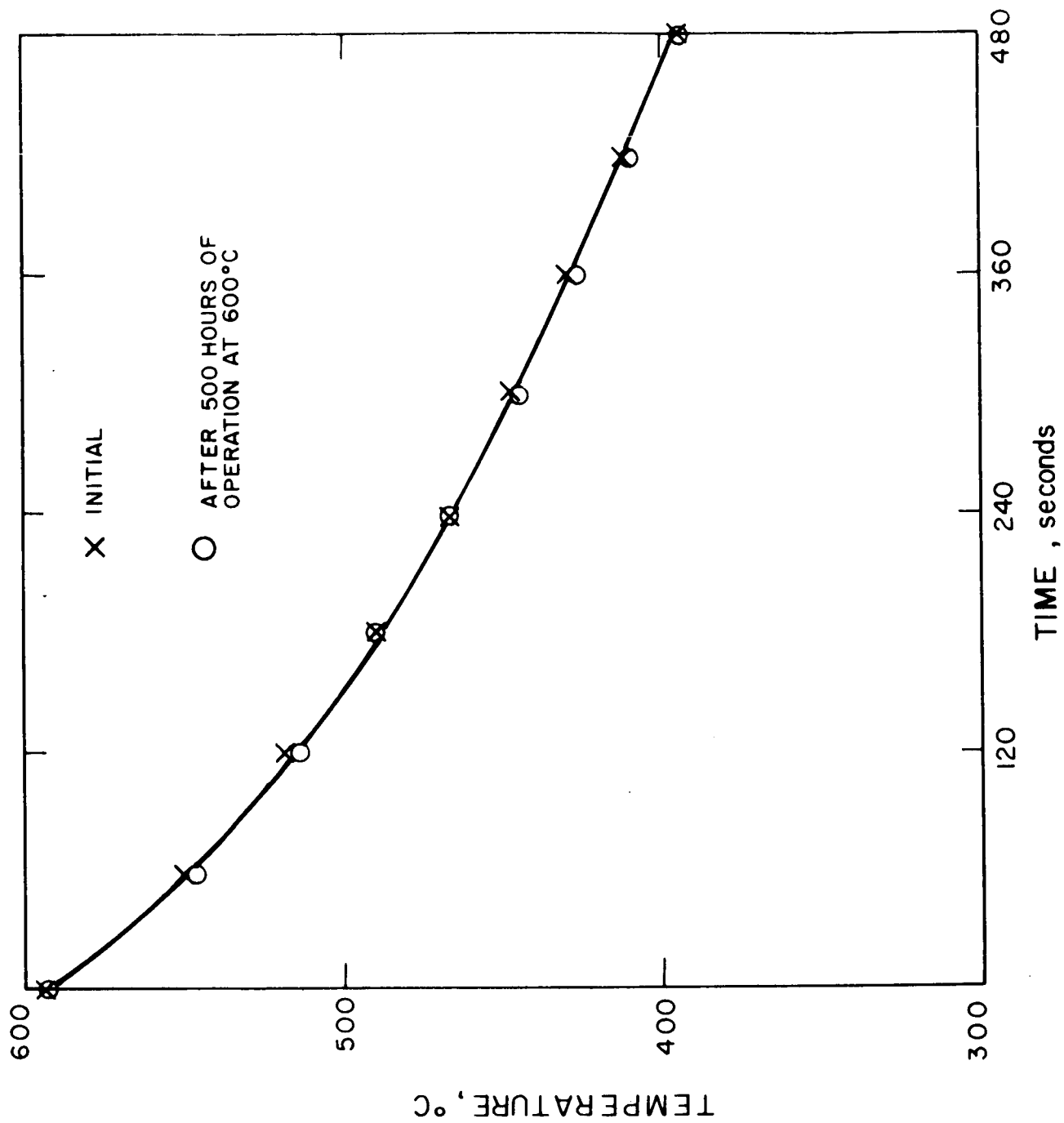


FIG. 3-4 COOLDOWN CURVES OF ROXIDE-COATED COPPER SAMPLE

analyzed in the same manner as just described for the Rokide-molybdenum curves. The value for Rokide "C" on copper is identical with that of Rokide "C" on molybdenum (i.e.,  $\epsilon \approx 0.78$ ).

No degradation of the coating on copper occurred over an extended test period of 500 hours operation at 600°C. The sample was rapidly thermal cycled some 30 times during test; however, no scaling, blistering, cracking, or peeling occurred. Moreover, the invariance of the cooldown curves over the 500-hour period attests to the coating stability. A slight haze, similar to that which appeared during the Rokide-molybdenum experiment, formed on the bell jar surface, which resulted in a transmission loss of the same order.

To insure that the coating thickness of 2.5 to 3.0 mils was adequate for achieving the maximum emittance value of Rokide "C", the molybdenum sample was stripped of thermocouples and resprayed using the same process schedule for an overall coating thickness of 7 mils. New couples were attached and the resulting sample was operated again at 600°C. The identical nature of the coatings is best described as follows.

1. The identical sample temperature distribution was measured for the identical power input (filament plus bombardment).
2. An identical cooldown curve, point for point, was measured along the entire time axis.

### 3.1.2 Nonintegral Collector-Radiator Investigation

The 1964 EOS production prototype converter contained an integral collector-radiator which was die-forged from molybdenum bar stock. The major advantages of the molybdenum integral collector-radiator are: (1) a continuous heat transfer path unimpaired by any braze interface or similar thermal impedances, (2) a mass-production technique for fabrication, and (3) a mechanically strong, high-temperature structural member. The sole disadvantage of the forged molybdenum collector-radiator is a lower specific performance compared

to materials such as copper, which due to their higher thermal conductivity have a reduced fin weight for equivalent radiator heat rejection capability.

An investigation was initiated which pertained to the problems of reliably bonding a molybdenum collector to a copper radiator for use at high heat rejection rates under thermal cycling conditions. The scheme shown in Fig. 3-5 was selected to evaluate a braze joint design which captivated the copper radiating fin so that the thermal expansion mismatch between the copper and the molybdenum always kept the copper part in compression. Shim-stock Nioro braze material (82 percent gold - 18 percent nickel) 0.002 inch thick was inserted in the slot on either side of the copper. Nioro wire (0.030 inch diameter) was placed at the copper-molybdenum interface on either side of the fin. The assembly was vacuum brazed at 925°C, the melting point of Nioro. This resulted in a braze fillet that contained no voids or cracks. As indicated in Fig. 3-5, the assembly is dimensioned to permit simulation of actual converter operation at thermal fluxes through the bonded area on the order of 200 to 250 watts. Over 100 cm<sup>2</sup> of copper radiator were Rokided to provide ample heat dissipation area for the experiment. The molybdenum portion of the assembly is an integrally forged part in which the mounting holes and braze joint were machined.

For the simulated thermal tests, the assembly was mounted in a vacuum bell jar and heated indirectly at the collector end by electron bombardment. Thermocouples were attached at several locations on either side of the braze interface to measure the temperature drop across the joint for various thermal loads. An average temperature difference of 5°C was measured across the braze joint for a thermal flux of approximately 210 watts. The heat load was computed using an EOS-measured value of 0.78 for the total emissivity of Rokide "C" at a measured radiator spade temperature of 520°C.

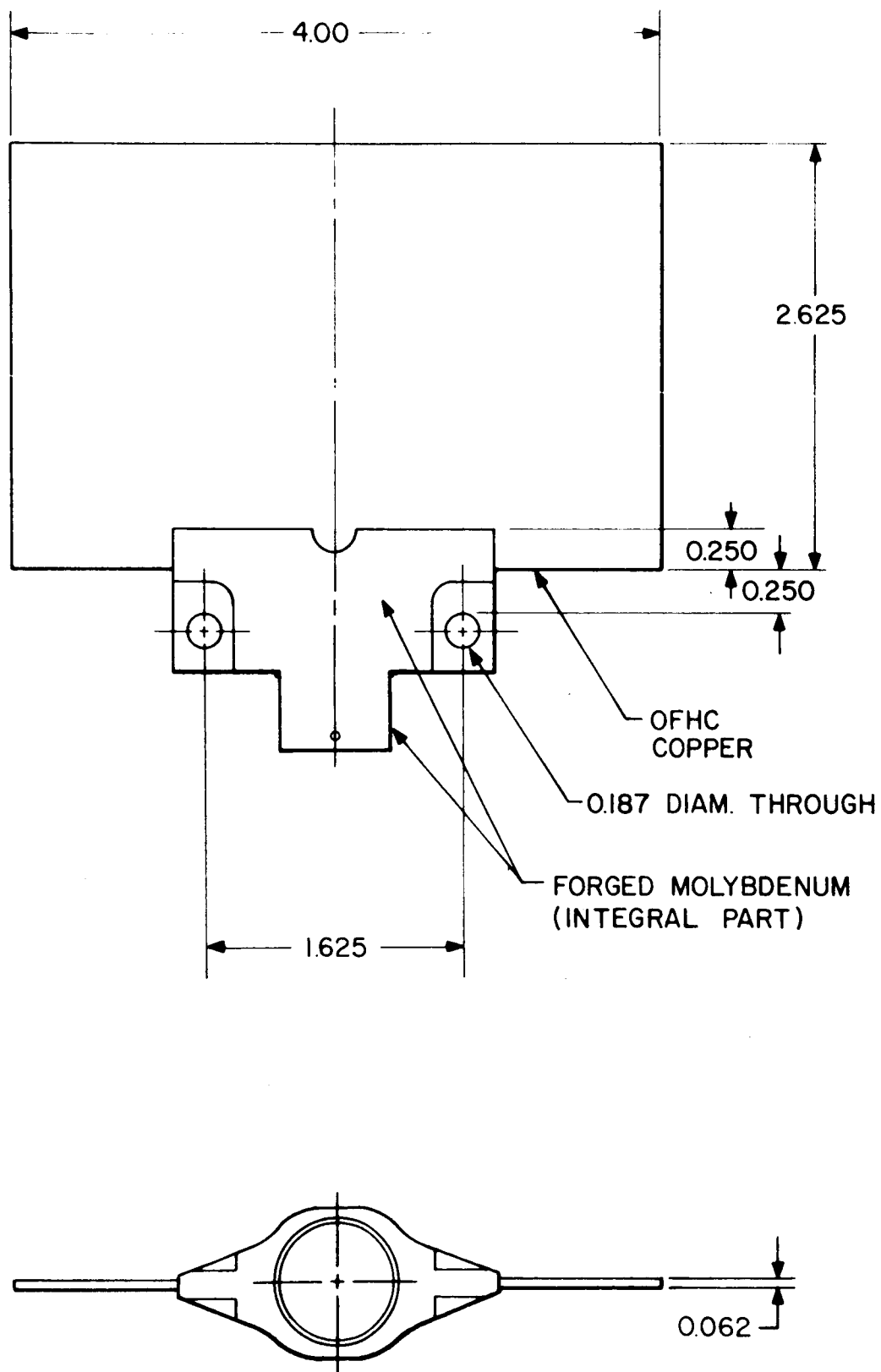


FIG. 3-5 NONINTEGRAL COLLECTOR-RADIATOR ASSEMBLY

After the initial temperature measurements, the bond between the copper and molybdenum was subjected to 329 thermal cycles from 600°C to 200°C. The thermal cycle consisted of the application of an on-off thermal load of 210 watts where the structure was allowed to come to equilibrium at 600°C at which time the input was shut off and the structure allowed to decay in temperature to 200°C. The temperature rise and fall rate was limited solely by the basic constants of the system. Throughout the series of thermal cycle tests, the measured temperature drop remained 5°C across the bonded interface. In addition, no peeling, cracking, or blistering of the Rokide "C" coating occurred. It was concluded that the braze joint results in a high quality thermal bond and performs reliably under severe test conditions.

The weight of the entire assembly is 220 grams, as compared to 230 grams for an integral molybdenum collector-radiator. Therefore, for approximately the same weight, the amount of heat rejected is almost double that of the all-molybdenum EOS production converter collector-radiator which dissipated about 120 thermal watts.

### 3.1.3 L/A Design Curves for Collector " $\Delta T$ "

The collector heat load in a thermionic converter may be calculated by summing the individual contributions of electron heating, net radiation heat transfer from emitter to collector, and the conduction heat transfer from cesium atoms, i.e.

$$Q_{\text{collector}} = Q_{\text{eh}} + Q_{\text{rad}} + Q_{\text{cs. cond.}}$$

The first term, electron heating, may be written as:

$$Q_{\text{eh}} = I \left( \phi_{\text{coll}} + \frac{e k T_{\text{pl}}}{e} \right) \quad (3-3)$$

since the drift electrons dissipate the energy acquired by falling through the potential of the collector work function plus random potential energy in the plasma. The value of  $\epsilon$  is chosen such that  $1.3 \leq \epsilon \leq 1.5$  depending on the plasma electron energy distribution (see Appendix B). The value of  $T_{pl}$  is selected to be  $6000^\circ\text{K}$ . The collector work function of cesium on molybdenum,  $\phi_{coll}$ , has been measured at 1.55 eV. Therefore, the electron heating contribution is

$$Q_{eh} = I(2.2)$$

where  $I$  is the drift current or external circuit current from an operating current.

The second term, net radiation heat transfer from emitter to collector, is

$$Q_{rad} = \epsilon_{eff} \sigma (T_{em}^4 - T_{coll}^4) \quad (3-4)$$

where  $\epsilon_{eff}$  is the effective emissivity of electrode system.

$$\epsilon_{eff} = \frac{1}{\frac{1}{\epsilon_{em}} + \frac{1}{\epsilon_{coll}} - 1} \quad (3-5)$$

The net radiation heat transfer for  $T_{em} = 2,000^\circ\text{K}$ ,  $T_{coll} = 1,100^\circ\text{K}$ ,  $\epsilon_{em} = 0.3$ , and  $\epsilon_{coll} = 0.25$ , and for two square centimeters of area is

$$Q_{rad} = 26 \text{ watts}$$

The last term, cesium conduction, has been experimentally determined to be

$$Q_{cs} = 16 \text{ watts}$$

The sum of these contributions is substituted into the heat conduction equation, and  $\Delta T$ 's (temperature differences between collector surface and collector root) are computed for various converter current loads. Figure 3-6 is a plot of this  $\Delta T$  as a function of the converter current with the collector L/A ratio as the parameter. Actually, the collector cross-sectional area, A, is fixed by design to accommodate a 2.0 cm<sup>2</sup> emitter area. To define the emitter area without drawing current from the emitter support structure (envelope), it is necessary to provide 0.010 to 0.012 inch spacing between the envelope and collector. The collector area, A, is therefore 1.9 cm<sup>2</sup>.

Consequently, at the design point of 50 amperes of current flow, a collector barrel length of 0.6 inch results in a temperature drop of 110°C. It is important to note that any slotted or stepped portions in the collector barrel increase the thermal impedance since the lines of heat flux are disturbed and do permit a simple, linear treatment.

### 3.2 Feasibility Experiments Related to Converter Fabrication

#### 3.2.1 Converter Seal-Off

An experimental investigation was concluded which established the necessary procedures for effecting a highly reliable converter seal-off. Copper tubulation seal-offs performed in the past with hand-operated pinch-off tools have always been vacuum tight, but some were of marginal quality.

The seal-off operation is performed with a pinch-off tool which applies pressure sufficient to cold-weld the converter reservoir tubulation. A cold-weld may be leak tight and have the external appearance of being a good pinch-off, but in microsection, the actual sealing area may be only about 0.001 inch. A pinch-off such as this is considered marginal since it cannot suffer any accidental damage in the pinch-off area without loss of the vacuum seal on the converter.



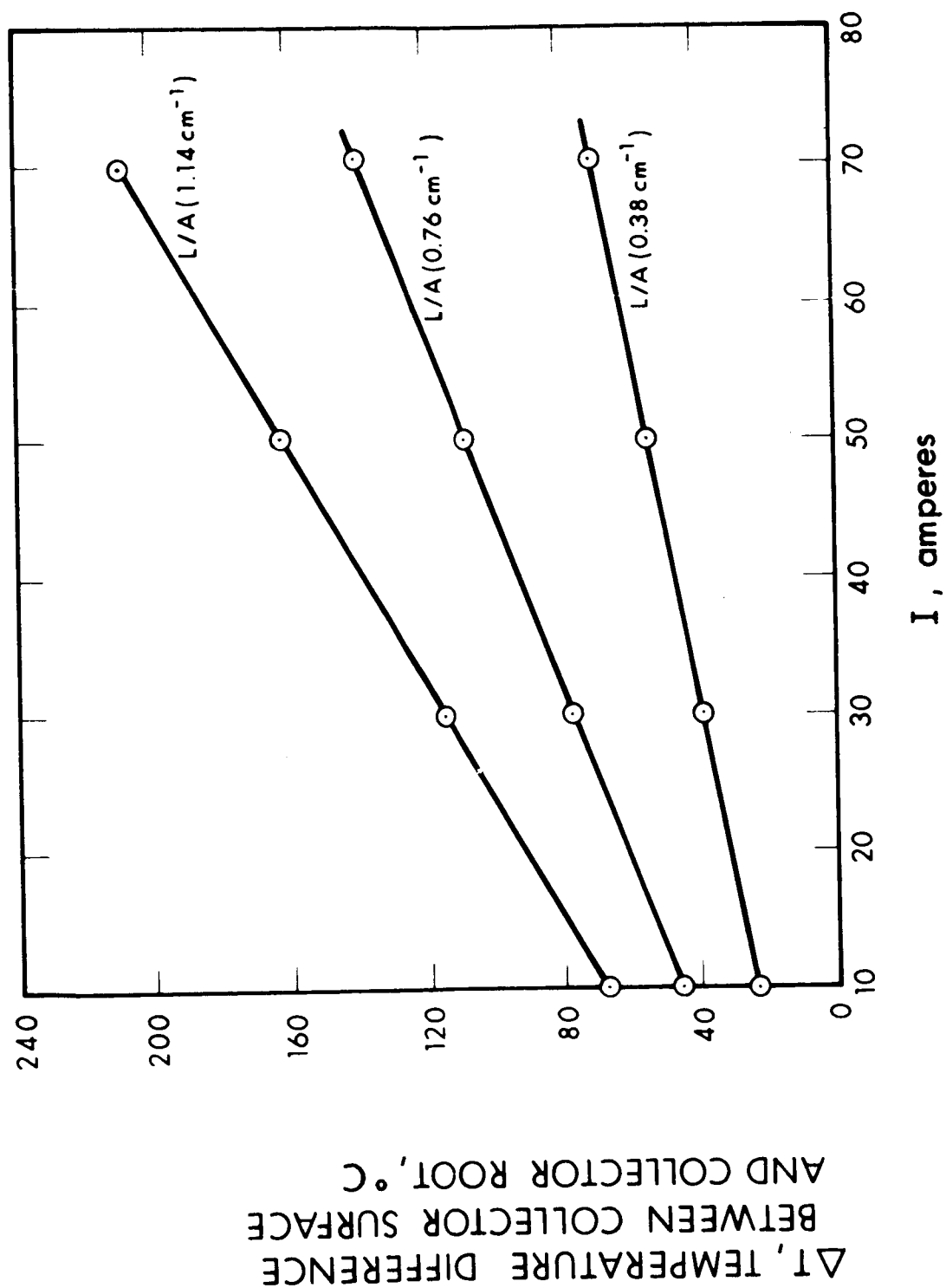


FIG. 3-6 THERMAL DESIGN CURVES FOR MOLYBDENUM COLLECTOR

Six pinch-offs were made with two different hand tools (Varian and Kane). The pinch-offs were then cross-sectioned, and examined for seal thickness. Of the six pinch-offs, only one had a seal thickness greater than 0.005 inch, the rest were 0.001 inch or less. Figures 3-7 and 3-8 show micro-sections of these marginal seals. In general, the hand tools required continuous adjustment to insure that the rollers mated properly. The rollers, though case-hardened, require periodic replacement. Moreover, the actual pinch operation using a hand tool is dependent upon the steadiness and skill of the operator.

Six additional pinch-offs were made from the same length of sample tubing. The tool used for these pinch-offs was a Kane hydraulic tool having 1/4-inch and 1/8-inch diameter, fully hardened tool-steel rollers. All pinch-off samples were examined for seal thickness and were found to vary between 0.006 inch and 0.009 inch with no preference for roller diameter (Figs. 3-9 and 3-10). The hydraulic tool requires only initial adjustment and occasional readjustment; the rollers appear to be capable of lasting almost indefinitely and the pinch-off operation proceeds with a smooth stroke, independent of operator skill or experience.

A few general observations on pinch-off procedures are outlined below which, if followed, should lead to consistent, highly reliable OFHC copper tubing pinch-offs.

1. The copper (OFHC) must be first chemically cleaned to remove all contamination induced by mill handling.
2. The copper must be annealed (after chemical cleaning) in a high-vacuum environment at temperatures in the 700°C area for 1/2 hour.
3. The pinch area should be preflattened with a flattening tool and re-annealed.
4. The pinch-off rollers or jaws should be made of fully treated tool steel and they should be periodically checked for evidence of warpage or misalignment.

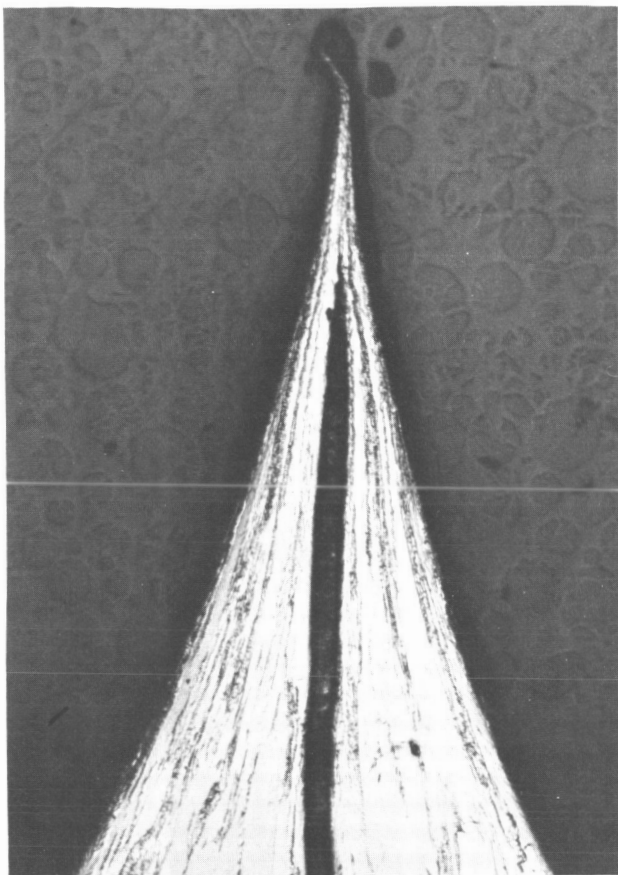


FIG 3-7

ANNEALED OFHC COPPER TUBING  
1/4" O.D., 0.030" WALL. KANE  
HAND PINCH-OFF TOOL. (X75)

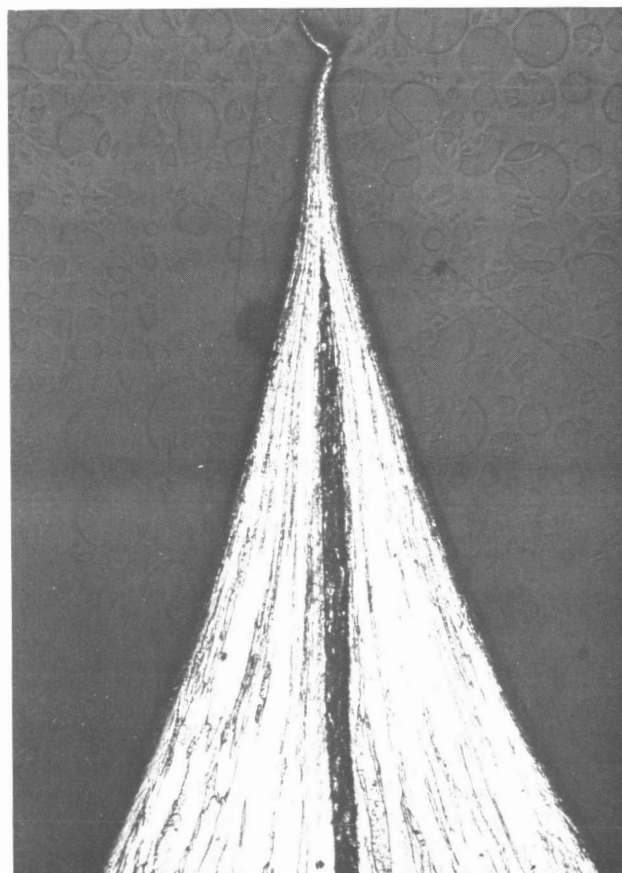


FIG. 3-8

ANNEALED OFHC COPPER TUBING  
1/4" O.D., 0.030" WALL.  
VARIAN HAND PINCH-OFF TOOL.  
(X75)

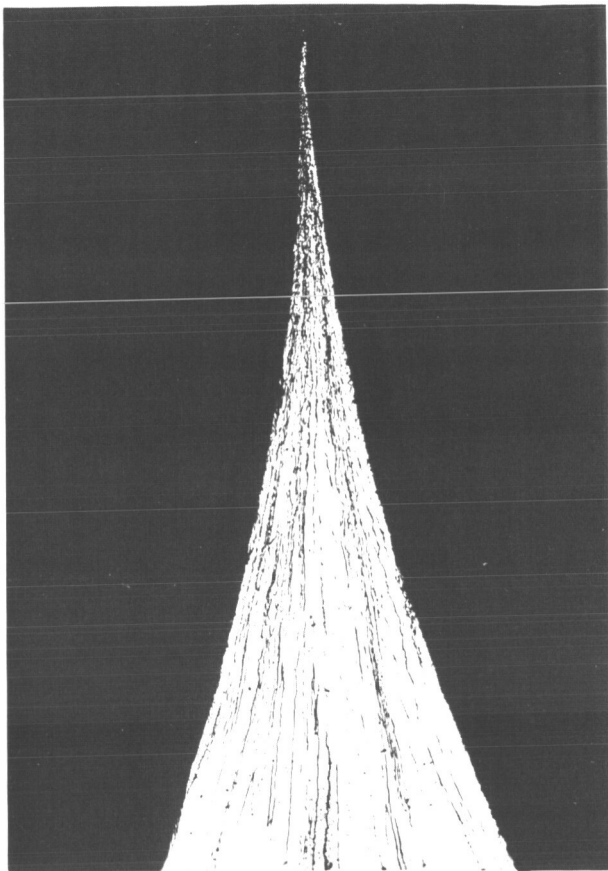
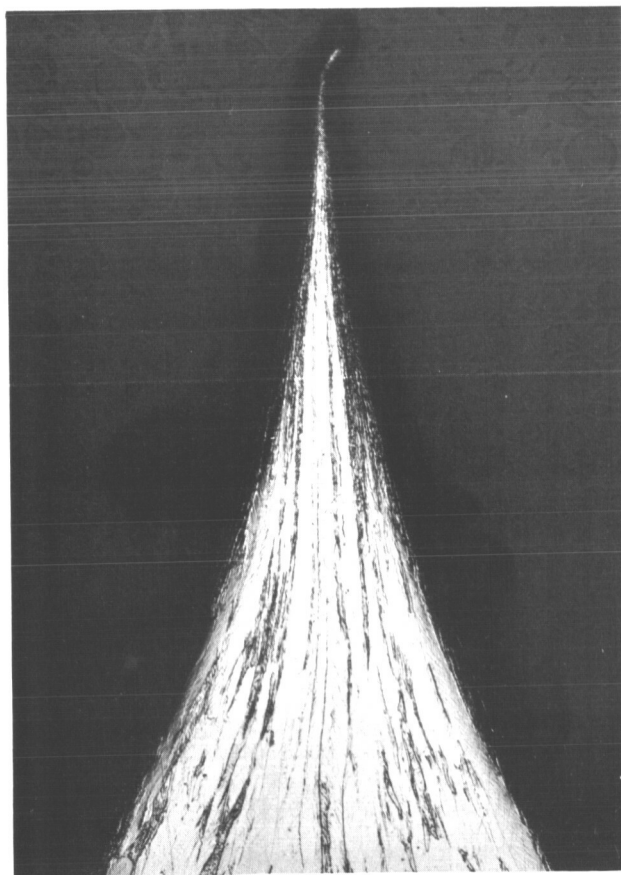


FIG. 3-9

ANNEALED OFHC COPPER TUBING  
 1/4" O.D., 0.030" WALL. KANE  
 HYDRAULIC PINCH-OFF TOOL WITH  
 1/4"-RADIUS ROLLER. (X100)

FIG. 3-10

ANNEALED OFHC COPPER TUBING  
 1/4" O.D., 0.030" WALL. KANE  
 HYDRAULIC PINCH-OFF TOOL WITH  
 1/8"-RADIUS ROLLER. (X75)



5. The pinch-off tool should be hydraulically actuated to provide maximum sealing area and consistent pinching action.

### 3.2.2 Ceramic-Metal Seal

A ceramic-metal seal study was conducted to examine seal reliability upon repeated thermal shock and also to establish a thicker sealing flange for preserving and improving converter structural rigidity in the absence of a retaining member employed in previous EOS converter designs. In addition, limited life testing after thermal shock testing was performed.

Three seal assemblies have been fabricated and leak tested with a helium mass spectrometer leak detector of calibrated sensitivity in the  $10^{-10}$  cc-atm/sec range. Each assembly consists of two niobium flanges with a right-angle spun surface that is flat to within 0.001 inch. An alumina ring of high-purity (Wesgo AL 995) and precision flatness (less than 0.0005 inch) was sealed between the niobium flanges with a eutectic mixture of nickel and zirconium. Brazing was accomplished in accordance with Specification GMP-34200/020-GEN. The assemblies were identical in dimensions, except that the flanges for each assembly were 0.020 inch, 0.030 inch, and 0.040 inch thick, respectively, as compared to previous EOS production and experimental converter flanges with 0.010-inch thicknesses.

The testing program and its results are summarized below:

1. The 0.020-inch-thick niobium flange/alumina seal assembly was thermally cycled 250 times from  $220^{\circ}\text{C}$  to  $610^{\circ}\text{C}$  at a rate of  $100^{\circ}\text{C}/\text{min}$  and tested to be leak tight.
2. The 0.030-inch-thick niobium flange/alumina seal assembly was thermally cycled 252 times from  $220^{\circ}\text{C}$  to  $610^{\circ}\text{C}$  at a rate of  $100^{\circ}\text{C}/\text{min}$  and tested to be leak tight. This assembly was subsequently operated for 1500 continuous hours at  $700^{\circ}\text{C}$  and tested to be leak tight.

3. The 0.040-inch-thick niobium flange/alumina seal assembly was thermally cycled 189 times between 200°C and 600°C at 100°C/min and tested to be leak tight. The assembly was subsequently cycled to a total of 289 times under the same cycling conditions. The ceramic cracked during the last 100 cycles.

The 0.020-inch and 0.030-inch-thick niobium flange/alumina seals have performed well under conditions of moderate to severe thermal shock for a ceramic-metal seal assembly (alumina itself is limited to heating and cooling rates of 200°C/min). In addition, the active alloy seal appears to be capable of long-life operation at elevated temperatures.

The fabrication and testing experience acquired from this secondary study was directly applied to the fabrication of converters, since the assembly procedure for the converters included the electron beam welding of prefabricated seals to converter subassemblies.

### 3.2.3 Electron Beam Welding

#### 3.2.3.1 Electron Beam Welding of Niobium-Molybdenum and Niobium-Niobium

An experimental investigation was conducted to examine the feasibility of electron beam welding prefabricated ceramic-metal seals to the collector. Sample welds of niobium sheet to molybdenum plate were made to determine a schedule that resulted in good penetration into the molybdenum. A schedule of 150 kV x 4.2 mA at a part speed of 91 in./min yielded penetration through the 0.020 inch niobium sheet and approximately 0.025 inch into the molybdenum plate. A niobium flange was subsequently welded to a molybdenum rod utilizing this schedule; however, the assembly leaked. A subsequent assembly also leaked.

There has been a notable lack of binary phase diagrams and information concerning the niobium-molybdenum system. Hansen (Ref. 9) devotes only a paragraph to niobium-molybdenum

concluding that: "Nb and Mo form an uninterrupted series of body-centered-cubic solid solutions." However, more recent work on the Nb-Mo system indicates:

1. Intermediate alloys of Nb-Mo contain large pores indicating that Nb-Mo and Mo-Nb diffusion rates in the melt are quite different.
2. An increase in hardness from 200 kg/mm<sup>2</sup> for 100 percent molybdenum, to 420 kg/mm<sup>2</sup> for molybdenum with only 15 percent addition of niobium.

Niobium-niobium, as the materials to be welded, was selected for weld feasibility. A niobium ring 0.060-inch thick, was first titanium brazed to a molybdenum bar and then used as a backing part for a 0.020 inch niobium flange. A schedule of 150 kV x 2.8 mA at a part speed of 40 rpm resulted in a leak-tight joint. In microsection, Fig. 3-11 displays a weld of good penetration into the backup ring (approximately 0.020 inch).

With an electron beam welding schedule for welding the flange seals of a prefabricated ceramic-metal seal to the converter subassembly structure, the feasibility of a "modular" assembly was established. That is, all major subassemblies of a thermionic converter are brought together and in two passes of an electron beam welder an exhaust assembly is completed.

#### 3.2.3.2 Electron Beam Welding of Rhenium-Rhenium

The choice of rhenium as an emitter material for a high performance, long-life thermionic converter also establishes rhenium as the emitter support (envelope) material. There are two principal reasons supporting this: First, rhenium and the more common structural materials, such as tantalum, tungsten, niobium, etc., form low melting point eutectics and brittle intermetallic compounds, which lack mechanical strength. Second, even if two such dissimilar materials welded reliably, the emitter becomes "contaminated" with envelope material diffusing onto the emitter surface. Electron beam welding

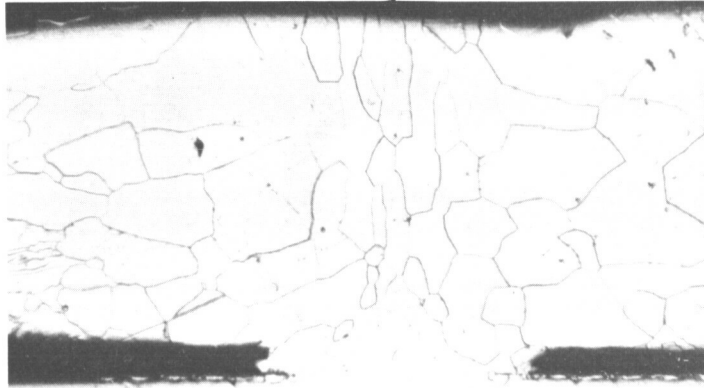


FIG. 3-11 ELECTRON-BEAM WELD OF 0.020-INCH THICK NIOBIUM RING TO 0.060-INCH THICK NIOBIUM RING. BEAM VOLTAGE OF 150 kV X CURRENT OF 2.8 mA. PART ROTATION SPEED OF 40 rpm (Mag 100X)



has proven to be a most effective means of joining converter parts, in particular, the emitter/emitter-support structure. The welding is done in a high vacuum chamber operating in the high  $10^{-6}$  or low  $10^{-5}$  range. The application of heat is instantaneous, which prevents part warpage; also, the heat-affected zone is small and ductile, which permits thermal cycling.

An experimental investigation was undertaken and completed to establish the proper electron beam welding schedules for rhenium-rhenium. Two rhenium sheet strips, each 0.020-inch thick, were ground flat, chemically cleaned, and clamped together to serve as feasibility samples for different electron beam parameters. Five separate weld passes of minimum spot diameter (0.012 inch) were made on the EOS Hamilton-Zeiss electron beam welder in a  $4 \times 10^{-5}$  torr vacuum environment. Figure 3-12 illustrates that a beam power of 150 kV x 3.4 mA at a part speed of 100 in./min is not sufficient to achieve penetration into the bottom part. However, a reduced part speed of 90 in./min for the same beam power produced penetration, as shown in Fig. 3-13. A higher beam power and lower part speed of 150 kV x 4.7 mA at 80 in./min yields good penetration into the bottom sheet, as shown in Fig. 3-14. It is interesting to note that while the weld shown in Fig. 3-12 would be leak tight, the degree of bonding is much greater for the latter schedule. Figure 3-15 illustrates the effect of a weld schedule sufficient to cause blow-through in the bottom sheet. The recommended schedule for electron beam welding a 0.020-inch-thick rhenium envelope to a rhenium emitter is 150 kV x 4.9 mA at a part speed of 80 in./min. If the weld is circumferential, the part speed, which is linear in this investigation, would be corrected to revolutions/min. A minimum electron beam diameter of approximately 0.012 inch is recommended for this type of welding since such a beam is more easily controlled and requires less total beam power to achieve the same penetration. The standard practice of requiring clean parts and good fit is essential to electron beam welding.

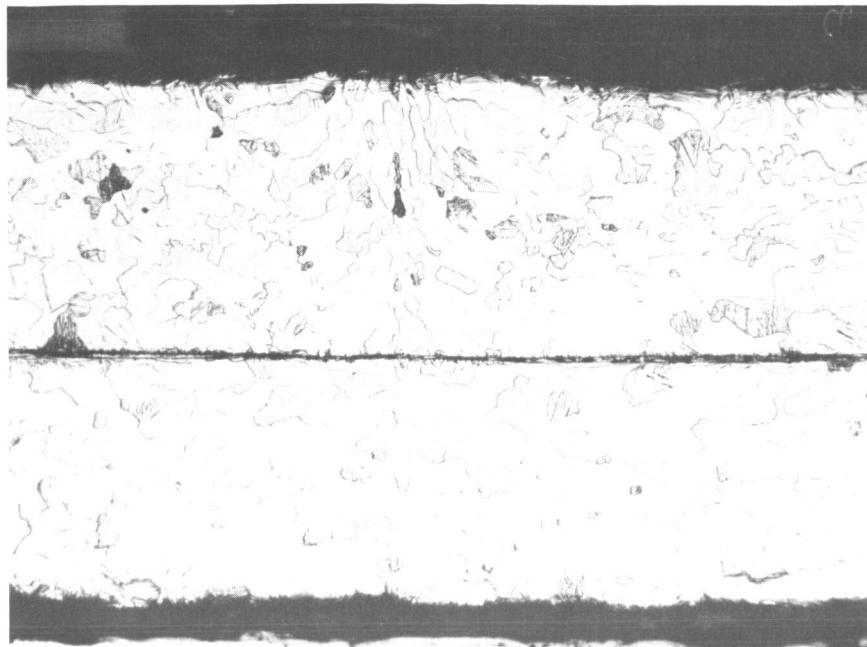


FIG. 3-12 RHENIUM SHEET TO RHENIUM SHEET ELECTRON BEAM WELD. BEAM VOLTAGE OF 150 kV X CURRENT OF 3.4 mA. PART SPEED OF 100 IN/MIN. (X75)

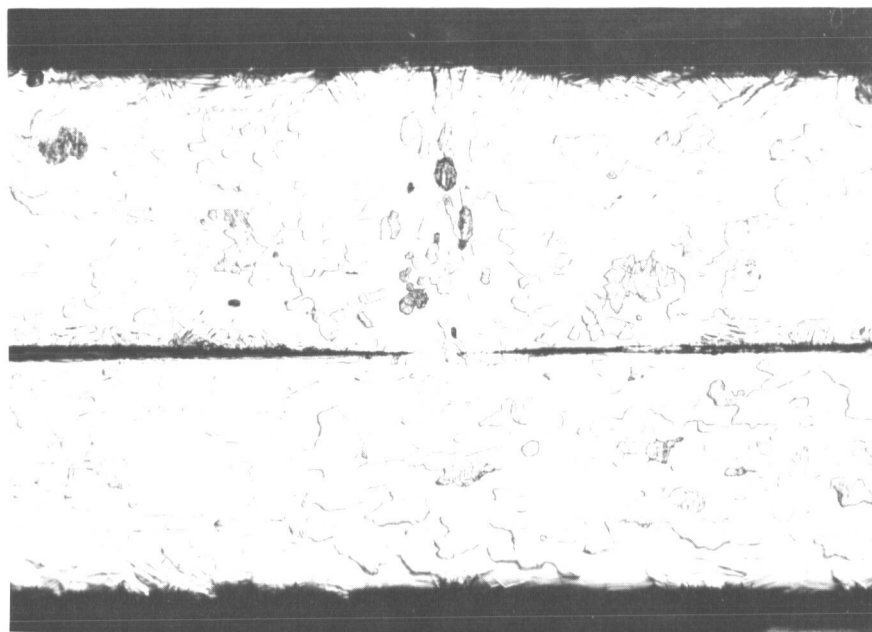


FIG. 3-13 RHENIUM SHEET TO RHENIUM SHEET ELECTRON-BEAM WELD. BEAM VOLTAGE OF 150 kV X CURRENT OF 3.4 mA. PART SPEED OF 90 IN/MIN. (X75)

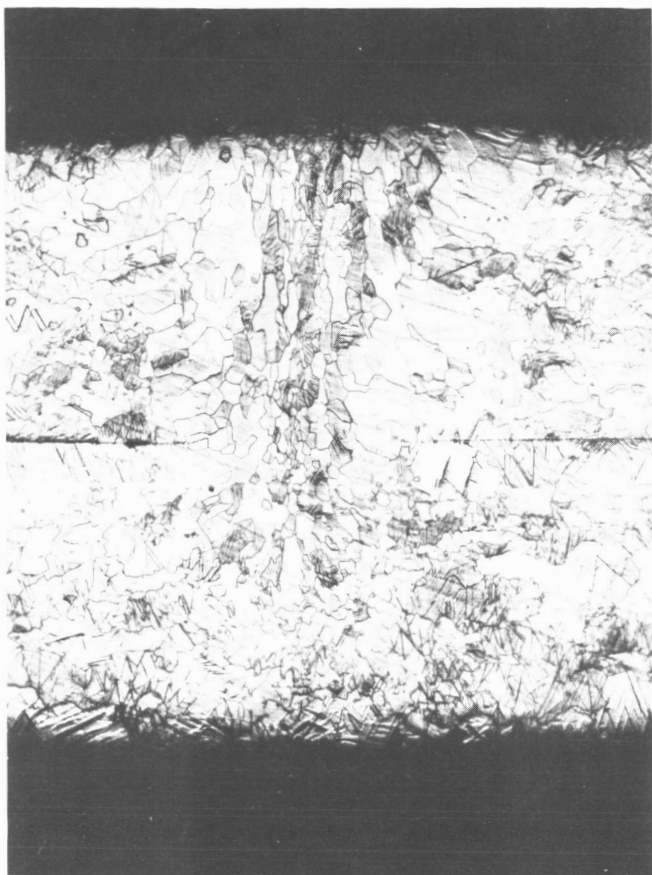
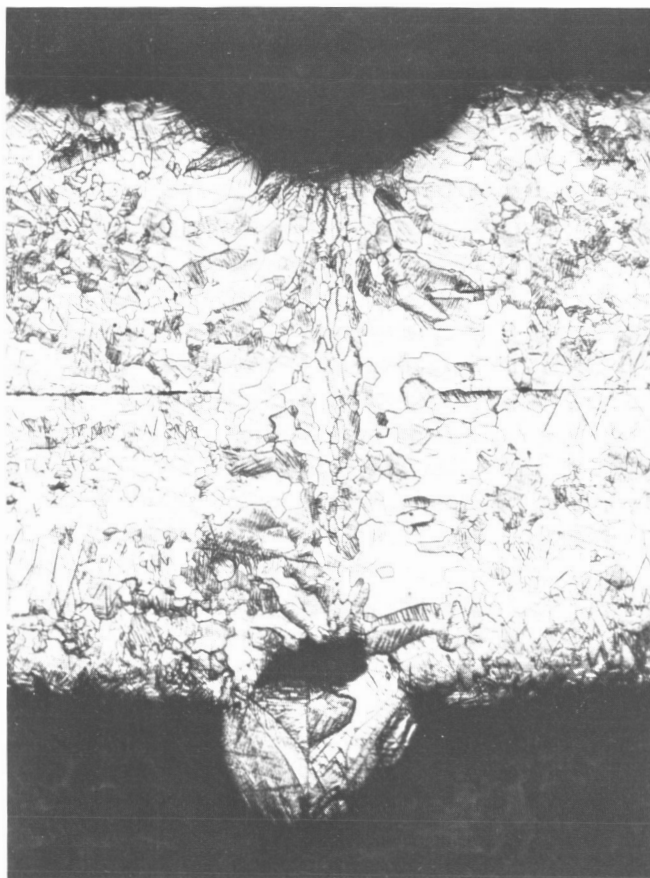


FIG. 3-14

RHENIUM SHEET TO RHENIUM SHEET  
ELECTRON-BEAM WELD. BEAM VOLTAGE  
OF 150 kV X CURRENT OF 4.7 mA.  
PART SPEED OF 80 IN/MIN.

FIG. 3-15

RHENIUM SHEET TO RHENIUM SHEET  
ELECTRON-BEAM WELD BEAM VOLTAGE  
OF 150 kV X CURRENT OF 6 mA.  
PART SPEED OF 80 IN/MIN.



### 3.2.4 Interelectrode Spacing Experiments

A thermal mockup of a converter was fabricated to directly measure the at-temperature interelectrode spacing of a thermionic converter.

The following paragraphs describe the interelectrode spacing vehicle and show experimental results and theoretical calculations. Spacing information from the test vehicle is correlated to converter fabrication techniques.

#### 3.2.4.1 Theoretical Calculations of the Converter Thermal Mockup

Figure 3-16 is a cross section of the interelectrode spacing vehicle thermal mockup. The emitter heat choke was machined to give a L/A ratio similar to that of a converter. It has a 0.003-inch-thick wall for a length of 0.200 inch.

$$L/A = \frac{0.200 \times 2.54}{3.14 \times 0.633 \times 3 \times 6.45 \times 10^{-3}}$$

$$L/A = \frac{5.08 \times 10^{-1}}{3.85 \times 10^{-2}}$$

$$L/A = 13.2 \text{ cm}^{-1}$$

To minimize the cost of the emitter heat choke it was made of tantalum rather than rhenium. The thermal expansion characteristics of tantalum are very similar to rhenium over the temperature range from 0 to 1000°C, the limit of literature data.

To calculate the interelectrode spacing, a temperature distribution of the emitter heat choke was taken. Figure 3-17 shows the temperature distribution of the envelope. The interelectrode spacing is the expansion of the emitter envelope plus the expansion of the seal minus the collector expansion. Assuming that the emitter at room temperature is stress-free, the thermal expansion

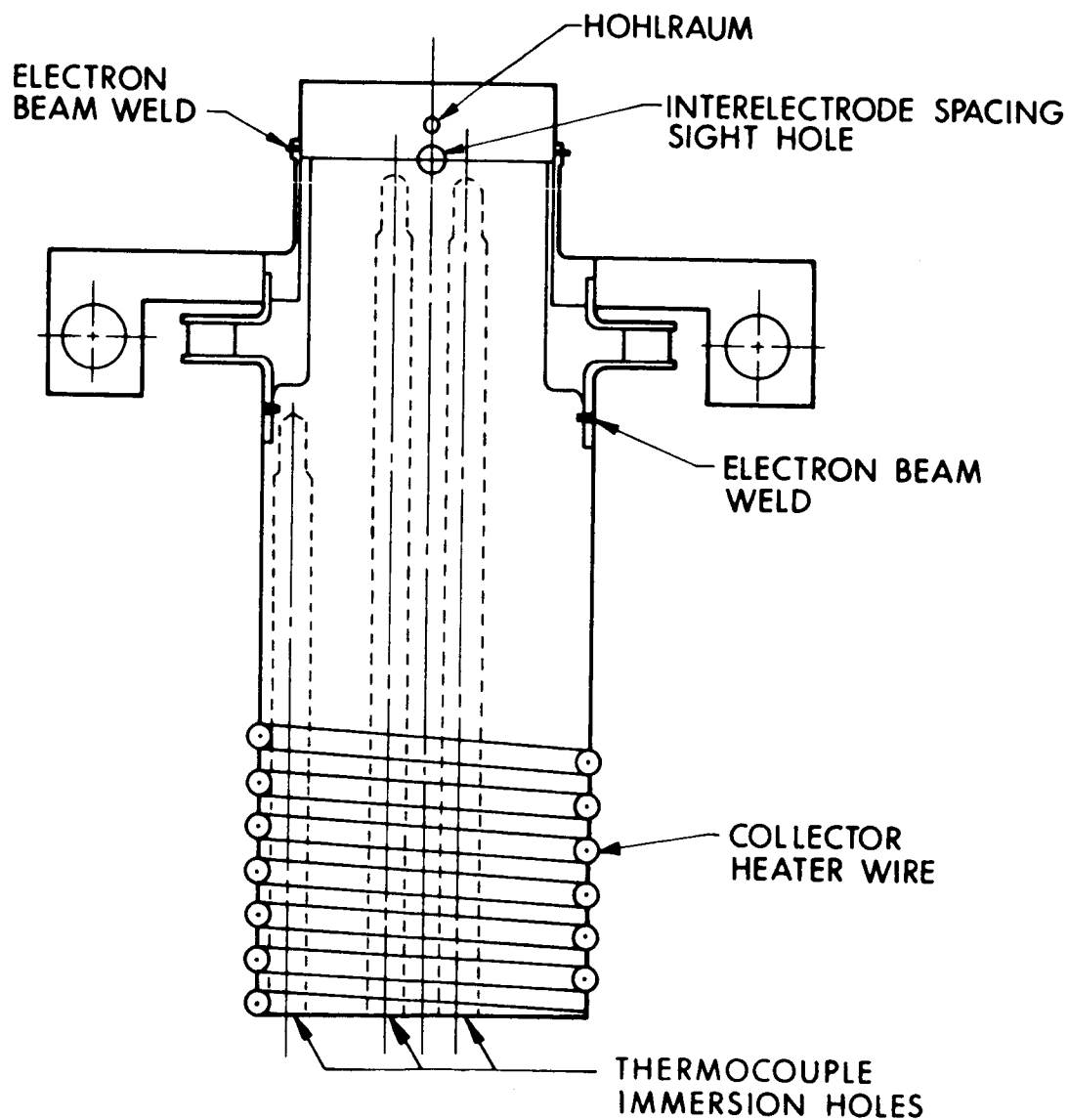


FIG. 3-16 THERMAL MOCK-UP FOR INTERELECTRODE SPACING MEASUREMENTS

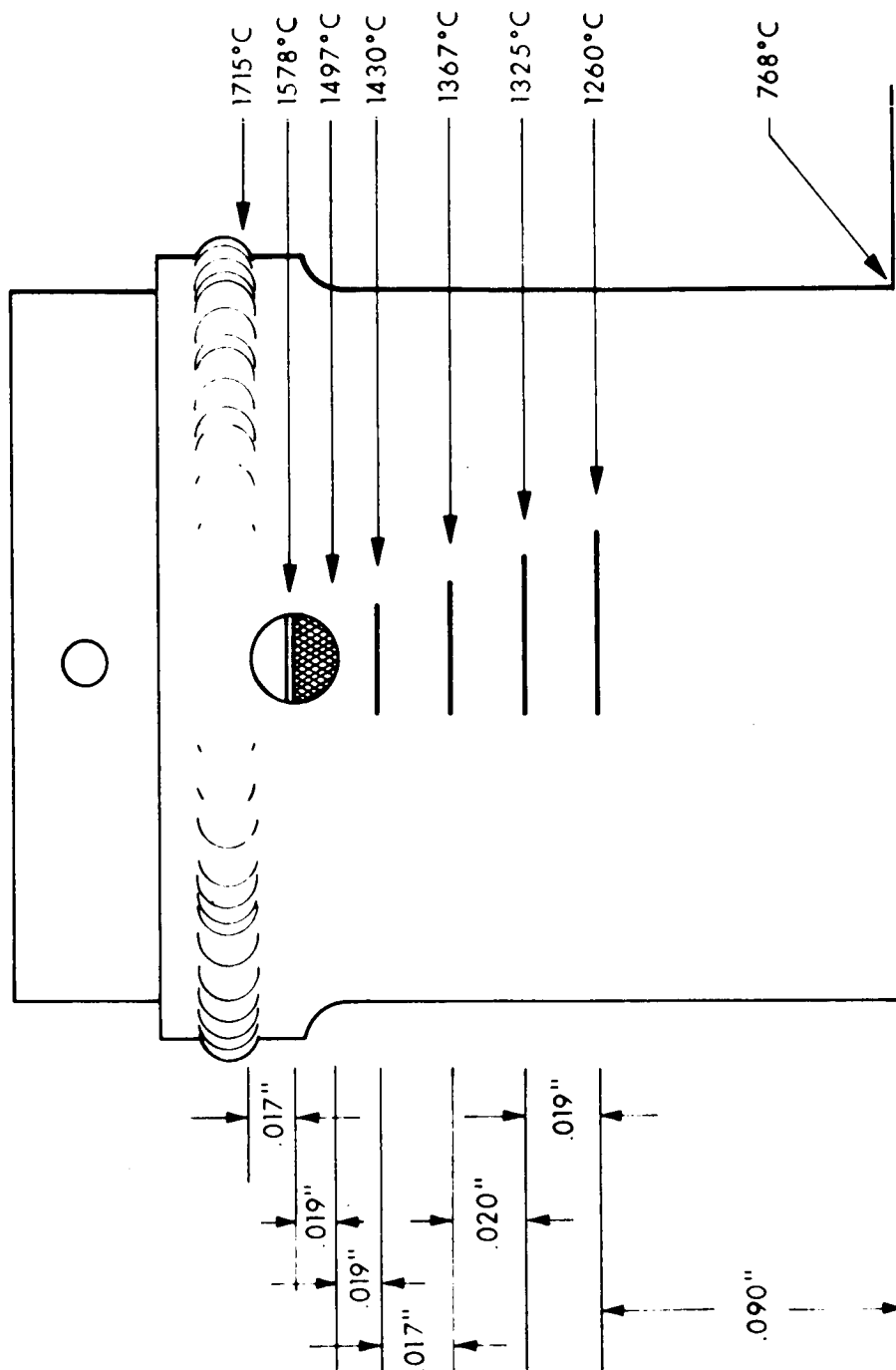


FIG. 3-17 EMITTER HEAT CHOKE TEMPERATURE (true) DISTRIBUTION

of the emitter envelope can be calculated using a piecewise solution. It is felt that a piecewise solution is valid because a sufficient number of pieces (seven) will be taken. The expansion is  $\Delta l = l_0 \alpha \Delta T$ , where  $\Delta l$  is the change in length,  $l_0$  is the initial length at room temperature,  $\alpha$  is the coefficient of thermal expansion of tantalum (Ref. 8) and  $\Delta T$  is the change in temperature.

The total expansion of the envelope is a summation of the smaller members.

$$\Delta l = \Delta l_1 + \Delta l_2 + \Delta l_3 + \Delta l_4 + \dots + \Delta l_7$$

$$\Delta l_1 = 01.7 \text{ inches} \times 1.27 \times 10^{-4} = 2.06 \times 10^{-4}$$

$$\Delta l_2 = 01.9 \text{ inches} \times 1.16 \times 10^{-4} = 2.20 \times 10^{-4}$$

$$\Delta l_3 = 01.9 \text{ inches} \times 1.10 \times 10^{-4} = 2.09 \times 10^{-4}$$

$$\Delta l_4 = 01.7 \text{ inches} \times 1.06 \times 10^{-4} = 1.80 \times 10^{-4}$$

$$\Delta l_5 = 02.0 \text{ inches} \times 1.01 \times 10^{-4} = 2.02 \times 10^{-4}$$

$$\Delta l_6 = 01.9 \text{ inches} \times 0.96 \times 10^{-4} = 1.82 \times 10^{-4}$$

$$\Delta l_7 = 09.0 \text{ inches} \times 0.7 \times 10^{-4} = \frac{6.30 \times 10^{-4}}{18.29 \times 10^{-4}}$$

Therefore, the calculated change in the emitter envelope is 0.00183 inch.

Likewise, the thermal expansion of the seal assembly can also be calculated. Assuming that the ceramic member has the same coefficient of thermal expansion as the niobium metal member (Ref. 8), with an average seal temperature of  $650^\circ\text{C}$ , the  $\alpha$  of niobium is  $0.51 \times 10^{-2} \text{ }^\circ\text{C}^{-1}$ ; for a 0.50 inch we have

$$0.50 \text{ inch} \times 0.51 \times 10^{-2} = 0.0026 \text{ inch}$$

Therefore, the seal expansion is 0.0026 inch.

The molybdenum collector expansion for a collector measuring length ( $l_o$ ) of 0.650 inch, assuming an average collector temperature of  $700^{\circ}\text{C}$ , is  $\Delta L_C = 0.650 \text{ inch} \times 0.35 \times 10^{-2} = 0.00228 \text{ inch}$ . Therefore, the calculated change in the interelectrode spacing is:  $\Delta l = (0.00183 \text{ inch} + 0.0026 \text{ inch}) - 0.00228 \text{ inch} = 0.00215 \text{ inch}$  with an operating temperature of  $1735^{\circ}\text{C}$  on the emitter, an average collector temperature of  $700^{\circ}\text{C}$ , and a seal temperature of  $650^{\circ}\text{C}$ .

#### 3.2.4.2 Direct Experimental Measurement of Interelectrode Spacing

Direct measurements of the interelectrode spacing were made by optically measuring the gap distance at temperature by sighting through a 0.038-inch-diameter hole which was drilled in the side of the emitter envelope assembly.

Figure 3-18 shows the testing setup. A self-contained 40-liter/second vacuum ion pump was used to minimize floor vibrations. Precision optical measurements are taken through an optically flat quartz window in a quartz bell jar. The spacing was directly measured by sighting through a Bausch and Lomb micrometer drum cross-hair eyepiece mounted on a 75 power microscope. The micrometer drum was calibrated against a ruled micrometer stage (Bausch and Lomb 31-16-89). The established accuracy of this optical system is  $\pm 0.0001 \text{ inch}$ . The emitter temperature of the converter mockup was varied from  $1250^{\circ}\text{C}$  to  $1800^{\circ}\text{C}$  with an electron bombardment heater. The tantalum emitter has a 10:1 depth-to-diameter hohlraum for micro-optical pyrometer temperature measurements.

The seal and envelope were fabricated as an assembly and electron beam welded to the collector.

The molybdenum collector was bored to accommodate an immersion thermocouple. Tantalum-sheathed heaters were brazed to the collector root. The heaters allow the average collector temperature to be varied in order to allow the determination of the effects of collector temperature on the interelectrode spacing.



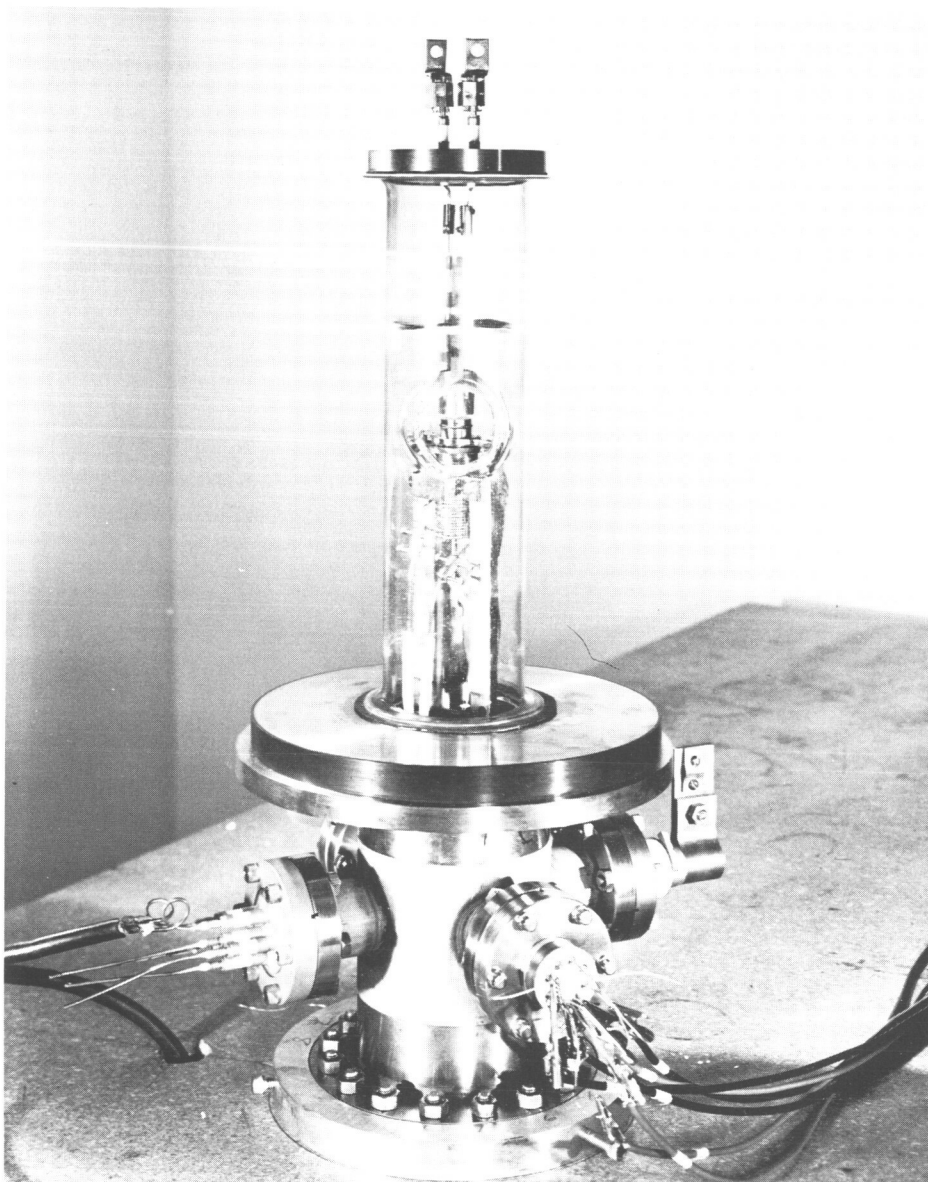


FIG. 3-18 SPACING EXPERIMENT SETUP. Note high-quality quartz window for optical measurements

The emitter collector spacing was set at 0.003 inch when fabricated. This spacing insures that the emitter envelope is in a stress-free state at room temperature.

Distances between the emitter and collector were measured by focusing on the selected electrode and aligning the cross-hair of the micrometer drum at the surface of that electrode; the cross-hair was then moved, counting the number of drum revolutions, until it was aligned with the surface of the other electrode. This procedure was then reversed. At least six readings were taken for each set of parameters.

Direct optical determination of the spacing yielded variations up to 0.0002 inch from reading to reading. The variation in the readings is dependent upon the ability to precisely focus on the electrode faces when they are at temperature. Figure 3-19 shows a typical temperature picture of the gap region looking through the microscope. (The cross-hairs in the picture are out of focus to accommodate the camera.)

Figure 3-20 shows the change in interelectrode spacing for various emitter temperatures, and seal temperatures of 608°C and 650°C. The calculated change in interelectrode spacing of 0.00215 inch and the experimentally measured spacing changes of 0.0023 inch at  $T_{\text{emitter}} = 1735$ ,  $T_{\text{coll.}} = 700^{\circ}\text{C}$ ,  $T_{\text{seal}} = 650^{\circ}\text{C}$  show close agreement.

Calculated values for the spacing change cannot be more accurate than  $\pm 5$  percent, because the best published data available for the coefficient of thermal expansion ( $\alpha$ ) vary by this amount. For example, 99.90 percent pure niobium has an  $\alpha$  of  $8.03 \times 10^{-6}/^{\circ}\text{C}$ , and 99.92 percent pure niobium has an  $\alpha$  of  $8.45 \times 10^{-6}/^{\circ}\text{C}$  (Ref. 10). This variation in  $\alpha$  is due to differences in the purity of the material involved. As a rule, the higher the purity of a particular material the larger its thermal expansion ( $\alpha$ ).

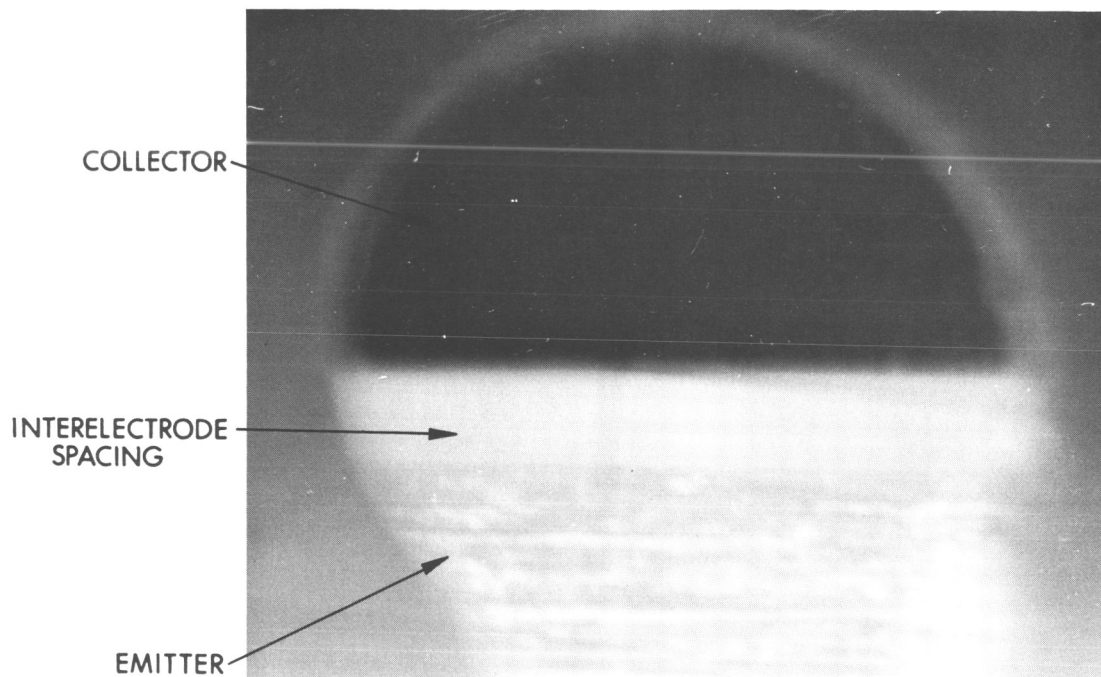


FIG. 3-19 PHOTOGRAPH OF INTERELECTRODE SPACING AT AN  
EMITTER TEMPERATURE OF  $1735^{\circ}\text{C}$

$T_{\text{COLLECTOR}} = 700^{\circ}\text{C}$  INTERELECTRODE SPACING  
MEASURED TO BE 5.6 MILS

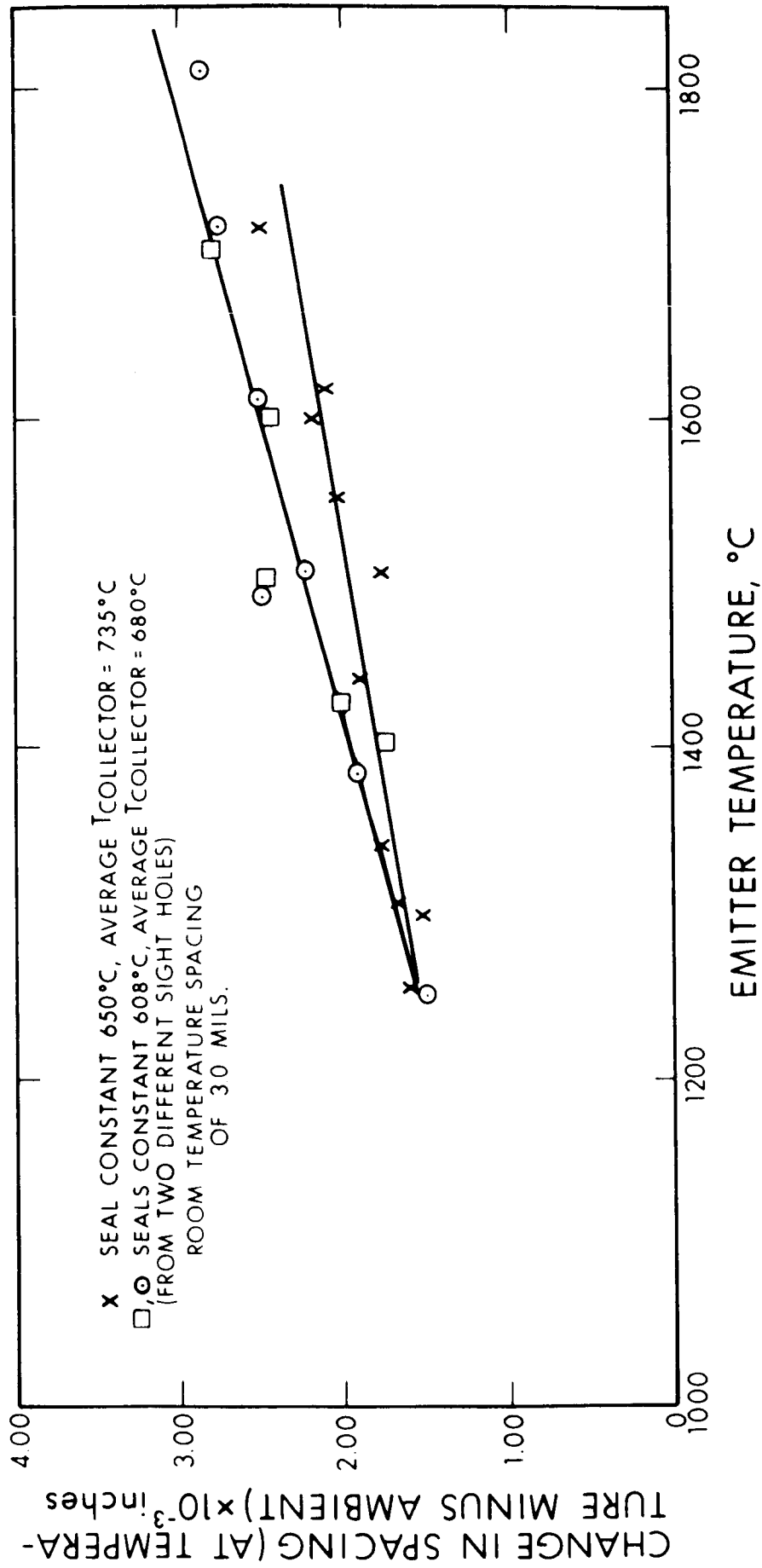


FIG. 3-20 CHANGE IN INTERELECTRODE SPACING AS A FUNCTION OF EMITTER TEMPERATURE

#### 3.2.4.3 Problems in Achieving Precision Interelectrode Spacing in Thermionic Converter Hardware

In converter operation, a large  $\Delta T$  is present in the collector due to the thermal load caused by the converter current. This  $\Delta T$  must be considered when correlating the spacing data obtained from the interelectrode spacing device with an operating converter. With a 50 ampere converter current and a  $1.88 \text{ cm}^2$  collector cross-sectional area, the  $\Delta T$  in the molybdenum collector is  $110^\circ\text{C}$ . At 70 amperes of converter current, the collector  $\Delta T$  is  $150^\circ\text{C}$ .

When fabricating a converter, the ability to achieve an operating spacing that is accurate to  $\pm 0.0001$  inch is decidedly a function of the fabrication processes such as machine tolerances, annealing, electron beam welding, and brazing.

The final fabrication procedure entails electron-beam welding the emitter on the rest of the converter as the final subassembly step. This insures not only the desired spacing but also eliminates stress in the metal-to-ceramic seal. If the emitter-envelope subassembly is seal-brazed to the collector subassembly as the final fabrication process, the spacing at operating temperature will be determined by variable brazing temperatures, variable braze run-out, and the annealing state of flange materials. Also, if the emitter and collector surfaces are in contact, the seal braze is made in compression and stresses are induced in the seal and envelope.

A realistic tolerance for practical converter interelectrode spacings should be  $\pm 0.0002$  inch.

#### 4. HIGH PERFORMANCE THERMIONIC CONVERTER DESIGN

The thermionic converter design goals for this program are:

1. A power density of 20 watts/cm<sup>2</sup> at 0.8 volt terminal output from a 2.0 cm<sup>2</sup> emitter area. The emitter temperature for this output is 1735°C true, as measured in a 10:1 depth-to-diameter blackbody hole with corrections for bell jar transmission loss.
2. An efficiency of 14 percent, measured at the conditions of output power density just described, using a flat, counter-wound, 0.020-inch-diameter tungsten filament.
3. Minimum converter weight consistent with a four-converter generator weighing 4 pounds.
4. Improved heat transfer from the converter collector surface to the radiator and sufficient radiator area to reject the generated heat loads during dc operation of the converter.

The design and fabrication of the converters proceeded in an iterative fashion wherein each converter is designed utilizing operational information from previous converters, the variable-parameter vehicle data, and the secondary experiments.

In 1964 EOS thermionic converters achieved 20 watts/cm<sup>2</sup> at 0.7 volt terminal output for an emitter temperature of 2000°K true. The emitter was 0.020-in. rhenium shim hot-pressed onto a tantalum substrate, a system that, a priori, is life-limited by the basic incompatibility of tantalum-rhenium at 2000°K. The useful life of this type of converter was at that time estimated to be: (1) a few hundred hours before some initial degradation due to emitter surface contamination, and (2) final catastrophic failure of the tantalum-rhenium bond after 1000 to 3000 hours of operation. Upon extended test these

predictions were proven correct; moreover, the recommendations for a solid rhenium emitter supported by a rhenium envelope for reliable, long-life operation was adopted.

#### 4.1 Converter Efficiency

The efficiency of a thermionic converter is calculated by way of standard considerations in the following manner:

$$\eta = P_{\text{out}} / (P_{\text{elec cool}} + P_{\text{rad}} + P_{\text{cs cond}} + P_{\text{env cond}}) \quad (4-1)$$

where  $P_{\text{out}}$  is set at 20 watts/cm<sup>2</sup> from 2 cm<sup>2</sup>,  $P_{\text{elec cool}}$  is the thermal power carried away from the emitter by electrons "evaporating" from the emitter surface,  $P_{\text{rad}}$  is the net heat lost from the emitter surface by radiation,  $P_{\text{cs cond}}$  is the net thermal "gas" conduction loss from the emitter surface, and  $P_{\text{env cond}}$  is the conduction heat transferred from the emitter to its envelope support structure.

Each of the loss terms is now examined at the power output design point.

$$P_{\text{elec cool}} = I (\phi_{\text{eff}} + 2kT/e) \quad (4-2)$$

where  $\phi_{\text{eff}}$  is the effective emitter work function obtained from the Richardson-Dushman equation by setting A, the preexponential multiplier, equal to 120 amperes/cm<sup>2</sup> - °K<sup>2</sup>; T, the emitter temperature, at 2000°K; and  $J_s$ , the saturated electron emission, at 25 amps/cm<sup>2</sup>.

$$J_s = A T^2 e^{-e\phi/kT}$$

$$\frac{25 \text{ amps}}{\text{cm}^2} = \frac{120 \text{ amps}}{\text{cm}^2 - ^\circ\text{K}^2} \times 4 \times 10^6 - ^\circ\text{K}^2 e^{-\frac{1.6 \times 10^{-12} \phi_{\text{eff}}}{1.38 \times 10^{-16} \times 2 \times 10^3}} \quad (4-3)$$

solving for  $\phi_{\text{eff}}$ ,

$$\phi_{\text{eff}} = 2.9 \text{ volts}$$

The term  $2kT/e$  is an additive energy term, divided by the electron charge for conversion to units of potential energy, which accounts for the energy distribution of emitted electrons. For an emitter temperature,  $T$ , of  $2000^{\circ}\text{K}$  this additive term is equal to 0.32 volt.

The total electron cooling loss for  $2.0 \text{ cm}^2$  of emitting area with a 50-ampere current is:

$$P_{\text{elec cool}} = 50 (2.9 + 0.32) = 160 \text{ watts}$$

$$P_{\text{rad}} = e_{\text{eff}} \sigma (T_{\text{em}}^4 - T_{\text{coll}}^4)$$

where  $e_{\text{eff}}$  is the effective emissivity of the electrode system which, in Section 3, was determined to be 0.16.

$$P_{\text{rad}} = 0.16 \times 5.7 \times 10^{-12} \times \left[ (2 \times 10^3)^4 - (1.1 \times 10^3)^4 \right]$$

$$P_{\text{rad}} = 13 \text{ watts/cm}^2$$

For  $2.0 \text{ cm}^2$ , the heat loss from the emitter surface is 26 watts.

The power loss via cesium conduction loss has been experimentally reported to be approximately 16 watts in the cesium pressure range of interest (i.e., from 2 to 10 torr).

The final loss term to be considered is the envelope conduction,  $P_{\text{env cond}}$ . The design of the envelope, which acts as the emitter support structure as well as the emitter current lead strap, requires a tradeoff between the electrical losses and thermal losses. The usual lead analysis, which follows, derives an  $L/A$  ratio for the envelope which is obtained by examining the ratio of electrical to thermal losses. Let  $\alpha$  be defined as the ratio of electrical to thermal loss:

$$\alpha = \frac{I^2 \rho L/A}{K \Delta T \left( \frac{A}{L} \right) - (1/2) I^2 \rho \left( \frac{L}{A} \right)} \quad (4-4)$$



The thermal loss term in the denominator is the sum of the simple heat conduction minus half the joule heating losses since the joule heating losses will modify the envelope temperature distribution in a manner which will reduce the straight conduction loss. For an  $\alpha$  value of 0.1, the L/A ratio for a rhenium envelope with  $\rho = 80 \times 10^{-6}$  ohm-cm,  $K = 0.48$  watt/cm -  $^{\circ}\text{C}$ ,  $I = 50$  amperes, and  $\Delta T = 1000^{\circ}\text{C}$  is:

$$L/A = \frac{1}{50} \sqrt{\frac{0.48 \times 0.1 \times 1000}{80 \times 10^{-6} [1 + 1/2 (0.1)]}}$$

$$L/A = 15 \text{ cm}^{-1}$$

From a fabrication standpoint, an envelope wall thickness of less than 0.003 inch is difficult to produce with a high yield. Therefore, a minimum wall dimension of 0.004 inch has been selected, and the resultant length, L, is approximately 0.22 inch for an envelope diameter of 0.631 inch. The electrical loss  $I^2 \rho L/A$ , by substitution, is  $(50)^2 \times 80 \times 10^{-6} \text{ ohm-cm} \times 15 \text{ cm}^{-1} = 3$  watts, while the thermal loss, or  $P_{\text{env cond}}$ , is 30 watts.

Returning to the efficiency expression,  $\eta$  may be written as:

$$\eta = \frac{40 \text{ watts}}{160 \text{ watts} + 26 \text{ watts} + 16 \text{ watts} + 30 \text{ watts}}$$

$$\eta = 17 \text{ percent}$$

which compares to the program goal of 14 percent with bombardment gun losses.

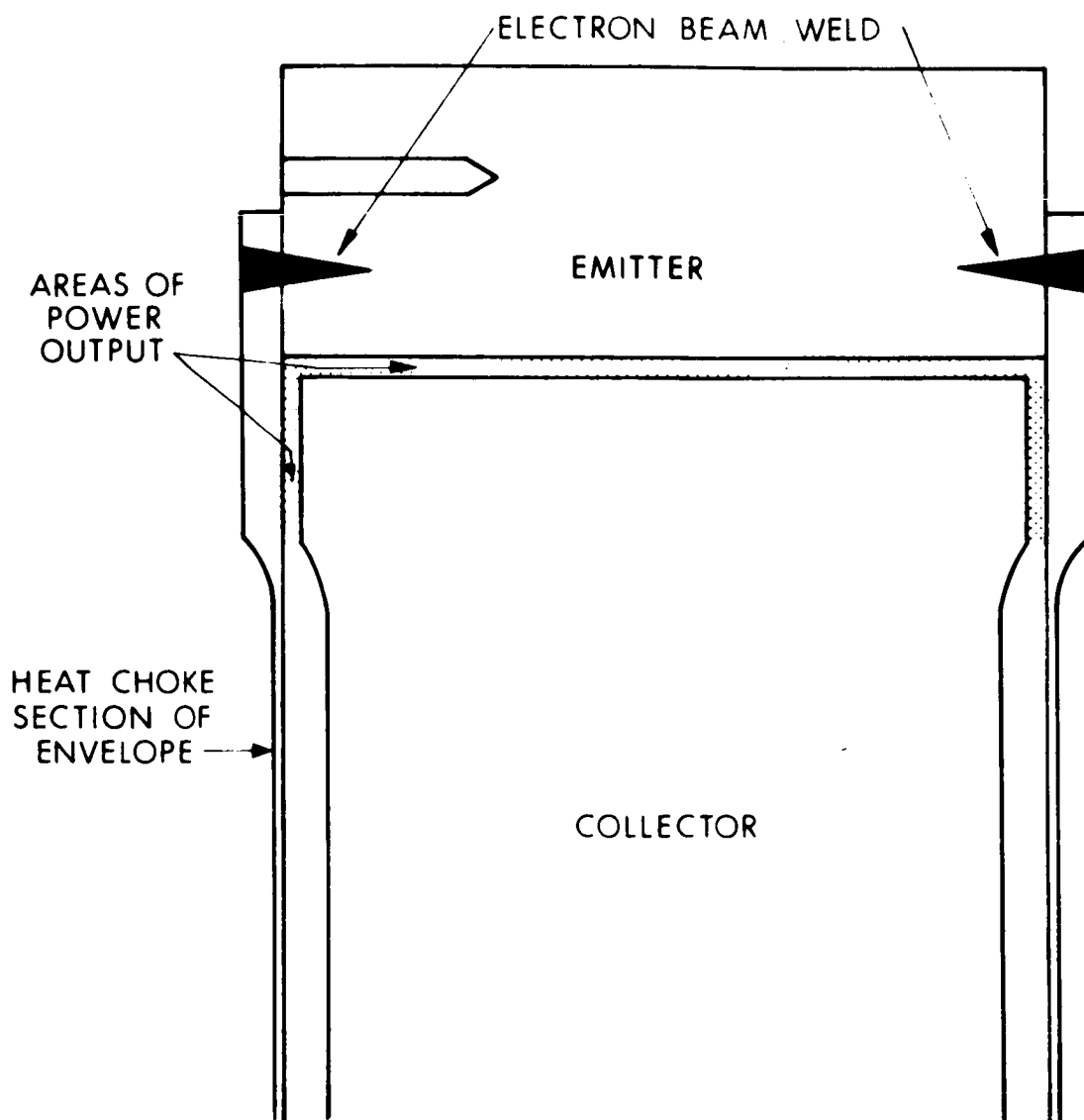
An EOS converter, fabricated and tested on Contract JPL 950699, which had a power output density of  $20 \text{ watts/cm}^2$  at a terminal voltage of 0.7 Vdc, yielded an efficiency of 11 percent when measured according to the methods defined in the present program design goals. However, the converter current level on that particular test was higher since the power output was obtained at an output voltage of

0.7 Vdc instead of 0.8 Vdc. For 0.8 Vdc output at 20 watts/cm<sup>2</sup> and at an emitter temperature of 1735°C, the projected test efficiency would have been 13.8 or 14 percent, measured.

#### 4.2 Definition of Emitter Area

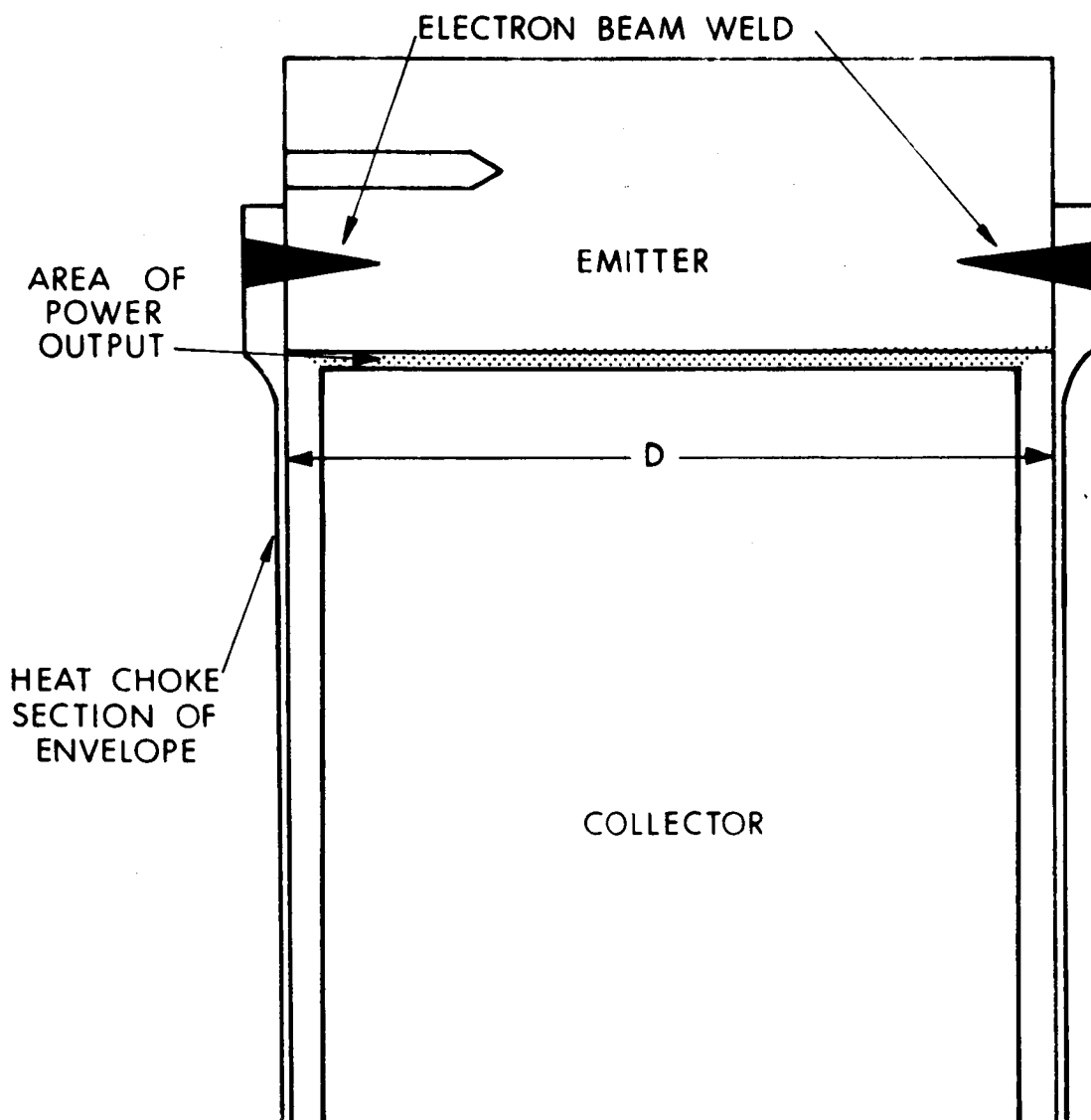
The emitter area of a plane-parallel, thermionic converter has lacked universal definition for some time. For example, some converters are assigned an emitter area based only on the area of the collector surface, other converters are assigned an area based on the entire emitter area as supported by the internal diameter of the envelope. For a selected level of power output from a converter, the collector area definition yields 10 to 15 percent greater power density than the emitting area definition. Although this difference in area definition seems small, it is sufficient to reject or accept deliverable hardware.

A more serious problem in plane-parallel converters is sidewall emission from the emitter support structure. There are two factors that enter into sidewall emission: (1) the sidewall (or envelope) - collector distance; and (2) the envelope temperature which implies sufficient contact potential difference to generate voltage output. A sidewall distance, as noted in Section 2, of 0.005 to 0.006 inch yields as much power output as an interelectrode spacing of 0.002 inch provided that the sidewall itself is at, or approximately at, the emitter temperature. If the envelope heat choke section is positioned 0.100 to 0.125 inch below the emitter electron beam weld, as shown in Fig. 4-1, the temperature of the envelope above the heat choke section will approximate the emitter temperature to within 50 to 70°C. However, if the envelope heat choke section is positioned such that it forces a sharp temperature gradient on the envelope opposing the collector, as shown in Fig. 4-2, the emission collected by the collector is minimal, particularly if the spacing between the envelope and collector is 0.010 to 0.012 inch. To estimate the additional emitting area from the envelope sidewall depicted in Fig. 4-1, assume that only one-fourth of the thick wall envelope is at the emitter temperature. For an emitter of 0.631 inch diameter (2.0 cm<sup>2</sup>), the surface area of the 0.03-inch length opposing



NOTE: NOT TO SCALE

FIG. 4-1 THERMIONIC CONVERTER DESIGN WITH ENVELOPE SIDEWALL CONTRIBUTING TO PERFORMANCE OUTPUT



NOTE: NOT TO SCALE

FIG. 4-2 THERMIONIC CONVERTER DESIGN WITH ENVELOPE SIDEWALL UNABLE TO PROVIDE PERFORMANCE OUTPUT

the collector is  $0.4 \text{ cm}^2$ . That is, a converter design which utilizes sidewall emission but does not consider the sidewall area realizes a 20 percent "increase" in power output density. A  $16.5 \text{ watt/cm}^2$  converter may therefore, be incorrectly referred to as a  $20 \text{ watt/cm}^2$  converter when sidewall emission area is neglected.

The question may be put forward: Why not use sidewall emission in a planar geometry? The answer is simply that there is no increase in efficiency for the sidewall system. It has the same losses as the emitter surface (to wit: electron cooling, radiation heat transfer, etc.), and since the final criterion for a SET converter (or any other converter) in a space power supply is power output versus power input, there is no system advantage to sidewall emission that cannot be obtained by just adding more converters or the same number of converters with a larger emitter area.

The EOS converter design is predicated to minimizing emitter sidewall emission by employing the geometry shown in Fig. 4-2. Temperature measurements which have been obtained on the emitter support structure of EOS converters indicate that the sidewall temperature immediately opposite the collector is some 200 to  $250^\circ\text{C}$  lower than the emitter temperature. Moreover, the spacing between collector and sidewall is consistently 0.011 inch and concentric, a measurement taken before the emitter is electron beam welded in place.

The emitter area of all EOS converters, unless otherwise specified, is taken as:

$$A_{\text{emitter}} = 1/4 \pi D^2$$

where D is the inside diameter of the emitter support structure shown in Fig. 4-2.

#### 4.3 Collector-Radiator Structure

As a starting point in the collector-radiator design, it is necessary to calculate the collector heat load that must be rejected

at the dc design operating point of 50 amperes (i.e., 40 watts at 0.8 Vdc). The following paragraphs contain these calculations and reexamine the molybdenum-copper spade in terms of heat rejection per unit weight.

#### 4.3.1 Collector Heat Load

The collector heat load,  $Q$ , may be written as the sum of three terms:

$$Q = Q_{el\ ht} + Q_{rad} + Q_{cs\ cond} \quad (4-5)$$

where  $Q_{el\ ht}$  is the heat generated by the drift current electrons in transit from the plasma (a region of higher potential energy) to the collector Fermi level (a region of lower potential energy). In concept, it is exactly opposite to the electron cooling term associated with the emitter, wherein electrons are lifted from the emitter Fermi level to the virtual emitter and remove heat from the emitter in the process. The terms  $Q_{rad}$  and  $Q_{cs\ cond}$  are equivalent to those discussed in the analysis of heat lost from the emitter. We may write  $Q_{el\ ht}$  as:

$$Q_{el\ ht} = kI, \quad (4-6)$$

where  $I$  is the drift or output current and  $k$  is defined as the summation of the kinetic energy of the plasma electrons and the potential energy fall represented by the effective work function of the collector.

$$k = \frac{4kT_{pl}}{\pi e} + \left( \phi_{coll} \pm \frac{V_s}{s} \right) \quad (4-7)$$

(A discussion of the origin and nature of the plasma potential energy term is presented in Appendix B.) For an electron plasma temperature of 6000°K

$$\frac{4kT_{pl}}{\pi e} = \frac{4 \times 1.38 \times 10^{-16} \times 6000}{\pi \times 1.6 \times 10^{-12}} = 0.66V$$

The measured minimum work function of cesium on rhenium has been determined to be 1.47 volts. Setting the collector sheath at zero for optimized operation,  $k$  is determined as:

$$k = 0.66V + 1.47V$$

$$k = 2.13V$$

and

$$Q_{el\ ht} = 2.13 (50\ \text{amps})$$

$$Q_{el\ ht} = 107\ \text{watts for 50 amperes current load}$$

To operate at 70 amperes without conduction cooling, the radiator would be required to reject a total heat load,  $Q$ , of

$$Q = (2.13) 70\ \text{watts} + 26\ \text{watts} + 10\ \text{watts}$$

the latter two terms being  $Q_{rad}$  and  $Q_{cs\ cond}$

$$Q = 190\ \text{watts}$$

#### 4.3.2 Radiator Heat Rejection

The molybdenum collector-copper radiator discussed previously in Subsection 3.1.2 provided a full-scale test for rejection of the computed collector heat load of 200 watts. The results of the testing program are repeated:

1. At a collector root temperature of  $600^{\circ}\text{C}$ , 200 to 225 thermal watts were dissipated by radiation.
2. The structure was thermal-cycled (on-off) 350 times under heat rejection loads of 200 to 225 watts. A  $\Delta T$  of  $5^{\circ}\text{C}$  across the molybdenum-copper interface was measured before and after thermal cycling.
3. No deterioration of the Rokide coating was observed.

The structure just described weighed 220 grams compared to the all-molybdenum collector-radiator weight of 250 grams which dissipated 125 watts thermal at lower power output. The molybdenum-copper system is, therefore, capable of rejecting twice the heat load of the molybdenum system for the same weight. A total weight of 240 grams is estimated for the high performance converter, yielding a specific power of 13 lb/kW(e).

#### 4.4 Assembly Procedure

As a method of improving diode fabrication, the design of the advanced prototype converters includes prefabrication of the ceramic-metal seals, their pretest, and final assembly into the diode configuration, utilizing electron-beam welding. Converters built previously were dependent upon the ceramic-metal sealing operation as the final assembly step. Two disadvantages resulted: First, a seal failure generally rendered one subassembly, and perhaps two, useless with minimal chance of recovery. Second, the vapor pressure of seal brazing materials is often high enough at the melting point (1/2 micron for copper) that the converter interior, including the electrodes, was coated with several monolayers of contaminant materials.

Figure 4-3 is a layout of the principal subassemblies including the prefabricated seal.

The collector-radiator subassembly is comprised of a molybdenum collector barrel, OFHC copper radiator fins, a niobium welding ring, a rhenium collector shim, and a tantalum reservoir. The rhenium shim is vanadium-brazed to the collector barrel since the resultant bond is made without the formation of a brittle intermetallic or low melting point eutectic alloy. The other components are titanium-brazed. The niobium welding ring is selected to provide a base material identical to that of the sealing flanges to avoid the apparent incompatibility of a solid solution of niobium and molybdenum formed during electron-beam welding.



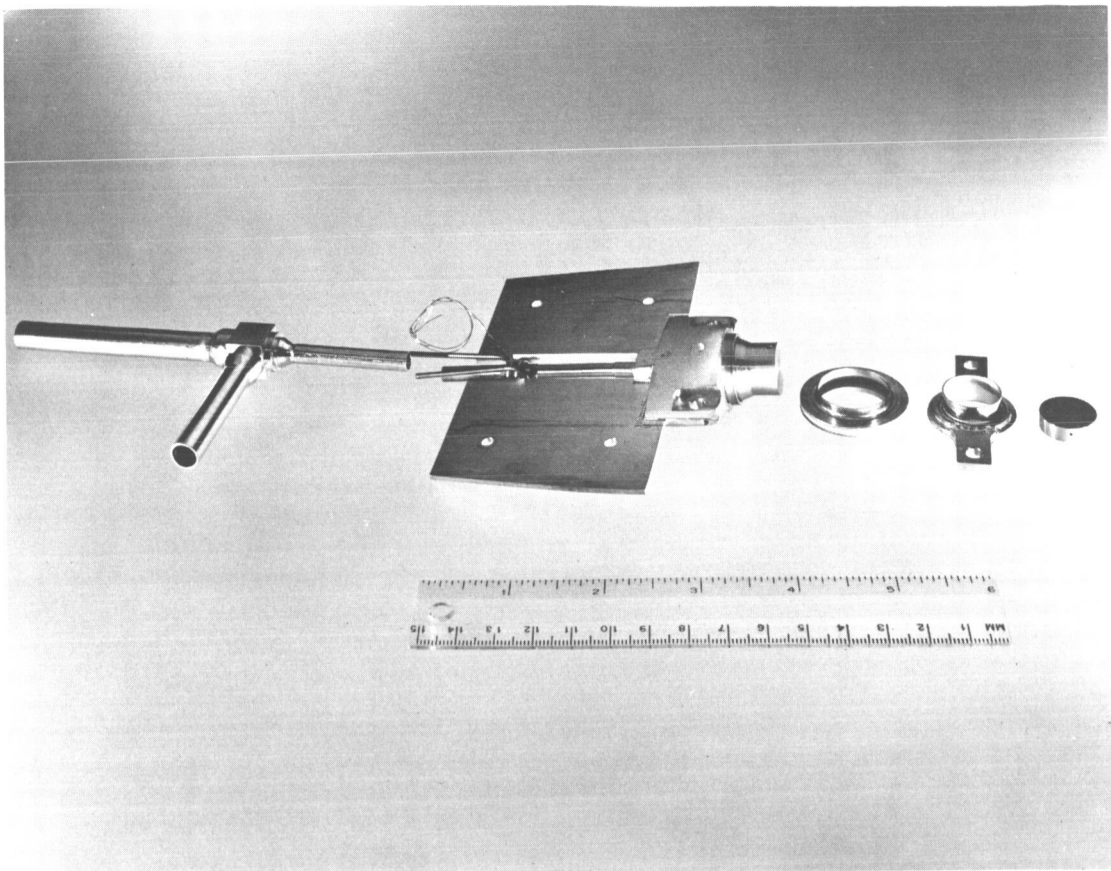


FIG. 4-3 LAYOUT OF PRINCIPAL SUBASSEMBLIES OF EOS HIGH-PERFORMANCE THERMIONIC CONVERTERS

The emitter envelope subassembly is comprised of a rhenium envelope, a niobium transition ring, and tantalum lead straps. All parts are vanadium-brazed. The niobium transition ring contains a 0.060-inch-thick lip section to which the upper flange of the pre-fabricated seal is electron-beam welded.

The final assembly operation is the electron-beam welding of the rhenium emitter to the envelope subassembly. The weld schedule follows the parameters established from the secondary experiments, that is, an electron-beam voltage of 150 kV at a current of 4.9 mA, with a part revolution speed of 40 rpm. Attaching the emitter last has several advantages: (1) It allows for visual inspection of the concentricity of the envelope and collector, (2) It permits a high temperature emitter outgas and grain stabilization treatment independent of the converter structure. In particular, the outgassed emitter impurities will contaminate the collector surface and prevent an optimum cesiated work function during converter operation, (3) It provides a means of setting the interelectrode spacing to a predetermined value by grinding or shaping the emitter before welding.

The final diode is depicted in Fig. 4-4. As noted, only three electron-beam welds are necessary for assembly — two welds at the flanges and one at the emitter. The exhaust tubulation is joined to the diode assembly, and high purity cesium is distilled into the converter.

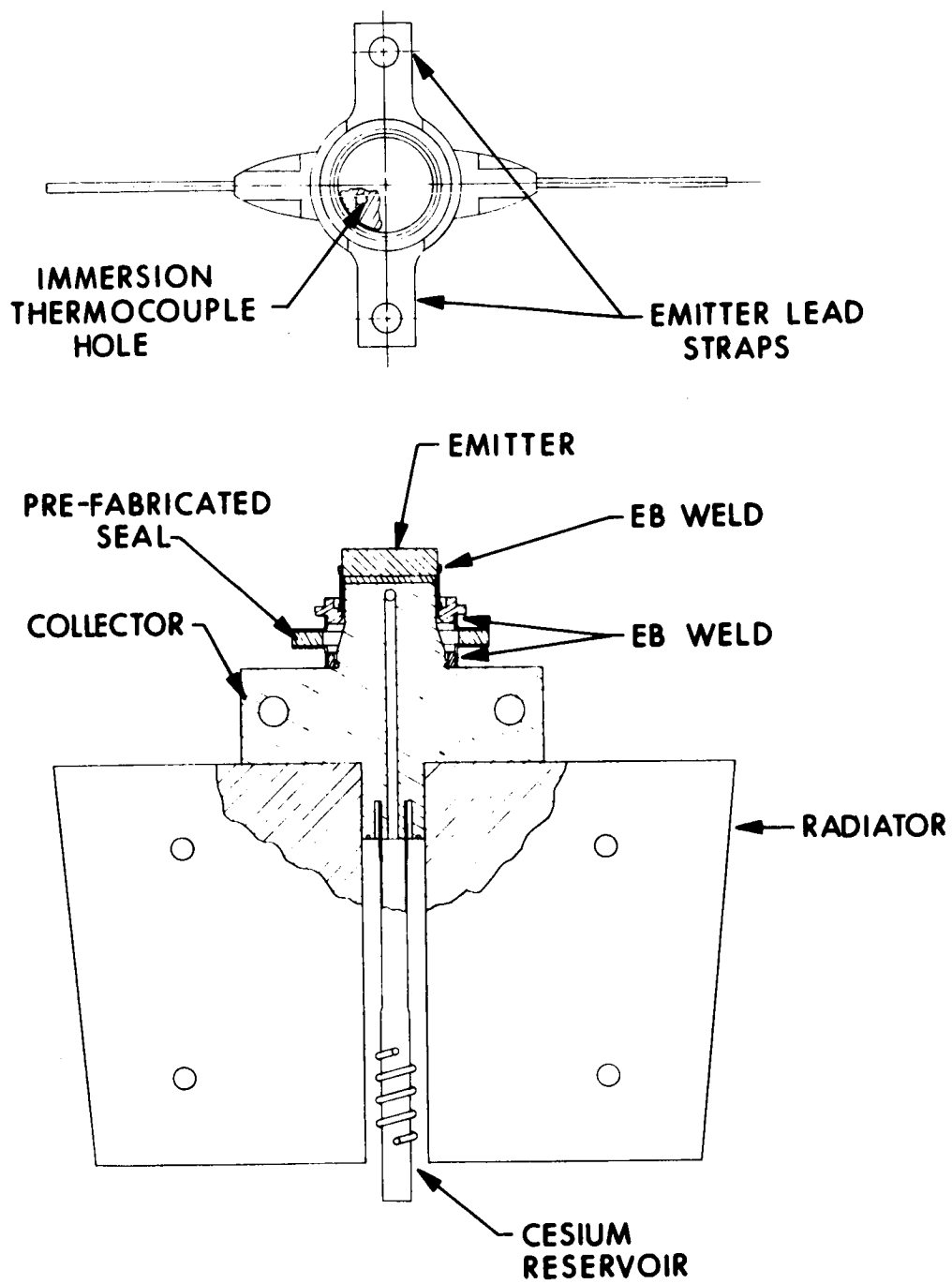


FIG. 4-4 COMPLETED DIODE ASSEMBLY

## 5. THERMIONIC CONVERTER PERFORMANCE

### 5.1 Methods of Measurement

#### 5.1.1 Current-Voltage Data

EOS uses two methods of testing thermionic converters and both methods yield equivalent data. The first method or technique, involves the steady state, dc measurement of optimized converter current and voltage from a simply instrumented circuit as shown in Fig. 5-1. For ease of testing, the usual passive resistor is replaced by an electronic load that is capable of controlling either constant current or voltage output from the converter. Emitter temperature is held constant at  $1735^{\circ}\text{K}$  while the cesium reservoir temperature and collector temperature are adjusted for maximum converter output at various specified voltage levels. To insure that the output is stable, all element temperatures are held constant for 10 to 15 minutes; the final current and voltage are then recorded.

The second method of obtaining current-voltage data is the impression of a 60 cycle voltage source upon a fixed converter operating point. This has the effect of continuously and rapidly changing the converter load line about the dc operating point. An oscilloscope of sufficient precision and stability may be employed to monitor the sweep characteristic. The main advantage of this technique is that an entire I-V characteristic may be photographed with all element temperatures unchanged. Figure 5-2 shows the circuit for this type of testing. Since there has been considerable controversy involved with ac sweeping methods or the interpretation of ac sweep data, the following discussion has been included. First, the sweep transformer should have a low inductance, low impedance secondary capable of sustaining at

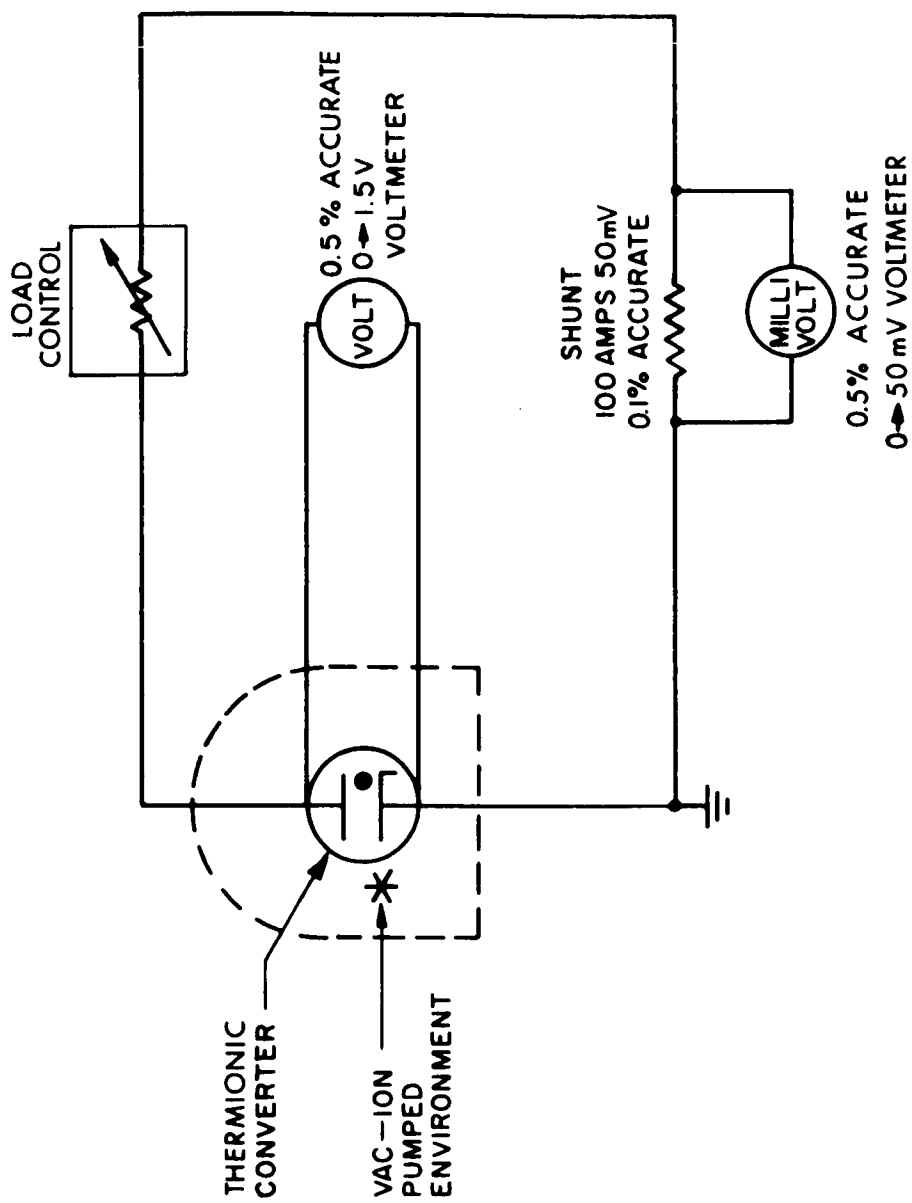


FIG. 5-1 ELECTRICAL CIRCUIT FOR dc PERFORMANCE TESTING OF THERMIONIC CONVERTERS

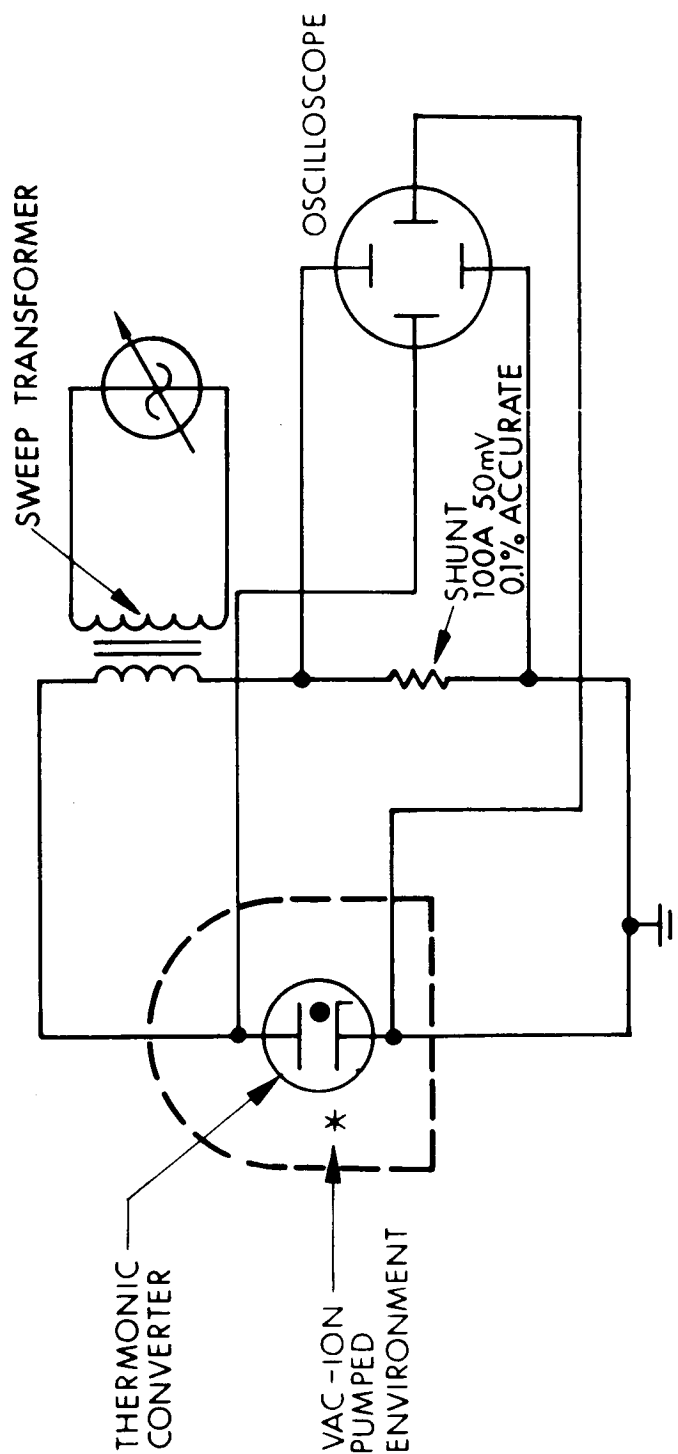


FIG. 5-2 ELECTRICAL CIRCUIT FOR ac PERFORMANCE TESTING OF THERMIONIC CONVERTERS

least 400 amperes steady state. High inductance transformers often lead to a voltage displacement or hysteresis in the characteristic caused by high values of  $L \, dI/dt$ . Second, grounding problems should be avoided by providing a common ground since oscilloscope grounds are made by the neutral line in the three-wire electrical system servicing the laboratory. On the other hand, the converter emitter is usually tied to water-pipe ground. Therefore, a voltage difference of several tenths of volts may exist between two reference points in the system. Third, the oscilloscope must have a high degree of stability, such that millivolt responses are displayed without drifting. If the oscilloscope is accurately calibrated, its display will register the true I-V characteristic for a fixed set of operating conditions. It is true that an ac sweep superimposed on an operating converter will cause the circuit dc meters to read a different value than the static dc level, but this is to be expected since these meters generally have rectifying junctions which will average out an ac signal. At any rate, a useful technique that EOS employs is to double expose the film on an oscillograph - the first exposure records the dc operating level, the second records the ac sweep about the dc level and must contain the original operating point if the element temperatures have not changed.

In summary, there are advantages to both methods. The dc yields unequivocal, acceptance-type data for hardware. On the other hand, the ac sweep method is useful for diagnostic testing where the effects of cesium pressure and collector temperature are quickly required. Moreover, such important items as saturated electron emission, breakdown voltage, arc impedance, etc., are available from an I-V sweep picture. The important point about sweep or dynamic testing is that, if done properly, it gives absolute agreement with the dc method. Any point on a sweep picture can be statically reproduced within test accuracy.

### 5.1.2 Temperature Measurement

There are two types of temperature measuring instruments involved with thermionic converter testing: optical pyrometers and thermocouples. The converter emitter temperature is measured by sighting a micro-optical pyrometer in an 8:1 or 10:1 depth-to-diameter hohlraum drilled parallel to the emitter surface. The position of the hohlraum relative to the bombardment filament is such that radiation or reflection from the filament does not affect the line-of-sight pyrometer measurement. Micro-optical pyrometers with thin filament bulbs 1/3 to 1/6 the diameter of the hohlraum are used for converter testing at EOS, thus facilitating accurate temperature measurement. These same pyrometers are calibrated each month against a standard lamp certified by the National Bureau of Standards. Figure 5-3 is a summary plot of a micro-pyrometer whose calibration data at six-month intervals is plotted against an NBS standard. The variation of the data is within 7°C over a two-year period of time.

Thermocouple measurements on a converter are made at the cesium reservoir, the collector, the radiator, and the seals. All thermocouples have wire material continuity from the temperature measuring junction through the vacuum system and into the ice junction to prevent erroneous emf generation. All thermocouples are made from the same heat number as supplied by vendor source. The variation in millivolt response from these couples is approximately  $\pm 0.5$  per cent as determined by furnace calibration. Moreover, the couple response is  $\pm 0.5$  percent of the true temperature indicated by a secondary standard of platinum/platinum-10 percent rhodium.

### 5.2 Converter SN-101 (rhenium-rhenium)

Converter SN-101 was built to reproduce the performance from the rhenium-rhenium variable parameter test vehicle. In particular, it was desired to fabricate a hardware type converter with a wide interelectrode spacing (0.0035 inch) to demonstrate 15.4 watts/cm<sup>2</sup> at



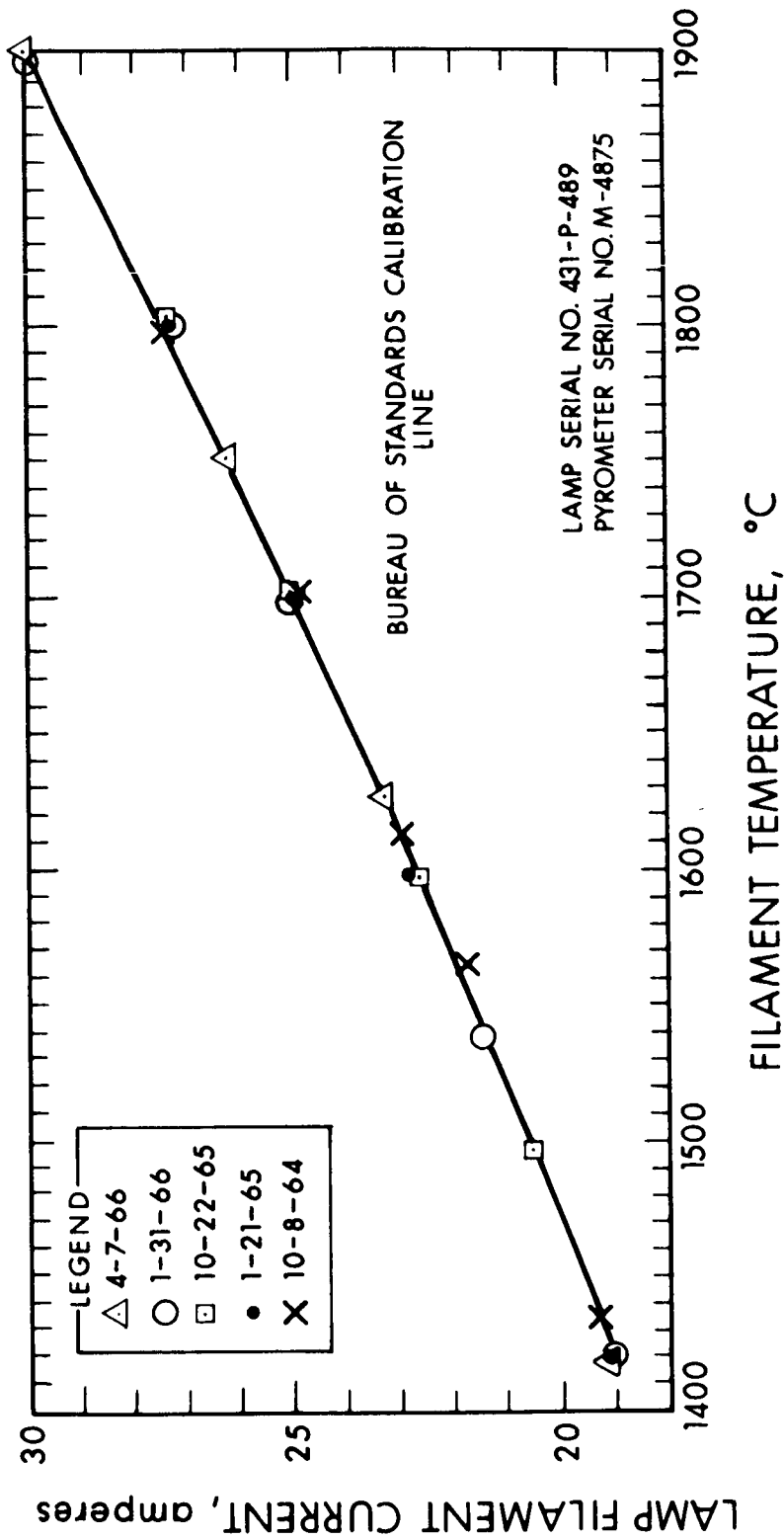


FIG. 5-3 CALIBRATION RECORD OF MICRO-OPTICAL PYROMETER USED FOR CONVERTER TESTING

0.8 Vdc and 21 watts/cm<sup>2</sup> and 0.7 Vdc for an emitter temperature of 1735°C. In addition, SN-101 utilized advanced concepts of converter design such as a solid rhenium emitter electron-beam welded to a rhenium envelope for long-life operation and stable performance, pre-fabricated seal assemblies for manufacturing reliability and ultraclean assembly, and a vanadium-brazed rhenium cap on the collector for output performance higher and more consistent than the rhenium-molybdenum system of electrodes.

The emitter area of SN-101 is 2.0 cm<sup>2</sup> as defined by the inside diameter of the emitter support structure or envelope. Sidewall emission from the envelope is designed to be minimal since the heat choke section commences 0.020 inch below the emitter weld and the sidewall spacing is between 0.010 and 0.012 inch.

The paragraphs that follow discuss the electrode processing, interelectrode spacing, optimized performance, and other data concerning SN-101.

#### 5.2.1 SN-101 Electrode Processing

The rhenium emitter for SN-101 was outgassed in a vac-ion pumped chamber at 2450°C for 3 hours. The chamber pressure, at outgassing temperature, was  $2 \times 10^{-7}$  torr. The heating was accomplished by electron bombardment from a counterwound rhenium filament. The emitter was supported on a rhenium fixture to insure that no materials interaction would contaminate the emitter. The temperature measurement is probably accurate to within  $\pm 25^\circ\text{C}$  since ordinary pyrometers and standard lamps rarely cover that range. As noted in Section 2, a heat treatment of 2450°C for three hours was found to produce a sufficiently stable emitting surface, i.e., absolutely no grain growth or grain boundary movement for 100 hours of subsequent operation at 1735°C.

The collecting surface of SN-101 is a planar cap of rhenium sheet vanadium-brazed at 1900°C for three minutes duration in a  $10^{-6}$  torr vacuum susceptor can environment. Since the collector

surface temperature in an operating converter is generally 800 to 850°C, treatment at 1900°C insures a stable surface for subsequent operation. Vanadium was selected as the braze material since the available literature indicates no low melting point eutectic nor brittle intermetallic formation. Metallurgical studies, at EOS, of the Re-V bond indicated a hardness increase at the braze interface of only ten percent over that of rhenium. Also, no voids were encountered in three separate cross sections of sample Re-V brazes, although it should be mentioned that overbrazing does result in void structure and significant increases in hardness at the braze interface.

#### 5.2.2 SN-101 Interelectrode Spacing

It was established from the variable parameter test vehicle that the maximum power output from a practical rhenium-rhenium system at 0.8V output occurred at 3.5 mils spacing and SN-101 was designed for this spacing. Furthermore, it was experimentally determined in a mockup structure that with the emitter and collector in a stress-free condition the converter structure, upon reaching operating temperature, differentially expanded 1.8 mils. To obtain 3.5 mils in SN-101 (the difference, 1.7 mils), four small flats were ground on the rhenium surface at a height of 1.7 mils. That is, 99.5 percent of the emitting area is 1.7 mils below the level of the flats; hence, the emitter may be brought in contact with the collector at room temperature and electron-beam welded in place to insure parallelism. Therefore, at temperature, 99.5 percent of the area emits at an interelectrode spacing of 3.5 mils; the remaining 0.5 percent, the surface area of the flats, emits at a spacing of 1.8 mils.

#### 5.2.3 SN-101 Optimized dc Performance

Figure 5-4 is an optimized performance plot of the dc output from converter SN-101 under the test conditions of: (1) an emitter temperature of 1735°C (true) hohlraum temperature; (2) potential voltage leads placed at the converter terminals, not electrodes; and (3) all data points recorded under steady-state, dc conditions.

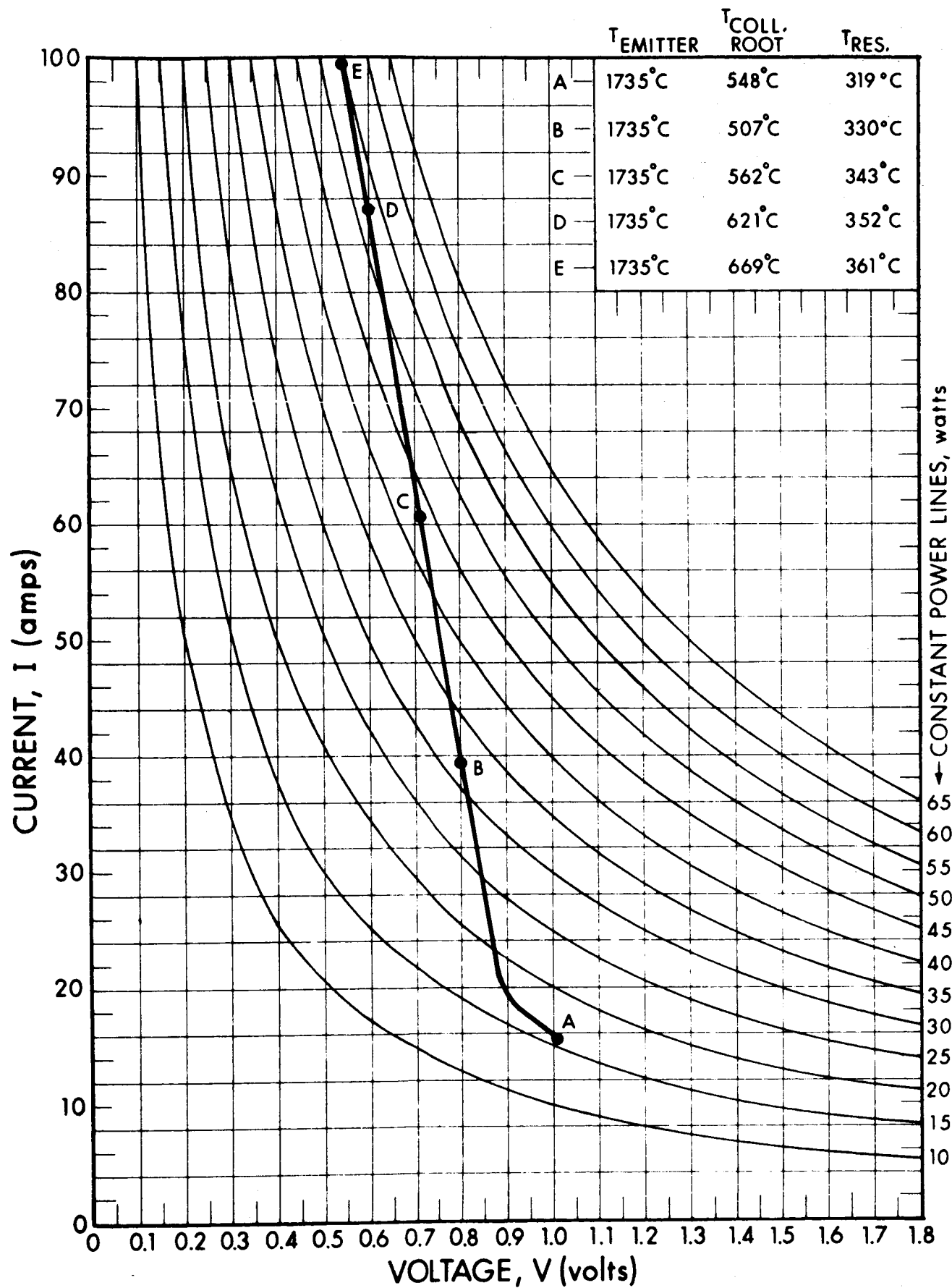


FIG. 5-4 CONVERTER SN-101 PERFORMANCE PLOT (all points are dc data)

Power output densities of  $15.2 \text{ watt/cm}^2$  at 0.8 Vdc and  $21.0 \text{ watts/cm}^2$  at 0.7 Vdc were measured from SN-101. The 0.8 Vdc data were less than the design goal; however, this was known as a virtual fact before SN-101 was built, since the variable parameter test vehicle measurements indicated that only interelectrode spacings of less than 0.0003 inch yielded any greater performance than  $15 \text{ watts/cm}^2$ . The tested efficiency of SN-101 operating at  $15.2 \text{ watts/cm}^2$  (0.8 Vdc) was 9 percent; however, the geometry of plane parallel converters is such that the bombardment heating is quite inefficient.

SN-101 was continuously operated for 40 hours at  $21 \text{ watts/cm}^2$  (0.7 Vdc output) as an acceptance test per the work statement. The output performance at all voltage output levels after 40 hours was identical to the initial data shown in Fig. 5-4.

#### 5.2.4 SN-101 Miscellaneous Data

Converter SN-101 was the first EOS converter built with a molybdenum-copper radiator; therefore, it was desirable to compare the thermal performance from operating data to the original design calculations. For a dc current load of 65 amperes, a temperature difference from the collector surface to the collector root of  $178^\circ\text{C}$  was measured, as compared to a calculated  $\Delta T$  of  $165^\circ\text{C}$ . It was further noted that no radiator heat input was required to optimize the output performance at 0.7V, nor was any artificial cooling of the radiator, including oversize lead straps, needed. SN-101 operated, therefore, in accord with the design calculations in Section 4.

Figure 5-5 is a performance plot of the electrode potential from SN-101 with a reference line indicating the terminal voltage output. Generally, these data are not useful from an applications standpoint, since the emitter support structure and emitter lead strap are an integral part of a power generating device. However, some investigators have recently reported converter performance using electrode potential in lieu of terminal voltage output. One final

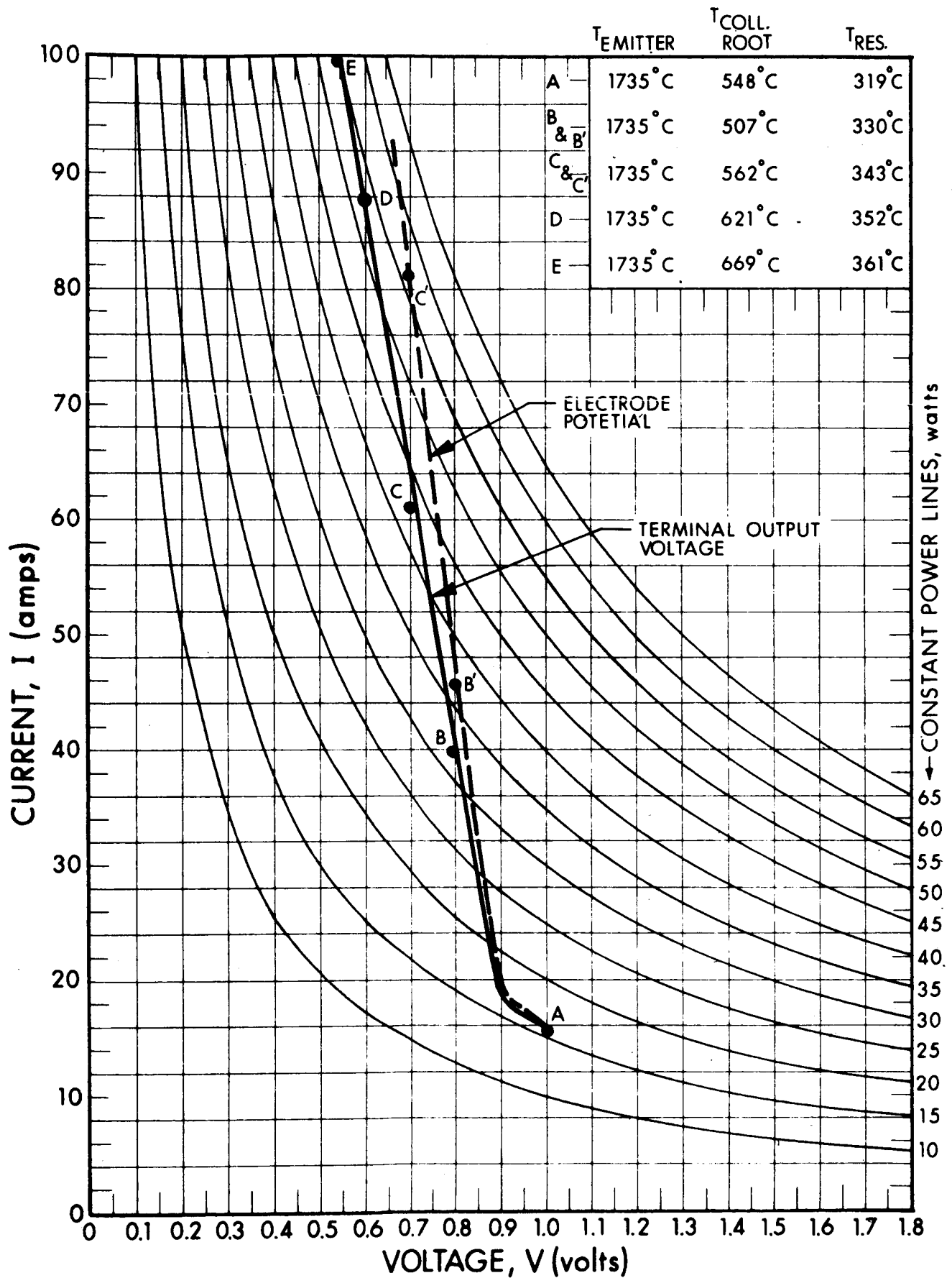


FIG. 5-5 CONVERTER SN-101 PERFORMANCE PLOT COMPARING ELECTRODE POTENTIAL TO TERMINAL OUTPUT VOLTAGE (all data points are dc)

precaution should be observed before comparing electrode potential performance: The emitter temperature measurements must be true hohlraum readings, and the emitter area must be carefully defined as discussed in Section 4.

Saturated electron emission data were taken from the emitter of SN-101 at an emitter temperature of  $1735^{\circ}\text{C}$  (true) hohlraum and  $330^{\circ}\text{C}$  cesium reservoir. A value of  $28 \text{ amps/cm}^2$  is reported. Bare work function measurements were also performed on the SN-101 emitter. The reduced data indicate a value of 4.80 to 4.85 eV for the polycrystalline rhenium surface.

### 5.3 Converter SN-102 (rhenium-rhenium)

#### 5.3.1 Electrode Processing

The electrodes of SN-102 were processed in an identical manner with those of SN-101; that is, the emitter was outgassed at  $2450^{\circ}\text{C}$  for three hours and the rhenium collector cap was outgassed at  $1900^{\circ}\text{C}$  for four minutes during the vanadium brazing operation.

#### 5.3.2 SN-102 Interelectrode Spacing

The interelectrode spacing of SN-102 was set at about 0.0002 inch to achieve the program goal of  $20 \text{ watts/cm}^2$  at 0.8 Vdc output. This spacing is almost impossible to reproduce from converter to converter and was considered as a performance demonstration only.

The most convincing evidence for the minimal spacing of SN-102 may be derived from the space-charge nature of its performance. For example, Fig. 5-6a is an I-V characteristic from SN-102 for operation at an emitter temperature of  $1735^{\circ}\text{C}$  (true) hohlraum and a cesium reservoir temperature of  $350^{\circ}\text{C}$ . Figure 5-6b is an I-V characteristic from the rhenium-rhenium test vehicle at the same emitter temperature of  $1735^{\circ}\text{C}$  (true hohlraum) and at a cesium reservoir temperature of  $349^{\circ}\text{C}$ . At these operating conditions the interelectrode spacing of the test vehicle was measured to be 0.0002 inch, with high precision 0.0001-inch indicators which may be read to within 0.00005 inch. The similarity of the characteristics shown in Figs. 5-6a and 5-6b for equivalent operating conditions strongly suggests that the interelectrode spacing of SN-102 was nearly the same as that of the test vehicle (i.e., 0.0002 inch).

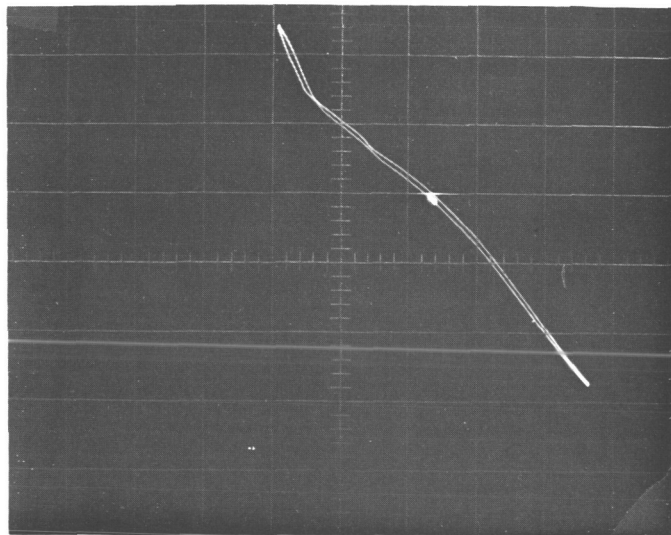


FIG. 5-6a SN-102 CHARACTERISTIC AT 1735°C.  
 EMITTER TEMPERATURE, 349°C CESIUM  
 RESERVOIR TEMPERATURE AND COLLECTOR  
 ROOT TEMPERATURE AT 592°C.

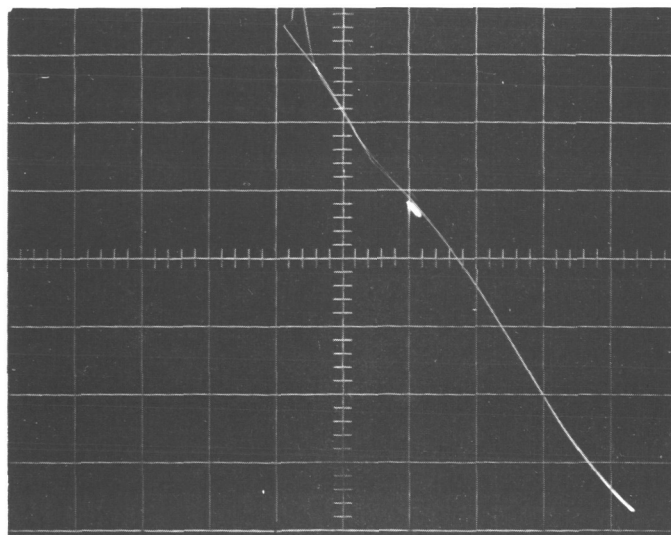


FIG. 5-6b RHENIUM-RHENIUM VARIABLE PARAMETER  
 TEST VEHICLE CHARACTERISTIC AT  
 1735°C EMITTER TEMPERATURE, 348°C  
 CESIUM RESERVOIR TEMPERATURE AND  
 COLLECTOR ROOT TEMPERATURE AT 600°C



At the uppermost portion of each characteristic curve, the arc discharge is just starting. One fact is obvious: The shape of the I-V curve in Fig. 5-6b ranging from 1.0V to 0.5V is not characteristic of the thermionic arc mode operation.

An additional point of interest about the voltage output of SN-102 (for constant current) is: The voltage output always increases with increasing collector temperature. This is an observation inconsistent with arc mode operation in a thermionic converter and suggests that the spacing between electrodes is so minimal that increasing the collector temperature by 50 to 70°C is sufficient to decrease the interelectrode spacing and increase the voltage output for a given space charge current in accordance with Child's Law. In one instance, the collector temperature was increased too much and the converter shorted internally between emitter and collector — further evidence of the close-spaced nature of SN-102.

Finally, it was noted that upon startup operation of SN-102, the electrodes did not open near ambient temperature but required excessive heat input resulting in emitter temperatures of 1200°C before electrode separation. The calculated interelectrode spacing of SN-102, based on the methods described in Section 3, was approximately 0.0004 inch assuming that the stress-free condition of the electrodes occurs at an emitter temperature of 1200°C rather than 20°C.

### 5.3.3 Converter SN-102 Performance

Figure 5-7 is a plot of the steady-state, dc performance from converter SN-102. The performance goal of 20 watts/cm<sup>2</sup> at 0.8 Vdc is identified on the plot. The testing procedures for SN-102, such as emitter temperature measurements, emitter area definition, and potential lead placement, were identical to those for SN-101.

The general shape of the performance plot in Fig. 5-7 is considerably different from that of SN-101, SN-103, or any other converter operating in the arc mode. For example, the power density

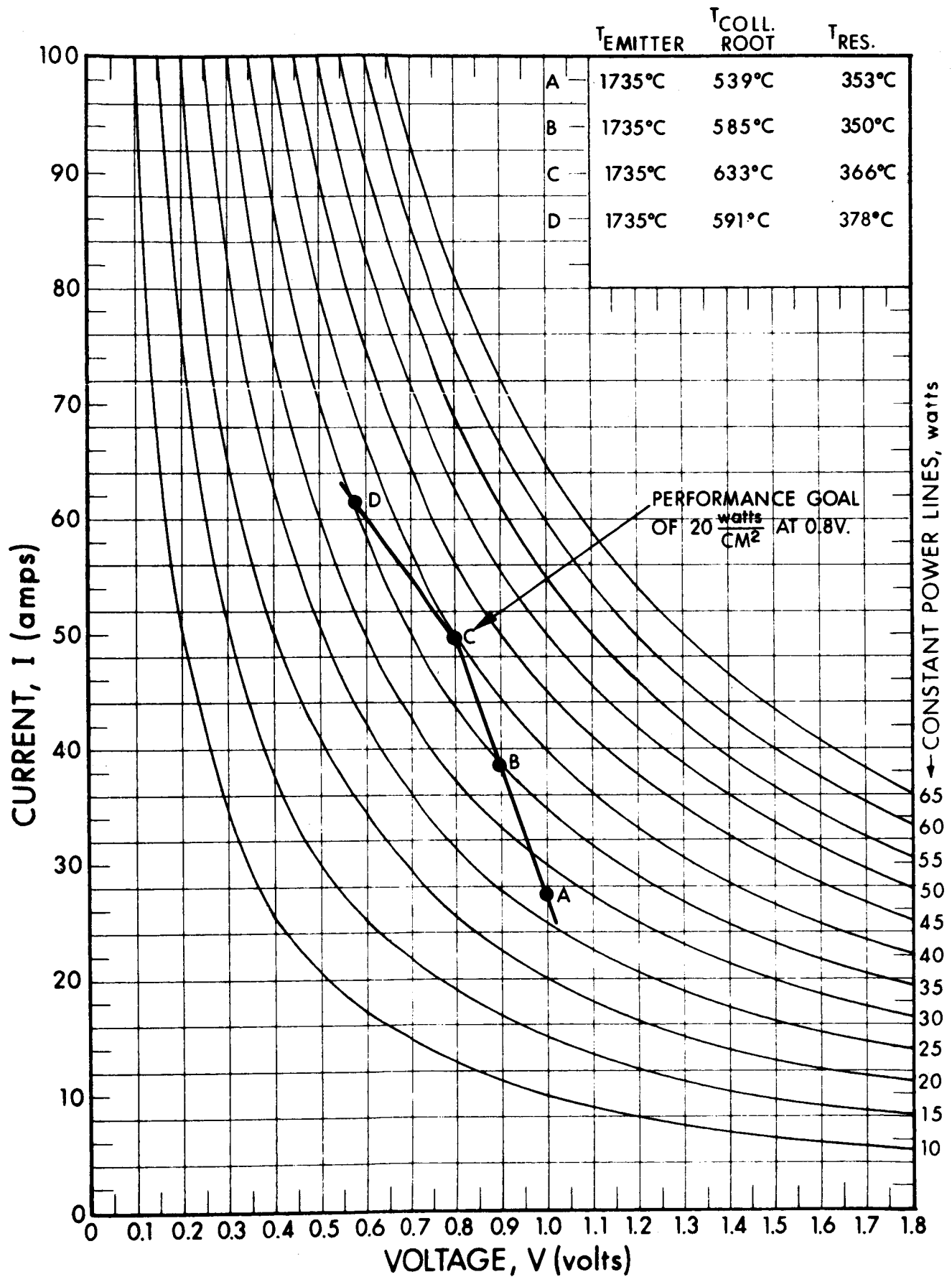


FIG. 5-7 CONVERTER SN-102 PERFORMANCE PLOT (all points are dc data)

output increases about 5 watts/cm<sup>2</sup> for 0.1 volt increments between 0.1V and 0.6V in an arc mode converter operating at an emitter temperature of 2000°K. In Fig. 5-7, the increase is much less, amounting to about 1 or 2 watts/cm<sup>2</sup> between 0.6V and 0.9V.

#### 5.4 Converter SN-103 (rhenium-molybdenum)

##### 5.4.1 Electrode Processing

The rhenium emitter of SN-103 was outgassed at 2450°C for three hours. The molybdenum collector was outgassed while titanium brazing the reservoir tubulation into the cesium vapor channel in the collector root (1700°C for three minutes).

##### 5.4.2 SN-103 Interelectrode Spacing

The interelectrode spacing of SN-103 was set in a manner identical with SN-101, wherein four flats were ground on the emitter face allowing for a stress-free expansion from ambient to operating temperature of 3.5 mils.

##### 5.4.3 Converter SN-103 Steady-State, Optimized Performance

Figure 5-8 is the initial performance plot of the dc output from SN-103. The performance is identical to that of SN-101, not only in terms of electrical output but also cesium reservoir temperature. This would normally be an unexpected result since the minimum work function of cesium on molybdenum is 1.55 eV as compared with cesium on rhenium at 1.47 eV. And consequently, the rhenium-molybdenum system of SN-103 should deliver less performance than the rhenium-rhenium system of SN-101. However, it was surmised that SN-103 displayed the same behavior as the rhenium-molybdenum test vehicle; that is, the molybdenum collector had received an evaporated layer of rhenium from the emitter during terminal exhaust and the performance was characteristic of a rhenium-rhenium/molybdenum system rather than just rhenium-molybdenum. After 31 hours of continuous operation at 20 watts/cm<sup>2</sup> (0.7 Vdc), a decrease in voltage output was

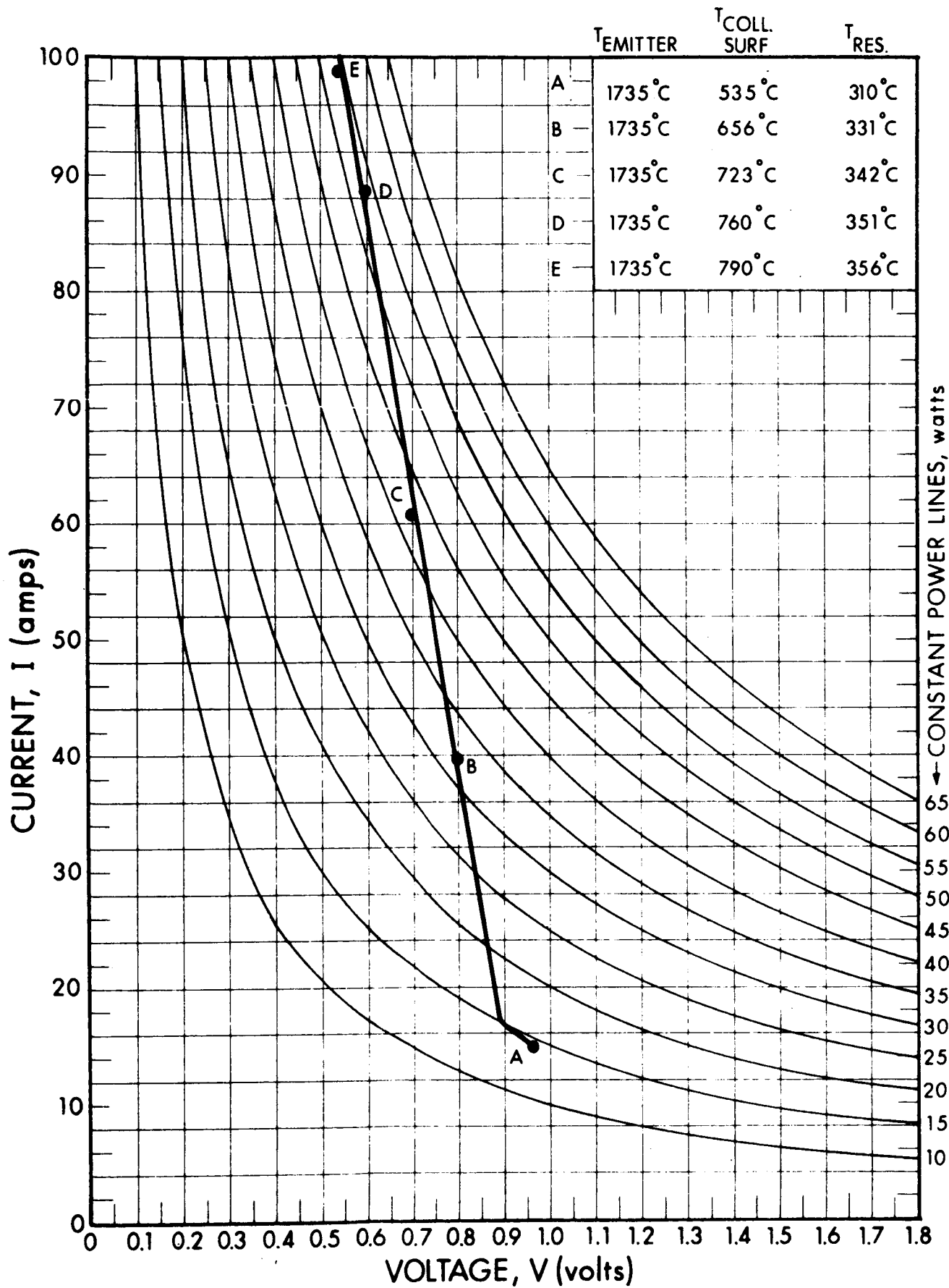


FIG. 5-8 CONVERTER SN-103 INITIAL PERFORMANCE PLOT (all points are dc data)

observed. Continued operation resulted in further output loss, and in addition it appeared that the conditions of cesium reservoir temperature and collector temperature for maximum output (at a specified voltage) had shifted. After 60 hours operation, the decrease in output terminated and steady-state, nonvarying operation resumed. Figure 5-9 is the performance plot for SN-103 after 60 hours of operation with the original performance included for comparison. It may be noted at once that the loss in voltage output is constant and equivalent to the difference in work function values of cesium on molybdenum and cesium on rhenium, namely 0.080 volt. To reestablish the original data of a presumed rhenium-rhenium/molybdenum system, the emitter temperature was increased to  $2200^{\circ}\text{C}$ , with the cesium reservoir heater secured for a period of two hours. The estimated thickness of the rhenium coating on the collector surface resulting from this high temperature operation is six angstrom layers based on elementary considerations of weight loss by evaporation. The low reservoir temperature of  $197^{\circ}\text{C}$  and an assumed wider interelectrode spacing of 4 mils at the elevated emitter temperature of  $2200^{\circ}\text{C}$  results only in negligible attenuation to a simple vacuum evaporation model.

The performance plot of SN-103 following the deliberate evaporation of rhenium from the emitter to the collector is illustrated in Fig. 5-10 wherein the original data are shown for comparison. The identity of performance and the similarity of operating conditions (such as cesium reservoir temperature and collector surface temperature) are readily apparent.

## 5.5 Converter SN-104 (rhenium-molybdenum)

### 5.5.1 Electrode Processing

The electrodes of SN-104 were processed in a manner identical with that of SN-103; namely, the rhenium emitter was outgassed at  $2450^{\circ}\text{C}$  for three hours and the molybdenum collector was outgassed at  $1700^{\circ}\text{C}$  for three minutes.

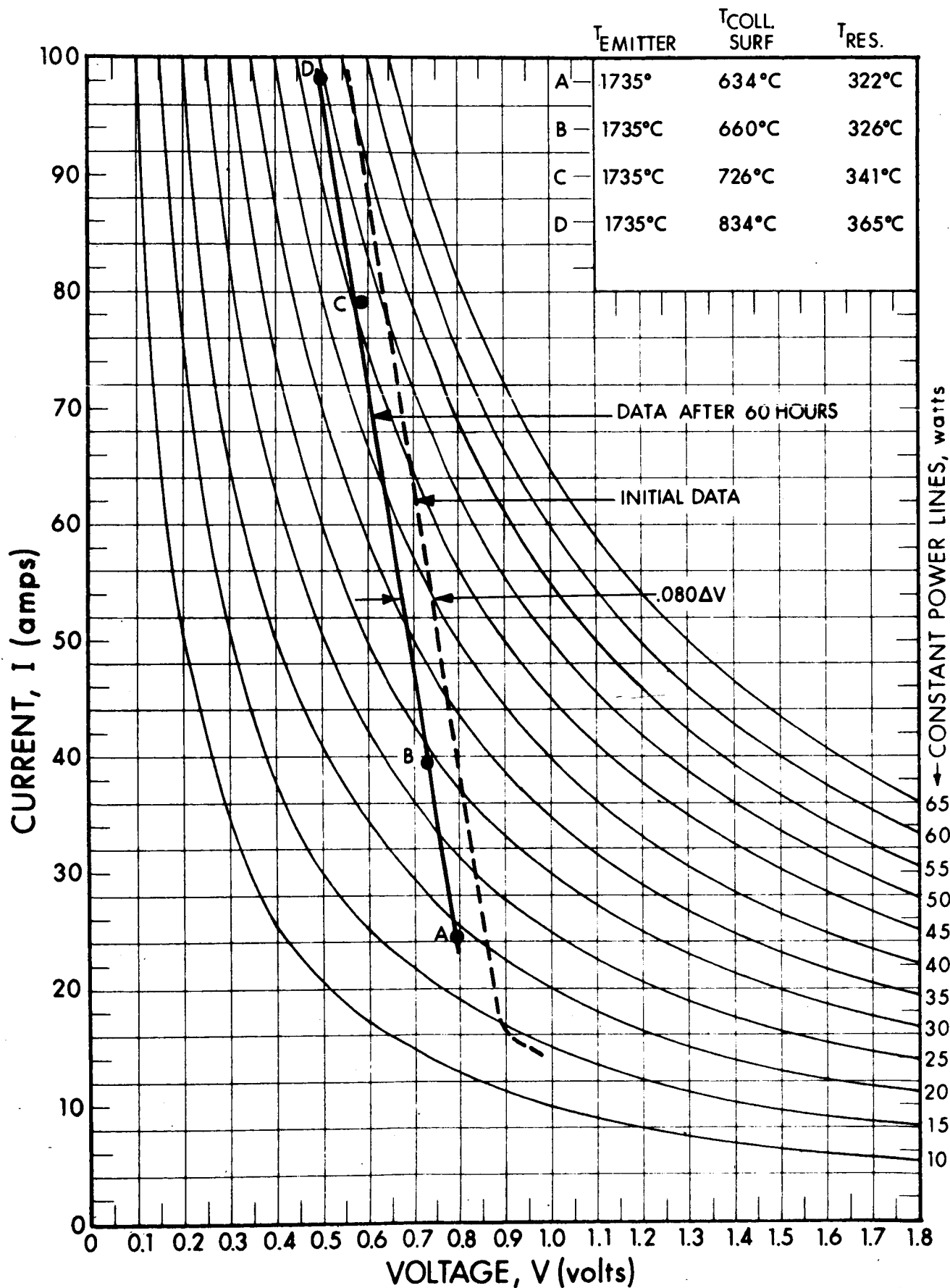


FIG. 5-9 CONVERTER SN-103 PERFORMANCE PLOT AFTER 60 HOURS. INITIAL DATA SHOWN FOR REFERENCE (all points are dc data)

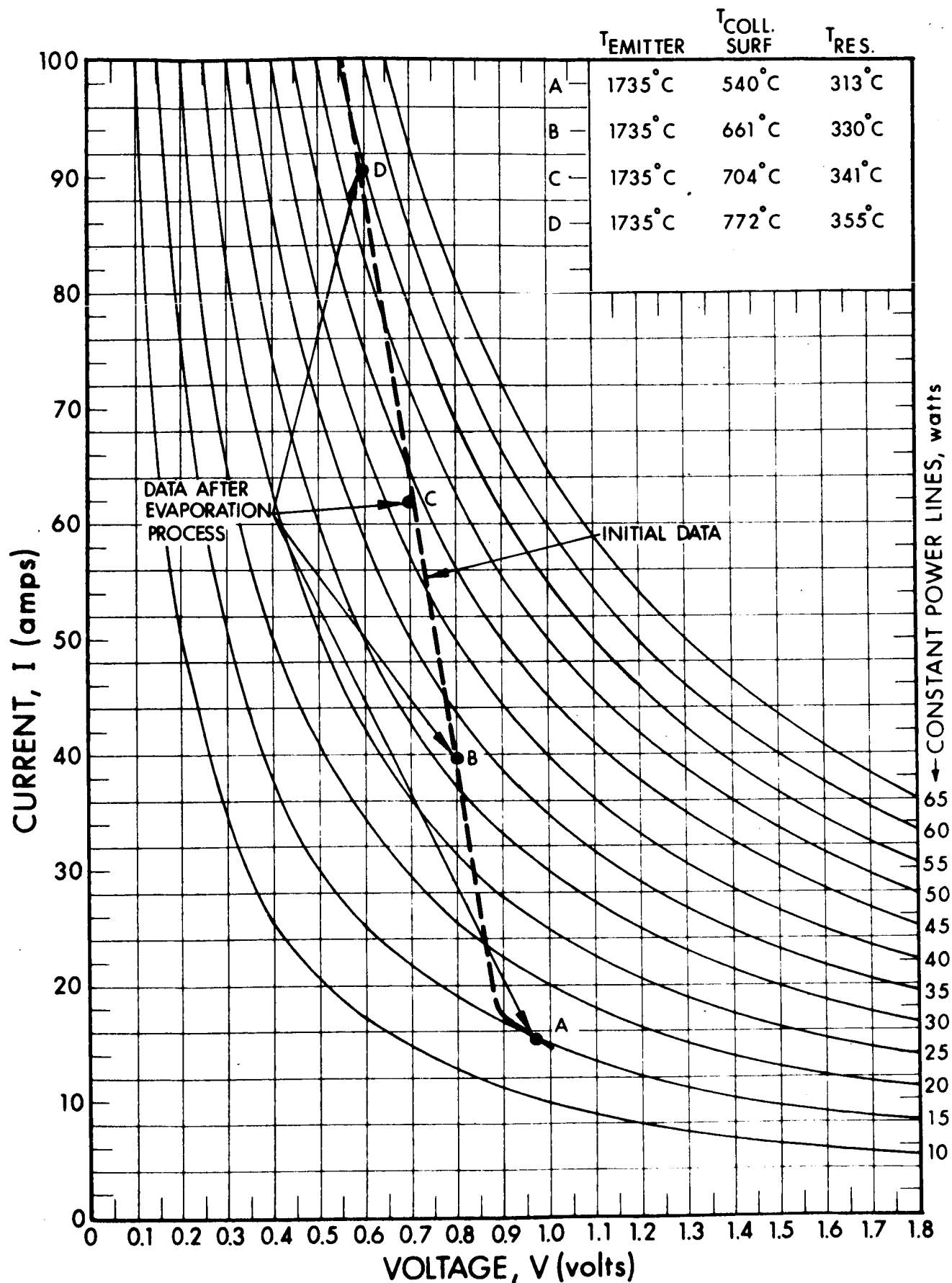


FIG. 5-10 CONVERTER SN-103 AFTER EVAPORATION OF RHENIUM ONTO THE COLLECTOR. INITIAL DATA SHOWN FOR REFERENCE (all points are dc data)

#### 5.5.2 SN-104 Interelectrode Spacing

The interelectrode spacing of SN-104 was set in an attempt to reproduce the spacing of SN-102. The space charge nature of the I-V characteristics and the high emitter temperature at electrode separation were quite similar to the behavior of SN-102. It is estimated that the actual spacing was 0.0003 inch since the electrodes separated at 1100°C emitter temperature during startup, 100°C less than for SN-102.

#### 5.5.3 Converter SN-104 Performance

Figure 5-11 is a plot of the steady-state, dc performance from SN-104. The testing procedures for SN-104, such as emitter temperature measurements, emitter area definition and potential lead placement, were identical with those of SN-101, SN-102, and SN-103 and in accordance with the test procedures previously discussed.



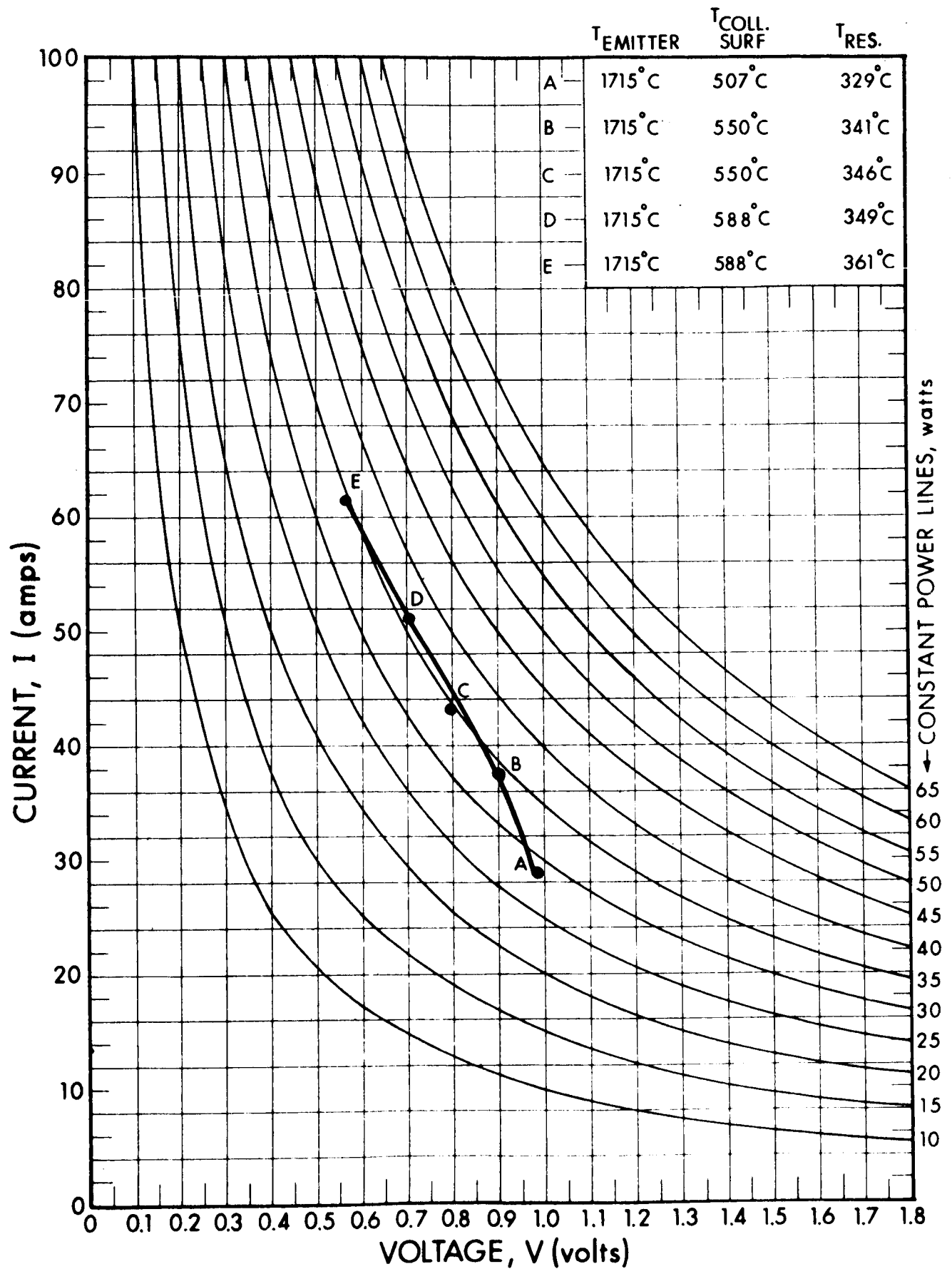


FIG. 5-11 CONVERTER SN-104 PERFORMANCE PLOT (all points are dc data)

6. CONTRIBUTOR LIST

The following contributors were actively engaged in technical performance on this program:

A. O. Jensen  
P. G. Worden  
A. E. Campbell  
D. H. Pollock  
B. Marchant  
R. W. Hamerdinger  
D. T. Dalinden  
L. Wolby

#### REFERENCES

1. A. O. Jensen, A. E. Campbell, Jr., and W. Dong, Proceedings of the Thermionic Specialist Conference, Gatlinberg, Tennessee, October 1963
2. E. A. Baum and A. O. Jensen, Proceedings of the 15th Annual Power Sources Conference, Atlanta, Georgia, May 1961
3. D. H. Pollock, Proceedings of the Thermionic Specialist Conference, San Diego, California, October 1965
4. S. Kitrilakis, and M. Meeker, "Experimental Determination of the Heat Conduction of Cesium Gas," Advanced Energy Conversion 3, 59-68, 1963
5. W. R. Martini, "Theoretical Calculation of the Thermal Conductivity of Cesium Vapor at Thermionic Temperatures," Advanced Energy Conversion 3, 49-58 1963
6. Neil N. Ault, "Optical Properties of Rokide Coatings," 6th Meeting of the Refractory Composite Working Group, June 1962
7. W. H. Askwyth, et al, "Determination of the Emissivity of Materials," (PWA-2128), Pratt & Whitney Aircraft, East Hartford, Connecticut
8. T. E. Waterman and H. J. Hirschhoren, Handbook of Thermophysical Properties of Solid Materials, MacMillan, New York, 1961
9. M. Hansen, Constitution of Binary Alloys, McGraw Hill, New York 1958
10. H. Miller, Tantalum and Niobium, Butterworths Scientific Publications, London, 1959

PRECEDING PAGE BLANK NOT FILMED.

APPENDIX A  
PROCEDURE FOR CHEMICAL CLEANING OF TANTALUM

I. DESCRIPTION

The following procedure describes a method for chemically cleaning tantalum prior to vacuum outgassing.

II. EQUIPMENT LIST

1. Beakers of assorted sizes
2. Hot plate
3. Ultrasonic cleaner (minimum of 60 watts average power)
4. Bunsen burner, stand, and hot pad
5. Forceps of assorted sizes
6. Lint-free and sulfur-free paper
7. Distilled water
8. Ethyl alcohol ( $C_2H_5OH$ )
9. Hydrochloric acid ( $HCl$ ), 37 percent
10. Chromic acid (saturated solution of chromium trioxide)
11. Sulfuric acid ( $H_2SO_4$ ), 96 percent
12. Stirring rod
13. Graduate
14. Balance, triple beam  $\pm 0.1$  gram
15. Glass storage container, 1 gallon

III. SAFETY PROCEDURE FOR PREPARATION OF CHROMIC ACID

All materials are corrosive. Avoid spilling. In case of spillage, wash away immediately with large quantities of water.

Sulfuric acid releases a large amount of heat when mixed with water. Therefore, use caution and follow instructions exactly. Add acid to water.

The following safety apparatus must be used while preparing the solution:

PRECEDING PAGE BLANK NOT FILMED.

1. Rubber gloves
2. Goggles or face mask
3. Full length rubber or plastic apron

#### IV. PREPARATION OF SATURATED CHROMIC ACID

##### 1. Materials

- a. Chromium trioxide (chromic acid), solid, technical grade
- b. Sulfuric acid, concentrated, 96 percent, ACS specification
- c. Distilled water

##### 2. Equipment

- a. Graduate (1 liter)
- b. Beaker (4 liters)
- c. Stirring rod
- d. Balance, triple beam,  $\pm 0.1$  gram
- e. Glass storage container, 1 gallon

##### 3. Procedure

- a. Measure 2 liters of distilled water into beaker.
- b. Add chromium trioxide and stir until solution is saturated.
- c. Slowly and while stirring, carefully add 1100 ml of concentrated sulfuric acid.
- d. Store in glass bottle, label "saturated chromic acid solution."

#### NOTE

Solution should be discarded if it shows a greenish cast. There may be legal restrictions on the disposal of chromate solutions.

#### V. SAFETY PROCEDURES FOR CLEANING PROCESS

All materials are corrosive. Avoid spilling. In case of spillage, wash away immediately with large quantities of water.

The following are mandatory while cleaning parts with acid solutions:

1. Rubber gloves
2. Goggles or face mask
3. Rubber or plastic apron

## VI. CLEANING PROCEDURE

### 1. Materials

- a. Ethyl alcohol ( $C_2H_5OH$ )
- b. Hydrochloric acid (HCl), 37 percent
- c. Chromic acid solution
- d. Distilled water
- e. Hot plate
- f. Ultrasonic cleaner (minimum of 60 watts average power)
- g. Lint-free and sulfur-free paper
- h. Beakers of assorted sizes

### 2. Procedure

- a. Place part to be cleaned in beaker of ethyl alcohol. Place beaker in ultrasonic cleaner. Clean for approximately 60 seconds.
- b. Remove parts from ethyl alcohol - allow to dry.
- c. Place parts in beaker of boiling hydrochloric acid for approximately 30 seconds.
- d. Remove from hydrochloric acid and rinse in beaker of boiling, distilled water for approximately 2 minutes.
- e. Remove from distilled water - allow to dry.
- f. Dip in ethyl alcohol - remove and allow to dry.
- g. Place parts in beaker of hot chromic acid ( $110^{\circ}C$ ).
- h. Remove from chromic acid and rinse vigorously in large beaker of cold, distilled water.
- i. Rinse parts in boiling, distilled water for approximately 2 minutes.
- j. Rinse parts in cold, distilled water for approximately 10 seconds.
- k. Remove parts from distilled water - allow to dry.
- l. Rinse parts in clean, ethyl alcohol - remove and dry with hot air blast.

- m. Visually inspect each part for contamination such as fingerprints, water stains, and discoloration. Parts must be free of any such contamination. PRESENCE OF ANY CONTAMINANTS DICTATES THE NEED FOR AN ENTIRE REPROCESSING OF THE AFFECTED PART.
- n. Wrap parts in lint-free, sulfur-free paper.
- o. Seal in polyethylene bag.

APPENDIX B  
DERIVATION OF COLLECTOR HEATING POWER

Plasma Electron Temperature in the Absence of a Collector Sheath

The plasma electron energy is the sum of the kinetic energy imparted to the electrons as they leave the emitter surface and the energy contributed by the emitter voltage fall. This is given by

$$\begin{aligned} E_{\text{eject}} + eV_{\text{sheath}} &= E_{\text{plasma}} \\ 2kT_{\text{emitter}} + eV_{\text{sheath}} &= E_{\text{plasma}} \end{aligned} \tag{1}$$

The controversy in this approach lies solely in the evaluation of the plasma energy. The mean electron energy, assuming a Maxwellian distribution, is defined by

$$\langle E \rangle = \frac{\int_0^{\infty} E dN_E}{\int_0^{\infty} dN_E} = \frac{\int_0^{\infty} \frac{1}{2} M v^2 dN_v}{\int_0^{\infty} dN_v} = \frac{3}{2} kT \tag{2}$$

where  $dN_v$  is the Maxwellian distribution function for electrons with velocity between  $v$  and  $v + dv$ . This is given by

$$dN_v = \left( \frac{4N}{\sqrt{\pi}} \right) \left( \frac{M}{2kT} \right)^{3/2} v^2 \exp\left( -\frac{Mv^2}{2kT} \right) dv \tag{3}$$



The energy associated with the electrons having the average velocity is

$$E = 1/2M \langle v \rangle^2 = 1/2M \left[ \frac{\int_0^\infty v dN_v}{\int_0^\infty dN_v} \right]^2 = \frac{4kT}{\pi} \quad (4)$$

Whether Eq. 2 or 4 is the correct expression for the plasma electron energy is the question. Now, the random plasma current density is given by

$$J_R = \frac{n_e e \langle v \rangle}{4}$$

where  $n_e$  is the electron density. Thus, Eq. 4 can be interpreted as the energy associated with the random electrons in the plasma. Since the random current densities exceed the drift current densities by greater than a factor of 10, it would seem appropriate to utilize Eq. 4 in evaluating the plasma electron temperature. Thus:

$$2kT_{\text{emitter}} + eV_{\text{sheath}} = \frac{4kT_{\text{plasma}}}{\pi} = 1.275kT_{\text{plasma}} \quad (5)$$

The error in plasma temperature determination and thus collector energy input can be as much as 20 percent, depending on which plasma energy term (Eq. 2 or 4) is utilized.

Thus the heating power input to the collector is given by

$$P = J_d A \left( \phi_c + \frac{2kT_{\text{emitter}}}{e} + V_{\text{sheath}} \right) = J_d A \left( \phi_c + \frac{4kT_{\text{plasma}}}{\pi} \right) \quad (6)$$

where

$$\begin{aligned} J_d &= \text{drift current density measured at the collector} \\ A &= \text{collecting area} \\ \phi_c &= \text{collector work function} \\ T_{\text{emitter}} &= \text{emitter temperature} \\ V_{\text{sheath}} &= \text{emitter sheath voltage} \end{aligned}$$

#### Plasma Electron Temperature with a Collector Sheath

In the case of a collector sheath, Eq. 6 is modified by the addition of a term representing the collector sheath voltage. That is,

$$P = J_d A \left( \phi_c + \frac{2kT_{\text{emitter}}}{e} + V_{\text{sheath}} \pm V_{\text{collector}} \right) \quad (7)$$

where  $V_{\text{collector}}$  is the height of the collector sheath and the sign is positive for an accelerating sheath and negative for a retarding sheath. There is a fine point in the evaluation of Eq. 7 since, when the collector sheath is retarding and the sign is negative,  $J_d$  will also decrease due to the loss of less energetic electrons. This will occur only in an "off" optimum mode of operation of a thermionic converter when the collector temperature is not high enough to emit sufficient electron density to equal the random plasma electrons impinging on the collector. In an optimized thermionic converter, the collector is analogous to an emitting probe that is matched to the plasma, i.e., the back emission from the collector is exactly equal to the positive x-directed random current. The positive x-direction is from the emitter toward the collector. In this instance there will be no sheath at the collector and a plasma-matched condition exists.